Eionet Report - ETC/ATNI 2021/1

European air quality maps for 2019

PM_{10}, $PM_{2.5}$, Ozone, NO_2 and NO_x
Spatial estimates and their uncertainties

September 2021

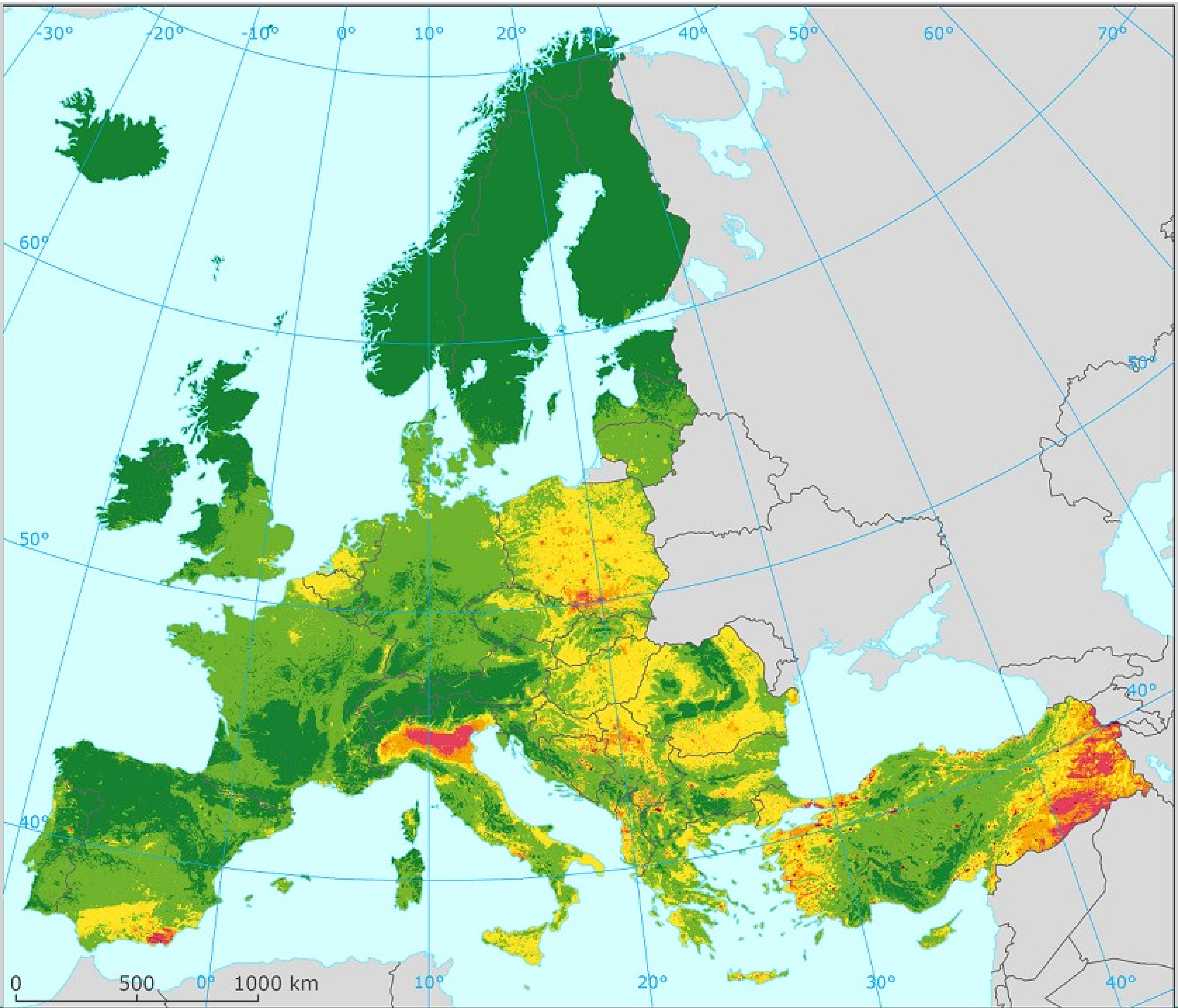

Authors:
Jan Horálek (CHMI), Leona Vlasáková (CHMI), Markéta Schreiberová (CHMI), Jana Marková (CHMI), Philipp Schneider (NILU), Pavel Kurfürst (CHMI), Frédéric Tognet (INERIS), Jana Schovánková (CHMI), Ondřej Vlček (CHMI)

ETC/ATNI consortium partners:
NILU – Norwegian Institute for Air Research, Aether Limited, Czech Hydrometeorological Institute (CHMI), EMISIA SA, Institut National de l'Environnement Industriel et des risques (INERIS), Universitat Autònoma de Barcelona (UAB), Umweltbundesamt GmbH (UBA-V), 4sfera Innova, Transport & Mobility Leuven NV (TML)

European Environment Agency
European Topic Centre on Air pollution, transport, noise and industrial pollution

Cover design: EEA
Cover picture: Concentration map of PM_{10} indicator 90.4 percentile of daily means for 2019. Units: $\mu g \cdot m^{-3}$. (Map 2.2 of this report.)
Layout: ETC/ATNI

The withdrawal of the United Kingdom from the European Union did not affect the production of the report.
Data reported by the United Kingdom are included in all analyses and assessments contained herein, unless otherwise indicated. Data refer to a year prior to the United Kingdom's withdrawal from the European Union. The withdrawal of the UK from the EU did not affect the data presented in this document. The terminology "EU-28" has been kept to refer to the current EU-27 and the UK. Possible exceptions to this approach will be clarified in the context of their use

Authors
Jan Horálek, Markéta Schreiberová, Leona Vlasáková, Jana Marková, Pavel Kurfürst, Jana Schovánková, Ondřej Vlček: Czech Hydrometeorological Institute (CHMI, CZ)
Philipp Schneider: Norwegian Institute for Air Research (NILU, NO)
Frédéric Tognet: National Institute for Industrial Environment and Risk (INERIS, FR)

ETC/ATNI c/o NILU
ISBN 978-82-93752-26-4

European Topic Centre on Air pollution,
transport, noise and industrial pollution
c/o NILU – Norwegian Institute for Air Research
P.O. Box 100, NO-2027 Kjeller, Norway
Tel.: +47 63 89 80 00
Email: etc.atni@nilu.no
Web : https://www.eionet.europa.eu/etcs/etc-atni

Contents

Summary

European air quality concentrations maps have been prepared for the year 2019. The maps are based primarily on air quality data as reported under the 2008 Ambient air quality directive by EEA member and cooperating countries and voluntary reporting countries (EC, 2008). The countries considered for mapping include the most of Europe, apart from its eastern part. Concentration maps have been produced to assess the situation with respect to the most stringent air quality limit values and the indicators most relevant for the assessment of impacts on human health and vegetation.

Methodology

The mapping method follows the methodology developed earlier (Horálek et al, 2021, and references cited therein); it combines the monitoring data with the results from a chemical transport model and other supplementary data (such as land cover, meteorological and satellite data). The method ('Regression – Interpolation – Merging Mapping') is based on a linear regression model followed by kriging of the residuals produced from that model (residual kriging). Next to this, maps of Phytotoxic Ozone Dose (POD) indicators have been presented since 2018, based on methodology described in CLRTAP (2017a) according to Emberson et al. (2000). These maps are prepared based on hourly ozone rural maps, hourly meteorological data and soil hydraulic properties data.

Population exposure

Concentrations of particulate matter continued to exceed the EU and WHO standards in large parts of Europe. 6 % of the considered European population is exposed to levels above the EU PM_{10} limit value of 40 µg·m^{-3}; 39 % of the considered European population is exposed to levels above the 2005 WHO PM_{10} Air Quality Guideline (AQG) level of 20 µg·m^{-3}(WHO, 2005)([1]). Table 2.2 shows that 16 % of the population is exposed to PM_{10} concentrations above the daily limit value in more than 35 days per year. Figure ES.1 shows that the countries with the highest values of annual averages PM_{10} are located in the central and south-eastern parts of Europe.

Figure ES.1: PM_{10} annual mean concentrations to which the population per country was exposed in 2019. The 2005 WHO AQG level (20 µg·m^{-3}) is marked by the green line, the EU annual limit value (40 µg·m^{-3}) is marked by the red line

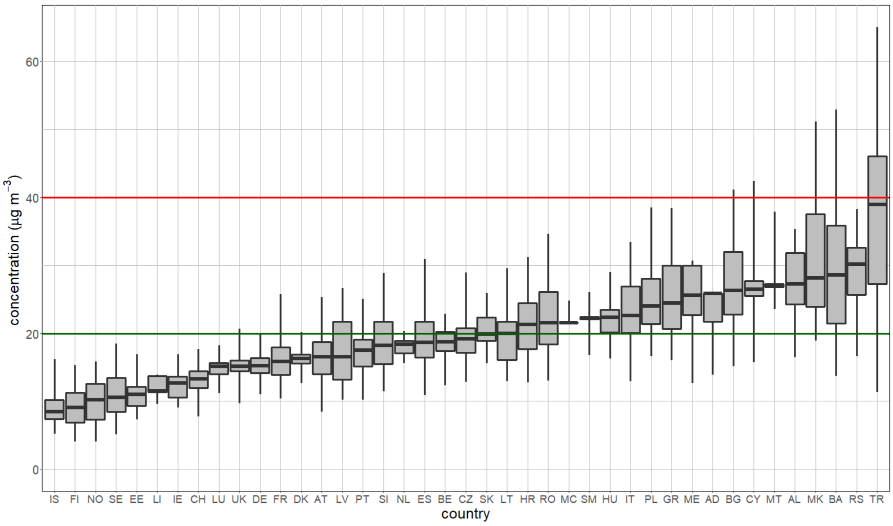

Note: For each country, the box plot shows the concentration to which a percentage of the population was exposed: 50 % is shown by the black marker, 25 % and 75 % by the box's edges, 2 % and 98 % by the whiskers' edges.

([1]) After the drafting of this report, WHO introduced its new Air Quality Guidelines (WHO, 2021). Throughout the report, the old 2005 WHO AQG levels are kept.

1.2 % of the considered European population (excluding Turkey in the case of $PM_{2.5}$) is exposed to levels above the EU $PM_{2.5}$ limit value of 25 µg·m^{-3}; 64 % of the considered European population is exposed to levels above the 2005 WHO $PM_{2.5}$ AQG level of 10 µg·m^{-3}, see Table 3.1. The concentrations of $PM_{2.5}$ and PM_{10} are often highly correlated, with the highest $PM_{2.5}$ exposures found in the central and south-eastern parts of Europe similarly as in the case of PM_{10}, see Figure ES.2.

Figure ES.2: $PM_{2.5}$ annual mean concentrations to which the population per country was exposed in 2019. The 2005 WHO AQG level (10 µg·m^{-3}) is marked by the green line, the EU annual limit value (25 µg·m^{-3}) is marked by the red line

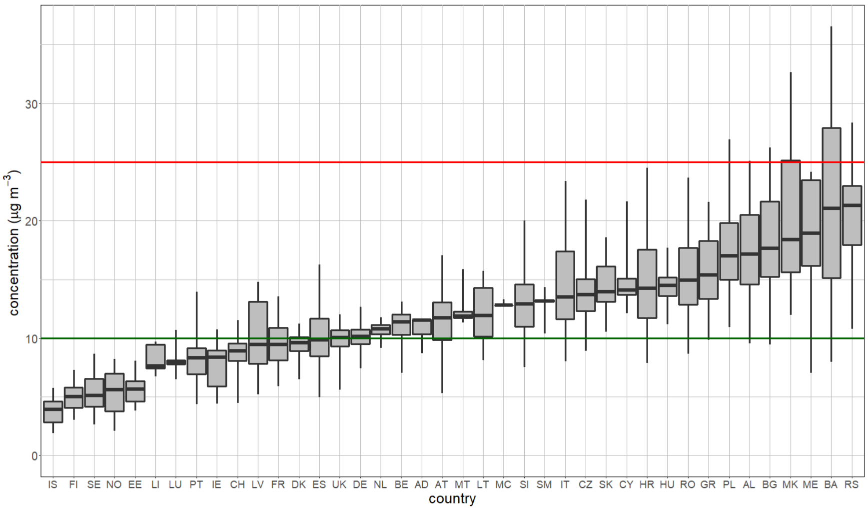

Note: For each country, the box plot shows the concentration to which a percentage of the population was exposed: 50 % is shown by the black marker, 25 % and 75 % by the box's edges, 2 % and 98 % by the whiskers' edges.

The NO_2 annual mean concentration map shows a different spatial distribution than the PM maps. Table 5.1 indicates that in 12 countries a limited fraction of the considered European population (3 % in total) is exposed to concentrations above the EU annual limit value of 40 µg·m^{-3} (which is the same as the 2005 WHO AQG level). Figure ES.3 shows that in all countries, the majority of population lived well below the limit value in 2019, according to the presented assessment.

Figure ES.3: NO_2 annual mean concentrations to which the population per country was exposed in 2019. The EU annual limit value and 2005 WHO AQG level (40 µg·m^{-3} in both cases) are marked by the red line

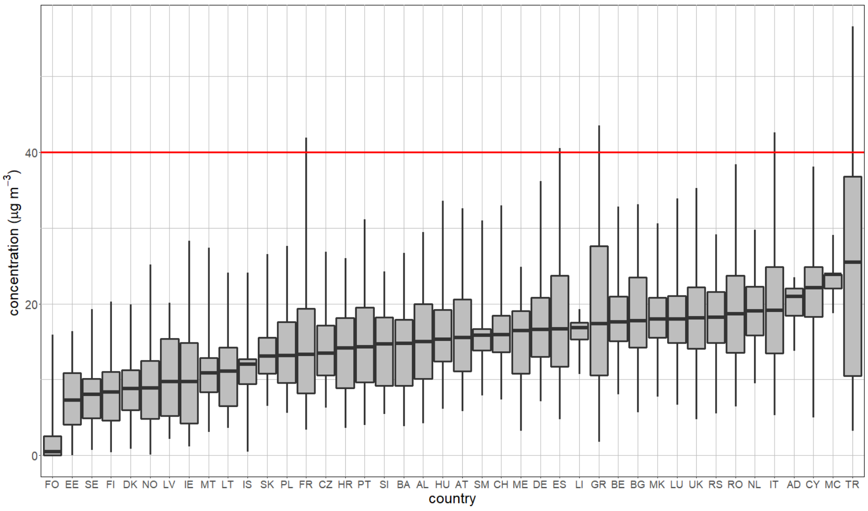

Note: For each country, the box plot shows the concentration to which a percentage of the population was exposed: 50 % is shown by the black marker, 25 % and 75 % by the box's edges, 2 % and 98 % by the whiskers' edges.

High exposures are observed in the larger urban areas (e.g. Milan, Naples, Rome, Turin, Paris, Barcelona, Madrid, London, Athens, Bucharest, Ankara, and Istanbul).

Exposure to ozone concentrations above the EU target value (TV) threshold (a maximum daily 8-hour average value of 120 µg·m^{-3} not to be exceeded on more than 25 days per year) occurs in 2019 in a large area of Europe, namely in most of Austria, Germany, Italy, Switzerland and Turkey, and in parts of Spain, France, west Balkan countries, Greece and Czechia. 22 % of the considered European population live in areas where the ozone TV is exceeded (Table 4.1). Figure ES.4 shows that the countries with the highest values of SOMO35 are located in the southern parts of Europe.

Figure ES.4: Ozone concentrations (expressed as the indicator SOMO35) to which the population per country was exposed in 2019

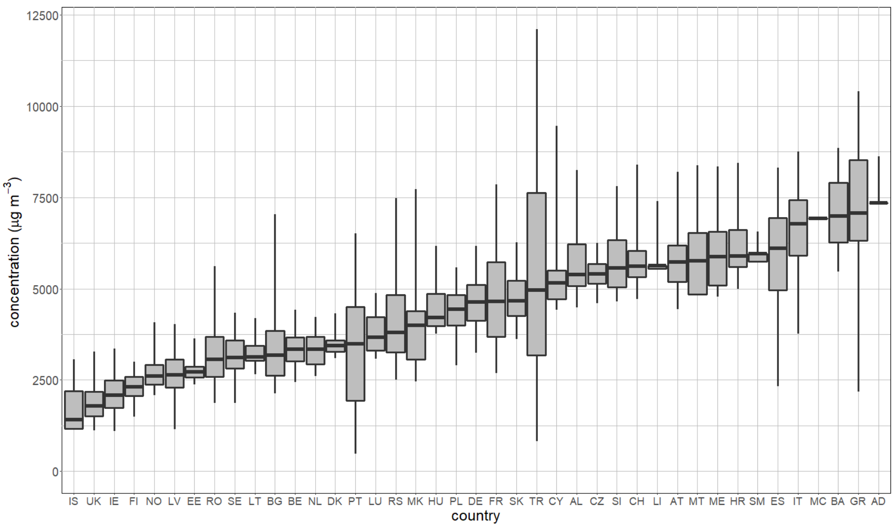

Note: For each country, the box plot shows the concentration to which a percentage of the population was exposed: 50 % is shown by the black marker, 25 % and 75 % by the box's edges, 2 % and 98 % by the whiskers' edges.

Accumulated risks

Although the spatial distributions of PM, NO_2 and ozone concentrations differ widely, the possibility of an accumulation of risk resulting from high exposures to all three pollutants cannot be excluded. The maps for the three most frequently exceeded EU standards (PM_{10} daily limit value, O_3 target value and NO_2 annual limit value) have been combined, see Map ES.1.

The combined population exposure shows the following results: out of the total population of 623 million in the mapping area, 6.9 % (43.0 million) people live in areas where two or three of these air quality standards are exceeded; and 0.3 % (2.2 million) people live in areas where all three standards are exceeded. The worst situation is observed in Italy (in particular the Po valley), where 2.5 % of the population live in areas where all three standards are exceeded; this is followed by Turkey, where it is also the case for 0.8 % of the population.

Map ES.1: Exceedance of Health-Related Air Quality Standards, 2019

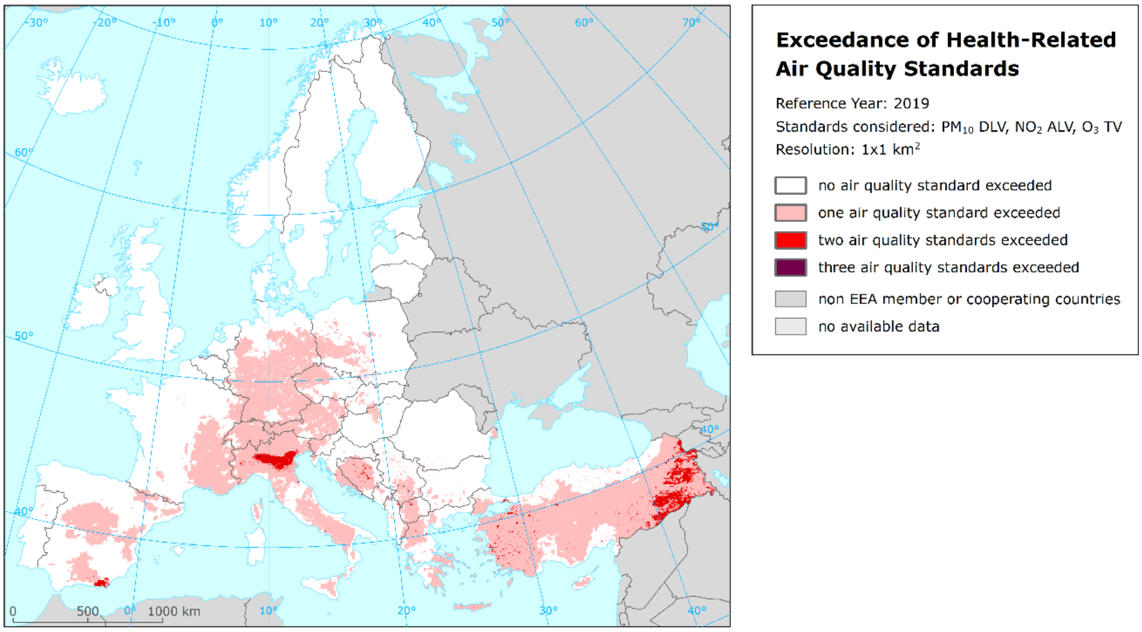

Vegetation exposure

Standards for the protection of vegetation have been set, among others, for NO_x and ozone. In a limited number of cases, the NO_x critical level has been exceeded, though this is relevant only if there is vegetation in those areas. A larger impact on vegetation can be expected from the direct exposure to ozone. The target value for the protection of vegetation (AOT40) is exceeded in about 37 % of the agricultural areas. The long-term objective is exceeded in 86 % of the agricultural areas. The critical level for the protection of forests (AOT40) is exceeded in about 85 % of the forested areas.

Critical levels of Phytotoxic Ozone Dose (POD) for wheat (both for grain yield and protein yield of wheat) has been exceeded in large parts of central, western and southern Europe. In most of Europe, critical levels for tuber yield of potato (in terms of POD for potato) have been exceeded, with the highest values of POD for potato in central Europe, the Baltic States, France and parts of Italy.

Changes over time

Since 2005, the maps have been prepared in an overall consistent way, although the mapping methodology has been subject to continuous improvement. This enables an analysis of changes in exposure over time. While PM_{10} and ozone maps have been prepared for the whole period 2005-2019, $PM_{2.5}$ maps have been routinely constructed since 2010 and NO_2 maps since 2014, with few maps for older years available. Thus, $PM_{2.5}$ maps are available for the whole period 2005-2019 apart from 2006, while in the case of NO_2 the maps for 2006, 2008, 2011 and 2012 are missing. Throughout the years, some methodology changes have been applied. Apart from minor changes, a major change was introduced for PM_{10} and $PM_{2.5}$ since 2017 maps, taking into account air quality in urban traffic areas, as was done for all the NO_2 maps.

The population-weighted concentration is calculated for the area of all countries considered in the report, both including and excluding Turkey, because the area of Turkey has not been mapped until 2016. For changes in population-weighted concentrations, excluding Turkey, see Figure ES.5. For comparability reasons, the results based on both the old and the new PM mapping methodology have been included in Figure ES.5.

The PM concentrations show a steady decrease of about 0.6 $\mu g \cdot m^{-3}$ per year for PM_{10} annual average and 0.4 $\mu g \cdot m^{-3}$ per year for $PM_{2.5}$ annual average. It is estimated that the considered European inhabitants have been exposed on average to an annual mean PM_{10} concentration of 19 $\mu g \cdot m^{-3}$ and to an annual mean $PM_{2.5}$ concentration of 12 $\mu g \cdot m^{-3}$ in 2019, being both the lowest values in the fifteen-year time series.

For the ozone concentration (expressed as SOMO35) no trend is observed for the period 2005-2019, due to the year-to-year variability. The NO_2 concentration (in terms of annual average) shows a decrease of about 0.5 $\mu g \cdot m^{-3}$ per year.

Figure ES.5: Population-weighted concentration of PM_{10} (annual mean), $PM_{2.5}$ (annual mean), ozone (SOMO35), and NO_2 (annual mean) in 2005-2019. For PM_{10} and $PM_{2.5}$, results based on both the old (blue dots) and the updated (red dots) mapping methodology are presented, where available

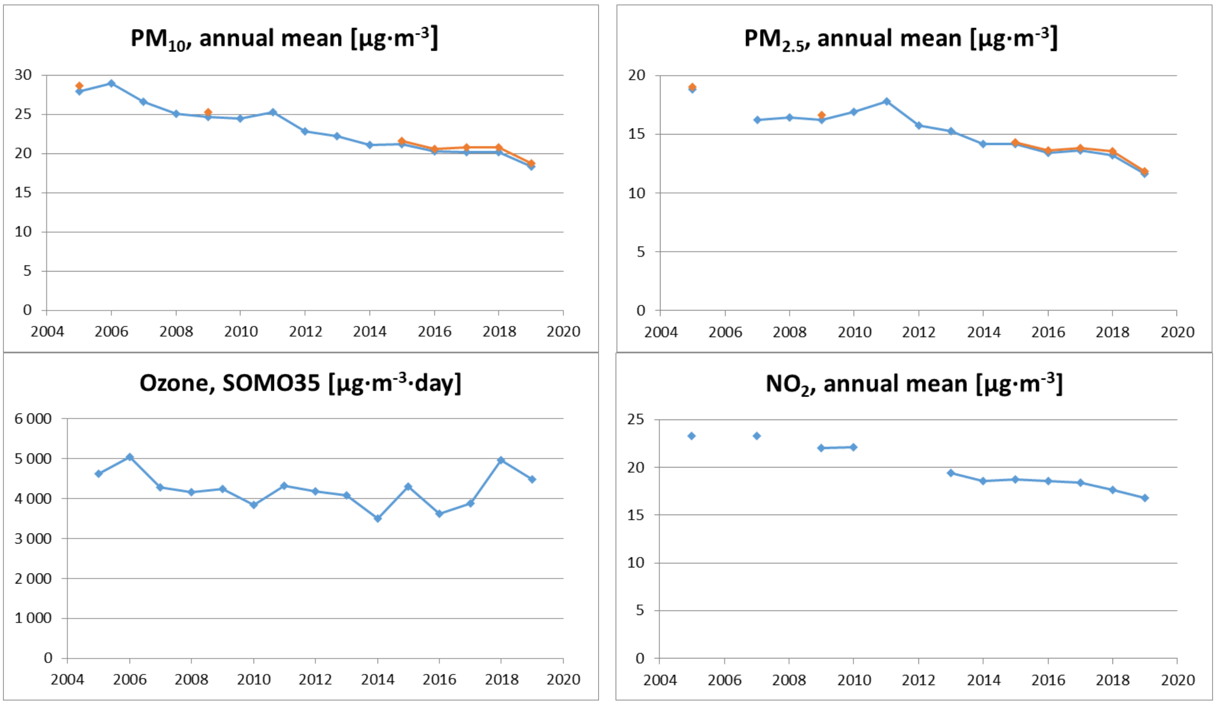

Again, the agricultural-weighted concentration is calculated for the area of all countries considered in the report, both including and excluding Turkey. For changes in agricultural-weighted concentrations (in terms of AOT40 for vegetation), excluding Turkey, see Figure ES.6. No trend is observed for the agricultural-weighted concentration over the period 2005-2019, in terms of AOT40 for vegetation.

Figure ES.6: Agricultural-weighted concentration of ozone indicator AOT40 for vegetation in 2005-2019

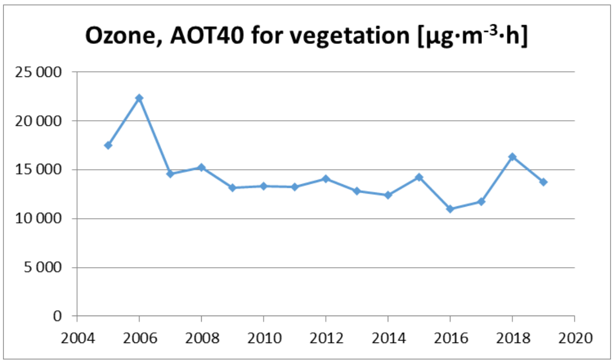

Acknowledgements

The EEA task manager was Alberto González Ortiz. The external task ETC/ATNI reviewer was Joana Soares (NILU, Norway).

The air quality monitoring data for 2019 were extracted from the AQ e-reporting database by Anna Ripoll and Jaume Targa (4sfera, Spain). The Obukhov length and the air density data for 2019 were calculated by Florian Couvidat (INERIS, France).

Thanks are due to Ignacio González Fernández (CIEMAT, Spain) from ICP Vegetation (UNECE Convention on Long-Range Transboundary Air Pollution) for providing his advice concerning the parametrisation of the phenology function for wheat in the Mediterranean (for POD_6 calculation) and for commenting the report.

1 Introduction

This report provides an update of European air quality concentration maps, population exposure and vegetation exposure estimates for 2019. It builds on the previous reports (Horálek et al., 2021, and references cited therein). The analysis is based on interpolation of annual statistics of validated monitoring data from 2019, reported by the EEA member and cooperating countries (and the voluntary reporting country of Andorra) in 2020. The paper presents mapping results and includes an uncertainty analysis of the interpolated maps, adopting the latest methodological developments, see Horálek et al. (2021) and references cited therein. The mapping area covers all of Europe apart from Belarus, Moldova, Ukraine and the European parts of Russia and Kazakhstan. Turkey (including both European and Asian areas) is included in the mapping area for all pollutants except $PM_{2.5}$, due to the lack of rural stations in Turkey for $PM_{2.5}$ in 2019 reported data to the AQ e-reporting database (EEA, 2021a).

In this report PM_{10}, $PM_{2.5}$, ozone, NO_2 and NO_x are considered for 2019, being the most relevant pollutants for annual updating due to their potential impacts on health and ecosystems. The analysis method applied is similar to that of previous years. Another potentially relevant pollutant, benzo[a]pyrene (BaP), is not presented, as the station coverage is not dense enough for enabling the regular mapping. The current status of mapping the BaP concentrations in Europe was discussed by Horálek et al. (2017a).

The mapping is primarily based on air quality measurements. It combines monitoring data, chemical transport model results and other supplementary data (such as altitude and meteorology). The method is a linear regression model followed by kriging of the residuals produced from that model ('residual kriging'). It should be noted that this methodology does not allow for formal compliance checking with the limit or target values as set by the Ambient air quality directive (EC, 2008).

The maps of health-related indicators of ozone are created for the rural and urban (including suburban) background areas separately on a grid at 10x10 km^2 resolution. Subsequently, the rural and urban background maps are merged into one final combined air quality indicator map using a 1x1 km^2 population density grid, following a weighting criterion applied per grid cell. This fine resolution takes into account the smaller settlements in Europe that are not resolved at the 10x10 km^2 grid resolution. The maps of health-related indicators of PM_{10}, $PM_{2.5}$, and NO_2 (not ozone) are constructed by the improved mapping methodology developed in Horálek et al. (2017b, 2018, 2019): together with the rural and urban background map layers, the urban traffic map layer is constructed and incorporated into the final merged map using the road data. All individual map layers are created at 1x1 km^2 resolution and land cover and road data are included in the mapping process as supplementary data.

The maps of ozone and NO_x vegetation-related indicators are constructed at a grid resolution of 2x2 km^2 and applicable for rural areas only. They are based on rural background measurements; in the case of ozone, they serve as input to the EEA's core set indicator CSI005 (EEA, 2021b).

Among the ozone vegetation-related indicators, maps of Phytotoxic Ozone Dose (POD6) indicators are also presented, following the conclusions of Colette et al. (2018). POD is the ozone flux through the stomata of leaves above a specific threshold accumulated during a specified time; it is calculated based on methodology described in CLRTAP (2017a) according to Emberson et al. (2000) based on Jarvis (1976).

Maps of the POD were presented for the first time in Horálek et al. (2021). This indicator takes into account the plant physiology, not only the ozone concentrations in the ambient air (as in the AOT40 indicators), and reflects the ozone actually absorbed by the vegetation. It is widely acknowledged that the impact of ozone on vegetation is more closely related to the ozone flux absorbed through the stomata than to the exposure to ozone in the atmosphere (Musselman and Massman, 1998; Nussbaum et al., 2003). The POD annual maps are calculated based on hourly ozone rural maps (created similarly to the annual ozone maps), hourly meteorological data and the soil hydraulic properties data. In the report, the maps of POD for representative species of crops in Europe (i.e., wheat, potato and tomato), in agreement with CLRTAP (2017a), are presented.

Next to the annual indicator maps, tables on the population exposure to PM_{10}, $PM_{2.5}$, O_3, and NO_2, and the exposure of vegetation to ozone in terms of AOT40 indicators are presented. Tables of population exposure are prepared using the population density map of 1x1 km^2 grid resolution. For PM_{10}, $PM_{2.5}$ and NO_2, the population exposure in each grid cell is calculated separately for urban areas directly influenced by traffic and for the background (both rural and urban) areas, in order to better reflect the population exposed to traffic emissions. The tables of the vegetation exposure are prepared with a 2x2 km^2 grid resolution based on the Corine Land Cover 2018 dataset (EU, 2020).

Chapters 2, 3, 4 and 5 present the concentration maps and exposure estimates for PM_{10}, $PM_{2.5}$, ozone and NO_2, respectively. Chapter 5 presents only the concentration map for NO_x; exceedances of the critical level for the protection of vegetation occur in very limited areas and, as such, it is considered not to provide relevant information from the European scale perspective. Chapter 6 summarizes the trends in exposure estimates in the period 2005-2019.

Annex 1 describes briefly the different methodological aspects. Annex 2 documents the input data applied in the 2019 mapping and exposure analysis. Annex 3 presents the technical details of the maps and their uncertainty analysis including the cross-validation results. Annex 4 shows concentration change in 2019 in comparison to the five-year average 2014-2018. Annex 5 presents the concentration maps including concentration values measured at the stations, in order to provide more complete information of the air quality in 2019 across Europe.

2 PM_{10}

The Ambient Air Quality Directive (EC, 2008) sets limit values for long-term and for short-term PM_{10} concentrations. The long-term annual PM_{10} limit value is set at 40 µg·m^{-3}. The Air Quality Guideline level recommended by the World Health Organization in 2005 (WHO, 2005) for the PM_{10} annual average is 20 µg·m^{-3}. The short-term limit value indicates that the daily average PM_{10} concentration should not exceed 50 µg·m^{-3} during more than 35 days per year. It corresponds to the 90.4 percentile of daily PM_{10} concentrations in one year. This daily limit value is the most frequently exceeded air quality PM limit value in Europe. The Air Quality Guideline level recommended by the World Health Organization in 2005 (WHO, 2005) for the short-term limit value indicates that the 99 percentile of the daily average PM_{10} concentrations should not exceed 50 µg·m^{-3} (meaning, three days of exceedance are allowed).

This chapter presents the 2019 updates of two PM_{10} indicators: the annual average and the 90.4 percentile of the daily averages. The latter is a more relevant indicator in the context of the Ambient Air Quality Directive (EC, 2008) than the formerly used 36th highest daily mean (Horálek et al., 2016b).

The maps of PM_{10} are based on the improved mapping methodology developed and tested in Horálek et al. (2019). The map layers are created for the rural, urban background and urban traffic areas separately on a grid at 1x1 km^2 resolution. Subsequently, the urban background and urban traffic map layers are merged together using the gridded GRIP road data (Meijer et al., 2018) into one urban map layer. This urban map layer is further combined with the rural map layer into the final PM_{10} map using a population density grid at 1x1 km^2 resolution. For both PM_{10} indicators, this final combined map in this 1x1 km^2 grid resolution is presented.

The population exposure tables are calculated based on these maps, according to the methodology described in Horálek et al. (2019), i.e., they are calculated separately for urban areas directly influenced by traffic and for the background (both rural and urban) areas, in order to better reflect the population exposed to traffic. For details, see Annex 1, Equation A1.6.

2.1 PM_{10} annual average

2.1.1 Concentration map

Map 2.1 presents the final combined concentration map for the 2019 PM_{10} annual average as the result of interpolation and merging of the separate map layers as described in Annex 1, Section A1.1 (for a more detailed description, see Horálek et al., 2007, 2019). Red and purple areas indicate exceedances of the limit value (LV) of 40 µg·m^{-3}.

The final combined concentration map presented in Map 2.1 is constructed on a 1x1 km^2 grid resolution (Annex 1, Section A1.1). The stations are not presented in the map, in order to better visualise the urban areas. However, concentration values from the station measurements used in the kriging interpolation methodology (Annex 3, Section A3.1) are considered to provide relevant information. In Map A5.1 of Annex 5 these point values are presented on top of Map 2.1 and illustrate the smoothing effect the interpolation methodology can have on the gridded concentration fields.

Map 2.1 shows annual LV exceedances in southern Spain near Almeria, in urban areas of southern and south-eastern Europe states (Bosnia and Herzegovina, Bulgaria, Greece, North Macedonia, and Serbia), in parts of Turkey and in southern Poland in the region around Katowice. The spatial extent of the exceedance area near Almeria has increased in 2019 compared to five-year average 2014-2018 (Map A4.1). Concerning the estimated exceedances in the Almeria area, it should be noted that they are primarily based on high concentration values indicated in this area by the chemical transport modelling, and not on measurements (which are not available in this area with the minimum data coverage required to be taken into account).

The uncertainty of the concentration map can be expressed in relative terms of the absolute Root Mean Square Error (RMSE) uncertainty related to the mean air pollution indicator value for all stations (see Annex 1, Section A1.4). This relative mean uncertainty (RRMSE) of the final combined map of PM_{10} annual average is 20 % for rural areas and 28 % for urban background areas including Turkish stations (i.e., quite similar to the last years), and respectively 18 % for rural areas and 20 % for urban background areas without Turkish stations (Annex 3, Section A3.1). The main reason for presenting the results without Turkish stations is to enable the comparison with previous years.

Be it noted that the final combined map in 1x1 km^2 resolution is representative for rural and urban background areas, but not for urban traffic areas (which are smoothed in this spatial resolution).

Map 2.1: Concentration map of PM_{10} annual average, 2019

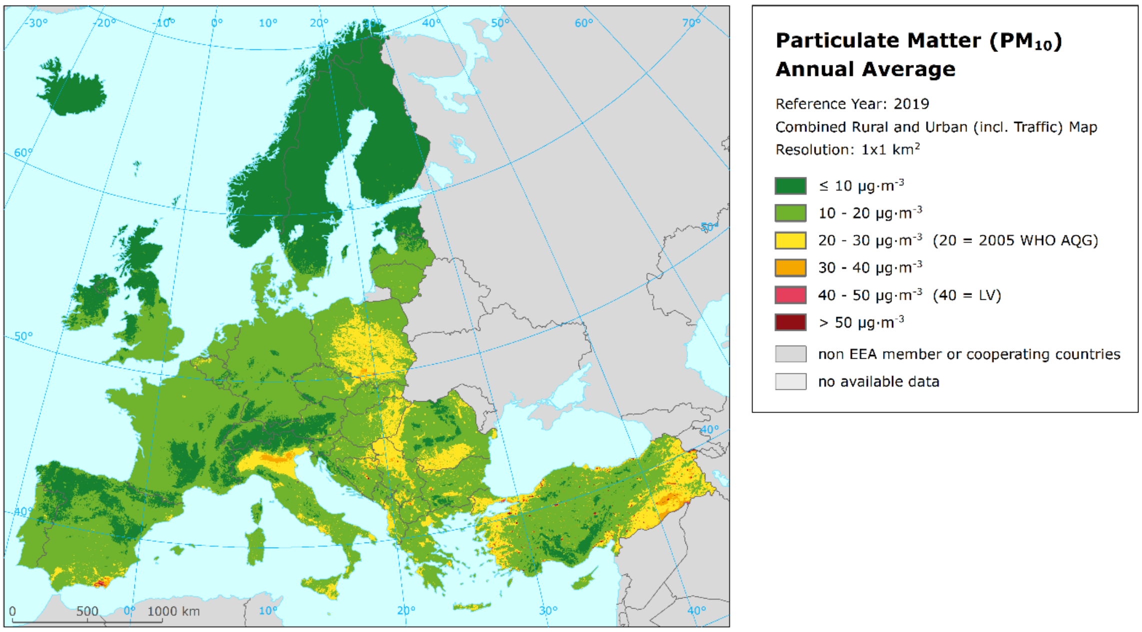

2.1.2 Population exposure

Table 2.1 and Figure 2.1 give the population frequency distribution for a limited number of exposure classes. Table 2.1 also presents the population-weighted concentration for individual countries, for EU-28 and for the total mapping area according to Equation A1.7.

About 39 % of the considered European population[2], including Turkey[3], has been exposed to annual average concentrations above the 2005 Air Quality Guideline level of 20 $\mu g \cdot m^{-3}$ recommended by the World Health Organization (WHO, 2005). The same is true for 33 % for the considered European population excluding Turkey and for 32 % of the EU-28 population.

([2]) We consider Europe apart from Belarus, Moldova, Ukraine and the European parts of Russia and Kazakhstan, due to the lack of the measurement air quality data for these countries.

([3]) The whole Turkish population, both European and Asian.

Table 2.1: Population exposure and population-weighted concentration, PM_{10} annual average, 2019

Country	ISO	Population [inhbs·1000]	PM_{10} – annual average, exposed population, 2019 [%]						PM_{10} ann. avg.
			< 10	10 - 20	20 - 30	30 - 40	40 - 50	> 50	Pop. weighted
Albania	AL	2 797	0.0	9.1	59.7	30.6	0.6		27.2
Andorra	AD	84	0.3	21.4	78.3				23.1
Austria	AT	8 381	5.7	86.1	8.3				16.1
Belgium	BE	10 944	0.0	72.6	27.4				18.5
Bosnia and Herzegovina	BA	3 802	0.0	18.4	38.4	25.4	10.8	7.0	29.8
Bulgaria	BG	7 363	0.0	13.3	56.7	24.0	5.9		27.2
Croatia	HR	4 288	0.1	39.8	57.7	2.4			21.1
Cyprus	CY	1 018		14.0	77.5	4.4	4.2		26.3
Czechia	CZ	10 423	0.1	64.3	34.9	0.7			19.3
Denmark (incl. Faroe Islands)	DK	5 577	0.2	97.5	2.3				16.2
Estonia	EE	1 291	35.0	65.0	0.0				11.1
Finland	FI	5 339	60.6	39.4	0.0				9.2
France (metropolitan)	FR	62 744	1.5	88.5	9.8	0.2			16.1
Germany	DE	80 174	0.7	97.4	1.9				15.3
Greece	GR	10 634	0.0	19.9	55.5	23.0	1.6	0.0	25.3
Hungary	HU	9 937		23.7	75.6	0.7			21.9
Iceland	IS	318	72.7	27.3					8.9
Ireland	IE	4 574	15.9	84.1	0.0				12.4
Italy	IT	59 409	0.5	24.1	65.3	10.1			23.3
Latvia	LV	2 080	1.3	65.5	32.1	1.1			17.6
Liechtenstein	LI	34	7.5	92.5					12.0
Lithuania	LT	3 028		50.5	47.9	1.6			19.4
Luxembourg	LU	511	0.0	100.0					14.9
Malta	MT	417		0.2	89.6	10.2			27.9
Monaco	MC	33			100.0				22.2
Montenegro	ME	620	0.1	18.6	57.6	23.7			24.7
Netherlands	NL	16 600		96.6	3.4				18.1
North Macedonia	MK	2 061		3.0	60.1	13.3	21.0	2.6	31.3
Norway	NO	4 906	48.7	51.3	0.0				10.0
Poland	PL	38 494	0.0	16.2	65.5	17.3	1.0		25.1
Portugal (excl. Azores, Madeira)	PT	10 047	1.6	81.6	16.7	0.0	0.0		17.3
Romania	RO	20 138	0.1	37.2	56.1	6.7			22.2
San Marino	SM	32		12.3	87.7				21.9
Serbia (incl. Kosovo*)	RS	8 896	0.0	5.7	42.3	51.0	0.3	0.7	29.3
Slovakia	SK	5 399	0.0	53.3	46.5	0.2			20.5
Slovenia	SI	2 042	0.3	65.9	33.8				18.8
Spain (excl. Canarias)	ES	44 722	1.1	59.5	36.9	1.5	0.7	0.2	19.3
Sweden	SE	9 539	43.3	56.1	0.6				10.9
Switzerland	CH	7 893	9.7	89.6	0.7				13.2
Turkey	TR	71 920	0.9	13.8	14.3	24.8	28.1	18.1	37.3
United Kingdom (& Crown dep.)	UK	63 415	2.5	95.0	2.5				15.0
Total		**601 926**	**2.9**	**57.9**	**26.0**	**7.3**	**3.7**	**2.2**	**21.0**
			60.7				**6.0**		
Total without Turkey		**530 007**	**3.1**	**63.9**	**27.6**	**4.9**	**0.4**	**0.1**	**18.7**
			67.0				**0.5**		
EU-28		**498 253**	**2.6**	**65.6**	**27.6**	**3.9**	**0.3**	**0.0**	**18.5**
			68.2				**0.3**		
Kosovo*	KS	1 748	0.0	6.2	56.4	37.4	0.0		27.7
Serbia (excl. Kosovo*)	RS	7 148	0.0	5.6	38.8	54.3	0.4	0.9	29.7

(*) under the UN Security Council Resolution 1244/99

Note: The percentage value "0.0" indicates that an exposed population exists, but it is small and estimated to be less than 0.05 %. Empty cells mean no population in exposure.

Approximately 6 % of population of the considered European area (including Turkey) has been exposed to concentrations exceeding the EU annual limit value (ALV) of 40 μg·m^{-3}; the same is the case for 0.5 % for the considered European population excluding Turkey and for less than 0.5 % of the EU-28 population. More than 45 % of the population has been exposed to concentrations above the ALV in Turkey, almost 24 % and 18 % of the population has been exposed to concentrations above the ALV in North Macedonia and Bosnia and Herzegovina, respectively. A limited fraction of the population (< 0.05-6 %) has been exposed to concentrations above the ALV in Albania, Bulgaria, Cyprus, Greece, Poland, Portugal, Serbia and Spain. However, as the current mapping methodology tends to underestimate high values (see Annex 3, Section A3.1), the exceedance percentage will most likely be underestimated. Additional population exposure above the ALV could therefore be expected in countries like Albania, Bosnia and Herzegovina, Bulgaria, Greece, Montenegro, Serbia and Turkey where a relatively large fraction (ca 20-50 %) of the population lives in areas with concentration levels above 30 μg·m^{-3}.

The population-weighted concentration of the annual average for 2019 for the considered European population is estimated to be about 21 μg·m^{-3} including Turkey and about 19 μg·m^{-3} both for the considered European population without Turkey and for EU-28 only. The value for EU-28 and considered European population without Turkey decreased by about 2 μg·m^{-3} compared to the previous five-year mean (for more details, see Annex 4, Section A4.1).

Figure 2.1: Percentage of the population (%) exposed of PM_{10} annual average (μg·m^{-3}), 2019

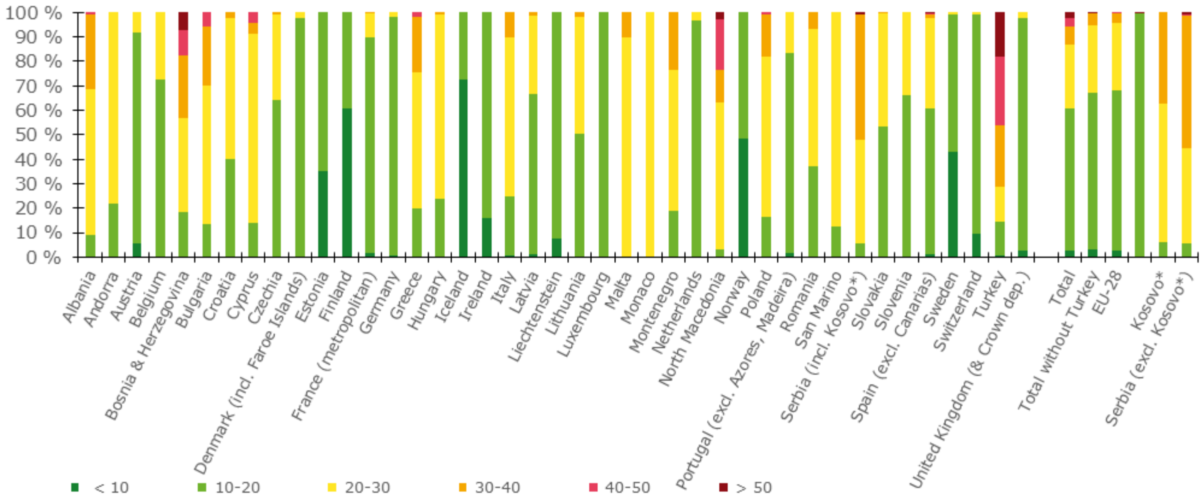

(*) under the UN Security Council Resolution 1244/99.

Figure 2.2 shows, for the whole mapped area (that is, all considered Europe including Turkey), the population frequency distribution for exposure classes of 1 μg·m^{-3}. One can see the highest population frequency for classes between 15 and 19 μg·m^{-3}. A quite continuous decline of population frequency is visible for classes between 20 and 35 μg·m^{-3} and beyond 40 μg·m^{-3}.

Figure 2.2: Population frequency distribution, PM_{10} annual average, 2019. The 2005 WHO AQG level (20 μg·m^{-3}) is marked by the green line, the EU annual limit value (40 μg·m^{-3}) is marked by the red line

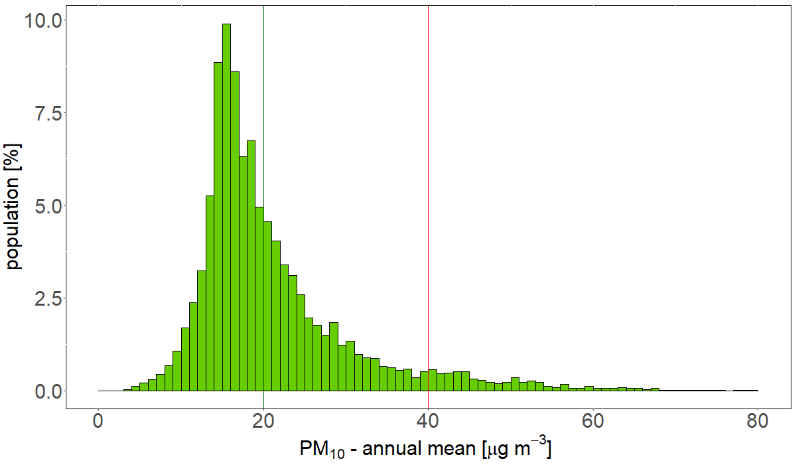

Note: Apart from the population distribution shown in graph, it was estimated that 0.03 % of population lived in areas with PM_{10} annual average concentration in between 80 and 175 μg·m^{-3}.

2.2 PM_{10} – 90.4 percentile of daily means

The Air Quality Directive (EC, 2008) describes the PM_{10} daily limit value (DLV) as "a daily average of 50 μg·m^{-3} not to be exceeded more than 35 times a calendar year". This requirement can be evaluated by the indicator 36th highest daily mean, which is in principle equivalent to the indicator 90.4 percentile of daily mean. However, for measurement data these two indicators are equivalent only if no data is missing, which is in general not the case. As shown in de Leeuw (2012), the additional uncertainty related to incomplete time series is substantially smaller when using percentile values instead of the x-th highest value. Furthermore, the Air Quality Directive requires the use of the 90.4 percentile when random measurements are used to assess the requirements of the PM_{10} DLV. As in the previous reports since the maps for 2014, the PM_{10} daily means are expressed as the 90.4 percentile instead of the formerly used 36th highest daily mean.

2.2.1 Concentration map

Map 2.2 presents the final combined map, where red and purple marked areas indicate values of the 90.4 percentile of daily means above 50 μg·m^{-3} (i.e., exceedances of the DLV of 50 μg·m^{-3} on more than 35 measurement days). The similar mapping procedure as in the case of the annual average is used. The mapping details and the uncertainty analysis are presented in Annex 3. Large areas above the DLV are observed in northern Italy (i.e., the Po Valley), in the region with the agglomerations Ostrava (Czechia) – Katowice (Poland) – Krakow (Poland) and in eastern parts of Turkey. Urban areas with concentrations above the DLV are observed in Albania, Andorra, Bosnia and Herzegovina, Bulgaria, Croatia, Cyprus, Czechia, France, Greece, Hungary, Italy, Malta, Montenegro, North Macedonia, Poland, Portugal, Romania, Serbia, Slovakia, Slovenia, Spain and Turkey.
In general, the central and the south-eastern parts of Europe appear with higher concentrations than the western and the northern parts. Similarly to the PM_{10} annual averages, the estimated exceedances in the Almeria area are based on the chemical transport modelling, not on measurements.

Map 2.2: Concentration map of PM_{10} indicator 90.4 percentile of daily means, 2019

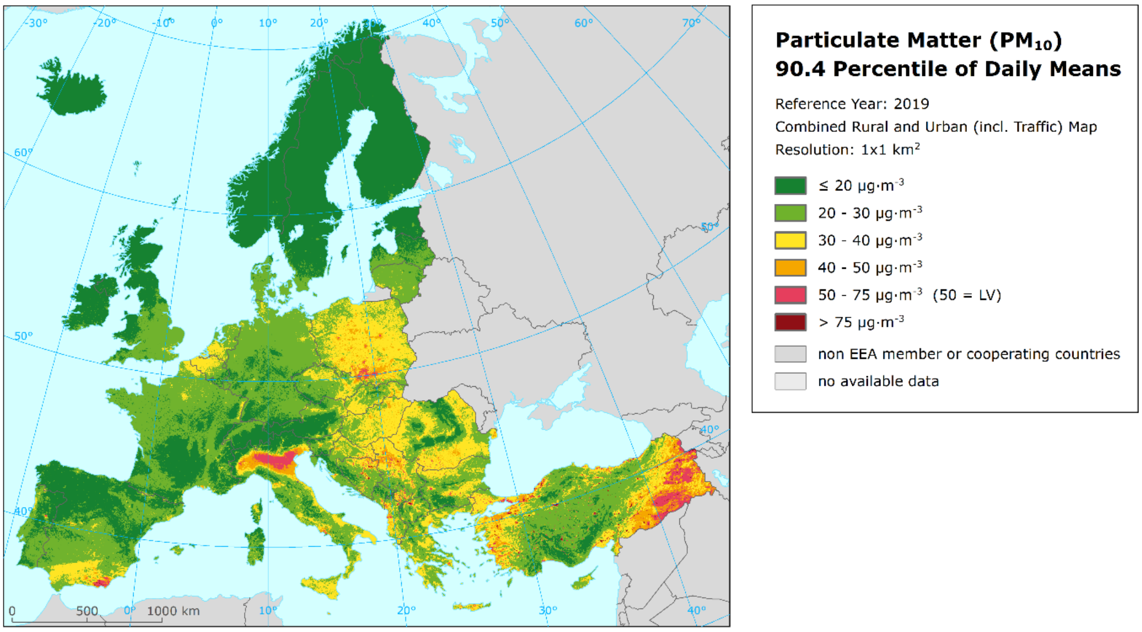

The relative mean uncertainty (relative RMSE) of the final combined map of the 90.4 percentile of PM_{10} daily means is 23 % for rural areas and 32 % for urban background areas including Turkish stations. The mean uncertainty for the map without Turkey is 20 % for rural areas and 21 % for urban background areas (Annex 3, Section A3.1).

For the comparison with five-year average 2014-2018 values, see Annex 4, Section A4.1. The final combined map including the indicator 90.4 percentile of daily means based on the actual measurement data at stations is presented in Map A5.2 of Annex 5.

2.2.2 Population exposure

Table 2.2 and Figure 2.3 give the population frequency distribution for a limited number of exposure classes calculated at 1x1 km^2 grid resolution. Table 2.2 also presents the population-weighted concentration for individual countries, for EU-28 and for the total mapping area.

In 2019 about 16 % of the considered European population including Turkey, 8 % of the considered European population excluding Turkey and 6 % of the EU-28 population are estimated to live in areas where the 90.4 percentile of the PM_{10} daily means exceeded the EU limit value of 50 µg·m^{-3}. In Albania, Bosnia and Herzegovina, Kosovo, Montenegro, North Macedonia, Serbia (both including and excluding Kosovo) and Turkey, more than half of the population (ca >50-74 %) was exposed to concentrations exceeding the DLV. In Bulgaria, Greece, Italy, Malta and Poland the portion of the population living in areas with concentrations above the DLV was between 10 % and 50 %. Less than 10 % (ca. <0.05-8 %) of the population living in areas with concentrations above the DLV was estimated in Andorra, Croatia, Cyprus, Czechia, France, Hungary, Portugal, Romania, Slovakia, Slovenia and Spain.

The European-wide population-weighted concentration of the 90.4 percentile of PM_{10} daily means is estimated for 2019 at about 37 µg·m^{-3} for the total mapped area (including Turkey), 33 µg·m^{-3} (without Turkey), and 32 µg·m^{-3} for the EU-28. The value for both EU-28 and the considered European population without Turkey decreased by about 4 µg·m^{-3} compared to the previous five-year mean (for more details, see Annex 4, Section A4.1).

Table 2.2: Population exposure and population-weighted concentrations, PM_{10} indicator 90.4 percentile of daily means, 2019

Country	ISO	Population [inhbs·1000]	PM_{10} - perc90.4, exposed population, 2019 [%]						PM_{10} - perc90.4
			< 20	20 – 30	30 - 40	40 - 50	50 - 75	> 75	Pop. Weighted
Albania	AL	2 797	0.0	3.3	14.3	31.9	49.3	1.2	50.4
Andorra	AD	84	0.3	9.6	13.4	76.3	0.3		44.1
Austria	AT	8 381	11.2	44.5	41.7	2.7			28.3
Belgium	BE	10 944	0.2	14.4	85.3	0.1			33.1
Bosnia and Herzegovina	BA	3 802	0.1	6.9	13.9	16.0	42.0	21.2	59.6
Bulgaria	BG	7 363	0.2	5.8	22.3	35.7	36.0		46.8
Croatia	HR	4 288	0.4	15.4	31.7	44.5	8.1	0.0	39.8
Cyprus	CY	1 018	0.0	7.2	15.1	69.3	8.5		42.6
Czechia	CZ	10 423	0.3	23.8	60.0	13.1	2.9		34.4
Denmark (incl. Faroe Islands)	DK	5 577	0.7	90.8	8.6				28.0
Estonia	EE	1 291	54.8	40.3	4.9				20.4
Finland	FI	5 339	75.5	22.6	1.9	0.0			17.2
France (metropolitan)	FR	62 744	4.8	59.8	32.9	2.4	0.0		27.8
Germany	DE	80 174	2.0	83.1	14.8	0.1			26.9
Greece	GR	10 634	0.0	5.4	45.1	35.3	14.1	0.1	41.3
Hungary	HU	9 937	0.0	4.2	50.7	42.5	2.5		38.6
Iceland	IS	318	78.6	16.6	4.8				17.9
Ireland	IE	4 574	31.9	66.6	1.5				22.1
Italy	IT	59 409	0.8	10.9	44.2	20.4	23.7		40.9
Latvia	LV	2 080	4.4	47.1	45.9	2.6			30.2
Liechtenstein	LI	34	11.0	89.0					21.9
Lithuania	LT	3 028	0.0	33.1	61.0	6.0			32.9
Luxembourg	LU	511	0.4	91.1	8.5				26.3
Malta	MT	417		0.0	9.5	80.2	10.2		42.2
Monaco	MC	33			100.0				34.3
Montenegro	ME	620	0.7	11.9	9.3	7.4	70.7		50.2
Netherlands	NL	16 600		36.6	63.4				30.4
North Macedonia	MK	2 061	0.0	1.2	5.4	36.4	32.3	24.7	60.1
Norway	NO	4 906	50.7	46.1	3.2				19.1
Poland	PL	38 494	0.0	1.8	36.1	36.9	24.3	0.9	45.0
Portugal (excl. Azores, Madeira)	PT	10 047	5.8	58.0	35.6	0.5	0.2	0.0	28.3
Romania	RO	20 138	0.2	15.8	45.7	31.6	6.8		38.2
San Marino	SM	32		2.4	84.6	12.9			38.9
Serbia (incl. Kosovo*)	RS	8 896	0.0	3.0	8.9	17.4	69.4	1.2	55.9
Slovakia	SK	5 399	0.0	4.8	64.7	30.0	0.5		37.5
Slovenia	SI	2 042	0.9	31.6	49.1	18.4	0.1		33.6
Spain (excl. Canarias)	ES	44 722	3.0	43.0	48.4	3.6	1.8	0.2	30.9
Sweden	SE	9 539	48.5	47.8	3.2	0.5			20.8
Switzerland	CH	7 893	13.1	77.8	9.0	0.0			24.5
Turkey	TR	71 920	1.0	8.9	8.2	8.0	42.1	31.8	64.7
United Kingdom (& Crown dep.)	UK	63 415	3.9	84.2	11.8				26.5
Total		**601 926**	**4.3**	**40.3**	**29.0**	**10.5**	**11.9**	**4.1**	**36.6**
			44.6				**16.0**		
Total without Turkey		**530 007**	**4.8**	**44.5**	**31.8**	**10.8**	**7.8**	**0.4**	**32.8**
			49.3				**8.1**		
EU-28		**498 253**	**4.3**	**45.5**	**33.2**	**10.7**	**6.2**	**0.1**	**32.2**
			49.8				**6.3**		
Kosovo*	KS	1 748	0.0	3.4	9.4	12.4	74.7		56.5
Serbia (excl. Kosovo*)	RS	7 148	0.0	2.9	8.8	18.6	68.1	1.5	55.8

(*) under the UN Security Council Resolution 1244/99

Note: The percentage value "0.0" indicates that an exposed population exists, but it is small and estimated to be less than 0.05 %. Empty cells mean no population in exposure.

As in previous years, the daily limit value was more widely exceeded than the annual limit value in 2019.

Figure 2.3: Percentage of the population (%) exposed of PM_{10} indicator 90.4 percentile of daily means, 2019

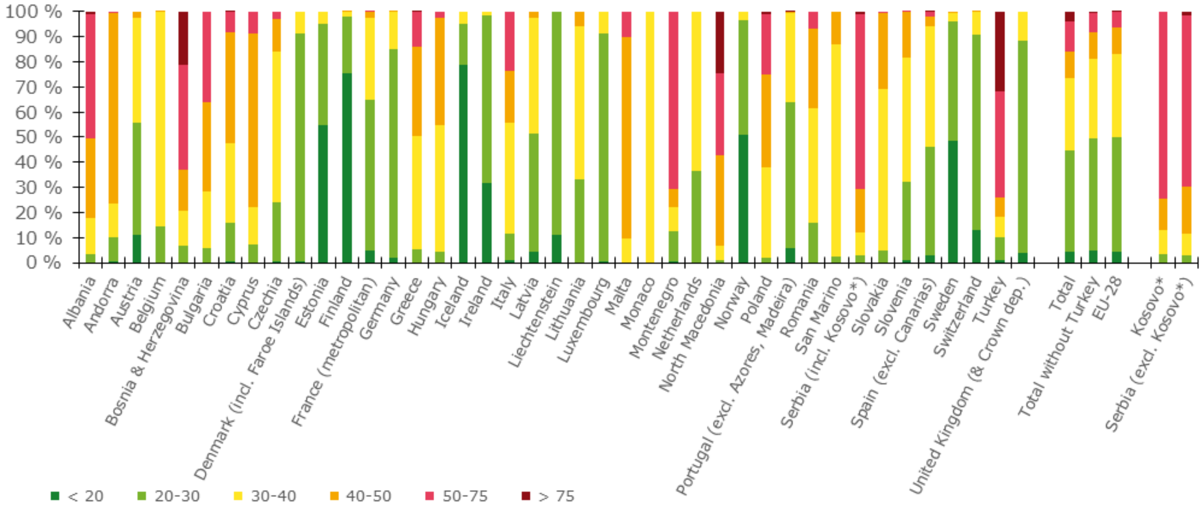

(*) under the UN Security Council Resolution 1244/99.

Figure 2.4 shows, for the whole mapped area, the population frequency distribution for exposure classes of 2 µg·m^{-3}. One can see the highest population frequency for classes between 24 and 32 µg·m^{-3}, continuous decline of population frequency for classes between 22 and 34 µg·m^{-3} and continuous mild decline of population frequency for classes between 36 and 70 µg·m^{-3}.

Figure 2.4: Population frequency distribution, PM_{10} indicator 90.4 percentile of daily means, 2019. The EU daily limit value (50 µg·m^{-3}) is marked by the red line

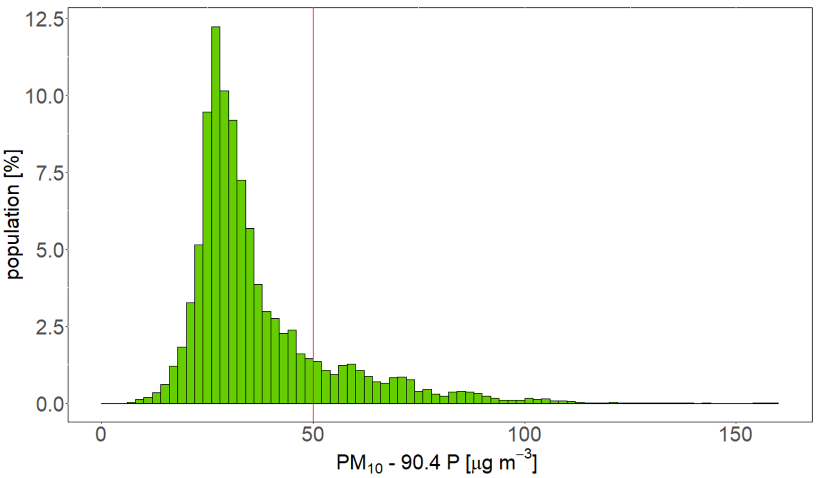

Note: Apart from the population distribution shown in graph, it was estimated that 0.014 % of population lived in areas with values of PM_{10} indicator 90.4 percentile of daily means in between 160 and 250 µg·m^{-3}.

Figure 2.5 shows for individual countries the PM_{10} daily concentrations to which the population per country was exposed in 2019. It can be seen that the countries with the highest values of PM_{10} indicator 90.4 percentile of daily means are located in the central and south-eastern parts of Europe.

Figure 2.5: PM_{10} expressed as indicator 90.4 percentile of daily means to which the population per country was exposed in 2019. The EU daily limit value (50 µg·m^{-3}) is marked by the red line

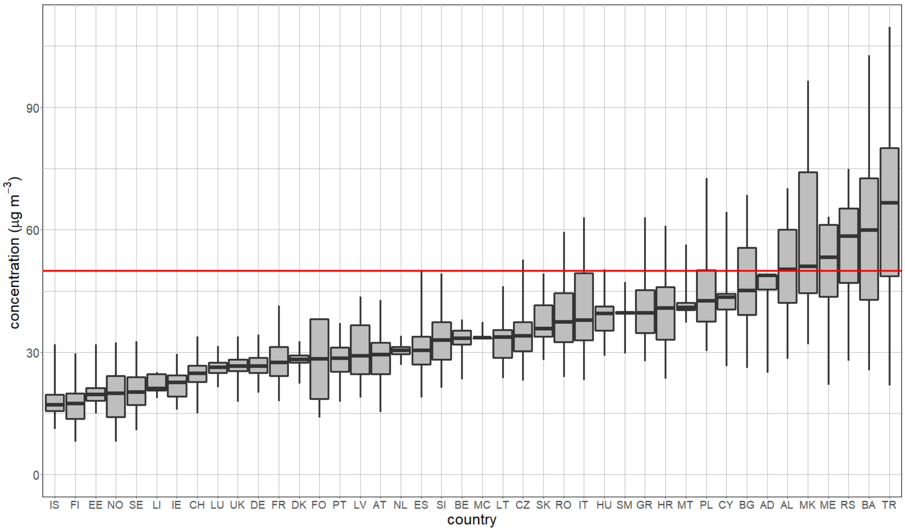

Note: For each country, the box plot shows the concentration to which a percentage of the population was exposed: 50 % in the case of the black marker, 25 % and 75 % in the cases of the box's edges, 2 % and 98 % in the cases of the whiskers' edges.

3 $PM_{2.5}$

In the Ambient Air Quality Directive (EC, 2008), the limit value (LV) for the annual average $PM_{2.5}$ concentrations was set at 25 µg·m^{-3}. In the Air Quality Directive there is also an indicative limit value (ILV) of 20 µg·m^{-3} defined as Stage 2, in place since 2020. The Air Quality Guideline level recommended by the World Health Organization in 2005 (WHO, 2005) for the $PM_{2.5}$ annual average is 10 µg·m^{-3}.

The current number of $PM_{2.5}$ measurement stations is still somewhat limited and its spatial distribution is irregular over Europe. Therefore, in this paper the mapping of the health-related indicator $PM_{2.5}$ annual average is based on a mapping methodology developed in Denby et al. (2011a, 2011b). This methodology derives additional pseudo $PM_{2.5}$ annual mean concentrations from PM_{10} annual mean measurement concentrations. As such, it increases the number and spatial coverage of $PM_{2.5}$ 'data points' and these data are used to derive a European wide map of annual mean $PM_{2.5}$. Pseudo $PM_{2.5}$ stations data are estimated using PM_{10} measurement data, surface solar radiation, latitude and longitude.

Like for PM_{10}, the map of $PM_{2.5}$ is based on the improved mapping methodology developed in Horálek et al. (2019). The map layers are created for the rural, urban background and urban traffic areas separately on a grid at 1x1 km^2 resolution. Subsequently, the urban background and urban traffic map layers are merged together using the gridded road data into one urban map layer. This urban map layer is further combined with the rural map layer into the final $PM_{2.5}$ map using a population density grid at 1x1 km^2 resolution. This final combined map is presented at this 1x1 km^2 grid resolution.

Annex 3, Section A3.2 provides details on the regression and kriging parameters applied for deriving the $PM_{2.5}$ annual average map, as well as the uncertainty analysis of the map. Annex 4, Section A4.3 discusses briefly the concentration and population exposure change in 2019 in comparison to the five-year average 2014-2018.

3.1 $PM_{2.5}$ annual average

3.1.1 Concentration map

Map 3.1 presents the final combined map for the 2019 $PM_{2.5}$ annual average as a result of the interpolation and merging of the separate rural and urban map layers as described in Annex 1, Section A1.1. The dark red areas show exceedances of the ALV of 25 µg·m^{-3}. Red areas show exceedances of the indicative LV of 20 µg·m^{-3} defined as Stage 2 (ILV_{2020}).

Due to the lack of rural $PM_{2.5}$ stations in Turkey, no proper interpolation results could be estimated for this country in a rural map. Therefore, the estimated $PM_{2.5}$ values for Turkey are not presented in the final map.

According to Map 3.1, the areas with the highest $PM_{2.5}$ concentrations appear to be the Po Valley in northern Italy, the areas around the Balkan cities of Belgrade, Podgorica, Sarajevo, Sofia, Skopje and Tirana, the Krakow – Katowice (Poland) – Ostrava (Czechia) industrial region and the area around Warsaw. Different other cities in Bosnia and Herzegovina, Bulgaria, Greece, North Macedonia, Poland and Serbia including Kosovo also show elevated $PM_{2.5}$ annual average concentrations, as well as some areas near Almeria in southern Spain (estimated based on the chemical transport modelling, not on measurements). Like in the case of PM_{10}, the central and the south-eastern parts of Europe show higher concentrations than the western and the northern parts.

The relative mean uncertainty of the 2019 map of $PM_{2.5}$ annual average is 20.5 % for both rural and urban background areas and determined exclusively on the actual $PM_{2.5}$ measurement data points, i.e., not on the pseudo stations (Annex 3, Section A3.2).

Map 3.1: Concentration map of $PM_{2.5}$ annual average, 2019

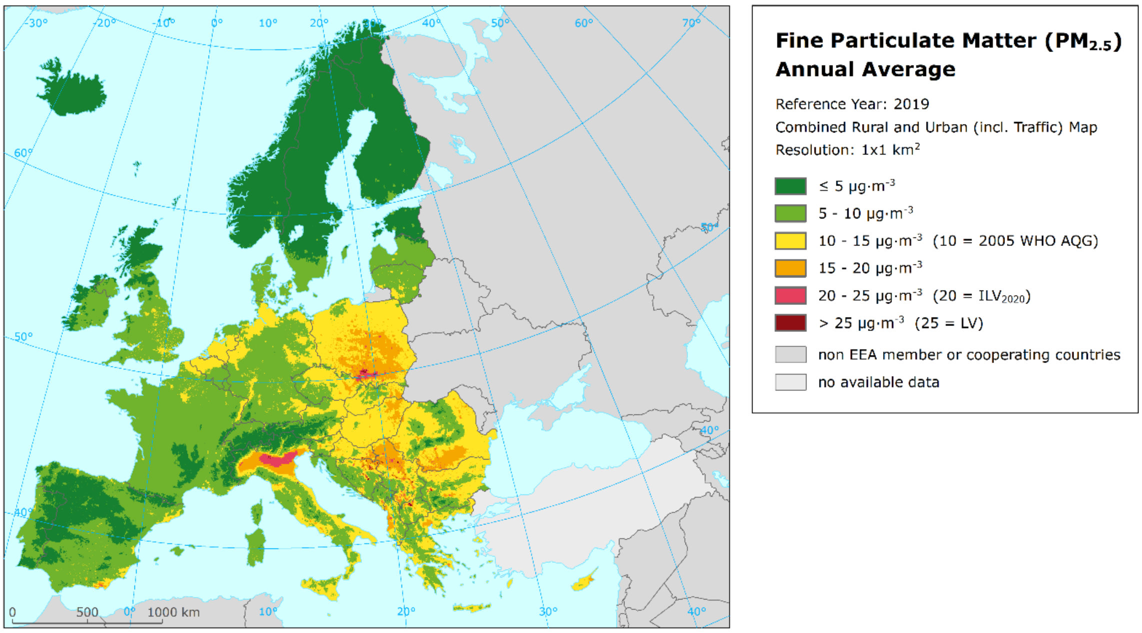

Similarly to the PM_{10}, the final map in 1x1 km^2 resolution is representative for the rural and the urban background areas, but not for the urban traffic areas (which are smoothed in the 1x1 km^2 resolution).

In order to provide more complete information of the air quality across Europe, the final combined map including the measurement data at stations is presented in Map A5.3 of Annex 5.

For the comparison with five-year average 2014-2018 values, see Annex 4, Section A4.2.

3.1.2 Population exposure

Table 3.1 and Figure 3.1 give the population frequency distribution for a limited number of exposure classes calculated on a grid of 1x1 km^2 resolution. Table 3.1 also presents the population-weighted concentration for individual countries, for EU-28 and for the total mapping area.

The population exposure has been calculated according to Equation A1.6 of Annex 1, i.e., it has been calculated separately for urban areas directly influenced by traffic and for the background (both rural and urban) areas, in order to better reflect the population exposed to traffic.

In 2019, 64 % of considered European (excluding Turkey) and 65 % of the EU-28 population has been exposed to $PM_{2.5}$ annual mean concentrations above the 2005 Air Quality Guideline level of 10 µg·m^{-3} as defined by the World Health Organization (WHO, 2005). Since $PM_{2.5}$ is one of the most relevant pollutants linked to health problems and premature mortality (EEA, 2019) it should be mentioned that more than half of the population has been exposed to $PM_{2.5}$ annual mean concentrations above the 2005 WHO AQG level in more than two thirds of countries. The only countries, where the $PM_{2.5}$ annual mean concentrations did not exceed the 2005 WHO AQG level, were Finland, Iceland, Liechtenstein, and Norway.

Table 3.1: Population exposure and population-weighted concentration, $PM_{2.5}$ annual average 2019

Country	ISO	Population [inhbs·1000]	$PM_{2.5}$ – annual average, exposed population, 2019 [%]						$PM_{2.5}$ ann. avg.
			< 5	5 - 10	10 - 15	15 - 20	20 - 25	> 25	Pop. weighted
Albania	AL	2 797	0.0	2.8	25.4	42.7	26.3	2.8	17.5
Andorra	AD	84	0.5	22.3	77.2				10.8
Austria	AT	8 381	1.6	24.7	68.8	4.9			11.3
Belgium	BE	10 944		20.5	79.5				11.0
Bosnia and Herzegovina	BA	3 802	0.0	5.7	18.9	21.3	18.1	36.0	21.6
Bulgaria	BG	7 363	0.0	2.8	20.3	46.4	23.2	7.3	18.0
Croatia	HR	4 288	0.0	9.2	47.2	35.4	6.4	1.8	14.6
Cyprus	CY	1 018		0.1	68.6	23.3	8.0		14.7
Czechia	CZ	10 423	0.0	7.0	67.6	21.3	4.1		13.8
Denmark (incl. Faroe Islands)	DK	5 577	0.8	71.4	27.8				9.4
Estonia	EE	1 291	37.9	61.7	0.5				5.5
Finland	FI	5 339	48.8	51.2					5.0
France (metropolitan)	FR	62 744	0.7	59.5	39.0	0.8			9.5
Germany	DE	80 174	0.1	43.8	56.1	0.0			10.1
Greece	GR	10 634		2.3	43.7	43.0	11.0		15.7
Hungary	HU	9 937		0.1	68.0	32.0			14.5
Iceland	IS	318	77.1	22.9					3.9
Ireland	IE	4 574	7.7	87.1	5.2				7.7
Italy	IT	59 409	0.3	8.7	56.0	22.6	11.9	0.5	14.5
Latvia	LV	2 080	1.0	55.8	41.8	1.5			10.1
Liechtenstein	LI	34	0.4	99.6					8.1
Lithuania	LT	3 028		22.6	66.2	11.2			12.1
Luxembourg	LU	511		91.2	8.8				8.1
Malta	MT	417			90.5	9.5			12.2
Monaco	MC	33			100.0				12.9
Montenegro	ME	620	0.1	10.3	12.0	31.2	46.5		18.4
Netherlands	NL	16 600		16.9	83.1				10.7
North Macedonia	MK	2 061	0.0	0.7	15.8	41.7	16.7	25.0	20.6
Norway	NO	4 906	39.7	60.3					5.4
Poland	PL	38 494		0.4	25.0	51.5	16.9	6.2	17.6
Portugal (excl. Azores, Madeira)	PT	10 047	5.7	79.8	14.4				8.3
Romania	RO	20 138	0.0	5.7	45.1	43.4	5.7	0.2	15.1
San Marino	SM	32		0.8	99.2				13.0
Serbia (incl. Kosovo*)	RS	8 896	0.0	1.4	7.3	28.1	49.0	14.2	20.6
Slovakia	SK	5 399	0.0	1.2	63.0	35.6	0.2		14.5
Slovenia	SI	2 042	0.0	15.2	62.9	20.3	1.6		13.1
Spain (excl. Canarias)	ES	44 722	2.1	49.8	43.0	4.9	0.2	0.0	10.2
Sweden	SE	9 539	47.1	52.9	0.0				5.4
Switzerland	CH	7 893	2.9	84.7	12.3	0.0			8.7
United Kingdom (& Crown dep.)	UK	63 415	0.9	47.6	51.5				9.7
Total (no Turkey) ([a])		**530 007**	**2.5**	**33.5**	**45.1**	**12.9**	**4.7**	**1.2**	**11.8**
			36.0				**5.9**		
EU-28		**498 253**	**2.2**	**32.7**	**48.1**	**12.6**	**3.7**	**0.7**	**11.7**
			34.9				**4.4**		
Kosovo*	KS	1 748	0.0	1.1	10.5	28.3	57.5	2.6	20.1
Serbia (excl. Kosovo*)	RS	7 148		1.5	6.5	28.1	46.9	17.0	20.8

(*) under the UN Security Council Resolution 1244/99.
([a]) Turkey not included due to the lack of the rural stations.

Note: The percentage value "0.0" indicates that an exposed population exists, but it is small and estimated to be less than 0.05 %. Empty cells mean no population in exposure.

The total considered and EU-28 population exposure exceeding the EU limit value (LV) of 25 $\mu g{\cdot}m^{-3}$ has been 1 % and <1 %, respectively. In Bosnia and Herzegovina, North Macedonia and Serbia (both including and excluding Kosovo), more than 10 % of the population (ca. 14-36 %) suffers from exposures above this limit value; in Albania, Bulgaria, Croatia, Italy, Kosovo, Poland, Romania and Spain it has been between <0.05 and 7 %. The Stage 2 indicative limit value (ILV_{2020}) of 20 µg·m^{-3} has been exceeded in areas with 6 % of the considered European population and with 4 % of the EU-28 population. In Bosnia and Herzegovina and Serbia including Kosovo, a half or more of the population has been exposed to concentrations above the ILV_{2020}. In Albania, Bulgaria, Greece, Italy, Montenegro, North Macedonia and Poland it has been between 11 and 47 %.

As the current mapping methodology tends to underestimate high values (Annex 3, Section A3.2), the exceedance percentages and/or the number of countries with population exposed to concentrations above both the current ALV and the indicative ILV_{2020} will most likely be higher.

The population-weighted concentration of the $PM_{2.5}$ annual means has been estimated for 2019 at about 12 µg·m^{-3} for both total mapped area and for the EU-28, which means a decrease about 2 µg·m^{-3} compared to five-year mean for both characteristics (Annex 4, Section A4.2).

Figure 3.1: Percentage of the population (%) exposed of $PM_{2.5}$ annual average (µg·m^{-3}), 2019

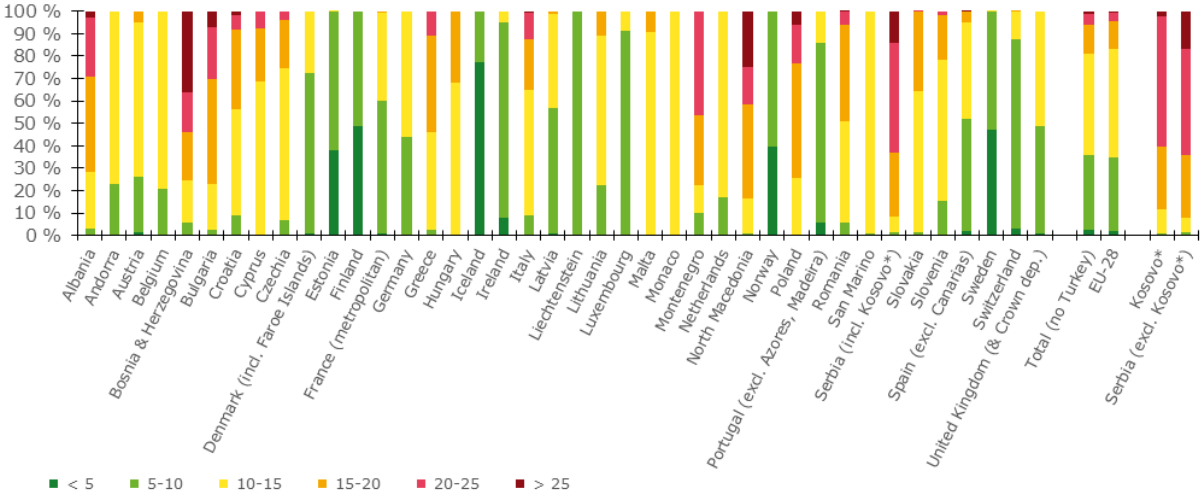

(*) under the UN Security Council Resolution 1244/99.

Figure 3.2 shows, for the whole mapped area, the population frequency distribution for exposure classes of 1 µg·m^{-3}. The highest population frequency is found for classes between 8 and 12 µg·m^{-3}.

Figure 3.2: Population frequency distribution, $PM_{2.5}$ annual average, 2019. The EU annual limit value (25 µg·m^{-3}) is marked by the red line, the 2005 WHO AQG level (10 µg·m^{-3}) is marked by the green line.

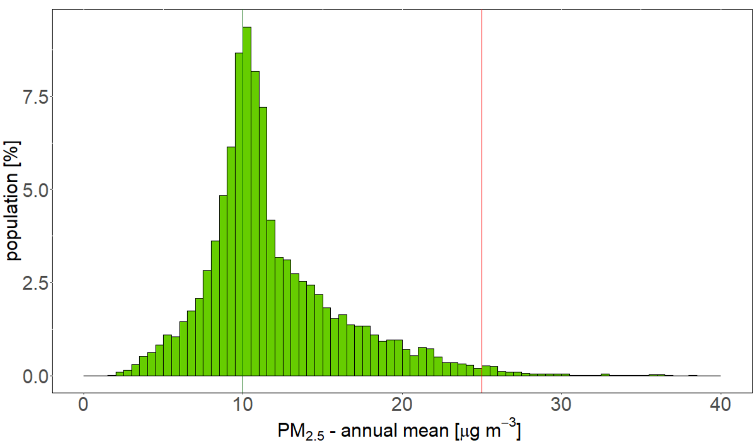

4 Ozone

For ozone, three health-related indicators, i.e., 93.2 percentile of maximum daily 8-hour means (see below), SOMO35 and SOMO10, and five vegetation-related indicators, i.e., AOT40 for vegetation, AOT40 for forests, POD_6 for wheat, potato and tomato are considered. For the definition of the SOMO35, SOMO10 and AOT40 and POD indicators, see following sections and Annex 2.

The separate rural and urban background health-related indicator fields are calculated at a resolution of 10x10 km^2. Subsequently, the final health-related indicator maps are created by combining rural and urban areas based on the 1x1 km^2 gridded population density map. These maps are presented on this 1x1 km^2 grid resolution. The population exposure tables are calculated on the basis of these health-related indicator maps.

The vegetation-related indicator maps are calculated from observations at rural background stations and are representative for rural areas only (assuming urban areas do not cover vegetation). The maps have a resolution of 2x2 km^2. This resolution serves the needs of the EEA Core Set Indicator 005 (EEA, 2021b) on ecosystem exposure to ozone.

Annex 3, Section A3.3 provides details on the regression and kriging parameters applied for deriving the maps of the ozone indicators, as well as the uncertainty analysis of the maps. Annex 4, Section A4.3 discusses briefly the inter-annual changes observed in the concentration maps and the relevant population and vegetation exposure.

4.1 Ozone – 93.2 percentile of maximum daily 8-hour means

The Air Quality Directive (EC, 2008) describes the ozone target value (TV) for the protection of human health as “a maximum daily 8-hour mean of 120 $\mu g \cdot m^{-3}$ not to be exceeded on more than 25 times a calendar year, averaged over three years”. On an annual basis, it can be evaluated by the indicator 26^{th} highest maximum daily 8-hour mean, which is in principle equivalent to the indicator 93.2 percentile of maximum daily 8-hour means. However, for measurement data these two indicators are equivalent only if no data is missing, which is in general not the case. As shown in de Leeuw (2012), the additional uncertainty related to incomplete time series is substantially smaller when using percentile values instead of the x-th highest value. As in the previous reports since 2014 maps, this ozone indicator is expressed as the 93.2 percentile of maximum daily 8-hour means instead of the formerly used 26^{th} highest maximum daily 8-hour mean.

4.1.1 Concentration map

Map 4.1 presents the final combined map for 93.2 percentile of maximum daily 8-hour means as a result of combining the separate rural and urban interpolated maps following the procedures as described in Annex 1, Section A1.1 (for a more detailed description, see Horálek et al., 2007, 2010). The supplementary data used are EMEP model output, altitude and surface solar radiation for rural areas and EMEP model output, wind speed and surface solar radiation for urban areas (Annex 3).

In the final combined map the red and dark red areas show values of the 93.2 percentile of maximum daily 8-hour means above 120 $\mu g \cdot m^{-3}$ in 2019, i.e., above the TV threshold of 120 $\mu g \cdot m^{-3}$ on more than 25 days in 2019. Note that in the Air Quality Directive (EC, 2008) the TV is actually defined as 120 $\mu g \cdot m^{-3}$ not to be exceeded on more than 25 days per calendar year averaged over three years. Here only 2019 data are presented, and no three-year average has been calculated.

The map shows that in 2019 percentile values above 120 $\mu g \cdot m^{-3}$ occur in a large area of Europe, namely in most of Austria, Germany, Italy, Switzerland and Turkey and in parts of Bosnia and Herzegovina, Czechia, France, Greece, Slovenia, Spain and North Macedonia. In general, the southern parts of

Europe show higher ozone concentrations than the northern parts, which is caused mainly by higher solar radiation and temperature in these areas. Nevertheless, concentrations above the TV can occur even in northern Europe during warm year as it was presented for 2018 (Horálek et al., 2021). For the comparison with five-year average 2014-2018 values, see Annex 4, Section A4.3.

The relative mean uncertainty of the 2019 map of the 93.2 percentile of maximum daily 8-h ozone means is about 8 % for rural and 10 % for urban areas (Annex 3, Section A3.3).

In order to provide more complete information of the air quality across Europe, the final combined map including the measurement data at stations is presented in Map A5.4 of Annex 5.

Map 4.1: Concentration map of ozone indicator 93.2 percentile of maximum daily 8-hour means, 2019

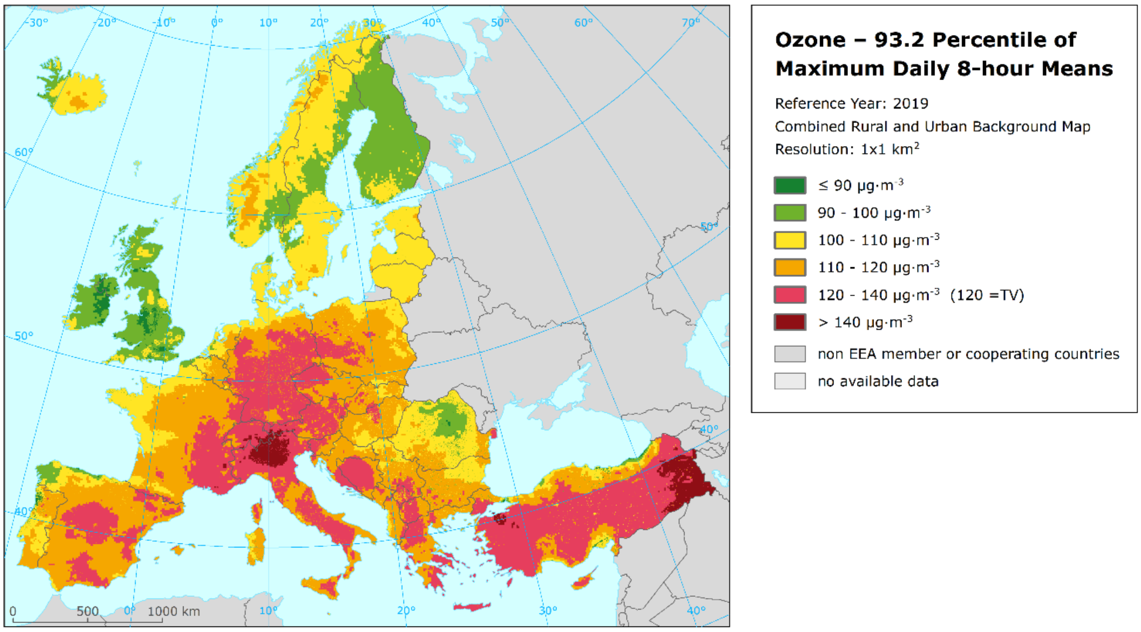

4.1.2 Population exposure

Table 4.1 and Figure 4.1 give, for the 93.2 percentile of maximum daily 8-hour means, the population frequency distribution for a limited number of exposure classes. Table 4.1 also presents the population-weighted concentration for individual countries, for EU-28 and for the total mapping area.

It has been estimated that in 2019 about 22 % of the considered European population including Turkey, 20 % of the considered European population excluding Turkey and 20 % of the EU-28 population lived in areas where the ozone concentration exceeded the health related target value threshold (TV of 120 $\mu g \cdot m^{-3}$).

In the following countries (apart from the microstates) at least 50 % of the population suffered exposures above the TV threshold: Austria, Bosnia and Herzegovina and Switzerland. In Croatia, Czechia, France, Germany, Greece, Italy, Slovenia, Spain and Turkey it has been between 13 and 49 %. Only in states of northern Europe and in the United Kingdom and Ireland no exposure to above the TV threshold has occurred.

Table 4.1: Population exposure and population-weighted concentrations, ozone indicator 93.2 percentile of maximum daily 8-hour means, 2019

Country	ISO	Population [inhbs·1000]	Ozone - perc93.2, exposed population, 2019 [%]						Ozone - perc93.2
			< 90	90 - 100	100 - 110	110 - 120	120 - 140	> 140	Pop. weighted
Albania	AL	2 797		0.7	57.2	40.9	1.1		109.2
Andorra	AD	84				95.8	4.2		116.5
Austria	AT	8 381			1.4	45.2	53.3	0.1	119.9
Belgium	BE	10 944		8.3	56.4	35.4	0.0		107.7
Bosnia and Herzegovina	BA	3 802			0.1	49.9	50.0		123.5
Bulgaria	BG	7 363	0.7	59.6	31.2	8.3	0.2		99.2
Croatia	HR	4 288			2.9	84.0	13.0		116.0
Cyprus	CY	1 018			22.3	69.4	8.3		113.5
Czechia	CZ	10 423			0.2	71.0	28.8		118.1
Denmark (incl. Faroe Islands)	DK	5 577		7.6	91.5	0.9			103.3
Estonia	EE	1 291		35.4	64.4	0.2			100.7
Finland	FI	5 339		82.2	17.8	0.0			97.5
France (metropolitan)	FR	62 744		6.3	29.7	41.2	22.9	0.0	112.8
Germany	DE	80 174			7.9	47.0	45.1		118.5
Greece	GR	10 634	5.1	2.7	33.6	39.8	18.8		113.2
Hungary	HU	9 937		0.6	71.0	26.9	1.4		108.3
Iceland	IS	318	41.4	51.3	7.2				92.8
Ireland	IE	4 574	40.1	57.1	2.8				90.2
Italy	IT	59 409	0.0	2.3	11.3	37.2	34.9	14.3	123.6
Latvia	LV	2 080	18.7	12.8	68.0	0.5	0.0		98.8
Liechtenstein	LI	34					100.0		122.9
Lithuania	LT	3 028			97.7	2.3			105.2
Luxembourg	LU	511			40.3	56.9	2.9		111.3
Malta	MT	417		32.9	52.8	13.1	1.3		106.0
Monaco	MC	33					100.0		121.0
Montenegro	ME	620			24.7	74.5	0.8		112.3
Netherlands	NL	16 600		15.6	51.4	31.2	1.7		106.5
North Macedonia	MK	2 061		36.3	54.6	7.0	2.1		103.7
Norway	NO	4 906		66.5	33.3	0.3			98.6
Poland	PL	38 494		2.0	19.4	74.9	3.7		112.6
Portugal (excl. Azores, Madeira)	PT	10 047	30.0	20.7	39.7	9.6	0.0		96.5
Romania	RO	20 138	6.9	65.0	26.1	2.0	0.0		97.5
San Marino	SM	32				29.5	70.5		119.0
Serbia (incl. Kosovo*)	RS	8 896		30.3	41.0	26.4	2.3		104.9
Slovakia	SK	5 399			46.7	46.8	6.5		110.9
Slovenia	SI	2 042			0.9	82.4	16.7		116.1
Spain (excl. Canarias)	ES	44 722	1.7	11.2	20.1	53.1	13.8		111.6
Sweden	SE	9 539		18.4	79.2	2.4	0.0		103.0
Switzerland	CH	7 893				18.5	79.0	2.5	123.2
Turkey	TR	71 920	14.5	12.8	19.0	22.0	29.3	2.5	109.9
United Kingdom (& Crown dep.)	UK	63 415	51.8	47.1	1.1	0.0			89.9
Total		601 926	**8.5**	**15.0**	**21.6**	**33.2**	**19.9**	**1.7**	**109.9**
			23.6				**21.6**		
Total without Turkey		530 007	**7.7**	**15.3**	**21.9**	**34.7**	**18.6**	**1.6**	**109.9**
			23.1				**20.3**		
EU-28		498 253	**8.2**	**14.9**	**21.7**	**35.4**	**18.1**	**1.7**	**109.9**
			23.1				**19.8**		
Kosovo*	KS	1 748		31.8	45.1	16.9	6.1		104.9
Serbia (excl. Kosovo*)	RS	7 148		30.0	40.0	28.8	1.3		104.9

(*) under the UN Security Council Resolution 1244/99.

Note: The percentage value "0.0" indicates that an exposed population exists, but it is small and estimated to be less than 0.05 %. Empty cells mean no population in exposure.

As the current mapping methodology tends to underestimate high values due to interpolation smoothing (Annex 3, Section A3.3), the exceedance percentage is most likely somewhat underestimated; additional population exposure above the TV threshold might be expected in additional countries: Croatia, Cyprus, Czechia, Montenegro, Poland and Slovenia. The reason is that in these countries the estimated percentage population exposed to the concentrations above 110 μg·m^{-3} is considerable.

The overall population-weighted ozone concentrations in terms of the 93.2 percentile of maximum daily 8-hour means has been estimated for 2019 as being 110 μg·m^{-3}. Both for the EU-28 area and the considered European area without Turkey, population-weighted ozone concentrations has been also estimated as being 110 μg·m^{-3}, i.e., of about 2.5 μg·m^{-3} less than five-year 2014-2018 mean concentration (Annex 4, Section A4.3).

Figure 4.1: Percentage of the population (%) exposed to ozone indicator 93.2 percentile of maximum daily 8-hour means, 2019

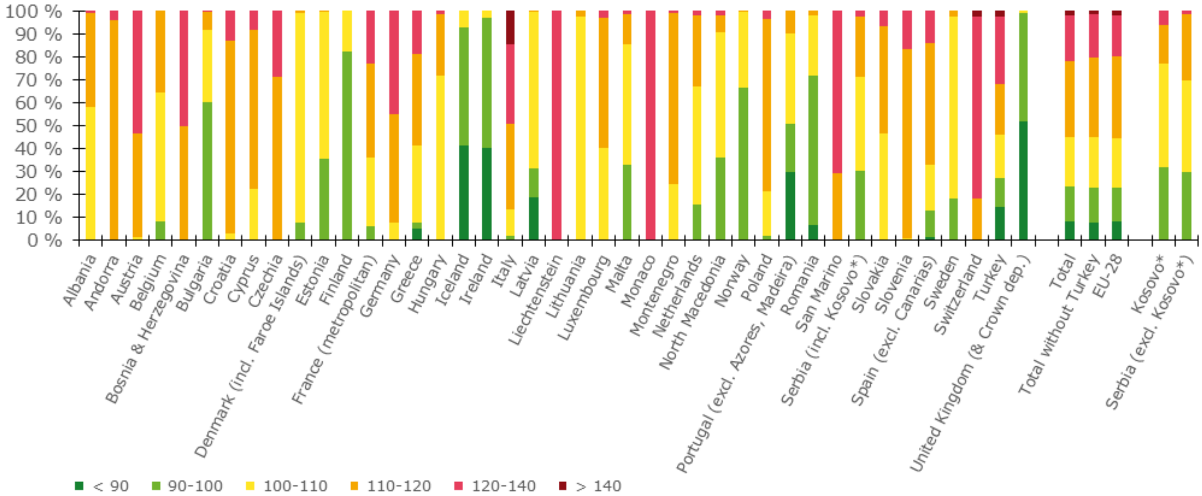

(*) under the UN Security Council Resolution 1244/99.

Figure 4.2 shows, for the whole mapped area, the population frequency distribution for exposure classes of 2 μg·m^{-3}. The highest population frequency is found for classes between 108 and 124 μg·m^{-3}.

Figure 4.2: Population frequency distribution, O_3 indicator 93.2 percentile of maximum daily 8-hour means, 2019. The EU target value (120 μg·m^{-3}) is marked by the red line

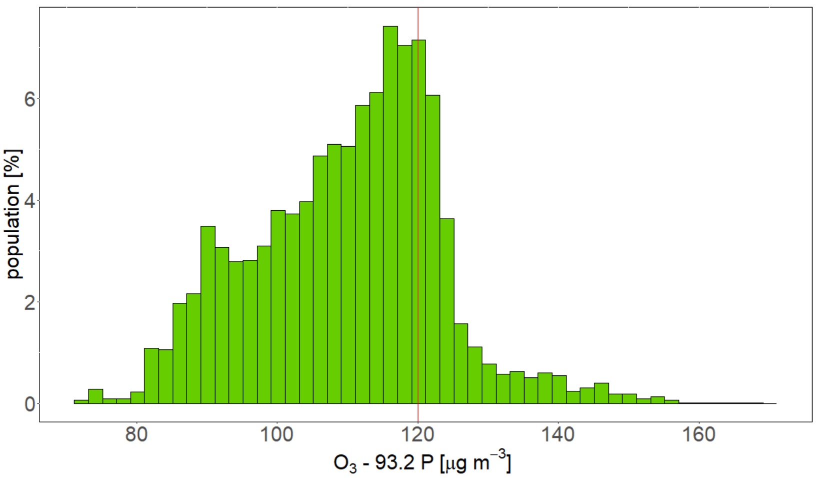

Figure 4.3 shows for individual countries the ozone to which the population per country was exposed in 2019. It can be seen that the countries with the highest ozone concentrations are located in the southern parts of Europe.

Figure 4.3: Ozone concentrations expressed as indicator 93.2 percentile of maximum daily 8-hour means to which the population per country was exposed in 2019. The EU target value (120 µg·m^{-3}) is marked by the red line

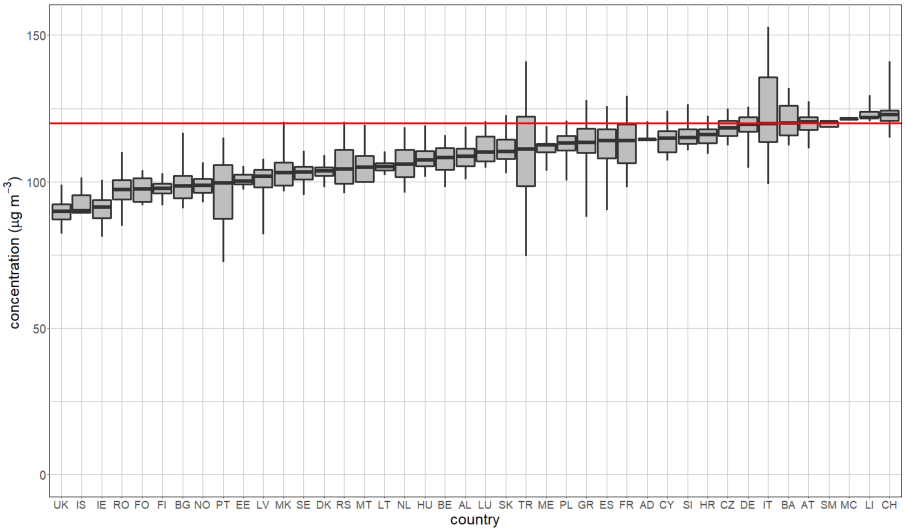

Note: For each country, the box plot shows the concentration to which a percentage of the population was exposed: 50% in the case of the black marker, 25% and 75% in the cases of the box's edges, 2% and 98% in the cases of the whiskers' edges.

4.2 Ozone – SOMO35 and SOMO10

SOMO35 is the annually accumulated ozone maximum daily 8-hourly means in excess of 35 ppb (i.e., 70 µg·m^{-3}). It is not subject to any of the EU air quality directives and there are no limit or target values defined. Comparing the 93.2 percentile of maximum daily 8-hour means versus the SOMO35 for all background stations shows no simple relationship between the two indicators. However, it seems that the TV of the 93.2 percentile of maximum daily 8-hour means (being 120 µg·m^{-3}) is related approximately with a SOMO35 value in the range of 6 000-8 000 µg·m^{-3}·d. This comparison motivates a somewhat arbitrarily chosen threshold of 6 000 µg·m^{-3}·d, in order to facilitate the discussion of the observed distributions of SOMO35 levels in their spatial and temporal context. This threshold is used in this and previous papers (Horálek et al., 2021, and the references cited therein) when dealing with the population exposure estimates.

SOMO10 is the annually accumulated ozone maximum daily 8-hourly means in excess of 10 ppb (i.e., 20 µg·m^{-3}). This indicator was introduced in Horálek et al. (2020), due to its link to the health impact assessment. Be it noted that the WHO recommends using the SOMO10 as an alternative to the SOMO35 when estimating the health impact of ozone (WHO, 2013).

4.2.1 Concentration maps

Maps 4.2 and 4.3 presents the final combined map for SOMO35 and SOMO10 as a result of combining the separate rural and urban interpolated maps following the same procedure as for 93.2 percentile of the maximum daily 8-hour means. The mapping details and the uncertainty analysis are presented in Annex 3. In the final combined map of SOMO35, the red and dark red areas show values above 8 000 µg·m^{-3}·d, while the orange areas show values above 6 000 µg·m^{-3}·d. In the case of SOMO10, the boundaries of concentration classes have been chosen quite arbitrary, in order to reflect the concentration distribution of this indicator. In the final combined map of SOMO10, the red and dark red areas show values above 24 000 µg·m^{-3}·d.

Map 4.2: Concentration map of ozone indicator SOMO35, 2019

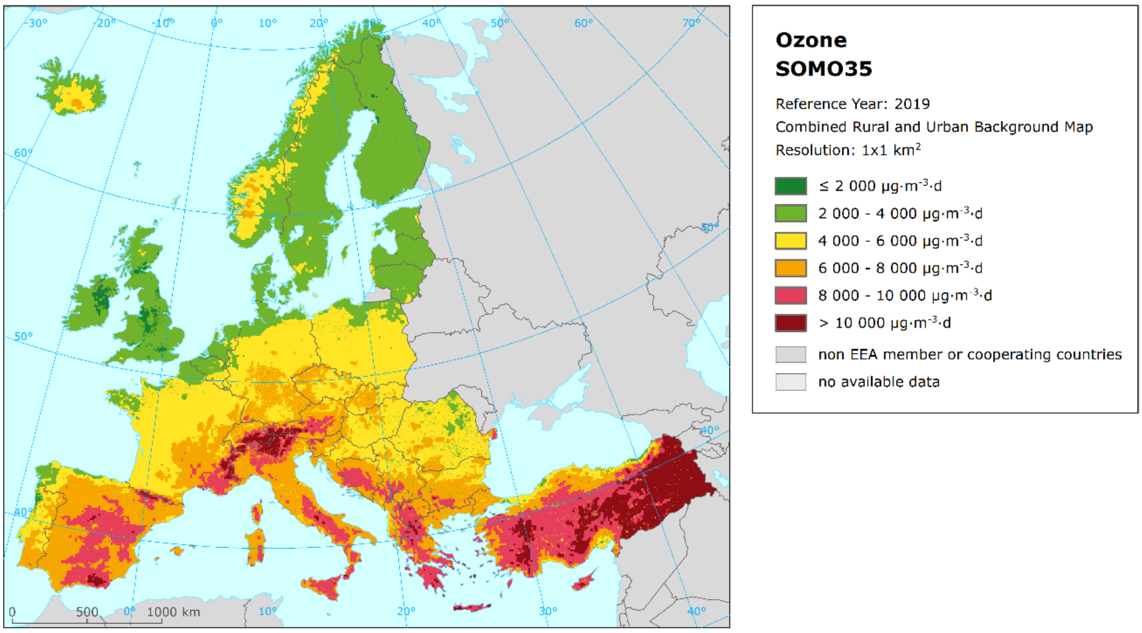

Map 4.3: Concentration map of ozone indicator SOMO10, 2019

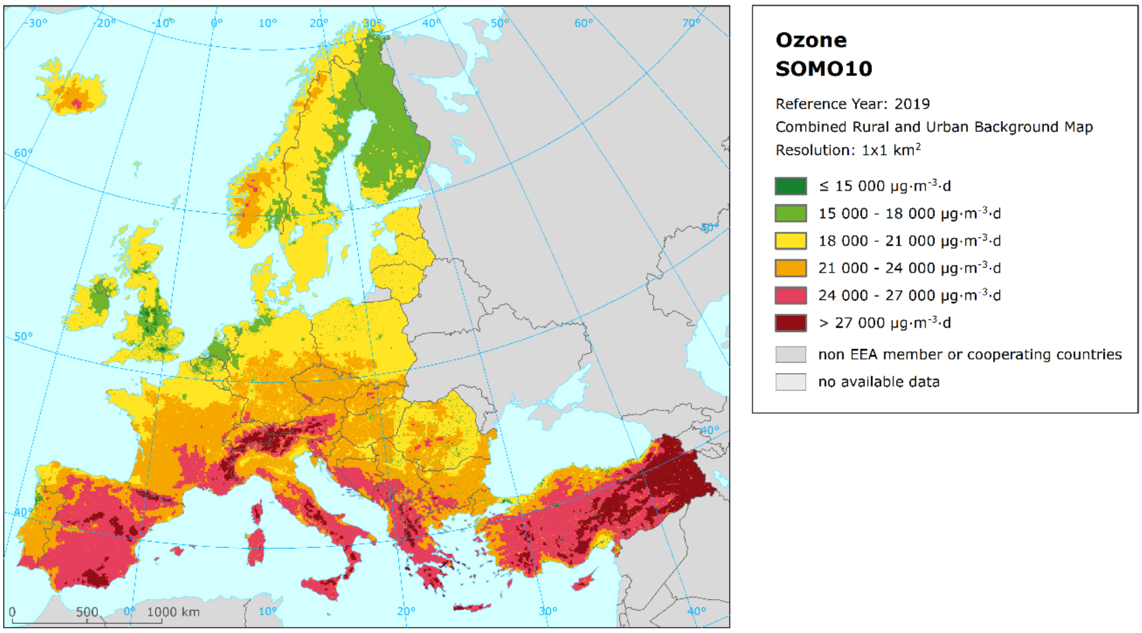

Like in the case of the 93.2 percentile of the maximum daily 8-hour means, generally the southern parts of Europe show higher ozone SOMO35 concentrations than the northern parts. Higher levels of ozone also occur more frequently in mountainous areas south of 50 degrees latitude than in lowlands. The relative mean uncertainty of the 2019 map of the SOMO35 is about 30 % for rural and 32 % for urban areas (see Annex 3).

Compared to the five-year average 2014-2018, highest increase has (in terms of SOMO35) been observed in northern Europe, in large areas in Spain, France and Germany and in smaller areas in south and south-eastern Europe, while a decline occurred in several coastal parts in southern and south-eastern Europe, in larger areas of Romania and Hungary and on the borders of Czechia, Poland and Slovakia, see Annex 4, Section A4.3.

4.2.2 Population exposure

Table 4.2 and Figure 4.4 give for SOMO35 the population frequency distribution for a limited number of exposure classes. Table 4.2 also presents the population-weighted concentration for individual countries, for EU-28 and for the total mapping area.

It has been estimated that in 2019 about 23 % of the considered European population (including Turkey), about 20 % both of the considered European population without Turkey and of the EU-28 population, lived in areas with SOMO35 values above 6 000 $\mu g \cdot m^{-3} \cdot d$ (see above on the motivation of this criterion).

In 2019, like in the previous several years, the northern and north-western European countries have had almost no inhabitants exposed to SOMO35 concentrations above 6 000 $\mu g \cdot m^{-3} \cdot d$. In Iceland and Norway there have been areas with SOMO35 above 6 000 $\mu g \cdot m^{-3} \cdot d$ (see map 4.2), but they mostly correspond to non-populated areas. Most of the countries in southern and central and eastern Europe have shown exposures above or well above 6 000 $\mu g \cdot m^{-3} \cdot d$, most notably (at least 50 % of population) Bosnia and Herzegovina, Greece, Italy and Spain. This corresponds with the concentrations observed in Map 4.2.

In 2019, the population-weighted ozone concentration in terms of SOMO35 was estimated to be almost 4 600 $\mu g \cdot m^{-3} \cdot d$ for the total mapping area. For both total area without Turkey and the EU-28, it was almost 4 500 $\mu g \cdot m^{-3} \cdot d$, which is the fourth highest in the fifteen years period 2005-2019 (Table 6.3). Compared to the five-year average 2014-2018, notably higher values have occurred in northern Europe, in large areas in Spain, France and Germany and in smaller areas in south and south-eastern Europe, while lower values have occurred in some parts of Romania and Hungary (Annex 4, Section A4.3).

Table 4.3 and Figure 4.5 give for SOMO10 the population frequency distribution for a limited number of exposure classes. Table 4.3 also presents the population-weighted concentration for individual countries, for EU-28 and for the total mapping area.

The population-weighted ozone concentrations, in terms of SOMO10, were estimated to be about 19 000 $\mu g \cdot m^{-3} \cdot d$ and 19 100 $\mu g \cdot m^{-3} \cdot d$ for the total mapping area and the EU-28, respectively. For the total mapping area without Turkey, it was also 19 100 $\mu g \cdot m^{-3} \cdot d$.

Table 4.2: Population exposure and population-weighted concentrations, ozone indicator SOMO35, 2019

Country	ISO	Population [inhbs·1000]	Ozone - SOMO35, exposed population, 2019 [%]						Ozone - SOMO35
			< 2000	4000	6000	8000	10000	> 10000	Pop, weighted
Albania	AL	2 797			71.0	25.7	3.3	0.0	5 727
Andorra	AD	84				78.5	21.0	0.5	7 536
Austria	AT	8 381			60.5	36.7	2.5	0.3	5 802
Belgium	BE	10 944		91.7	8.3				3 336
Bosnia and Herzegovina	BA	3 802			13.5	68.9	17.6		7 062
Bulgaria	BG	7 363	0.2	78.6	14.3	6.7	0.3	0.0	3 515
Croatia	HR	4 288			53.5	39.5	7.0		6 191
Cyprus	CY	1 018		0.1	79.4	7.2	12.8	0.6	5 653
Czechia	CZ	10 423			93.5	6.5			5 400
Denmark (incl. Faroe Islands)	DK	5 577		94.5	5.5				3 477
Estonia	EE	1 291		99.4	0.6				2 739
Finland	FI	5 339	20.7	79.3	0.0				2 297
France (metropolitan)	FR	62 744		32.0	48.2	18.4	1.4	0.0	4 791
Germany	DE	80 174		20.4	76.5	3.0	0.0	0.0	4 612
Greece	GR	10 634		6.6	13.7	45.3	30.4	4.0	7 094
Hungary	HU	9 937		30.1	66.7	3.2			4 473
Iceland	IS	318	69.5	30.4	0.0				1 662
Ireland	IE	4 574	44.1	55.6	0.3				2 125
Italy	IT	59 409	0.0	2.1	25.6	62.4	9.7	0.3	6 659
Latvia	LV	2 080	18.7	77.0	4.4				2 552
Liechtenstein	LI	34			90.2	9.6	0.1		5 719
Lithuania	LT	3 028		97.0	3.0				3 222
Luxembourg	LU	511		56.5	43.5				3 808
Malta	MT	417			74.6	21.1	3.8	0.6	5 872
Monaco	MC	33				100.0			6 930
Montenegro	ME	620			51.4	43.6	5.0		6 017
Netherlands	NL	16 600		91.1	8.9				3 331
North Macedonia	MK	2 061		50.0	44.2	4.3	1.5	0.0	4 038
Norway	NO	4 906	0.3	97.5	2.2	0.0			2 709
Poland	PL	38 494		25.0	74.9	0.2			4 390
Portugal (excl. Azores, Madeira)	PT	10 047	26.0	37.7	31.5	4.9	0.0		3 332
Romania	RO	20 138	5.5	76.1	17.8	0.6	0.0		3 222
San Marino	SM	32			78.0	22.0			5 956
Serbia (incl. Kosovo*)	RS	8 896		54.5	36.9	7.7	0.9	0.0	4 143
Slovakia	SK	5 399		13.4	80.0	6.7			4 778
Slovenia	SI	2 042			62.0	36.9	1.1	0.0	5 758
Spain (excl. Canarias)	ES	44 722	0.8	13.9	33.4	47.9	3.9	0.0	5 816
Sweden	SE	9 539	2.8	90.6	6.7				3 148
Switzerland	CH	7 893			73.1	23.5	2.8	0.5	5 847
Turkey	TR	71 920	10.7	28.2	19.5	20.8	11.7	9.0	5 493
United Kingdom (& Crown dep.)	UK	63 415	63.4	36.3	0.3				1 892
Total		**601 926**	**9.3**	**31.4**	**36.7**	**17.7**	**3.6**	**1.2**	**4598.9**
			40.7			**22.6**			
Total without Turkey		**530 007**	**9.1**	**31.8**	**39.1**	**17.3**	**2.5**	**0.1**	**4477.5**
			40.9			**20.0**			
EU-28		**498 253**	**9.6**	**31.6**	**39.0**	**17.2**	**2.5**	**0.1**	**4453.6**
			41.3			**19.8**			
Kosovo*	KS	1 748		56.7	25.0	16.4	2.0	0.0	4 086
Serbia (excl. Kosovo*)	RS-	7 148		54.0	39.8	5.6	0.6		5 727

(*) under the UN Security Council Resolution 1244/99.

Note: The percentage value "0.0" indicates that an exposed population exists, but it is small and estimated to be less than 0.05 %. Empty cells mean no population in exposure.

Table 4.3: Population exposure and population-weighted concentrations, ozone indicator SOMO10, 2019

Country	ISO	Population [inhbs·1000]	Ozone – SOMO10, exposed population, 2019 [%]						Ozone – SOMO10
			< 15000	18000	21000	24000	27000	> 27000	Pop, weighted
Albania	AL	2 797			31.4	56.6	11.8	0.2	21 910
Andorra	AD	84				97.6	1.9	0.6	22 728
Austria	AT	8 381		3.8	49.4	41.5	5.0	0.4	20 707
Belgium	BE	10 944	3.4	79.5	17.1	0.0			17 237
Bosnia and Herzegovina	BA	3 802			12.6	69.2	18.2		22 745
Bulgaria	BG	7 363	14.5	56.5	19.6	8.7	0.7	0.0	17 137
Croatia	HR	4 288			47.7	37.0	15.3		21 625
Cyprus	CY	1 018			74.6	11.6	13.3	0.5	21 304
Czechia	CZ	10 423			76.3	23.6	0.1		20 475
Denmark (incl. Faroe Islands)	DK	5 577		0.5	99.4	0.1			18 918
Estonia	EE	1 291		76.4	23.6	0.0			17 594
Finland	FI	5 339		93.6	6.4				16 872
France (metropolitan)	FR	62 744		16.2	47.2	31.7	4.8	0.1	20 273
Germany	DE	80 174		27.1	67.7	5.1	0.1	0.0	18 719
Greece	GR	10 634		7.4	10.4	43.4	34.7	4.2	22 955
Hungary	HU	9 937		47.4	43.7	8.9			18 649
Iceland	IS	318		90.6	9.4	0.0			16 807
Ireland	IE	4 574		68.8	31.2	0.0			17 436
Italy	IT	59 409		0.7	41.2	46.7	11.0	0.3	21 625
Latvia	LV	2 080	18.7	55.5	25.8	0.1			16 339
Liechtenstein	LI	34			91.4	7.1	1.4	0.1	20 049
Lithuania	LT	3 028		69.7	30.2	0.0			17 584
Luxembourg	LU	511		52.1	47.8	0.2			18 126
Malta	MT	417				75.0	24.1	0.9	23 683
Monaco	MC	33				100.0			23 101
Montenegro	ME	620			41.5	43.7	14.7	0.1	21 930
Netherlands	NL	16 600		76.9	23.1				17 232
North Macedonia	MK	2 061		43.9	46.3	7.5	2.3	0.1	18 335
Norway	NO	4 906		68.8	30.4	0.8	0.0		17 338
Poland	PL	38 494		25.8	71.2	3.0	0.0		18 784
Portugal (excl. Azores, Madeira)	PT	10 047	27.1	14.4	37.9	19.5	1.2		18 010
Romania	RO	20 138	12.9	60.6	23.3	3.2	0.0		16 828
San Marino	SM	32			78.0	22.0			21 020
Serbia (incl. Kosovo*)	RS	8 896	3.7	61.5	22.3	10.6	2.0	0.0	17 627
Slovakia	SK	5 399		5.6	79.9	14.5	0.1		19 636
Slovenia	SI	2 042			53.3	40.4	6.4	0.0	20 963
Spain (excl. Canarias)	ES	44 722	0.8	4.9	26.6	46.4	21.0	0.2	21 951
Sweden	SE	9 539		38.6	60.9	0.5			18 368
Switzerland	CH	7 893			77.5	19.2	2.8	0.6	20 521
Turkey	TR	71 920	33.7	17.9	12.6	17.3	12.0	6.5	18 223
United Kingdom (& Crown dep.)	UK	63 415	38.4	53.8	7.7	0.1			15 662
Total		**601 926**	**9.4**	**27.1**	**38.3**	**18.6**	**5.7**	**0.9**	**19036.4**
			36.5.				**6.7**		
Total without Turkey		**530 007**	**6.1**	**28.4**	**41.8**	**18.7**	**4.9**	**0.2**	**19146.7**
			34.4				**5.1**		
EU-28		**498 253**	**6.4**	**28.1**	**41.9**	**18.5**	**4.9**	**0.2**	**19127.1**
			34.5				**5.0**		
Kosovo*	KS	1 748		50.6	29.1	15.4	4.9	0.0	17 364
Serbia (excl. Kosovo*)	RS-	7 148	4.5	64.2	20.6	9.4	1.3		21 910

(*) under the UN Security Council Resolution 1244/99.

Note: The percentage value "0.0" indicates that an exposed population exists, but it is small and estimated to be less than 0.05 %. Empty cells mean no population in exposure.

Figure 4.4: Percentage of the population (%) exposed to ozone indicator SOMO35, 2019

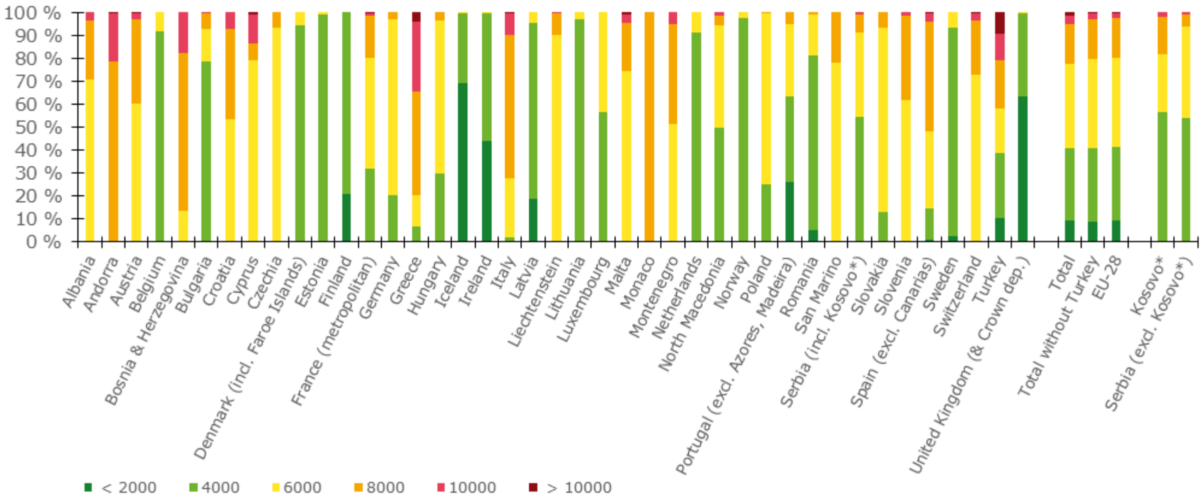

(*) under the UN Security Council Resolution 1244/99.

Figure 4.5: Percentage of the population (%) exposed to ozone indicator SOMO10, 2019

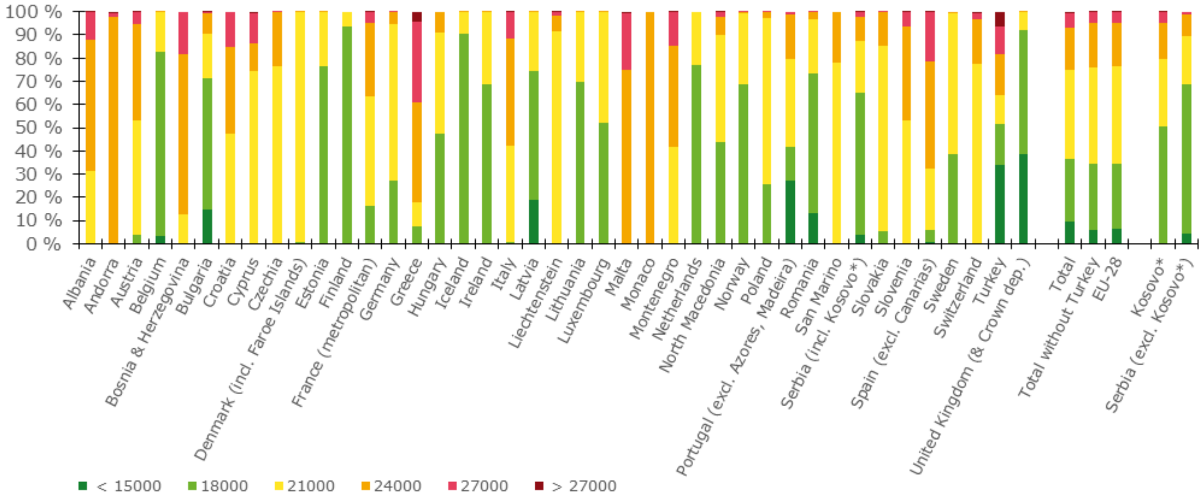

(*) under the UN Security Council Resolution 1244/99.

Figure 4.6 shows, for the whole mapped area, the frequency distribution of SOMO35 for population exposure classes of 250 $\mu g \cdot m^{-3} \cdot d$. The highest frequencies are found for classes between 2 000 and 7 000 $\mu g \cdot m^{-3} \cdot d$. One can see a steep decline of population frequency for exposure classes between 7 000 and 9000 $\mu g \cdot m^{-3} \cdot d$ and a continuous mild decline of population frequency for classes above 9 000 $\mu g \cdot m^{-3} \cdot d$.

Figure 4.7 shows the population frequency distribution of SOMO10 for population exposure classes of 500 $\mu g \cdot m^{-3} \cdot d$. The graph shows the highest frequencies for classes between 15 500 and 23 000 $\mu g \cdot m^{-3} \cdot d$.

Figure 4.8 shows for individual countries the ozone indicator SOMO10 to which the population per country was exposed in 2019. (For similar figure for SOMO35, see Figure ES.4.) It can be seen that the countries with the highest ozone concentrations are located in the southern parts of Europe.

Figure 4.6: Population frequency distribution, ozone indicator SOMO35, 2019

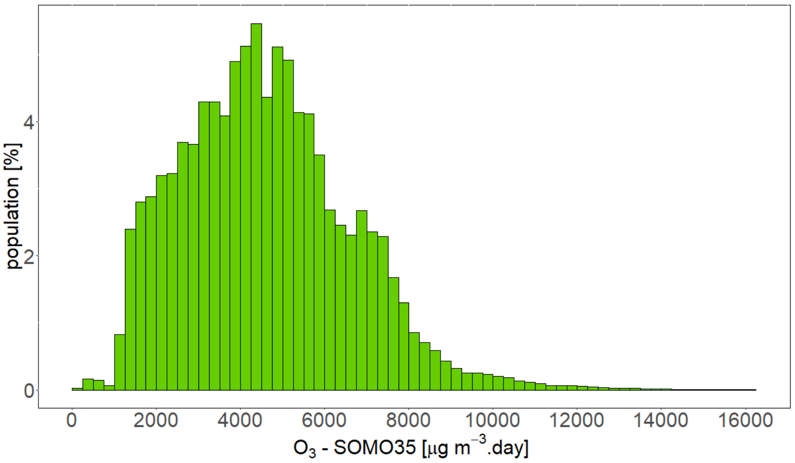

Figure 4.7: Population frequency distribution, ozone indicator SOMO10, 2019

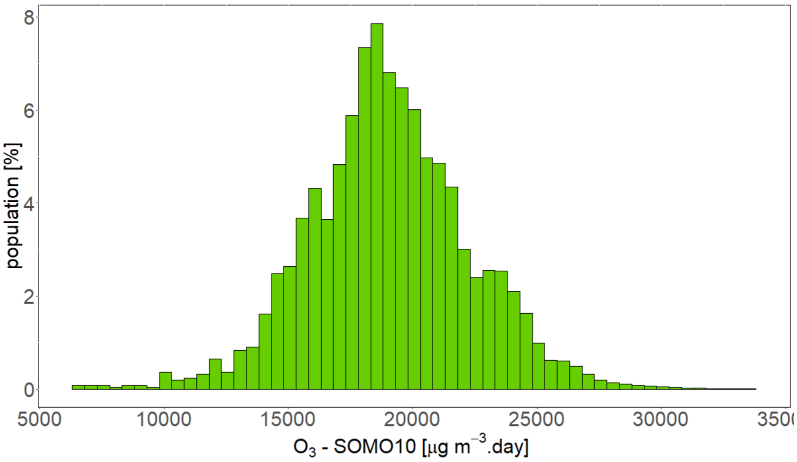

Figure 4.8: Ozone concentrations expressed as indicator SOMO10 to which the population per country was exposed in 2019

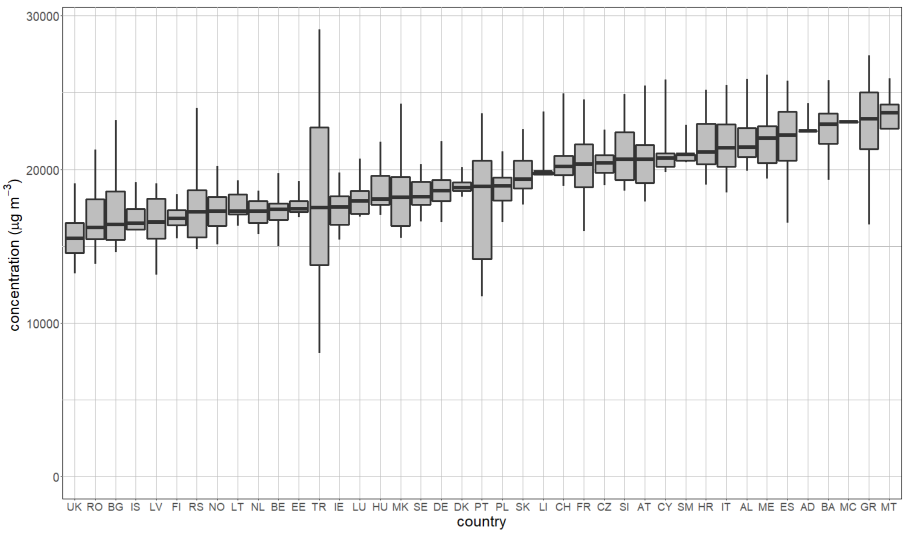

Note: For each country, the box plot shows the concentration to which a percentage of the population was exposed: 50 % in the case of the black marker, 25 % and 75 % in the cases of the box's edges, 2 % and 98 % in the cases of the whiskers' edges.

4.3 Ozone – AOT40 vegetation and AOT40 forests

In the Ambient Air Quality Directive (EC, 2008) a target value (TV) and a long-term objective (LTO) for the protection of vegetation from high ozone concentrations accumulated during the growing season have been defined. TV and LTO are specified using "accumulated ozone exposure over a threshold of 40 parts per billion" (AOT40). This is calculated as a sum of the difference between hourly concentrations greater than 80 $\mu g{\cdot}m^{-3}$ (i.e. 40 parts per billion) and 80 $\mu g{\cdot}m^{-3}$, using only observations between 08:00 and 20:00 Central European Time (CET) each day, calculated over three months from 1 May to 31 July. The TV is 18 000 $\mu g{\cdot}m^{-3}{\cdot}h$ (averaged over five years) and the LTO is 6 000 $\mu g{\cdot}m^{-3}{\cdot}h$.

Note that the term vegetation as used in the Air Quality Directive (EC, 2008) is not further defined. Nevertheless, the TV used in the directive is quite similar as the critical level used in the Mapping Manual (CLRTAP, 2017a) for "agricultural crops" (although the definitions of AOT40 by EU and CLRTAP are slightly different), so the term vegetation in the Air Quality Directive has been interpreted as primarily agricultural crops. Therefore, the exposure of agricultural crops has been evaluated here based on the AOT40 for vegetation as defined in the Air Quality Directive and the agricultural areas, defined as the CORINE Land Cover level-1 class 2 Agricultural areas (encompassing the level-2 classes 2.1 Arable land, 2.2 Permanent crops, 2.3 Pastures and 2.4 Heterogeneous agricultural areas), see Section 4.3.2. Note that in addition to these agricultural areas there are several other CLC classes that could be considered "vegetation", namely level-2 classes 1.4 Artificial, non-agricultural vegetated areas (encompassing the level-3 classes 1.4.1 Green urban areas and 1.4.2 Sport and leisure facilities), 3.1 Forests (see below) and 3.2 Scrub and/or herbaceous vegetation associations.

Next to the AOT40 for vegetation protection, the Air Quality Directive (EC, 2008) defines also the AOT40 for forest protection, which is calculated similarly as the AOT40 for vegetation, but is summed over six months from 1 April to 30 September. For AOT40 for forests there is no TV defined. However, there is a Critical Level (CL) established by CLRTAP (2017a). This Critical Level is set at 10 000 $\mu g{\cdot}m^{-3}{\cdot}h$. Although CLRTAP (2017a) calculates the AOT40 indicators somewhat differently (e.g. it uses the ozone concentration corrected at canopy height), we further use this CL level for the AOT40 for forests calculated according to the EC (2008).

For the exposure of forests evaluation, the CLC level-2 class 3.1 Forests has been used.

The ecosystem based accumulative ozone indicators described in this section are specifically prepared for calculation of the EEA Core Set Indicator 005 (EEA, 2021b). For the estimation of the vegetation and forested area exposure to accumulated ozone, the maps in this section are created on a grid of 2x2 km^2 resolution. The exposure frequency distribution outcomes are based on the overlay with the 100x100 m^2 grid resolution of the CLC2016 land cover classes.

4.3.1 Concentration maps

The interpolated maps of AOT40 for vegetation and AOT40 for forests are created for rural areas only, as urban areas are considered not to represent agricultural or forested areas. These maps are therefore applicable to rural areas only, and as such they are based on AOT40 data derived from rural background station observations only. These AOT40 monitoring data are combined in the mapping with the supplementary data sources EMEP model output, altitude and surface solar radiation. These supplementary data sources are the same as those selected at the human health related ozone indicators.

Map 4.4 presents the final map of AOT40 for vegetation in 2019. Note that in the Air Quality Directive (EC, 2008) the TV is actually defined as 18 000 $\mu g{\cdot}m^{-3}{\cdot}h$ averaged over five years. Here only 2019 data are presented, and no five-year average has been calculated.

The areas in the map with concentrations above the TV threshold of 18 000 $\mu g{\cdot}m^{-3}{\cdot}h$ are marked in red and dark red. The areas below the long-term objective (LTO) are marked in green. The high and very high AOT40 levels for vegetation occur specifically in southern, south-western and south-eastern regions of Europe and in Turkey; they also occurred in central regions of Europe in 2019. Highest levels (dark red) were estimated in the middle of Greece, in the south-west and south-east of Turkey, both in the north and in the south (Sicilia) of Italy, in other smaller parts in North Macedonia, in the middle of Spain and in a small other part, France and Switzerland. The relative mean uncertainty of the 2019 map of the AOT40 for vegetation is about 32 % (Annex 3, Section A3.3).

Map 4.5 presents the final map of AOT40 for forests in 2019. The areas in the map with concentrations above the Critical Level (CL) defined by CLRTAP (2017a) are marked in yellow, orange, red and dark red. One can see large European forested areas exceeding this level.

Like for the AOT40 for vegetation indicator, the highest levels of the AOT40 for forests are found in the south-western, southern and south-eastern European region and Turkey. In 2019, high levels of the AOT40 are found also in central Europe (Austria, Czechia, Germany, Poland and Switzerland). Nevertheless, values exceeding CL are found everywhere in Europe except the Atlantic areas in the north-west of Spain, larger parts of the United Kingdom, Ireland and Finland and only smaller parts in Iceland, Norway and Sweden. The relative mean uncertainty of the 2019 map of the AOT40 for forests is about 33 % (Annex 3, Section A3.3).

Map 4.4: Concentration map of ozone indicator AOT40 for vegetation, rural map, 2019

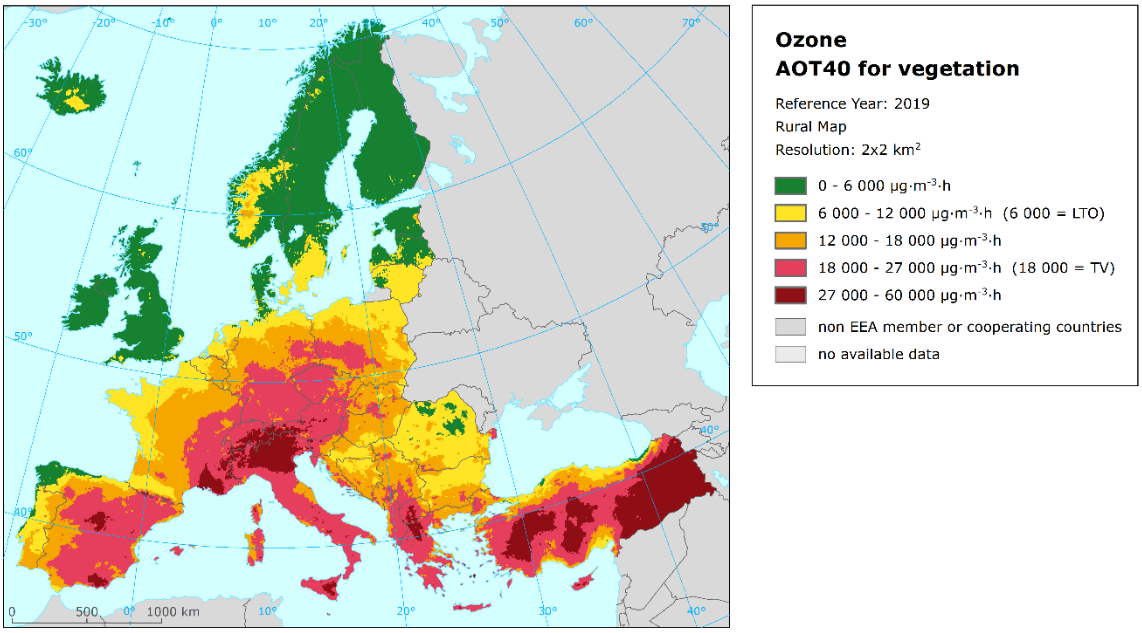

For the comparison with five-year average 2014-2018 values, see Annex 4, Section A4.3.

In order to provide more complete information of the air quality across Europe, the AOT40 maps including the AOT40 values based on the actual rural background measurement data at stations are presented in Maps A5.7 and A5.8 of Annex 5.

Map 4.5: Concentration map of ozone indicator AOT40 for forests, rural map, 2019

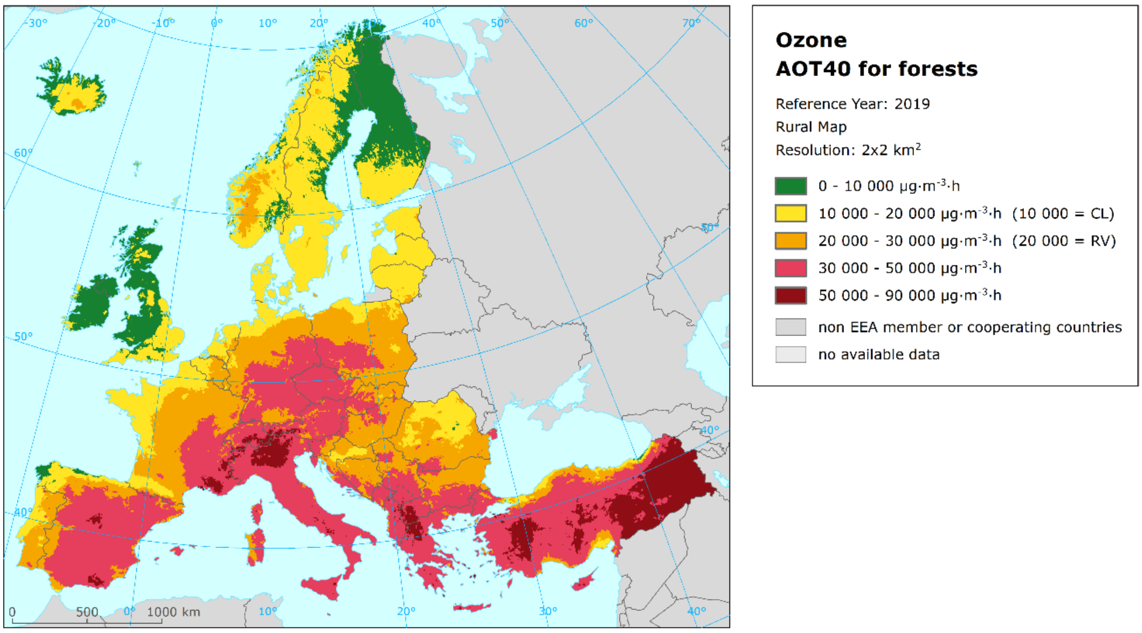

4.3.2 Vegetation exposure

Agricultural crops

The rural map with the ozone indicator AOT40 for vegetation has been combined with the land cover CLC2018 map. Following a similar procedure as described in Horálek et al. (2007), the exposure of agricultural areas (as defined above) has been calculated at the country-level.

Table 4.4 gives the absolute and relative agricultural area for each country and for four European regions where the ozone target value (TV) threshold and long-term objective (LTO) for protection of vegetation as defined in the Air Quality Directive (EC, 2008) are exceeded. The frequency distribution of the agricultural area over some exposure classes per country is presented as well. The table presents the country grouping of the following regions: 1) Northern Europe: Denmark, Estonia, Finland, Latvia, Lithuania, Norway, and Sweden, 2) North-western Europe: Belgium, France north of 45 degrees latitude, Ireland, Iceland, Luxembourg, the Netherlands, and United Kingdom, 3) Central and South-Eastern Europe: Austria, Bulgaria, Czechia, Germany, Hungary, Liechtenstein, Poland, Romania, Slovakia and Switzerland, and 4) Southern Europe: Albania, Bosnia and Herzegovina, Croatia, Cyprus, France south of 45 degrees latitude, Greece, Italy, Malta, Monaco, Montenegro, North Macedonia, Portugal, San Marino, Serbia (including Kosovo under the UN Security Council Resolution 1244/99), Slovenia, Spain and Turkey.

Table 4.4 illustrates that in 2019, about 37 % of all European agricultural land including Turkey has been exposed to ozone exceeding the TV of 18 000 $\mu g \cdot m^{-3} \cdot h$. For the areas excluding Turkey and for the EU-28, it has been about 30 %, which is in the mean of the fifteen-year period mean 2005-2019, see Table 6.4. More than 90 % of the agricultural area present ozone levels in excess of the TV in Austria, Cyprus, Malta and Switzerland. And more than half of the agricultural area in Albania, Czechia, Greece, Italy, North Macedonia, Spain and Turkey.

Considering the LTO of 6 000 $\mu g \cdot m^{-3} \cdot h$, the total European area including Turkey in excess has been about 86 %. For the areas excluding Turkey and for the EU-28, it has been 84 %. In 2019, values of the AOT40 for vegetation above the LTO have occurred in all countries with the exception of Iceland.

Nevertheless, very small areas (< 1 %) with the values above LTO have also occurred in Finland and Ireland. On the other hand, in most of the countries about or more than 90 % of the agricultural area has been exposed to ozone levels in excess of the LTO. Only in a few countries (Denmark, Estonia, Latvia, Norway, Sweden and the United Kingdom), the agricultural area exposed above the LTO in 2019 has been lower than 50 %.

Forests

The rural map with ozone indicator AOT40 for forests was combined with the land cover CLC2018 map. Following a similar procedure as described in Horálek et al. (2007), the exposure of forest areas (as defined above) has been calculated for each country, for the same four European regions as for crops and for Europe as a whole. Table 4.5 gives the absolute and relative forest area where the Critical Level (CL set at 10 000 $\mu g \cdot m^{-3} \cdot h$), at the same level as defined in CLRTAP (2017a), and the value 20 000 $\mu g \cdot m^{-3} \cdot h$ (which is equal to the earlier used Reporting Value, RV, as was defined in the repealed ozone directive 2002/3/EC) are exceeded. Next to the forest area in exceedance, the table presents the frequency distribution of the forest area over some exposure classes.

The Critical Level was exceeded in 2019 at about 85 % of all European forested area including Turkey. For the area excluding Turkey and for the EU-28 it was exceeded at about 84 %, which is the third highest exceedance observed for the fifteen-year period 2005-2019 (Table 6.4). As in previous years, most countries continue to have in 2019 the whole or considerable forest areas in excess to the CL, with specifically almost all forest area in southern and central, eastern and western European countries. In 2019, areas in excess to the CL occurred also in Northern Europe. The CL was not exceeded only in the most of Iceland, United Kingdom, Ireland and Finland, and in smaller parts of Norway, Sweden and Spain (north-western part).

In this context, it should be mentioned that the AOT40 indicator is probably not the best proxy for vegetation damage assessment. AOT40 does not take into account plant physiological control of ozone absorbed doses, which is taken into account in the POD (i.e. Phytotoxic Ozone Dose) indicators, as discussed in Section 4.4 for main crops. POD indicators are known to be more related with ozone effects on plant growth than ambient air ozone concentrations alone. The AOT40 does not take into account either the influence of meteorological conditions on growing season timing. Growing season´s start and end dates can change across Europe, and between years for a given site, depending on factors such as air temperature, solar radiation, photoperiod or rainfall. High temperature and dry weather favouring ozone pollution cause a reduction of ozone absorbed doses by plants due to plant physiological response to drought (i.e., the vegetation closes its stomata protecting itself from the exposure to ozone). However, plants may still be sensitive to ozone in such weather conditions, as illustrated by foliar injury records in Aleppo pine stands growing in southern France (CLRTAP, 2016) or controlled experimental results (e.g. Alonso et al., 2014).

Table 4.4: Agricultural area exposure and exceedance and agricultural-weighted concentrations, ozone indicator AOT40 for vegetation, 2019

Country	Agricultural area, 2019					Percentage of agricultural area, 2019 [%]					Agricult.-weighted conc.
	Total area	> LTO (6 000 μg·m⁻³·h)		> TV (18 000 μg·m⁻³·h)		< 6 000	6 000 - 12 000	12 000 - 18 000	18 000 - 27 000	> 27 000	
	[km²]	[km²]	[%]	[km²]	[%]	μg·m⁻³·h	μg·m⁻³·h	μg·m⁻³·h	μg·m⁻³·h	μg·m⁻³·h	[μg·m⁻³·h]
Albania	8 017	8 017	100.0	4 852	60.5			39.5	60.4	0.1	18 773.9
Andorra	13	13	100.0	12	85.5			14.5	71.7	13.9	23 484.1
Austria	26 827	26 827	100.0	25 528	95.2			4.8	93.7	1.4	20 912.5
Belgium	17 473	17 473	100.0				47.1	52.9			11 588.8
Bosnia and Herzegovina	17 023	17 023	100.0	69	0.4		54.1	45.5	0.4		12 216.1
Bulgaria	57 390	57 390	100.0	1 620	2.8		58.6	38.6	2.8		11 897.1
Croatia	22 168	22 168	100.0	2 316	10.4		41.5	48.0	10.4	0.0	13 282.4
Cyprus	4 291	4 291	100.0	3 954	92.2			7.8	88.2	4.0	21 921.2
Czechia	44 784	44 784	100.0	33 381	74.5		0.0	25.5	74.5		19 379.9
Denmark (incl. Faroe Is.)	31 235	10 554	33.8			66.2	33.5	0.3			5 930.6
Estonia	14 251	641	4.5			95.5	4.5				4 772.7
Finland	27 504	63	0.2			99.8	0.2				3 161.9
France (metropolitan)	323 377	323 199	99.9	63 499	19.6	0.1	37.7	42.6	17.3	2.3	14 222.0
Germany	204 463	198 594	97.1	79 015	38.6	2.9	20.5	38.0	38.6	0.0	15 708.8
Greece	50 051	50 051	100.0	38 059	76.0		0.2	23.8	69.7	6.3	20 492.8
Hungary	60 387	60 387	100.0	7 154	11.8		17.9	70.3	11.8		14 505.5
Iceland	2 517					100.0					945.6
Ireland	46 756	28	0.1			99.9	0.1				2 430.8
Italy	155 718	155 718	100.0	139 534	89.6			10.4	65.2	24.4	23 989.8
Latvia	25 530	7 191	28.2			71.8	28.2	0.0			5 679.6
Liechtenstein	37	37	100.0	37	100.0				96.3	3.7	24 252.9
Lithuania	38 148	34 089	89.4			10.6	89.4	0.0			7 202.3
Luxembourg	1 351	1 351	100.0				13.1	86.9			14 337.6
Malta	125	125	100.0	113	90.3			9.7	79.0	11.4	21 420.1
Monaco											
Montenegro	2 242	2 242	100.0	679	30.3			69.7	30.3		16 557.3
Netherlands	23 644	23 222	98.2			1.8	82.1	16.1			9 828.3
North Macedonia	9 146	9 146	100.0	6 967	76.2		4.6	19.2	61.7	14.5	21 866.3
Norway	15 636	883	5.6			94.4	5.6	0.0			2 871.6
Poland	183 258	183 183	100.0	26 910	14.7	0.0	43.4	41.8	14.7		13 241.8
Portugal (excl. Az., Mad.)	42 566	40 470	95.1	10	0.0	4.9	52.8	42.3	0.0		10 918.5
Romania	135 270	123 619	91.4	1 035	0.8	8.6	76.1	14.5	0.8		9 394.0
San Marino	42	42	100.0	42	100.0				100.0		19 719.9
Serbia (incl. Kosovo*)	46 768	46 768	100.0	6 489	13.9		21.1	65.1	13.9		14 445.2
Slovakia	23 100	23 100	100.0	3 439	14.9		7.9	77.2	14.9		15 630.1
Slovenia	6 986	6 986	100.0	3 170	45.4		3.7	50.9	44.4	1.0	17 835.9
Spain (excl. Canarias)	241 014	230 903	95.8	164 081	68.1	4.2	2.8	24.9	66.0	2.1	18 956.1
Sweden	39 035	13 588	34.8			65.2	34.8	0.1			5 212.3
Switzerland	11 359	11 359	100.0	11 102	97.7			2.3	88.6	9.1	22 887.7
Turkey	339 966	337 168	99.2	266 402	78.4	0.8	8.1	12.7	33.1	45.3	24 827.1
United Kingdom (& dep.)	135 759	4 926	3.6			96.4	3.6	0.0			3 641.9
Total	**2 435 233**	**2 097 621**	**86.1**	**889 467**	**36.5**	**13.9**	**23.7**	**25.9**	**27.9**	**8.7**	**15 281.4**
Total without Turkey	**2 095 267**	**1 760 453**	**84.0**	**623 065**	**29.7**	**16.0**	**26.3**	**28.0**	**27.0**	**2.7**	**13 734.5**
EU-28	**1 981 926**	**1 664 701**	**84.0**	**592 817**	**29.9**	**16.0**	**26.7**	**27.3**	**27.2**	**2.7**	**13 720.9**
France over 45N	256 784	256 606	99.9	45 662	17.8	0.1	40.8	41.3	17.8	0.0	13 676.9
France bellow 45N	66 594	66 594	100.0	17 837	26.8		25.7	47.5	15.7	11.1	16 324.4
Kosovo	4 167	4 167	100.0	2 932	70.4			29.6	70.4		19 574.0
Serbia (without Kosovo*)	42 601	42 601	100.0	3 556	8.3		23.1	68.5	8.3		13 943.5
Northern	191 340	67 009	35.0			65.0	35.0	0.1			5 270.0
North-western	484 285	303 606	62.7	45 662	9.4	37.3	28.4	24.8	9.4	0.0	9 450.6
Central & south-eastern	746 876	729 280	97.6	189 221	25.3	2.4	36.2	36.1	25.1	0.2	14 083.7
Southern	1 012 731	997 726	98.5	654 584	64.6	1.5	10.2	23.7	44.0	20.7	20 830.0

(*) under the UN Security Council Resolution 1244/99.

Note: The percentage value "0.0" indicates that an exposed population exists, but it is small and estimated to be less than 0.05 %. Empty cells mean no population in exposure.

Table 4.5: Forested area exposure and exceedance and forest-weighted concentrations, ozone indicator AOT40 for forests, 2019

Country	Forested area, 2019					Percentage of forested area, 2019 [%]					Forest - weighted conc.
	Total area	> CL (10 000 µg·m⁻³·h)		> RV (20 000 µg·m⁻³·h)		< 10 000	10 000 - 20 000	20 000 - 30 000	30 000 - 50 000	> 50 000	
	[km²]	[km²]	[%]	[km²]	[%]	µg·m⁻³·h	µg·m⁻³·h	µg·m⁻³·h	µg·m⁻³·h	µg·m⁻³·h	[µg·m⁻³·h]
Albania	7 104	7 104	100.0	7 104	100.0			0.5	92.2	7.3	42 927.2
Andorra	129	129	100.0	129	100.0			10.2	89.8		36 993.4
Austria	36 667	36 667	100.0	36 667	100.0			9.6	89.5	0.9	34 385.3
Belgium	6 089	6 089	100.0	5 352	87.9		12.1	87.9			21 931.0
Bosnia and Herzegovina	23 911	23 911	100.0	23 422	98.0		2.0	80.8	17.1		26 767.6
Bulgaria	34 674	34 674	100.0	34 671	100.0		0.0	50.6	49.4		30 831.6
Croatia	19 734	19 734	100.0	15 354	77.8		22.2	50.1	27.7	0.0	26 113.9
Cyprus	1 458	1 458	100.0	1 458	100.0				89.3	10.7	44 368.6
Czech Republic	25 867	25 867	100.0	25 867	100.0			11.4	88.6		33 242.3
Denmark (incl. Faroe Is.)	3 747	3 747	100.0	108	2.9		97.1	2.9			14 563.7
Estonia	21 078	21 078	100.0	3	0.0		100.0	0.0			12 952.8
Finland	211 647	60 626	28.6			71.4	28.6				9 166.8
France (metropolitan)	143 376	143 376	100.0	125 076	87.2		12.8	49.8	34.6	2.8	28 949.1
Germany	108 031	108 031	100.0	103 056	95.4		4.6	35.5	59.9	0.0	30 179.6
Greece	26 122	26 122	100.0	26 116	100.0		0.0	0.8	87.0	12.2	41 860.9
Hungary	17 407	17 407	100.0	17 364	99.8		0.2	67.1	32.7		27 963.9
Iceland	536	37	6.9			93.1	6.9				7 804.7
Ireland	4 510	487	10.8			89.2	10.8				7 534.1
Italy	79 052	79 052	100.0	79 052	100.0			1.6	83.8	14.5	41 710.0
Latvia	24 256	24 255	100.0	46	0.2	0.0	99.8	0.2			14 161.7
Liechtenstein	79	79	100.0	79	100.0				100.0		38 591.4
Lithuania	19 450	19 450	100.0	2 053	10.6		89.4	10.6			17 618.1
Luxembourg	937	937	100.0	833	88.9		11.1	88.9			23 792.7
Malta	2	2	100.0	2	100.0				86.9	13.1	42 654.7
Monaco	1	1	100.0	1	100.0			40.0	60.0		31 606.5
Montenegro	5 777	5 777	100.0	5 777	100.0			6.4	93.5	0.0	36 934.0
Netherlands	3 118	3 118	100.0	1 155	37.0		63.0	37.0			19 024.9
North Macedonia	8 144	8 144	100.0	8 144	100.0			1.2	57.7	41.1	46 398.5
Norway	103 486	77 544	74.9	4 026	3.9	25.1	71.0	3.9			12 494.1
Poland	96 954	96 954	100.0	87 840	90.6		9.4	66.4	24.2		25 901.3
Portugal (excl. Az., Mad.)	16 512	16 512	100.0	9 706	58.8		41.2	56.8	2.0		20 008.3
Romania	71 264	71 111	99.8	34 466	48.4	0.2	51.4	46.1	2.2		20 239.4
San Marino	6	6	100.0	6	100.0				100.0		35 994.1
Serbia (incl. Kosovo)	27 211	27 211	100.0	27 208	100.0		0.0	26.7	72.9	0.5	34 235.9
Slovakia	20 483	20 483	100.0	20 127	98.3		1.7	59.5	38.8		28 222.9
Slovenia	11 441	11 441	100.0	11 271	98.5		1.5	35.2	63.2	0.1	31 664.4
Spain (excl. Canarias)	107 927	103 419	95.8	88 449	82.0	4.2	13.9	16.8	63.1	2.1	31 203.4
Sweden	261 757	210 038	80.2	45	0.0	19.8	80.2	0.0			11 807.8
Switzerland	11 850	11 850	100.0	11 850	100.0			7.6	83.7	8.7	37 918.8
Turkey	114 856	114 639	99.8	106 800	93.0	0.2	6.8	23.8	55.3	13.9	36 404.4
United Kingdom (& dep.)	20 247	5 014	24.8	1	0.0	75.2	24.8	0.0			8 582.2
Total	**1 696 893**	**1 443 579**	**85.1**	**920 684**	**54.3**	**14.9**	**30.8**	**21.6**	**30.1**	**2.5**	**23 294.0**
Total without Turkey	**1 582 038**	**1 328 940**	**84.0**	**813 884**	**51.4**	**16.0**	**32.6**	**21.5**	**28.3**	**1.7**	**22 343.0**
EU-28	**1 393 765**	**1 167 109**	**83.7**	**726 139**	**52.1**	**16.3**	**31.6**	**22.1**	**28.5**	**1.5**	**22 331.4**
France over 45N	90 007	90 007	100.0	77 519	86.1		13.9	56.5	29.5	0.2	26 764.4
France bellow 45N	53 369	53 369	100.0	47 558	89.1		10.9	38.6	43.3	7.2	32 634.0
Kosovo	4 316	4 316	100.0	4 316	100.0				97.0	3.0	42 599.7
Serbia (without Kosovo)	22 894	22 894	100.0	22 892	100.0		0.0	31.7	68.3		32 659.7
Northern	645 419	416 737	64.6	6 282	1.0	35.4	63.6	1.0			11 368.8
North-western	125 443	105 688	84.3	84 859	67.6	15.7	16.6	46.4	21.2	0.1	22 608.4
Central & eastern	423 276	423 124	100.0	371 987	87.9	0.0	12.1	43.6	44.0	0.3	28 163.2
Southern	502 755	498 030	99.1	457 556	91.0	0.9	8.1	23.5	59.4	8.1	34 638.4

(*) under the UN Security Council Resolution 1244/99.

Note: The percentage value "0.0" indicates that an exposed population exists, but it is small and estimated to be less than 0.05 %. Empty cells mean no population in exposure.

4.4 Ozone – Phytotoxic Ozone Dose (POD)

Ozone is generally recognized to be the most relevant pollutant for plants. Visible injury, reduction in growth, changes in biomass partitioning, or a higher susceptibility to pathogen attack can be the effect of ozone influence (Krupa et al., 2000). Scientific evidence suggests that observed effects of ozone on vegetation are more strongly related to the uptake of ozone through the stomatal leaf pores (stomatal flux) than to the concentration in the atmosphere around the plants (Mills et al., 2011). It is generally accepted that the most severe ozone effects on plants are caused by ozone that is taken up through the stomata into the leaf interior (Reich, 1987; Ashmore et al., 2004).

The cumulative stomatal ozone fluxes (F_{sto}) through the stomata of leaves found at the top of the canopy are calculated over the course of the growing season based on ambient ozone concentration and stomatal conductance (g_{sto}) to ozone. The stomatal conductance has been calculated using a multiplicative stomatal conductance model (Emberson et al., 2000) based on Jarvis (1976) as a function of species-specific maximum g_{sto} (expressed on a single leaf-area basis), phenology, and prevailing environmental conditions (photosynthetic photon flux density, PPFD), air temperature, vapour pressure deficit (VPD), and soil moisture.

POD_Y (Phytotoxic Ozone Dose) is the accumulated plant uptake (flux) of ozone above a threshold of Y during a specified time or growth period. The flux-based POD_Y metrics are preferred in risk assessment over the concentration-based AOT40 exposure index. AOT40 accounts for the atmospheric ozone concentration above the leaf surface and is therefore biologically less relevant for ozone impact assessment than POD_Y as it does not take into account how ozone uptake is affected by climate, soil and plant factors.

Several POD_Y indicators are described in CLRTAP (2017a). POD_YSPEC is a species or group of species-specific POD_Y that requires comprehensive input data and is suitable for detailed risk assessment. POD_YIAM is a vegetation-type specific POD_Y that requires less input data and is suitable for large-scale modelling, including integrated assessment modelling. POD_YSPEC is further used in this report.

For the wheat as for other crop species including potato and tomato, the Y value is taken equal to 6 nmol m^{-2} PLA s^{-1} (i.e. per unit projected leaf area). For the details of POD_Y (and specifically POD_6SPEC as used in this report) calculation, see Annex 1, Section A1.3.

The species-specific flux models and associated response functions and critical levels for ozone-sensitive crops and cultivars can be used to quantify the potential negative impacts of O_3 on the security of food supplies at the local and regional scale. They can be used to estimate yield losses, including economic losses. A flux-threshold Y of 6 (POD_6SPEC) provides the strongest flux-effect relationships for crops (Pleijel et al., 2007). O_3 effects proved to be significant at a 5 % reduction of the effect parameter (Mills et al., 2011), hence Critical Levels (CL) were determined for this 5 % reduction of the effect parameter (i.e. yield, weight or quality of grain, tuber or fruit), based on the slope of the relationship. The POD_6SPEC Critical Levels (CL) for crops were determined based on this reduction of relevant yield or weight, as shown in Table 4.6.

Wheat, potato and tomato are considered as representative species of crops in Europe (tomato can be regarded as representative horticultural crop for the Mediterranean and Black Sea regions, while potato for other regions). Therefore, POD_6SPEC for these crops (labelled further simply as POD_6 for wheat, potato and tomato, respectively) are recommended for regular map construction. This report presents maps of POD_6 for wheat (*Triticum aestivum*), potato (*Solanum tuberosum*) and tomato (*Solanum lycopersicum*).

Table 4.6: POD_6SPEC Critical Levels for crops as determined by CLRTAP

Crop	Effect parameter	POD_6SPEC Critical Level
Wheat	grain yield	1.3 $mmol.m^{-2}$ PLA
Wheat	1000-grain weight	1.5 $mmol.m^{-2}$ PLA
Wheat	protein yield	2.0 $mmol.m^{-2}$ PLA
Potato	tuber yield	3.8 $mmol.m^{-2}$ PLA
Tomato	fruit yield	2 $mmol.m^{-2}$ PLA
Tomato	fruit quality	3.8 $mmol.m^{-2}$ PLA

Source: CLRTAP, 2017a.

4.4.1 Phytotoxic Ozone Dose maps

The POD maps have been calculated based on the hourly ozone maps, together with the meteorological and soil hydraulic properties data, based on the methodology described in Annex 1, Section A1.3. The calculation has been executed in 0.1° x 0.1° resolution. The hourly ozone maps are created for rural areas only, based on rural background stations. The POD maps are therefore applicable to rural areas only. Next to this, it should be noted that in the POD calculations for wheat and potato, all growing areas are considered rain-fed (i.e. without irrigation), see Colette et al. (2018). Thus, the maps are directly applicable only for areas without irrigation. If applied for irrigated areas, the POD values for wheat and potato might be somewhat underestimated. On the other hand, no limitation of stomatal conductance due to soil moisture can be assumed for tomato, since it is an irrigated horticultural crop (see Annex 1, Section A1.3).
The hourly ozone maps needed for POD calculation have been calculated at the 2x2 km^2 resolution, based on rural background measurements. The maps for each hour of the year 2019 have been constructed using the same methodology like the annual maps, i.e. the multiple linear regression followed by the kriging of its residuals (see Annex 1, Section A1.1) based on the measurement data, EMEP model output, altitude and the surface solar radiation. For details, see Annex 3, Section A3.3.

Maps 4.6 to 4.8 present the final map of Phytotoxic Ozone Dose (POD_6) for wheat, potato and tomato in 2019. High values of the POD_6 can be found in different parts of Europe since the POD_6 is dependent not only on ozone levels but also on the environmental conditions and plant phenology. On the other hand, the lowest levels of the POD_6 usually occur in areas with lower ozone concentrations (e.g. northern European regions) and/or in areas where environmental conditions limit the ozone stomatal conductance (dry and warm areas, including parts of the southern, south-western and south-eastern Europe).

The areas in the Map 4.6 with POD_6 values above the Critical Level (CL) for protein yield of wheat (i.e. 2 $mmol.m^{-2}$ PLA) are marked in orange, red and dark red. The areas with POD_6 values below the CL for grain yield of wheat (i.e. 1.3 $mmol.m^{-2}$ PLA) are marked in green and dark green. The areas with POD_6 values in between CLs for grain yield and 1000-grain weight and in between CLs for 1000-grain weight and protein yield are marked in yellow and dark yellow, respectively. All these CLs were exceeded in large areas of central Europe and Denmark, western part of France, in most of Portugal, Italy and Greece and parts of Spain, the Balkan area and Turkey.

The highest levels of the POD_6 for wheat in 2019 are found in the south-western and southern Europe. Nevertheless, high values of the POD_6 for wheat have been found also in other European areas (e.g. central Europe, namely Czechia and Czech-Polish border in 2019). Low values of POD_6 for wheat in some areas in the south of Europe (i.e. with high ozone values, but limited ozone stomatal conductance) are in agreement with findings of Colette et al. (2018).

Map 4.7 presents the final map of POD_6 for potato in 2019. The areas with POD_6 values above the Critical Level (CL) for tuber yield of potato (i.e. 3.8 mmol.m^{-2} PLA) are marked in yellow, dark yellow, orange, red and dark red. Most of Europe showed values of POD_6 for potato above this CL in 2019. The highest POD_6 levels are found in the central European region, the Baltic States, France and parts of Italy. On the other hand, the lowest levels of the POD_6 for potato in 2019 are found in northern Europe with the exception of Denmark, the United Kingdom, Ireland, parts of Switzerland and Austria and parts of southern, south-western and south-eastern European regions.

Map 4.8 presents the final map of POD_6 for tomato in 2019. The areas with POD_6 values above the Critical Level (CL) for fruit yield are marked in red and dark red, the areas with POD_6 values above the Critical Level (CL) for fruit quality in dark red. The Modelling and Mapping Manual (CLRTAP, 2017a) defines the parameterization for tomato for the Mediterranean area. EU27 agriculture statistics show that ca 70 % of tomato in 2020 was produced in Italy, Spain, Portugal and Greece (EC, 2021). In the colder regions of Europe, tomato would be mostly grown in greenhouses. Most of the Mediterranean areas showed the values of POD_6 for tomato below these CLs in 2019. Only in very small parts of the coastal areas POD_6 values above CL have occurred.

For the purpose of completeness, the POD_6 has been modelled even for non-Mediterrranean areas using the same parameterization (lighter colours in the Map 4.8).

Map 4.6: Phytotoxic Ozone Dose (POD_6) for wheat, rural map, 2019

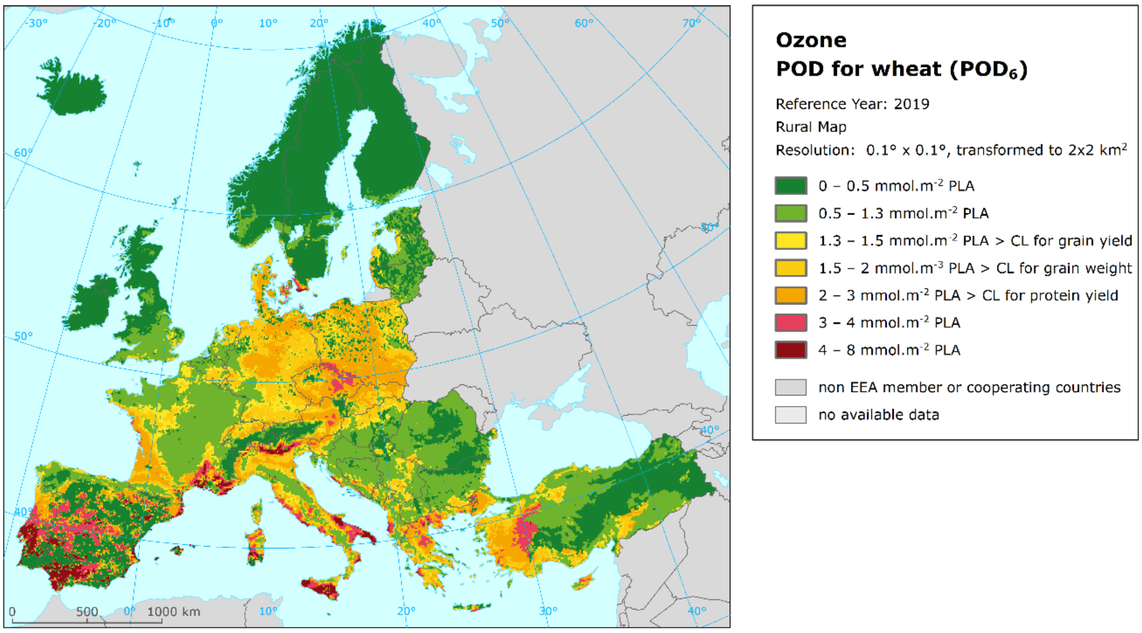

Map 4.7: Phytotoxic Ozone Dose (POD_6) for potato, rural map, 2019

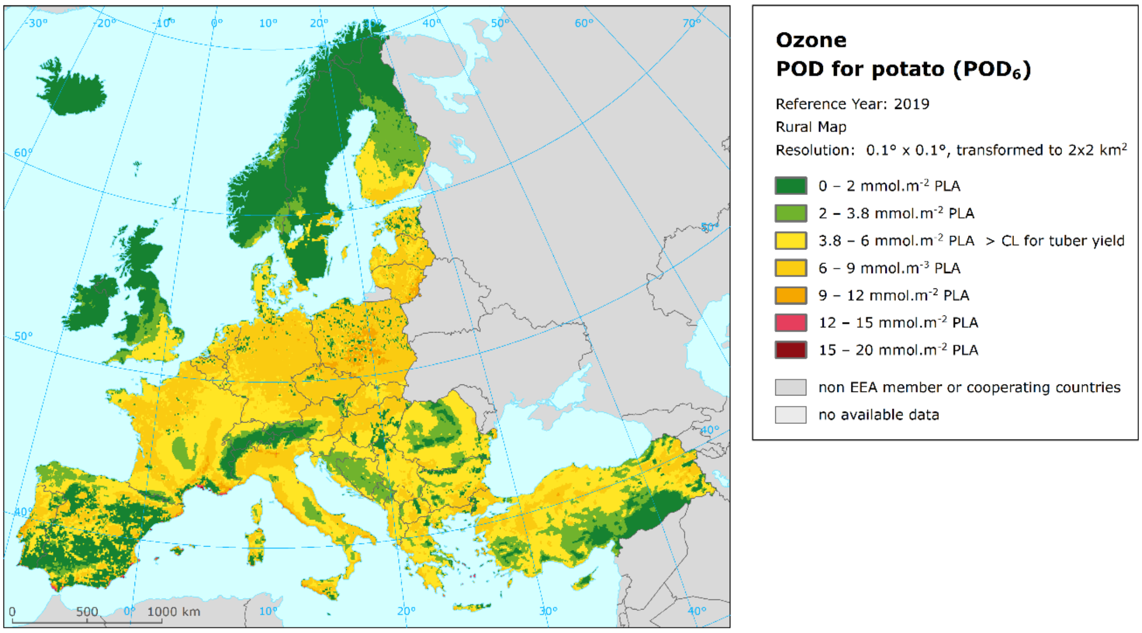

Map 4.8: Phytotoxic Ozone Dose (POD_6) for tomato, rural map, 2019

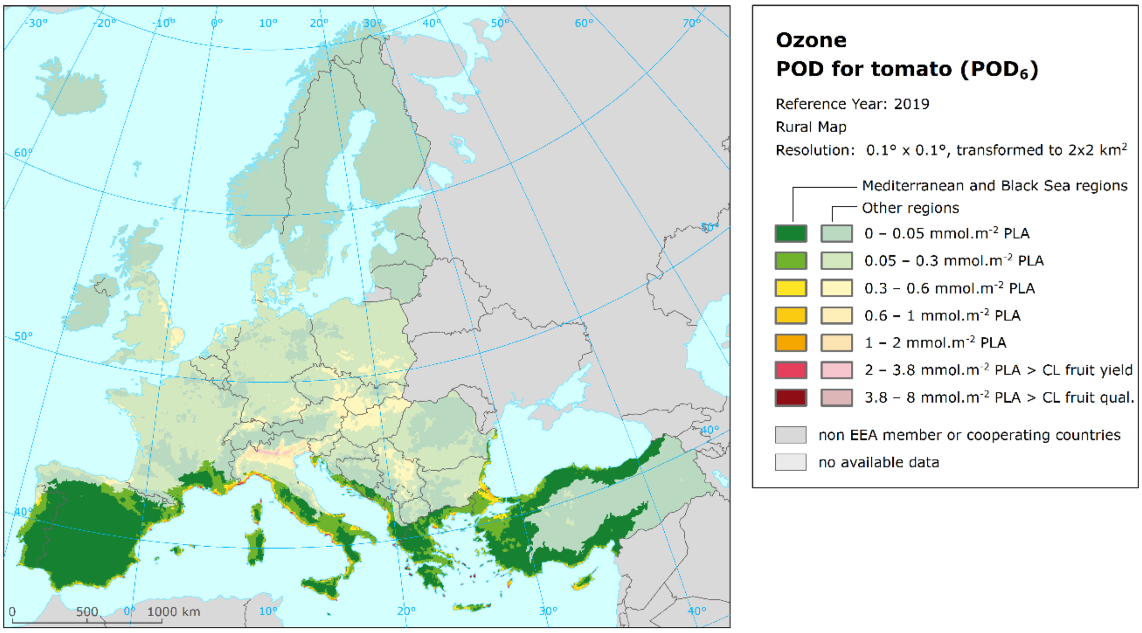

5 NO_2 and NO_x

Annual average maps for NO_2 (related to protection of human health) and for NO_x (related to protection of vegetation) have been produced and presented in the regular mapping report since the maps for year 2014.

The methodology for creating the concentration maps follows the same principle as for the rest of pollutants: a linear regression model on the basis of European wide station measurement data, followed by kriging of the residuals produced from that regression model (residual kriging).

The map on NO_2 is based on an improved mapping methodology developed in Horálek et al. (2017b, 2018). The map layers are created for the rural, urban background and urban traffic areas separately on a grid at 1x1 km^2 resolution. Subsequently, the urban background and urban traffic map layers are merged using the gridded road data into one urban map layer. This urban map layer is further combined with the rural map layer into the final NO_2 map using a population density grid at 1x1 km^2 resolution. This final combined map is presented in this 1x1 km^2 grid resolution.

The map of the vegetation-related indicator NO_x annual average is created on a grid at 2x2 km^2 resolution, based on rural background measurements only, as vegetation is considered not to be extensively present at urban and suburban areas. Hence, this map is applicable to rural areas only. The resolution is chosen equally to the one of the vegetation indicator for ozone.

Annex 3 provides details on the regression and kriging parameters applied for deriving the maps, as well as the uncertainty analysis of the maps.

5.1 NO_2 – Annual mean

5.1.1 Concentration maps

The Air Quality Directive (EC, 2008) sets two limit values (LV) for NO_2 for the human health protection. The first one is an annual LV (ALV) at the level of 40 $\mu g \cdot m^{-3}$. This is the same concentration level as recommended by the World Health Organization for the NO_2 annual average as the 2005 Air Quality Guideline level (WHO, 2005). The second one is an hourly LV (HLV, 200 $\mu g \cdot m^{-3}$ not to be exceeded on more than 18 hours per year). Concentrations above the HLV were observed in 0.3 % (11 stations) of all reporting stations only, mostly at urban traffic stations; they were observed in five countries (number stations): Turkey (seven), Bosnia and Herzegovina (one), Kosovo (one), Spain (one) and United Kingdom (one), see Targa et al. (2021). In view of this low number of exceedances, the short-term LV has not been included in the mapping procedures.

Map 5.1 presents the final combined concentration 1x1 km^2 gridded map for the 2019 NO_2 annual average as the result of interpolation and merging of the separate maps as described in Annex 1.

Supplementary data used in the linear regression are in principle the same as described in Horálek et al. (2017b). For rural areas they consist of EMEP model output, altitude, Sentinel-5P satellite data, wind speed, population density and land cover indicators; for urban background areas these are EMEP model output, altitude, Sentinel-5P satellite data, wind speed, population density and land cover indicators; for traffic areas the EMEP model output, altitude, and Sentinel-5P satellite data are used (Annex 3, Section A3.4).

According to Map 5.1, the areas where the ALV of 40 $\mu g \cdot m^{-3}$ was exceeded include urbanized parts of some large cities, particularly Milan, Naples, Rome, Turin, Paris, Barcelona, Madrid, London, Athens, Bucharest, Ankara, Istanbul, and some other smaller cities in Turkey. Some other cities show NO_2 levels above 30 $\mu g \cdot m^{-3}$, e.g., in Germany, Italy, the Netherlands, Belgium, United Kingdom, Turkey. Most of the European area shows NO_2 levels below 20 $\mu g \cdot m^{-3}$, with most of the rural areas below 10 $\mu g \cdot m^{-3}$. Some larger areas above 20 $\mu g \cdot m^{-3}$ can be found in the Po Valley, the Benelux, the German Ruhr region, in central and southern England, in the Île de France region and around Rome.

It should be noted that the interpolated map is created at 1x1 km^2 only. Although the urban traffic map layer is used in the map creation, the traffic locations are smoothed in the 1x1 km^2 resolution. Thus, the maps as such refers to the rural and urban background situations only, while the exceedances of the NO_2 limit values occur mostly at local hotspots such as dense traffic locations and densely urbanised and industrialised areas. Such exceedances are mostly not visible in the 1x1 km^2 map. The relative mean uncertainty of the NO_2 annual average map is 31 % for rural, 27 % for urban background and 24 % for urban traffic areas (Annex 3, Section A3.4).

For the comparison with five-year average 2014-2018 values, see Annex 4, Section A4.4.

In order to provide more complete information of the air quality across Europe, the final combined map including the measurement data at stations is presented in Map A5.9 of Annex 5.

Map 5.1: Concentration map of NO_2 annual average, 2019

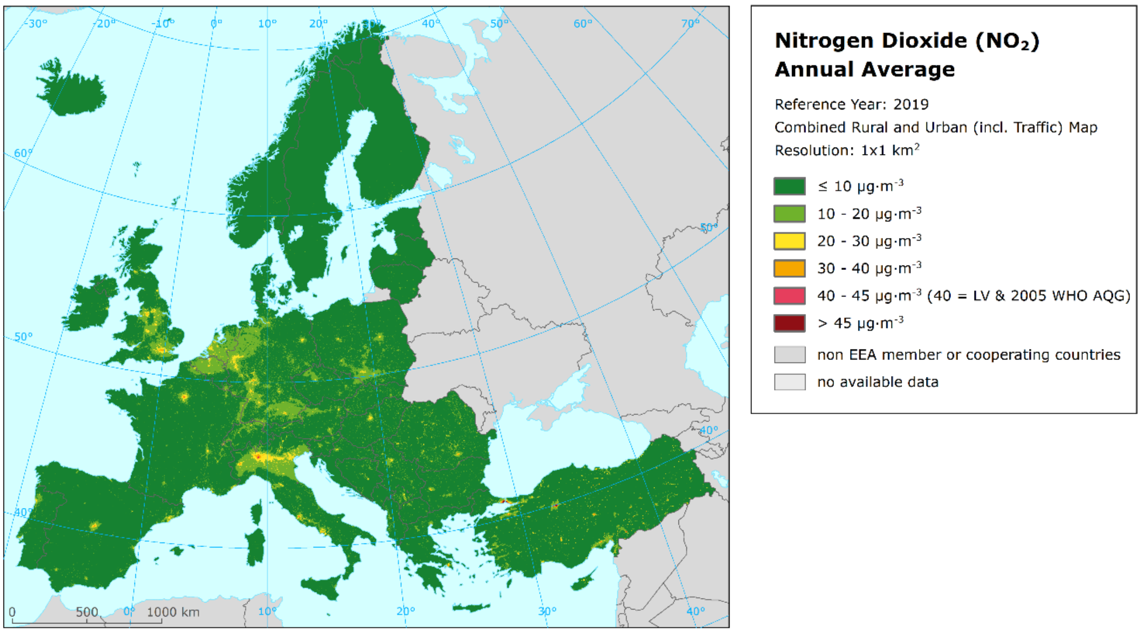

5.1.2 Population exposure

Table 5.1 and Figure 5.1 give the population frequency distribution for a limited number of exposure classes calculated on a grid of 1x1 km^2 resolution. Table 5.1 also presents the population-weighted concentration for individual countries, for EU-28 and for the whole mapping area according to Equation A1.7 of Annex 1.

The human exposure to NO_2 has been calculated based on the improved methodology as developed in Horálek et al. (2017b). The population exposure has been calculated according to Equation A1.6 of Annex 1, i.e. it has been calculated separately for urban areas directly influenced by traffic and for the background (both rural and urban) areas, in order to better reflect the population exposed to traffic. Based on this, the different concentration levels in urban background and traffic areas inside the 1x1 km^2 grid cells are taken into account.

Table 5.1: Population exposure and population-weighted concentration, NO_2 annual average 2019

<table>
<tr><th rowspan="2">Country</th><th rowspan="2">ISO</th><th rowspan="2">Population [inhbs·1000]</th><th colspan="6">NO_2 – annual average, exposed population, 2019 [%]</th><th>NO_2 ann. avg.</th></tr>
<tr><th>< 10</th><th>10 - 20</th><th>20 - 30</th><th>30 - 40</th><th>40 - 45</th><th>> 45</th><th>Pop. weighted</th></tr>
<tr><td>Albania</td><td>AL</td><td>2 797</td><td>24.5</td><td>50.7</td><td>23.2</td><td>1.5</td><td></td><td></td><td>15.2</td></tr>
<tr><td>Andorra</td><td>AD</td><td>84</td><td>1.7</td><td>39.8</td><td>58.5</td><td></td><td></td><td></td><td>20.0</td></tr>
<tr><td>Austria</td><td>AT</td><td>8 381</td><td>19.0</td><td>52.8</td><td>24.9</td><td>3.4</td><td></td><td></td><td>16.4</td></tr>
<tr><td>Belgium</td><td>BE</td><td>10 944</td><td>3.9</td><td>66.6</td><td>25.3</td><td>4.2</td><td>0.0</td><td></td><td>18.5</td></tr>
<tr><td>Bosnia and Herzegovina</td><td>BA</td><td>3 802</td><td>27.9</td><td>56.7</td><td>14.8</td><td>0.7</td><td></td><td></td><td>14.3</td></tr>
<tr><td>Bulgaria</td><td>BG</td><td>7 363</td><td>13.5</td><td>52.6</td><td>25.9</td><td>8.1</td><td></td><td></td><td>18.6</td></tr>
<tr><td>Croatia</td><td>HR</td><td>4 288</td><td>29.6</td><td>51.2</td><td>18.1</td><td>1.0</td><td></td><td></td><td>14.2</td></tr>
<tr><td>Cyprus</td><td>CY</td><td>1 018</td><td>13.1</td><td>22.1</td><td>56.4</td><td>8.4</td><td></td><td></td><td>20.9</td></tr>
<tr><td>Czechia</td><td>CZ</td><td>10 423</td><td>20.9</td><td>64.8</td><td>13.1</td><td>1.2</td><td></td><td></td><td>14.2</td></tr>
<tr><td>Denmark (incl. Faroe Islands)</td><td>DK</td><td>5 577</td><td>61.6</td><td>36.5</td><td>2.0</td><td></td><td></td><td></td><td>9.0</td></tr>
<tr><td>Estonia</td><td>EE</td><td>1 291</td><td>68.2</td><td>31.8</td><td></td><td></td><td></td><td></td><td>7.5</td></tr>
<tr><td>Finland</td><td>FI</td><td>5 339</td><td>68.3</td><td>29.6</td><td>2.1</td><td></td><td></td><td></td><td>8.2</td></tr>
<tr><td>France (metropolitan)</td><td>FR</td><td>62 744</td><td>32.9</td><td>43.5</td><td>16.1</td><td>4.7</td><td>1.5</td><td>1.2</td><td>15.2</td></tr>
<tr><td>Germany</td><td>DE</td><td>80 174</td><td>9.9</td><td>61.0</td><td>24.2</td><td>4.1</td><td>0.6</td><td>0.1</td><td>17.5</td></tr>
<tr><td>Greece</td><td>GR</td><td>10 634</td><td>23.2</td><td>35.6</td><td>22.4</td><td>16.2</td><td>0.9</td><td>1.8</td><td>19.0</td></tr>
<tr><td>Hungary</td><td>HU</td><td>9 937</td><td>14.4</td><td>63.0</td><td>18.2</td><td>4.1</td><td>0.3</td><td></td><td>16.6</td></tr>
<tr><td>Iceland</td><td>IS</td><td>318</td><td>27.7</td><td>66.7</td><td>5.6</td><td></td><td></td><td></td><td>11.0</td></tr>
<tr><td>Ireland</td><td>IE</td><td>4 574</td><td>51.7</td><td>38.8</td><td>7.9</td><td>1.6</td><td></td><td></td><td>10.5</td></tr>
<tr><td>Italy</td><td>IT</td><td>59 409</td><td>12.1</td><td>41.6</td><td>33.3</td><td>9.8</td><td>2.2</td><td>1.0</td><td>20.0</td></tr>
<tr><td>Latvia</td><td>LV</td><td>2 080</td><td>51.8</td><td>45.8</td><td>2.4</td><td></td><td></td><td></td><td>10.4</td></tr>
<tr><td>Liechtenstein</td><td>LI</td><td>34</td><td>1.6</td><td>97.3</td><td>0.2</td><td>0.9</td><td></td><td></td><td>16.5</td></tr>
<tr><td>Lithuania</td><td>LT</td><td>3 028</td><td>40.5</td><td>55.2</td><td>4.3</td><td></td><td></td><td></td><td>11.0</td></tr>
<tr><td>Luxembourg</td><td>LU</td><td>511</td><td>8.5</td><td>57.8</td><td>26.3</td><td>7.3</td><td></td><td></td><td>18.4</td></tr>
<tr><td>Malta</td><td>MT</td><td>417</td><td>44.9</td><td>44.9</td><td>10.2</td><td></td><td></td><td></td><td>11.5</td></tr>
<tr><td>Monaco</td><td>MC</td><td>33</td><td></td><td>4.7</td><td>95.3</td><td></td><td></td><td></td><td>23.9</td></tr>
<tr><td>Montenegro</td><td>ME</td><td>620</td><td>23.7</td><td>58.7</td><td>17.7</td><td></td><td></td><td></td><td>14.9</td></tr>
<tr><td>Netherlands</td><td>NL</td><td>16 600</td><td>2.6</td><td>55.5</td><td>40.2</td><td>1.7</td><td></td><td></td><td>19.1</td></tr>
<tr><td>North Macedonia</td><td>MK</td><td>2 061</td><td>4.4</td><td>65.3</td><td>27.9</td><td>2.3</td><td></td><td></td><td>18.0</td></tr>
<tr><td>Norway</td><td>NO</td><td>4 906</td><td>59.3</td><td>32.5</td><td>7.6</td><td>0.5</td><td></td><td></td><td>9.6</td></tr>
<tr><td>Poland</td><td>PL</td><td>38 494</td><td>28.6</td><td>54.7</td><td>15.4</td><td>0.9</td><td>0.4</td><td>0.0</td><td>14.2</td></tr>
<tr><td>Portugal (excl. Azores, Madeira)</td><td>PT</td><td>10 047</td><td>26.6</td><td>50.5</td><td>20.6</td><td>2.3</td><td></td><td></td><td>14.9</td></tr>
<tr><td>Romania</td><td>RO</td><td>20 138</td><td>14.4</td><td>43.9</td><td>29.7</td><td>10.3</td><td>0.9</td><td>0.9</td><td>19.5</td></tr>
<tr><td>San Marino</td><td>SM</td><td>32</td><td>5.1</td><td>90.2</td><td>0.1</td><td>4.5</td><td></td><td></td><td>15.8</td></tr>
<tr><td>Serbia (incl. Kosovo*)</td><td>RS</td><td>8 896</td><td>13.9</td><td>50.8</td><td>33.8</td><td>1.5</td><td>0.0</td><td></td><td>17.9</td></tr>
<tr><td>Slovakia</td><td>SK</td><td>5 399</td><td>19.3</td><td>74.7</td><td>5.5</td><td>0.5</td><td></td><td></td><td>13.5</td></tr>
<tr><td>Slovenia</td><td>SI</td><td>2 042</td><td>29.6</td><td>53.5</td><td>16.9</td><td></td><td></td><td></td><td>14.3</td></tr>
<tr><td>Spain (excl. Canarias)</td><td>ES</td><td>44 722</td><td>16.1</td><td>47.9</td><td>22.7</td><td>10.8</td><td>2.3</td><td>0.1</td><td>18.6</td></tr>
<tr><td>Sweden</td><td>SE</td><td>9 539</td><td>73.7</td><td>24.7</td><td>1.6</td><td></td><td></td><td></td><td>8.0</td></tr>
<tr><td>Switzerland</td><td>CH</td><td>7 893</td><td>7.5</td><td>75.0</td><td>12.6</td><td>4.8</td><td></td><td></td><td>16.7</td></tr>
<tr><td>Turkey</td><td>TR</td><td>71 920</td><td>24.1</td><td>14.2</td><td>22.7</td><td>19.4</td><td>6.8</td><td>12.7</td><td>25.6</td></tr>
<tr><td>United Kingdom (& Crown dep.)</td><td>UK</td><td>63 415</td><td>9.2</td><td>53.2</td><td>30.7</td><td>6.0</td><td>0.6</td><td>0.4</td><td>18.7</td></tr>
<tr><td rowspan="2">Total</td><td rowspan="2"></td><td rowspan="2">601 926</td><td>20.3</td><td>46.4</td><td rowspan="2">22.9</td><td rowspan="2">7.0</td><td>1.6</td><td>1.9</td><td rowspan="2">17.9</td></tr>
<tr><td colspan="2">66.7</td><td colspan="2">3.4</td></tr>
<tr><td rowspan="2">Total without Turkey</td><td rowspan="2"></td><td rowspan="2">530 007</td><td>19.8</td><td>50.8</td><td rowspan="2">22.9</td><td rowspan="2">5.3</td><td>0.9</td><td>0.4</td><td rowspan="2">16.8</td></tr>
<tr><td colspan="2">70.5</td><td colspan="2">1.3</td></tr>
<tr><td rowspan="2">EU-28</td><td rowspan="2"></td><td rowspan="2">498 253</td><td>19.6</td><td>50.5</td><td rowspan="2">23.1</td><td rowspan="2">5.5</td><td>0.9</td><td>0.4</td><td rowspan="2">16.9</td></tr>
<tr><td colspan="2">70.1</td><td colspan="2">1.3</td></tr>
<tr><td>Kosovo*</td><td>KS</td><td>1 748</td><td>13.6</td><td>51.5</td><td>33.8</td><td>1.0</td><td></td><td></td><td>17.5</td></tr>
<tr><td>Serbia (excl. Kosovo*)</td><td>RS-</td><td>7 148</td><td>13.9</td><td>50.7</td><td>33.8</td><td>1.6</td><td>0.0</td><td></td><td>18.0</td></tr>
</table>

(*) under the UN Security Council Resolution 1244/99.

Note: The percentage value "0.0" indicates that an exposed population exists, but it is small and estimated to be less than 0.05 %. Empty cells mean no population in exposure.

Thus – like for PM_{10} and $PM_{2.5}$ – the population exposure refers not only to the rural and urban background areas, but to the urban traffic locations as well. However, it should be mentioned that only population density data at 1x1 km^2 resolution has been used. This means that contrary to the concentration levels, the population density is constant within each 1x1 km^2 grid cell. This shortcoming can increase the uncertainty of the population exposure results.

It has been estimated that in 2019 about 3 % of the considered European population including Turkey and about 1 % of both the considered European population without Turkey and the EU-28 population lived in areas with NO_2 annual average concentrations above the EU limit value of 40 $\mu g \cdot m^{-3}$.

The population-weighted concentration of the NO_2 annual average for 2019 has been estimated to be about 18 $\mu g \cdot m^{-3}$ and 17 $\mu g \cdot m^{-3}$ for the total considered European and EU-28 only population, respectively, being this last value the same also for the total considered European population without Turkey, which means a decrease of almost 2 $\mu g \cdot m^{-3}$ compared to the previous five-year mean (Annex 4, Section A4.4).

Figure 5.1: Percentage of the population (%) exposed to NO_2 annual average ($\mu g \cdot m^{-3}$), 2019

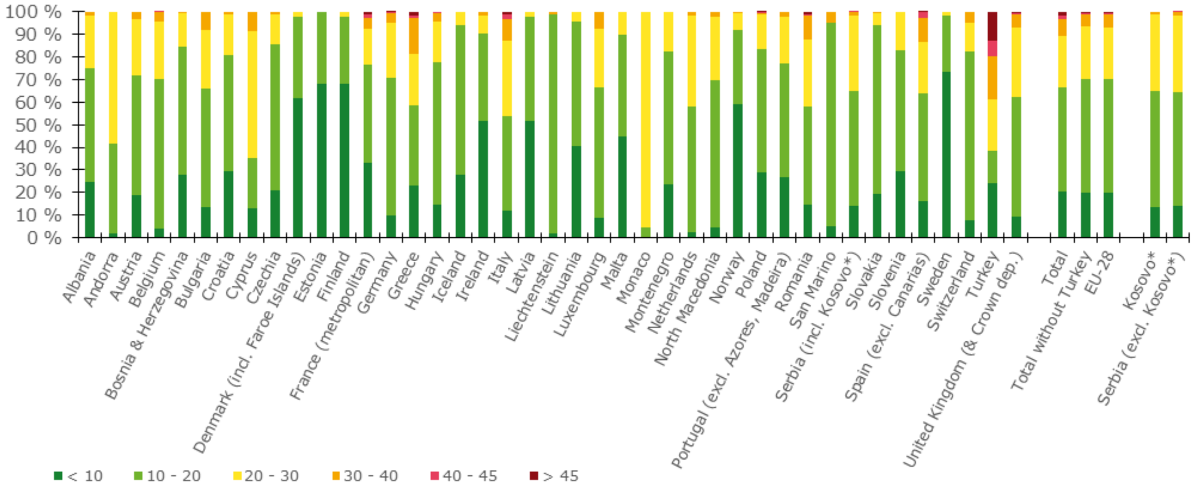

(*) under the UN Security Council Resolution 1244/99.

Figure 5.2 shows, for the whole mapped area, the population frequency distribution for exposure classes of 1 $\mu g \cdot m^{-3}$. One can see the highest population frequency for classes between 10 and 20 $\mu g \cdot m^{-3}$, continuous decline of population frequency for classes between 21 and 30 $\mu g \cdot m^{-3}$ and continuous mild decline of population frequency for classes between 31 and 60 $\mu g \cdot m^{-3}$.

Figure 5.2: Population frequency distribution, NO_2 annual average, 2019. The annual limit value and the 2005 WHO AQG level (40 µg·m^{-3} in both cases) are marked by the red line.

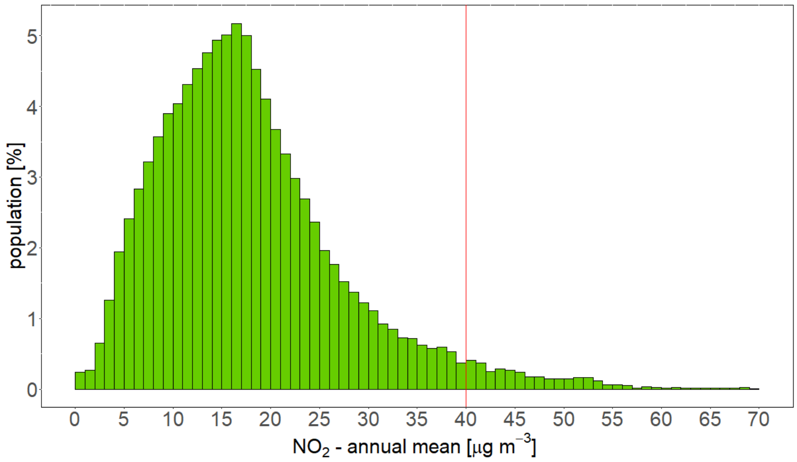

5.2 NO_x – Annual mean

5.2.1 Concentration maps

The Air Quality Directive (EC, 2008) sets a Critical Level (CL) for the protection of vegetation for the NO_x annual mean at 30 µg·m^{-3}. According to this directive, the sampling points targeted at the protection of vegetation and natural ecosystems shall be in general sited more than 20 km away from agglomerations or more than 5 km away from other built-up areas. Thus, only the observations at rural background stations are used for the NO_x mapping and the resulting map is representative for rural areas only.

The number of NO_x measurement stations is limited. The mapping of the NO_x annual average has been therefore performed on the basis of an approach presented in Horálek et al. (2007). This approach derives additional pseudo NO_x annual mean concentrations from NO_2 annual mean measurement concentrations and increases as such the number and spatial coverage of NO_x 'data points', and applies these data to the NO_x mapping. Section A1.1 of Annex 1 provides some details.

Map 5.2 presents the concentration map of NO_x annual average. It concerns rural areas only, representing an indicator for vegetation exposure to NO_x. The relative mean uncertainty of this rural map is 42 %.

Most of the European area shows NO_x levels below 20 µg·m^{-3}. However, in the Po Valley, southern part of the Netherlands, northern Belgium, the German Ruhr region and around some larger European cities (typically being the national capitals) elevated NO_x concentrations above the Critical Level (CL) are observed. Furthermore, around many larger European cities concentrations just below the CL are observed. These concentrations are expected to be the result of large emissions from transport in and around the cities, as well as energy production and industrial facilities taking place at these areas. This is relevant only for so called peri-urban vegetation where patches of agricultural land and of natural or planted vegetation can be found. On the contrary, low concentrations (below 10 µg·m^{-3}) are observed in large areas of Spain, France, Italy, Croatia, Bosnia and Herzegovina, Montenegro, Hungary, Scandinavia, Iceland, Ireland and the Baltic States.

For the comparison with five-year average 2014-2018 values, see Annex 4, Section A4.4.

The NO_x annual average rural map including the data measured at rural background stations is presented in Map A5.10 of Annex 5. The map illustrates the lack of the NO_x rural stations in the Balkan area.

Map 5.2: Concentration map of NO_x annual average, rural map, 2019

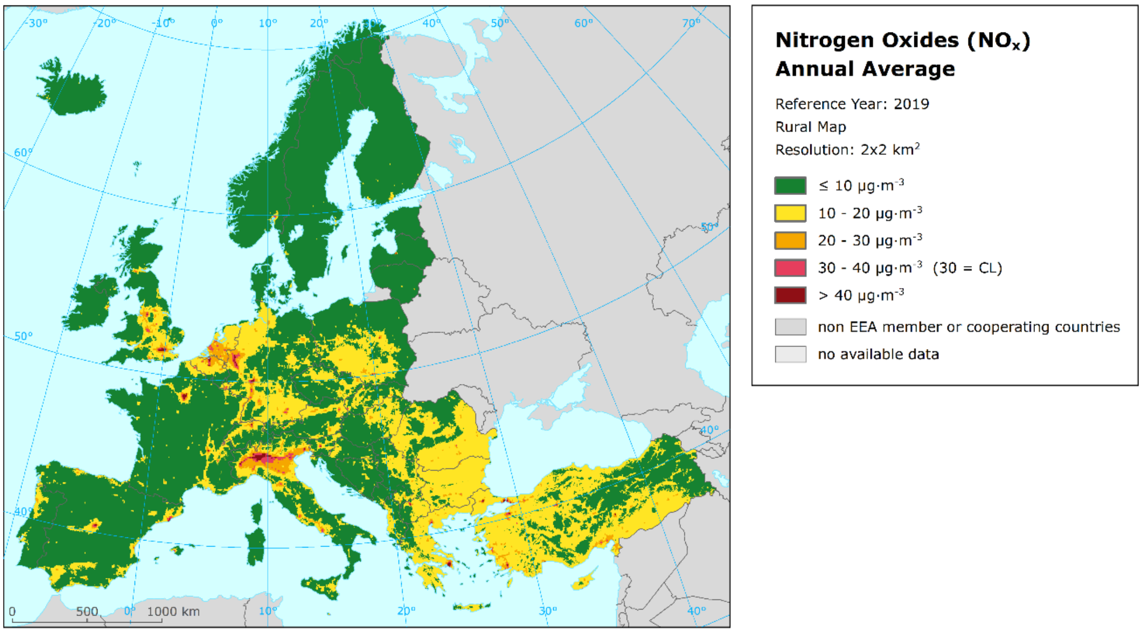

Vegetation exposure has not been calculated for NO_x, as the Critical Level (CL) applies actually to vegetation only, which is by nature mostly allocated in rural areas where there has been limited CL exceedance observed. Therefore, the vegetation exposure exceedance would occur in limited vegetation areas only and, as such, is considered not to provide essential information from the European scale perspective. Furthermore, contrary to vegetation exposure to high ozone concentrations in Europe that leads to considerable damage, vegetation exposure to NO_x pollution is of minor importance in terms of actual impacts. On the other hand, NO_x concentrations contribute in part to the total N-deposition, which leads to acidifying and eutrophying effects on vegetation. These effects, especially eutrophication, are still very important in Europe (e.g. EMEP, 2020). However, these effects on vegetation cannot be expressed by an exposure to NO_x as many oxidized and reduced nitrogen compounds contribute to total atmospheric nitrogen deposition.

Concerning the potential exposure estimate of vegetation and natural ecosystems to NO_x there is an additional dilemma: which receptor types should be selected to estimate the exposure and Critical Level exceedance of vegetation and natural ecosystems? An option would be the use of CLC classes (e.g. like in Horálek et al., 2008); nevertheless this classification is too general. Another option would be the NATURA 2000 database. However, that data source contains a wide series of receptor types, species and classes. Serious additional efforts would be needed to conclude on the most relevant set of receptors from the NATURA 2000 geographical database.

6 Exposure trend estimates

This report has presented the interpolated maps for 2019 on the PM_{10}, $PM_{2.5}$, ozone and NO_2 human health related air pollution indicators (annual average and the 90.4 percentile of PM_{10} daily means, annual average for $PM_{2.5}$, the 93.2 percentile of maximum daily 8-hour means, SOMO35 and SOMO10 for ozone, and the annual average for NO_2), together with tables showing the frequency distribution of the estimated population exposures and exceedances per country, EU-28 and the total mapping area.

Furthermore, interpolated maps of ozone and NO_x vegetation related air pollution indicators have been produced. More specifically, these include a map of the ozone indicator AOT40 for vegetation and AOT40 for forests, and tables with the frequency distribution of estimated land area exposures and exceedances per country, EU-28 and the total mapping area. In addition, the maps of the Phytotoxic Ozone Dose (POD) for wheat, potato and tomato, and the NO_x annual average map have been produced, but without exposure estimates.

A mapping approach similar to previous years (Horálek et al., 2021 and references therein) based primarily on observational data has been used. With the interpolated air pollution maps and exposure estimates for the year 2019 completed, a fifteen-year overview of comparable exposure estimates has been obtained (with full time series coverage for PM_{10} and ozone, except SOMO10 and POD indicators, with one year missing for $PM_{2.5}$ and with four years missing for NO_2). In this chapter these multi-annual overviews of exposure estimates are provided for each of the indicators of PM_{10}, $PM_{2.5}$ and ozone (except SOMO10 and POD), including a trend analysis.

For the previous years, mapping results as presented in Horálek et al. (2021) and previous mapping reports have been used. Since 2017, PM_{10} and $PM_{2.5}$ maps have been prepared based on the updated method (Horálek et al., 2019). For comparability reasons, results for 2015-2018 (and partly also for 2005 and 2009) are presented in two variants for these pollutants, i.e. based on the old and the updated methodologies.

For the human health indicators, the exposure estimates are expressed, on one hand, as population-weighted concentration and, on the other hand, as percentage of population exposed to concentrations above the limit/target value. For the vegetation related indicators, the exposure estimates are expressed as the agricultural- and forest-weighted concentrations, as well as the agricultural or forest areas exposed to concentrations above defined thresholds.

It should be noted that the percentage of population, agricultural area, or forest area exposed is a less robust indicator compared to the population-weighted, agricultural-weighted, or forest-weighted concentration, as a small concentration increase (or decrease) may lead to a major increase (or decrease) of population, agricultural or forest area exposed. This is not the case when taking the population-weighted or agricultural/forest-weighted concentration as indicator. Therefore, the trend analysis is done based on the population-weighted, agricultural-weighted and forest-weighted concentrations only.

When thinking about a trend, the following should be taken into account: (i) the meteorologically induced variations, (ii) the uncertainties involved in the interpolation (Annex 3), and (iii) the year-to-year variation of the station density and their spatial distribution, which induce a variation in interpolated maps from year to year. In addition, one should be aware of the fact that different trends in various parts of Europe may occur. However, bearing in mind these limitations here a trend analysis is provided for the period 2005-2019 on the population-, agricultural- and forest-weighted concentrations for the total mapping area.

For comparability reasons, in this chapter the results for the total mapped area without Turkey are presented, because 2016 was the first year for which the area of Turkey was mapped.

6.1 Human health PM_{10} indicators

Table 6.1 summarises the average concentration to which the considered European population has been exposed to over the fifteen-year period 2005-2019 for both human health PM_{10} indicators, expressed as the population-weighted concentration, and the percentage of population exposed to PM_{10} concentrations above limit values (LV), i.e. the annual (ALV) and daily (DLV) limit value, respectively.

For the years 2012 and 2013 both the 36th highest value and the 90.4 percentile of daily mean(s) have been calculated. Their results demonstrate an underestimation of almost 1 $\mu g \cdot m^{-3}$ at the 36th highest daily mean. One may conclude that this underestimation is caused by the fact that when calculating the 36th highest daily mean value there is no correction for the missing values at incomplete time series. Whereas the 90.4 percentile of daily means adjusts for such missing data.

As the PM_{10} maps for 2019 (as presented in Chapter 2) have been constructed using the updated methodology as developed and tested in Horálek et al. (2019), the table presents the results for 2015-2019 (and 2005 and 2009, for annual average) both based on the updated and the old methodologies, for comparability reasons.

Table 6.1: Population-weighted concentration and percentage of the considered European population (without Turkey) exposed to concentrations above the PM_{10} limit values (LV) for the protection of health for 2005 to 2019

PM_{10}		method	2005	2006	2007	2008	2009	2010	2011	2012	2013	2014	2015	2016	2017	2018	2019
Annual average																	
Population-weighted concentration	[$\mu g.m^{-3}$]	old	28.0	28.9	26.6	25.1	24.6	24.5	25.3	22.9	22.2	21.1	21.2	20.2	20.2	20.1	18.3
		new	28.6				25.3						21.6	20.5	20.8	20.8	18.7
Population exposed > ALV (40 $\mu g.m^{-3}$)	[%]	old	13.3	10.9	7.1	5.9	6.0	5.2	7.2	3.4	2.6	2.0	0.6	1.7	2.9	2.1	0.3
		new	11.5				6.2						0.7	1.7	3.3	2.4	0.5
36th highest daily mean / 90.4 percentile of daily means																	
Popul.-weighted conc. [$\mu g.m^{-3}$]	36th highest d. m.	old	47.4	48.3	44.7	41.9	41.6	42.0	44.9	40.0	38.6						
	90.4 perc. of d. m.	old								40.8	39.4	37.1	36.9	35.7	36.1	34.5	32.1
	90.4 perc. of d. m.	new											37.5	36.1	37.0	35.4	32.8
Popul. exposed > DLV (50 $\mu g.m^{-3}$) [%]	36th highest d. m.	old	35.9	37.2	27.6	20.3	17.0	20.8	24.8	16.9	16.4						
	90.4 perc. of d. m.	old								18.1	17.3	13.3	14.7	14.0	15.8	12.0	7.2
	90.4 perc. of d. m.	new											16.2	14.6	17.0	13.2	8.1

In 2019 the population exposed to annual mean concentrations of PM_{10} above the limit value of 40 $\mu g \cdot m^{-3}$ has been 0.5 % of the total population (calculated using the new methodology), which is the lowest percentage in the fifteen years' time series. Furthermore, it is estimated that the considered European inhabitants have been exposed on average to an annual mean PM_{10} concentration of 19 $\mu g \cdot m^{-3}$ (using the old methodology, it would be 18 $\mu g \cdot m^{-3}$), the lowest value in the fifteen years' time series. The comparison of results for 2015-2018 illustrates well that a clear decrease in the population-weighted concentration does not lead necessarily to a similar decrease in the percentage of population exposed to an exceedance.

In the fifteen-year time series, the number of people living in areas with concentrations above the annual LV is lower in the latest seven years (2013-2019) than in the first eight years. The overall picture of the population-weighted annual mean concentration of the whole mapping area (i.e. totals of 40 European countries considered) demonstrates a downward trend of about -0.6 $\mu g \cdot m^{-3}.year^{-1}$ for the years 2005-2019, based on the old mapping method results for the whole period (for trend estimation methodology, see Annex 1, Section A1.2). This trend is statistically significant (at the strongest level ***, i.e. 0.001) and expresses a mean decrease of 0.6 $\mu g \cdot m^{-3}$ per year.

In 2019 about 8 % of the considered European population have lived in areas where the PM_{10} daily limit value (calculated using the 90.4 percentile and the new methodology) has been exceeded (using the old methodology, it would be 7 %), being the lowest of the fifteen-year period (also in the case of the old methodology). The overall population-weighted concentration of the 90.4 percentile of the PM_{10} daily means (formerly the 36th highest daily mean) for the background areas is estimated to be about 33 µg·m^{-3} in 2019 for the whole mapping area (using the old methodology, it would be 32 µg·m^{-3}), which is again the lowest of the fifteen years considered . This is the case even though the 36th highest daily means (i.e. possibly underestimated data if applied instead of the 90.4 percentiles, see above) have been used in the 2005-2011 calculations. The population-weighted concentrations of the whole mapping area (i.e. total of 40 European countries considered) show a statistically significant (at the strongest level ***, i.e. 0.001) downward trend of about -0.9 µg·m^{-3} per year for the years 2005-2019, for the daily LV related indicator 90.4 percentile of daily means (formerly the 36th highest daily mean), as calculated based on the old mapping method results for the whole period.

6.2 Human health $PM_{2.5}$ indicators

Table 6.2 summarises for human health $PM_{2.5}$ indicator (annual average) the population-weighted concentration and the percentage of the considered European population exposed to $PM_{2.5}$ concentrations above the EU LV for the years 2005 to 2019 (without 2006, for which neither a map nor a population exposure was prepared).

As in the case of PM_{10}, the $PM_{2.5}$ maps for 2019 (as presented in Chapter 3) has been constructed using the updated methodology. The table presents the results for 2005, 2009 and 2015-2019 (all the years for which maps using both methods are available) both based on the updated and the old methodology, for comparability reasons.

Table 6.2: Population-weighted concentration and percentage of the considered European population (without Turkey) exposed to concentrations above the $PM_{2.5}$ limit value (LV) for the protection of health for 2005 to 2019

$PM_{2.5}$		method	2005	2006	2007	2008	2009	2010	2011	2012	2013	2014	2015	2016	2017	2018	2019
Annual average																	
Population-weighted concentration	[µg.m^{-3}]	old	18.8	not mapped	16.2	16.4	16.2	16.9	17.8	15.7	15.3	14.1	14.2	13.4	13.6	13.2	11.6
		new	19.0				16.6						14.3	13.6	13.8	13.5	11.8
Population exposed > LV (25 µg.m^{-3})	[%]	old			8.2	7.9	7.6	8.3	13.3	9.1	5.8	4.2	6.3	5.4	7.0	4.1	0.9
		new	16.8				7.6						6.5	5.4	7.2	4.5	1.2

The percentage of population exposed in 2019 to annual mean concentrations of $PM_{2.5}$ above the LV of 25 µg·m^{-3} has been 1.2 % (using the old methodology, it would be 0.9 µg·m^{-3}), which is the lowest value in the fifteen years' time series. Furthermore, it is estimated that the considered European inhabitants have been exposed on average to an annual mean $PM_{2.5}$ concentration of 12 µg·m^{-3} in 2019 (also using the old methodology), being again the lowest value in the time series.

The trend analysis of the population-weighted concentrations across the period 2005-2019 for the total mapping area has been executed, based on the old mapping method results for the whole period. At European scale a statistical significant (at the level ***, i.e. 0.001) downward trend can be observed, estimated to be -0.4 µg·m^{-3} per year.

6.3 Human health ozone indicators

Table 6.3 summarises the exposure levels of the considered European inhabitants in terms of population-weighted concentrations for both human health ozone indicators. Furthermore, it presents the percentage of considered European population exposed to concentrations above the target value (TV) and above a level of 6 000 µg·m^{-3}·d for the SOMO35 for the years 2005 to 2019.

Table 6.3: Population-weighted concentration and percentage of the considered European population (without Turkey) exposed to concentrations above the target value (TV) threshold for the protection of health and a SOMO35 threshold of 6 000 μg·m^{-3}·d for 2005 to 2019

Ozone		2005	2006	2007	2008	2009	2010	2011	2012	2013	2014	2015	2016	2017	2018	2019
26th highest daily max. 8-h mean / 93.2 percentile of daily max. 8-h means																
Pop.-weighted conc. [μg.m^{-3}]	26th highest d. max8h	111.4	117.6	110.0	109.4	107.7	106.5	108.4	107.3	108.3						
Pop.-weighted conc. [μg.m^{-3}]	93.2 perc. of d. max8h								107.9	108.9	102.9	110.4	104.8	105.0	114.4	109.9
Pop. exp. > TV (120 μg.m^{-3})	26th highest d. max8h	29.5	49.8	24.9	13.6	14.9	15.8	15.0	19.0	15.0						
Pop. exp. > TV (120 μg.m^{-3})	93.2 perc. of d. max8h								20.2	15.9	5.6	34.0	8.4	12.9	34.8	20.3
SOMO35																
Pop.-weighted concentration	[μg.m^{-3}.d]	4622	5045	4291	4164	4233	3850	4318	4174	4089	3500	4312	3619	3890	4962	4478
Pop. exposed > 6000 μg.m^{-}	[%]	26.8	27.1	26.3	17.0	23.2	15.9	22.0	23.2	18.8	9.4	22.2	11.7	19.1	31.3	20.0

The table presents the results obtained with the 1x1 km^2 merging resolution as tested on the 2006 data in Horálek et al (2010), then recomputed for 2005 and 2007, and finally implemented fully on the 2008 data and onwards. For 2012 and 2013, both the 26th highest value and the 93.2nd percentile of maximum daily 8-hour mean(s) have been calculated. It demonstrates an underestimation of about 0.6 μg·m^{-3} at the 26th maximum daily 8-hour mean, which is caused by the fact that when calculating this indicator there is no correction for the missing values in the incomplete measurement time series.

Using the 93.2 percentile of ozone maximum daily 8-hour means it is estimated that 20 % of the population have lived in 2019 in areas where concentrations were above the ozone target value (TV) of 120 μg·m^{-3}, which is the sixth highest number of the fifteen-year period. The overall population-weighted ozone concentration in terms of the 93.2 percentile maximum daily 8-hour means in the background areas is estimated at about 110 μg·m^{-3} for the total mapping area, which is ca. a mean value of the whole fifteen-year period (it should be noted that for 2005-2011 the 26th highest value of the maximum daily eight-hour mean was considered instead).

Examining the time series for 2005-2019, it can be concluded that 2006, but also 2005, 2015 and 2018 are exceptional years with high ozone concentrations, leading to increased exposure levels compared to the other eleven years. The years 2014, 2016 and 2017 show the lowest exposure levels in the fifteen years' time series for the 93.2 percentile of the maximum daily 8-hour means.

The trend analysis of the population-weighted concentrations for the 93.2 percentile of the maximum daily 8-hour means across the period 2005-2019 for the total mapping area (i.e. totals of 40 European countries considered) does not estimate a statistically significant trend.

A similar tendency is observed for SOMO35. In 2006-2007, a bit more than one-fourth of the population have lived in areas where a level of 6 000 μg·m^{-3}·d [4] has been exceeded, with the highest level in 2006. In the period of 2008-2019, it fluctuated from about 16 % to 23 % of the population, except 2014 with about 9 %, 2016 with about 12 %, and 2018 with about one-third of the population.

The population-weighted SOMO35 concentrations show the fourth highest value in 2019. Trend analysis on the population-weighted concentration for the total mapping area shows no trend for the period 2005-2019.

6.4 Vegetation related ozone indicators

Exposure indicators describing the agricultural and forest areas exposed to accumulated ozone concentrations above defined thresholds are summarised in Table 6.4. Those thresholds are the

([4]) Note that the 6 000 μg·m^{-3}·d does not represent a health-related legally binding 'threshold'. In this and previous papers it represents a somewhat arbitrarily chosen threshold to facilitate the discussion of the observed distributions of SOMO35 levels in their spatial and temporal context. For motivation of this choice, see Section 4.2.

target value (TV) of 18 000 μg·m^{-3}·h and the long-term objective (LTO) of 6 000 μg·m^{-3}·h for the AOT40 for vegetation, and the former Reporting Value (RV) of 20 000 μg·m^{-3}·h and the Critical Level (CL) of 10 000 μg·m^{-3}·h for the AOT40 for forests.

Table 6.4: Percentages of the considered European agricultural and forest area (without Turkey) exposed to ozone concentrations above the target value (TV) and the long-term objective (LTO) for AOT40 for vegetation, and above Critical Level (CL) and Reporting Value (RV) for AOT40 for forests and agricultural- and forest-weighted concentrations for 2005 to 2019

Ozone	2005	2006	2007	2008	2009	2010	2011	2012	2013	2014	2015	2016	2017	2018	2019
AOT40 for vegetation															
Agricult. area exp. > TV (18 000 μg·m^{-3}·h) [%]	48.5	69.1	35.7	37.8	26.0	21.3	19.2	30.0	22.1	17.8	31.4	14.7	23.8	39.7	29.7
Agricult. area exp. > LTO (6 000 μg·m^{-3}·h) [%]	88.8	97.6	77.5	95.5	81.0	85.4	87.9	86.4	81.0	85.5	79.7	74.1	73.4	95.1	84.0
Agricultural-weighted concentr. [μg·m^{-3}·h]	17481	22344	14597	15214	13157	13310	13255	14041	12838	12427	14223	10942	11750	16311	13735
AOT40 for forests															
Forest area exp. > RV (20 000 μg·m^{-3}·h) [%]	59.1	69.4	48.4	50.2	49.2	49.3	53.0	47.2	44.1	37.7	52.4	41.9	38.9	56.1	51.4
Forest area exp. > CL (10 000 μg·m^{-3}·h) [%]	76.4	99.8	62.1	79.6	67.4	63.4	68.6	65.0	67.2	68.2	59.8	60.0	55.4	86.7	84.0
Forest-weighted concentration [μg·m^{-3}·h]	25900	31154	23744	21951	23532	19625	21892	21580	21753	17124	21150	17573	16798	25397	22343

In 2019, some 30 % of all agricultural land (crops) has been exposed to accumulated ozone concentrations (AOT40 for vegetation) exceeding the target value (TV) threshold, which is in the half of the fifteen years considered. About 84 % of all agricultural land has been exposed to levels in excess of the long-term objective (LTO), which is in the lower half of the fifteen-year period.

The trend analysis of the agricultural-weighted concentrations for the AOT40 for vegetation across the period 2005-2019 for the total mapping area (i.e. totals of 40 European countries considered) does not estimate any statistically significant trend.

For the ozone indicator AOT40 for forests, the level of 20 000 μg·m^{-3}·h (earlier used Reporting Value, RV) has been exceeded in about 51 % of the considered European forest area in 2019, which is the sixth highest of the whole time series. The forest area exceeding the Critical Level (CL) has been in 2019 about 84 %, which is the third highest percentage of the fifteen years period.

The temporal pattern of the AOT40 for forests exceedances shows some similarity with those of the AOT40 for vegetation, despite their different definitions and receptors and their natural difference in area type characteristics and occurrence. Their annual variability is, however, heavily dependent on meteorological variability.

The trend analysis of the forest-weighted concentrations for the AOT40 for forests across the period 2005-2019 for the total mapping area (i.e. totals of 40 European countries considered) shows no statistically significant trend.

6.5 Human health NO_2 indicators

Table 6.5 summarises the development in exposure levels of the considered European population for the human health NO_2 indicator (annual average), in terms of population-weighted concentrations and of percentage population exposed to concentrations above the annual LV (40 μg·m^{-3}), for the years 2005, 2009, 2010 and 2013 to 2019, for which the maps based on the current methodology are available. The population-weighted concentration is presented additionally also for 2007, although based on different mapping methodology than the other years. This 2007 value is probably slightly underestimated; based on Horálek et al. (2017b), one can suppose the true value would be of about 1 % higher (i.e. it would be about 23.5 μg·m^{-3}).

Table 6.5: Population-weighted concentration and percentage of the considered European population (without Turkey) exposed to concentrations above the NO_2 limit value (LV) of 40 µg·m^{-3} for the protection of health for 2005 to 2019

NO_2	2005	2006	2007	2008	2009	2010	2011	2012	2013	2014	2015	2016	2017	2018	2019
Annual average															
Popul.-weighted concentr [µg.m^{-3}]	23.3	not mapped	23.3	not mapped	22.1	22.1	not mapped		19.4	18.6	18.8	18.6	18.4	17.6	16.8
Pop. exp. > LV (40 µg.m^{-3}) [%]	7.9				5.6	4.9			3.2	2.8	3.2	2.8	3.0	1.8	1.3

In 2019 the population exposed to NO_2 annual mean concentrations above the limit value of 40 µg·m^{-3} has been 1.3 % of the total population, which is the lowest in the whole series. Furthermore, it is estimated that considered European inhabitants have been exposed on average to an annual mean NO_2 concentration of 17 µg·m^{-3}, again the lowest in the whole series.

Trend analysis on the population-weighted concentration for the total mapping area shows a slight downward trend of about -0.5 µg·m^{-3}·d per year, for the period 2005-2019, which is statistically significant (at the highest level ***, i.e. 0.001).

List of abbreviations

ALV	Annual Limit Value
AOT40	Accumulated Ozone exposure over a Threshold of 40 ppb (i.e. 80 $\mu g/m^3$) in a specific period
AQ	Air Quality
CL	Critical Level
CLC	CORINE Land Cover
CLRTAP	Convention on Long-range Transboundary Air Pollution (Air Convention)
CORINE	Co-ORdinated INformation on the Environment
CTM	Chemical Transport Model
CSI	Core Set of Indicators
DLV	Daily Limit Value
ECMWF	European Centre for Medium-Range Weather Forecasts
EBAS	EMEP dataBASe
EEA	European Environment Agency
EMEP	European Monitoring and Evaluation Programme
ETC/ACM	European Topic Centre on Air pollution and Climate change Mitigation
ETC/ATNI	European Topic Centre on Air pollution, Noise, Transport and Industrial pollution
EU	European Union
GMTED	Global multi-resolution terrain elevation data
GRIP	Global Roads Inventory Dataset
HLV	Hourly Limit Value
ICP	International scientific Cooperative Programme
ILV	Indicative Limit Value
JRC	Joint Research Centre
LV	Limit Value
NILU	Norwegian Institute for Air Research
NO_2	Nitrogen dioxide
NO_2	Nitrogen oxides
O_3	Ozone
ORNL	Oak Ridge National Laboratory
PLA	Projected Leaf Area
PM_{10}	Particulate Matter with a diameter of 10 micrometres or less
$PM_{2.5}$	Particulate Matter with a diameter of 2.5 micrometres or less
POD_6	Phytotoxic Ozone Doze above a threshold of 6 nmol m^{-2} PLA s^{-1}
R^2	Coefficient of determination
RIMM	Regression – Interpolation – Merging Mapping
RMSE	Root Mean Square Error
SOMO10	Sum of Ozone Maximum daily 8-hour means Over 10 ppb (i.e. 20 $\mu g \cdot m^{-3}$)
SOMO35	Sum of Ozone Maximum daily 8-hour means Over 35 ppb (i.e. 70 $\mu g \cdot m^{-3}$)
TV	Target Value
UN	United Nations
UNECE	United Nations Economic Commission for Europe
UTC	Coordinated Universal Time
WHO	World Health Organization

7 References

Alonso, R., et al., 2014, ‘Drought stress does not protect Quercus ilex L. from ozone effects: results from a comparative study of two subspecies differing in ozone sensitivity’, *Plant Biology 16*, pp. 375-384 (https://onlinelibrary.wiley.com/doi/10.1111/plb.12073) accessed 21 January 2021.

Ashmore, M., et al., H., 2004, ‘New directions: a new generation of ozone critical levels for the protection of vegetation in Europe’, *Atmospheric Environment* 38, pp. 2213-2214 (https://doi.org/10.1016/j.atmosenv.2004.02.029) accessed 20 November 2020.

CLRTAP, 2016, *Forest condition in Europe*, 2016 Technical Report of ICP Forests, UNECE Convention on Long-range Transboundary Air Pollution (https://www.icp-forests.org/pdf/TR2016.pdf) accessed 19 November 2020.

CLRTAP, 2017a, *Manual for modelling and mapping critical loads & levels. Chapter III: "Mapping Critical levels for Vegetation"*, UNECE Convention on Long-range Transboundary Air Pollution (https://icpvegetation.ceh.ac.uk/chapter-3-mapping-critical-levels-vegetation) accessed 7 May 2021.

CLRTAP, 2017b, *Scientific Background Document A of Chapter 3 of "Manual on methodologies and criteria for modelling and mapping critical loads and levels of air pollution effects, risks and trends"*, UNECE Convention on Long-range Transboundary Air Pollution (https://icpvegetation.ceh.ac.uk/sites/default/files/ScientificBackgroundDocumentAOct2018.pdf) accessed 11 December 2020.

CLRTAP, 2020, *Scientific Background Document B of Chapter 3 of “Manual on methodologies and criteria for modelling and mapping critical loads and levels of air pollution effects, risks and trends”*, UNECE Convention on Long-range Transboundary Air Pollution (https://icpvegetation.ceh.ac.uk/sites/default/files/Scientific%20Background%20document%20B%20June%202020.pdf) accessed 11 December 2020.

Colette, A., et al., 2018, *Long term evolution of the impacts of ozone air pollution on agricultural yields in Europe. A modelling analysis for the 1990-2010 period*, Eionet Report – ETC/ACM 2018/15 European Environment Agency (https://www.eionet.europa.eu/etcs/etc-atni/products/etc-atni-reports/eionet_rep_etcacm_2018_15_o3impacttrends) accessed 26 August 2020.

Cressie, N., 1993, *Statistics for spatial data,* Wiley series, New York.

Danielson, J. J. and Gesch, D. B., 2011, *Global multi-resolution terrain elevation data 2010 (GMTED2010)*, U.S. Geological Survey Open-File Report, pp. 2011-1073 (https://pubs.er.usgs.gov/publication/ofr20111073) accessed 19 November 2020.

De Leeuw, F., 2012, *AirBase: a valuable tool in air quality assessments at a European and local level*, ETC/ACM Technical Paper 2012/4 (http://www.eionet.europa.eu/etcs/etc-atni/products/etc-atni-reports/etcacm_tp_2012_4_airbase_aqassessment) accessed 26 August 2020.

Denby, B., et al., 2008, ‘Comparison of two data assimilation methods for assessing PM_{10} exceedances on the European scale’, *Atmospheric Environment* 42, pp. 7122-7134 (https://doi.org/10.1016/j.atmosenv.2008.05.058) accessed 26 August 2020.

Denby, B., et al., 2011a, *Calculation of pseudo $PM_{2.5}$ annual mean concentrations in Europe based on annual mean PM_{10} concentrations and other supplementary data*, ETC/ACC Technical Paper 2010/9 (http://www.eionet.europa.eu/etcs/etc-atni/products/etc-atni-reports/etcacc_tp_2010_9_pseudo_pm2-5_stations) accessed 26 August 2020.

Denby, B., et al., 2011b, *Mapping annual mean $PM_{2.5}$ concentrations in Europe: application of pseudo $PM_{2.5}$ station data*, ETC/ACM Technical Paper 2011/5 (http://www.eionet.europa.eu/etcs/etc-atni/products/etc-atni-reports/etcacm_tp_2011_5_spatialpm2-5mapping) accessed 26 August 2020.

De Smet, P., et al., 2011, *European air quality maps of ozone and PM_{10} for 2008 and their uncertainty analysis*, ETC/ACC Technical Paper 2010/10 (http://www.eionet.europa.eu/etcs/etc-atni/products/etc-atni-reports/etcacc_tp_2010_10_spataqmaps_2008) accessed 26 August 2020.

Deumier, J. M. and Hannon, C., 2010, 'La période d' initiation de la tubérisation: comment la repérer?' (in French), CNIPT (http://www.cnipt.fr/wp-content/uploads/2013/10/Irrigation-juin-2010.pdf) accessed 8 February 2021.

EC, 2008, *Directive 2008/50/EC of the European Parliament and of the Council of 21 May 2008 on ambient air quality and cleaner air for Europe,* OJ L 152, 11.06.2008, 1-44 (http://eur-lex.europa.eu/LexUriServ/LexUriServ.do?uri=OJ:L:2008:152:0001:0044:EN:PDF) accessed 26 May 2021.

EC, 2021. *The tomato market in the EU: Vol. 1: Production statistics* (https://ec.europa.eu/info/sites/default/files/food-farming-fisheries/farming/documents/tomatoes-production_en.pdf) accessed 4 August 2021.

EEA, 2010, *ORNL Landscan 2008 Global Population Data conversion into EEA ETRS89-LAEA5210 1km grid* (by Hermann Peifer of EEA) (https://sdi.eea.europa.eu/catalogue/geoss/api/records/1d68d314-d07c-4205-8852-f74b364cd699) accessed 26 August 2020.

EEA, 2018, *Guide for EEA map layout. EEA operational guidelines*, January 2015, version 5 (https://www.eionet.europa.eu/gis/docs/GISguide_v5_EEA_Layout_for_map_production.pdf) accessed 26 August 2020.

EEA, 2019, Healthy environment, healthy lives: how the environment influences health and well-being in Europe, EEA Report 21/2019 (https://www.eea.europa.eu/publications/healthy-environment-healthy-lives) accessed 2 June 2021.

EEA, 2021a, *Air Quality e-Reporting. Air quality database* (https://www.eea.europa.eu/data-and-maps/data/aqereporting-8). Data extracted in March 2021.

EEA, 2021b, *Exposure of Europe's ecosystems to ozone* (https://www.eea.europa.eu/data-and-maps/indicators/exposure-of-ecosystems-to-acidification-15/assessment) accessed 2 June 2021.

Emberson, L. D., et al., 2000, 'Modelling stomatal ozone flux across Europe', *Environmental Pollution* 109, pp. 403-413 (https://doi.org/10.1016/S0269-7491(00)00043-9) accessed 26 May 2021.

EMEP, 2020, *Transboundary particular matter, photo-oxidants, acidifying and eutrophying components*, EMEP Report 1/2020 (https://emep.int/publ/reports/2020/EMEP_Status_Report_1_2020.pdf) accessed 22 January 2021.

ESA, 2019, *Land cover classification gridded maps from 1992 to present derived from satellite observations*, (https://cds.climate.copernicus.eu/cdsapp#!/dataset/satellite-land-cover) accessed 17 February 2021.

EU, 2020, *Corine land cover 2018 (CLC2018) raster data*, 100x100m^2 gridded version 2020_20 (https://land.copernicus.eu/pan-european/corine-land-cover/clc2018) accessed 19 November 2020.

Eurostat, 2014, *GEOSTAT 2011 grid dataset. Population distribution dataset* (http://ec.europa.eu/eurostat/web/gisco/geodata/reference-data/population-distribution-demography) accessed 26 August 2020.

Eurostat, 2021, *Total population for European states for 2019* (https://ec.europa.eu/eurostat/web/main/data/database) accessed 19 May 2021.

Gilbert, R. O., 1987, *Statistical Methods for Environmental Pollution Monitoring*, Van Nostrand Reinhold, New York.

Haberle, J. and Svoboda, P., 2015, 'Calculation of available water supply in crop root zone and the water balance of crop's, *Contributions to Geophysics and Geodesy* 45, pp. 285-298 (https://www.researchgate.net/publication/293194127_Calculation_of_available_water_supply_in_crop_root_zone_and_the_water_balance_of_crops) accessed 21 January 2021.

Horálek, J., et. al., 2005, *Interpolation and assimilation methods for European scale air quality assessment and mapping, Part II: Development and testing new methodologies*, ETC/ACC Technical paper 2005/8 (http://www.eionet.europa.eu/etcs/etc-atni/products/etc-atni-reports/etcacc_technpaper_2005_8_spatial_aq_dev_test_part_ii) accessed 26 August 2020.

Horálek, J., et. al., 2007, *Spatial mapping of air quality for European scale assessment*, ETC/ACC Technical paper 2006/6 (http://www.eionet.europa.eu/etcs/etc-atni/products/etc-atni-reports/etcacc_technpaper_2006_6_spat_aq) accessed 26 August 2020.

Horálek, J., et. al., 2008, *European air quality maps for 2005 including uncertainty analysis*, ETC/ACC Technical paper 2007/7 (http://www.eionet.europa.eu/etcs/etc-atni/products/etc-atni-reports/etcacc_tp_2007_7_spataqmaps_ann_interpol) accessed 26 August 2020.

Horálek, J., et. al., 2010, *Methodological improvements on interpolating European air quality maps*, ETC/ACC Technical Paper 2009/16 (http://www.eionet.europa.eu/etcs/etc-atni/products/etc-atni-reports/etcacc_tp_2009_16_improv_spataqmapping) accessed 26 August 2020.

Horálek, J., et. al., 2016a, *Application of FAIRMODE Delta tool to evaluate interpolated European air quality maps for 2012*, ETC/ACM Technical Paper 2015/2 (http://www.eionet.europa.eu/etcs/etc-atni/products/etc-atni-reports/etcacm_tp_2015_2_delta_evaluation_aqmaps2012) accessed 26 August 2020.

Horálek, J., et. al., 2016b, *European air quality maps of PM and ozone for 2013 and their uncertainty*, ETC/ACM Technical Paper 2015/5 (http://www.eionet.europa.eu/etcs/etc-atni/products/etc-atni-reports/etcacm_tp_2015_5_aqmaps2013) accessed 27 May 2021.

Horálek, J., et. al., 2017a, *Potential improvements on benzo(a)pyrene (BaP) mapping*, ETC/ACM Technical Paper 2016/3 (http://www.eionet.europa.eu/etcs/etc-atni/products/etc-atni-reports/etcacm_tp_2016_3_bap_improved_mapping) accessed 27 May 2021.

Horálek, J., et. al., 2017b, *Inclusion of land cover and traffic data in NO_2 mapping methodology*, ETC/ACM Technical Paper 2016/12 (http://www.eionet.europa.eu/etcs/etc-atni/products/etc-atni-reports/etcacm_tp_2016_12_lc_and_traffic_data_in_no2_mapping) accessed 27 May 2021.

Horálek, J., et. al., 2018, *Satellite data inclusion and kernel based potential improvements in NO_2 mapping*, ETC/ACM Technical Paper 2017/14 (http://www.eionet.europa.eu/etcs/etc-atni/products/etc-atni-reports/etcacm_tp_2017_14_improved_aq_no2mapping) accessed 27 May 2021.

Horálek, J., et. al., 2019, *Land cover and traffic data inclusion in PM mapping*, Eionet Report ETC/ACM 2018/18 (http://www.eionet.europa.eu/etcs/etc-atni/products/etc-atni-reports/etc-acm-report-18-2018-land-cover-and-traffic-data-inclusion-in-pm-mapping) accessed 27 May 2021.

Horálek, J., et. al., 2020, *European air quality maps for 2017,* Eionet Report ETC/ATNI 2019/9 (https://doi.org/10.5281/zenodo.4035928) accessed 28 May 2021.

Horálek, J., et. al., 2021, *European air quality maps for 2018*, Eionet Report ETC/ATNI 2020/10 (https://doi.org/10.5281/zenodo.4638651) accessed 27 May 2021.

Jarvis, P. G., 1976, 'The interpretation of the variation in leaf water potential and stomatal conductance found in canopies in the field', *Philosophical Transactions of the Royal Society of London*, Series B: Biological Sciences 273, pp. 593-610 (https://doi.org/10.1098/rstb.1976.0035) accessed 26 May 2021.

JRC, 2009, *Population density disaggregated with Corine land cover 2000,* 100x100 m^2 grid resolution, EEA version (http://www.eea.europa.eu/data-and-maps/data/population-density-disaggregated-with-corine-land-cover-2000-2) accessed 26 August 2020.

JRC, 2016, Maps of indicators of soil hydraulic properties for Europe, dataset/maps downloaded from the European Soil Data Centre (http://esdac.jrc.ec.europa.eu/content/maps-indicators-soil-hydraulic-properties-europe) accessed 8 December 2020.

Krupa, S., et al., 2000, 'Ambient ozone and plant health', *Plant Disease* 85, pp. 4-12 (https://apsjournals.apsnet.org/doi/pdf/10.1094/pdis.2001.85.1.4) accessed 8 December 2020.

Mareckova, K., et al., 2020, *Inventory Review 2019, Review of emission data reported under the LRTAP Convention and NEC Directive,* Technical Report CEIP 4/2020 (https://www.ceip.at/fileadmin/inhalte/ceip/00_pdf_other/2020/inventoryreport_2020.pdf) accessed 24 August 2021.

MDA, 2015, *World Land Cover at 30m resolution from MDAUS BaseVue 2013* (https://www.arcgis.com/home/item.html?id=1770449f11df418db482a14df4ac26eb) accessed 17 Fegruary 2021.

Meijer, J. R., et al., 2018, 'Global patterns of current and future road infrastructure', *Environmental Research Letters*, 13 0640, (https://doi.org/10.1088/1748-9326/aabd42) accesed 10 June 2019.

Mills, G., et al., 2011, 'New stomatal flux-based critical levels for ozone effects on vegetation', *Atmospheric Environment* 45, pp. 5064-5068 (https://doi.org/10.1016/j.atmosenv.2011.06.009) accessed 19 November 2020.

Musselman, R. C. and Massman, W. J., 1998, 'Ozone flux to vegetation and its relationship to plant response and ambient air quality standards', *Atmospheric Environment* 33, pp. 65-73 (https://doi.org/10.1016/S1352-2310(98)00127-7) accessed 26 May 2021.

NILU, 2021, *EBAS, database of atmospheric chemical composition and physical properties* (http://ebas.nilu.no) accessed 8 April 2021.

NMI, 2021, *EMEP/MSC-W modelled air concentrations and depositions, Gridded data for 2019, using 2018 emission (2020 Reporting)* (https://thredds.met.no/thredds/catalog/data/EMEP/2020_Reporting/catalog.html) accessed 22 January 2021.

Nussbaum, S., et al., 2003, 'High-resolution spatial analysis of stomatal ozone uptake in arable crops and pastures', *Environmental International* 129, pp. 385-392 (https://www.ncbi.nlm.nih.gov/pubmed/12676231) accessed 26 May 2021.

Pedersen, S. M., et al., 2005. Potato production in Europe - a gross margin analysis. University of Copenhagen, FOI WorkingPaper Vol. 2005 No. 5, pp. 1-39 (https://curis.ku.dk/ws/files/135440168/5.pdf) accessed 26 May 2021.

Pleijel, H., et al., 2007, 'Ozone risk assessment for agricultural crops in Europe: Further development of stomatal flux and flux-response relationships for European wheat and potato', *Atmospheric Environment* 41, pp.3022-3040 (https://doi.org/10.1016/j.atmosenv.2006.12.002) accessed 8 December 2020.

Reich, P. B., 1987, 'Quantifying plant response to ozone: a unifying theory', *Tree Physiology* 3, pp. 63-91 (https://doi.org/10.1093/treephys/3.1.63) accessed 19 November 2020.

Simpson, D., et al., 2012, 'The EMEP MSC-W chemical transport model – technical description', *Atmospheric Chemistry and Physics* 12, pp. 7825-7865 (https://doi.org/10.5194/acp-12-7825-2012) accessed 26 August 2020.

Targa, J., et al. (2021), *Status report of air quality in Europe for year 2019, using validated data*, Eionet Report ETC/ATNI 2021/7 (https://www.eionet.europa.eu/etcs/etc-atni/products/etc-atni-reports/etc-atni-report-7-2021-status-report-of-air-quality-in-europe-for-year-2019-using-validated-data) accessed 10 December 2021.

UN, 2020, *World Population Prospects 2019*, United Nations. Department of Economic and Social Affairs, Population Division (https://population.un.org/wpp/Download/Standard/Population/) accessed 19 May 2021.

van Geffen, J., et., 2019, 'TROPOMI ATBD of the total and tropospheric NO2 data products', KNMI (https://sentinel.esa.int/documents/247904/2476257/Sentinel-5P-TROPOMI-ATBD-NO2-data-products) accessed 30 August 2021.

van Geffen, J., et al., 2020, 'S5P TROPOMI NO_2 slant column retrieval: Method, stability, uncertainties and comparisons with OMI', *Atmospheric Measurement Techniques* 13, pp. 1315–1335 (https://doi.org/10.5194/amt-13-1315-2020) accessed 30 August 2021.

Veefkind, J. P., et al., 2012. 'TROPOMI on the ESA Sentinel-5 Precursor: A GMES mission for global observations of the atmospheric composition for climate, air quality and ozone layer applications', *Remote Sensing of Environment* 120, pp. 70–83 (https://doi.org/10.1016/j.rse.2011.09.027) accessed 30 August 2021.

WHO, 2005, *WHO Air quality guidelines for particulate matters, ozone, nitrogen dioxide and sulphur dioxide, Global update 2005,* World Health Organization (http://www.who.int/phe/health_topics/outdoorair/outdoorair_aqg/en/) accessed 26 May 2021.

WHO, 2013, *Health risks of air pollution in Europe – HRAPIE project,* World Health Organization (http://www.euro.who.int/__data/assets/pdf_file/0006/238956/Health_risks_air_pollution_HRAPIE_project.pdf) accessed 26 August 2020.

WHO, 2021, *WHO global air quality guidelines: particulate matter ($PM_{2.5}$ and PM_{10}), ozone, nitrogen dioxide, sulfur dioxide and carbon monoxide*, World Health Organization (https://apps.who.int/iris/handle/10665/345329) accessed 10 December 2021.

Annex 1
Methodology

A1.1 Mapping method

Previous technical papers prepared by Horálek et al. (2005, 2007, 2008, 2010, 2017b, 2018, 2019), De Smet et al. (2011) and Denby et al. (2011a, 2011b) discuss methodological developments and details on spatial interpolations and their uncertainties. No changes took place in the mapping methodology compared to the preceding report (Horálek et al., 2021). This annex summarizes the currently applied method for all the considered indicators. The mapping method has been evaluated with the FAIRMODE Delta tool in Horálek et al. (2016a). The method is called the *Regression – Interpolation – Merging Mapping* (RIMM).

Pseudo $PM_{2.5}$ and NO_x station data estimation

To supplement $PM_{2.5}$ measurement data, in the mapping procedure data from so-called pseudo $PM_{2.5}$ stations are also used. These data are the estimates of $PM_{2.5}$ concentrations at the locations of PM_{10} stations with no $PM_{2.5}$ measurement. These estimates are based on PM_{10} measurement data and different supplementary data, using linear regression:

$$\hat{Z}_{PM_{2.5}}(s) = c + b.Z_{PM_{10}}(s) + a_1X_1(s) + a_2X_2(s) + \cdots + a_nX_n(s) \qquad \text{(A1.1)}$$

where $\hat{Z}_{PM_{2.5}}(s)$ is the estimated value of $PM_{2.5}$ at the station *s*,
$Z_{PM_{10}}(s)$ is the measurement value of $PM_{2.5}$ at the station *s*,
c, *b*, a_1,…, a_n are the parameters of the linear regression model calculated based on the data at the points of stations with both $PM_{2.5}$ and PM_{10} measurements,
$X_1(s)$,…, $X_n(s)$ are the values of other supplementary variables at the station *s*,
n is the number of other supplementary variables used in the linear regression.

When applying this estimation method, all background stations (either classified as rural, urban or suburban) are handled together for estimating $PM_{2.5}$ values at background pseudo stations. For details, see Denby et al. (2011b). For estimating $PM_{2.5}$ values at urban traffic pseudo stations, Equation A1.1 is applied for the urban traffic stations. For details, see by Horálek et al. (2019).

To supplement NO_x measurement data, NO_x values are estimated at locations of NO_2 stations with no NO_x data. The estimates are calculated similarly as in Horálek et al. (2007), using regression:

$$\hat{Z}_{NO_x}(s) = a_1Z_{NO_2}(s)^2 + a_2Z_{NO_2}(s) + c \qquad \text{(A1.2)}$$

where $\hat{Z}_{NO_x}(s)$ is the estimated value of NO_x at the station s,
$Z_{NO_2}(s)$ is the measurement value of NO_2 at the station s,
a_1, a_2, *c* are the parameters of the regression calculated based on the data at the points of measuring stations with both NO_x and NO_2 measurements.

Interpolation

The mapping method used is a linear regression model followed by kriging of the residuals produced from that model (residual kriging). Interpolation is therefore carried out according to the relation:

$$\hat{Z}(s_0) = c + a_1X_1(s_0) + a_2X_2(s_0) + \cdots + a_nX_n(s_0) + \eta(s_0) \qquad \text{(A1.3)}$$

where $\hat{Z}(s_0)$ is the estimated value of the air pollution indicator at the point s_o,
$X_1(s_0)$, $X_2(s_0)$,…, $X_n(s_0)$ are *n* number of individual supplementary variables at the point s_o
c, a_1, a_2,,…, a_n are the *n+1* parameters of the linear regression model calculated based on the data at the points of measurement,
$\eta(s_0)$ is the spatial interpolation of the residuals of the linear regression model at the point s_o calculated based on the residuals at the points of measurement.

For different pollutants and area types (rural, urban background, and in the case of PM and NO_2 , also urban traffic), different supplementary data are used, depending on their improvement to the fit of the regression. Ordinary kriging is used to interpolate the residuals:

$$\hat{R}(s_i) = \sum_{i=1}^{N} \lambda_i R(s_i) \,, \sum_{i=1}^{N} \lambda_i = 1 \qquad \text{(A1.4)}$$

where $R(s_i)$ are the residuals in the points of the measuring stations s_i ,
$\lambda_1, \ldots, \lambda_N$ are the weights estimated based on variogram,
N is the number of the stations used in the interpolation.

The variogram (as a measure of a spatial correlation) is estimated using a spherical function (with parameters nugget, sill, range). For details, see Horálek et al. (2007), Section 2.3.5 and Cressie (1993).

For $PM_{2.5}$ and NO_x, both measurement data and the estimated data from the pseudo stations are used.

For the PM_{10} and $PM_{2.5}$ indicators, prior to linear regression and interpolation, a logarithmic transformation is applied to measurement and EMEP model concentrations. After interpolation, a back-transformation is applied. For details, see De Smet et al. (2011) and Denby et al. (2008).

For the vegetation related indicators (AOT40 for vegetation and forests, POD, and NO_x) only rural maps are constructed based on rural background stations, based on the assumption that no vegetation is located in urban areas. For the health related indicators, the rural and urban background map layers (and for PM and NO_2 also urban traffic map layer) are constructed separately and then merged.

Merging of rural and urban background (and urban traffic) map layers

Health related indicator map layers for ozone are constructed (using linear regression with kriging of its residuals) for the rural and urban background areas separately on a grid at 10x10 km^2 resolution, while for PM_{10}, $PM_{2.5}$ and NO_2 on a grid at 1x1 km^2 resolution. The rural map is based on rural background stations and the urban background map on urban and suburban background stations. Subsequent to this, the rural and urban background maps are merged into one combined air quality indicator map using a European-wide population density grid at 1x1 km^2 resolution. For the 1x1 km^2 grid cells with a population density less than a defined value of α_1, the rural map value is selected and for grid cells with a population density greater than a defined value α_2, the urban background map value. For areas with population density within the interval (α_1, α_2) a weighting function of α_1 and α_2 is applied (for details and the setting of the parameters α_1 and α_2, see Horálek et al., 2005, 2007, 2010). This applies to the grid cells where the estimated rural value is lower (PM_{10}, $PM_{2.5}$ and NO_2) or higher (ozone), than the estimated urban background map value. In limited areas when this criterion does not hold, a joint urban/rural map layer (created using all background stations regardless of their type) is applied, as far as its value lies in between the rural and urban background map value. Thus, the adjusted rural and urban background map layers are calculated and further used. For details, see De Smet et al. (2011).

In the case of ozone, the separate ozone rural and urban (adjusted) map layers are constructed at a resolution of 10x10 km^2; their merging however takes place on the basis of the 1x1 km^2 resolution population density grid, resulting in a final combined pollutant indicator map on this 1x1 km^2 resolution grid. This map is used both for the population exposure estimates and for presentational purposes.

In the case of PM_{10}, $PM_{2.5}$ and NO_2, separate map layers are created for rural, urban background and urban traffic areas on a grid at 1x1 km^2 resolution. The (adjusted) rural background map layer is based on the rural background stations, the (adjusted) urban background map layer on the urban and the suburban background stations, and the urban traffic map layer on the urban and the suburban traffic stations. For different map layers (rural, urban background, urban traffic) different supplementary data are used, depending on their improvement to the fit of the regression. The three map layers are merged into one final map using a weighting procedure

$$\hat{Z}_F(s_0) = (1 - w_U(s_0))\hat{Z}_R(s_0) + w_U(s_0)(1 - w_T(s_0))\hat{Z}_{UB}(s_0) + w_U(s_0)w_T(s_0)\hat{Z}_{UT}(s_0) \quad \text{(A1.5)}$$

where $\hat{Z}_F(s_0)$ is the resulting estimated concentration value in a grid cell s_o for the final map,
$\hat{Z}_R(s_0)$ is the estimated value in a grid cell s_o for the rural background map layer,
$\hat{Z}_{UB}(s_0)$ is the estimated value in a grid cell s_o for the urban background map layer,
$\hat{Z}_{UT}(s_0)$ is the estimated value in a grid cell s_o for the urban traffic map layer,
$w_U(s_0)$ is the weight representing the ratio of the urban character of the a grid cell s_o,
$w_T(s_0)$ is the weight representing the ratio of areas exposed to traffic air quality in a grid cell s_o.

The weight $w_U(s_0)$ is based on the population density grid, while $w_T(s_0)$ is based on the buffers around the roads. For further details, see Horálek et al. (2017b).

In all calculations and map presentations the EEA standard projection ETRS89-LAEA5210 (also known as ETRS89 / LAEA Europe, see www.epsg-registry.org) is used. The interpolation and mapping domain consists of the areas of all EEA member and cooperating countries, and other microstates, as far as they fall into the EEA map extent Map_2c (EEA, 2018). The mapping area covers the whole Europe apart from Belarus, Moldova, Ukraine and the European parts of Russia and Kazakhstan.

A1.2 Calculation of population and vegetation exposure

Population and vegetation exposure estimates are based on the interpolated concentration maps, population density data and land cover data.

Population exposure

Population exposure for individual countries, for EU-28 and for the whole mapping areas is calculated for ozone from the air quality maps and population density data, both at 1x1 km^2 resolution. For each concentration class, the total population per country as well as the European-wide total is determined.

For PM and NO_2, the population exposure is calculated separately for the areas where the air quality is considered to be directly influenced by traffic and for the background (both rural and urban) areas. For each concentration class 'j', the percentage population per country as well as the European-wide total is determined according to:

$$P_j = \frac{\sum_{i=1}^{N} I_{Bij}\,(1 - w_U(\mathrm{i})w_T(\mathrm{i}))p_i + \sum_{i=1}^{N} I_{Tij} w_U(\mathrm{i})w_T(\mathrm{i})p_i}{\sum_{i=1}^{N} p_i} . 100 \quad \text{(A1.6)}$$

where P_j is the percentage population living in areas of the *j*-th concentration class in either the country or in Europe as a whole,
p_i is the population in the *i*-th grid cell,
I_{Bij} is the Boolean 0-1 indicator showing whether the background air quality concentration (estimated by the combined rural/urban background map layer) in the *i*-th grid cell is within the *j*-th concentration class ($I_{Bij} = 1$), or not ($I_{Bij} = 0$),
I_{Tij} is the Boolean 0-1 indicator showing whether the traffic air quality concentration in the *i*-th grid cell is within the *j*-th concentration class ($I_{Tij} = 1$), or not ($I_{Tij} = 0$),
N is the number of grid cells in the country or in Europe as a whole.

In addition, per-country, and the total exposure are expressed as the population-weighted concentration, i.e. the average concentration weighted according to the population in a 1x1 km^2 grid cell:

$$\hat{c} = \frac{\sum_{i=1}^{N} c_i p_i}{\sum_{i=1}^{N} p_i} \quad \text{(A1.7)}$$

where $\hat{c}$ is the population-weighted average concentration in the country, EU-28 or in the whole mapping area,

p_i is the population in the i^{th} grid cell,

c_i is the concentration in the i^{th} grid cell (based on the final merged map),

N is the number of grid cells in the country or in Europe as a whole.

Estimation of trends

For detecting and estimating the trends in time series of annual values of population exposure, the non-parametric Mann-Kendall's test for testing the presence of the monotonic increasing or decreasing trend is used. Next to that, the non-parametric Sen's method for estimating the slope of a linear trend is executed. For details, see Gilbert (1987). The significance of the Mann-Kendal test is shown by the usual way, i.e. + for 0.1, * for 0.05, ** for 0.01, and *** for 0.001.

Vegetation exposure

Vegetation exposure for individual countries, for EU-28 and for the total mapping area is calculated based on the air quality maps and land cover data, both in 2x2 km^2 grid resolution. For each concentration class, the total agricultural and forest area per country as well as European-wide is determined.

Next to this, per-country and European-wide exposure are expressed as the agricultural- and forest-weighted concentration, i.e. the average concentration weighted according to the agricultural and forest area in a 1x1 km^2 grid cell, similarly like in Eq. A1.7.

A1.3 Phytotoxic Ozone Dose above a threshold flux Y (POD_Y) calculation

The calculation of the phytotoxic ozone dose above a threshold *Y* (POD_Y) as described below follows precisely the methodology described in the Manual for modelling and mapping critical loads & levels of the Long-Range Transboundary Air Pollution Convention (CLRTAP) in its most recent available revision (CLRTAP, 2017a), including some specifications presented in the Scientific background documents of this manual (CLRTAP, 2017b, 2020), as prepared by the International scientific Cooperative Programme on effects of air pollution on natural vegetation and crops of the Working Group on Effects of the CLRTAP (ICP Vegetation). The steps to be taken are presented in Table A1.1.

Table A1.1: Steps to calculate POD_Y and exceedance of flux-based critical levels

1	Decide on the species and biogeographical region(s) to be included.
2	Obtain the ozone concentrations at the top of the canopy for the species or vegetation-specific accumulation period.
3	Calculate the hourly stomatal conductance of ozone (g_{sto}).
4	Model the hourly stomatal flux of ozone (F_{sto}).
5	Calculation of POD_Y from F_{sto}.
6	Calculation of exceedance of flux-based critical levels.

Source: CLRTAP, 2017a

The cumulative stomatal ozone fluxes (F_{sto}) are calculated over the course of the growing season based on ambient ozone concentration and stomatal conductance (g_{sto}) to ozone. g_{sto} is calculated using a multiplicative stomatal conductance model proposed by Jarvis (1976) and modified by Emberson et al. (2000) as a function of species-specific maximum g_{sto} (expressed on a single leaf-area basis), phenology, and prevailing environmental conditions (photosynthetic photon flux density (PPFD)), air temperature, vapour pressure deficit (VPD), and soil moisture.

Hourly averaged stomatal ozone fluxes (F_{sto}) in excess of a threshold Y (expressed in mmol m^{-2} PLA ([5])) are accumulated over a species or vegetation-specific accumulation period during daylight hours, in order to get the phytotoxic ozone dose above the threshold *Y* (POD_Y).

For the wheat as for other crop species, the Y value is taken equal to 6 nmol m^{-2} PLA s^{-1}. Although several POD indicators are proposed in CLRTAP (2017a), POD_6 is recommended for wheat, as the hourly averaged stomatal ozone fluxes above a value of 6 are more relevant for that crop. For potato and tomato, POD_6 is also recommended. Two POD_6 versions are available in CLRTAP (2017a): POD_6IAM (which is a simplified version recommended for Integrated Assessment Modelling) and POD_6SPEC (which is specific to a given specie). Here, POD_6SPEC was preferred and used, in agreement with Colette et al. (2018).

Obtaining the ozone concentrations at the top of the canopy for the species or vegetation-specific accumulation period

The ozone concentration at canopy top (nmol.m^{-3}) in the given hour H is calculated according to

$$c(z_1) = c(z_{m,O3})*\left(1-\frac{R_a(z_{tgt}, z_{m,O3})}{R_a\left(d+z_0, z_{m,O3}\right) + R_b + R_{surf}}\right) \quad \text{(A1.8)}$$

where
- $c(z_1)$ is ozone concentration at the top of the canopy
- $c(z_{m,O3})$ is the ozone concentration measured at the height z_m
- $R_a(x, y)$ is the aerodynamic resistance between the height of y and the height of x
- R_b is the resistance to ozone diffusion in the laminar sub-layer
- R_{surf} is the overall resistance to ozone deposition to the underlying surfaces

while

$$R_a(z_{tgt}, z_{m,O3}) = \frac{1}{k.u*}\left[ln\left(\frac{z_{m,O3}-d}{z_{tgt}-d}\right) - \Psi_H\left(\frac{z_{m,O3}-d}{L}\right) + \Psi_H\left(\frac{z_{tgt}-d}{L}\right)\right] \quad \text{(A1.8a)}$$

$$R_a(d + z_0, z_{m,O3}) = \frac{1}{k.u*}\left[ln\left(\frac{z_{m,O3}-d}{z_0}\right) - \Psi_H\left(\frac{z_{m,O3}-d}{L}\right) + \Psi_H\left(\frac{z_0}{L}\right)\right] \quad \text{(A1.8b)}$$

$$R_b = \frac{2}{k.u*}\left(\frac{Sc}{Pr}\right)^{2/3} \quad \text{(A1.8c)}$$

$$R_{surf} = \frac{1}{\frac{LAI}{R_{sto}}+\frac{SAI}{R_{ext}}+\frac{1}{R_{inc}+R_{soil}}} \quad \text{(A1.8d)}$$

where
- k is the von Kármán constant (equal to 0.41)
- z_{tgt} is the top canopy height (the target height)
- $z_{m,O3}$ is the height of the available ozone measurement above the canopy
- z_0 is the roughness length, usually assumed as 1/10 of the canopy height
- L is the Obukhov length;
- d is the displacement height, usually assumed as 2/3 of the canopy height;
- $u*$ is the friction velocity;
- Sc is the Schmidt number for ozone (equal to 0.41);
- Pr is the Prandtl number of air (equal to 0.71);
- LAI is the projected leaf area in [$m^2.m^{-2}$];
- SAI is the surface area of the canopy in [$m^2.m^{-2}$];
- $\Psi_H(..) = \Psi_H(\zeta)$ is the similarity function for heat with ζ as the argument ([6]),

([5]) PLA, or the projected leaf area, is the total area of the sides of the leaves that are projected towards the sun. PLA is different to the total leaf area, which accounts for both sides of the leaves.

([6]) For more details see CLRTAP (2017b).

according to

$(\zeta) = 2$ when $\zeta < 0$

$= -5\zeta$ when $\zeta \geq 0$ (A1.8e)

with $x = (1 - 16 * \zeta)^{1/4}$ (A1.8f)

and R_{ext} is the resistance to cuticular deposition of ozone (equal to 2 500 $s.m^{-1}$);
R_{soil} is the soil resistance (equal to 200 $s.m^{-1}$),

while $R_{sto} = 1/g_{sto}$ (A1.8g)

$R_{inc} = b.SAI.h / u^*$ (A1.8h)

where g_{sto} is the actual stomatal conductance;
b is the empirical constant (equal to 14 m^{-1});
h is the height of the canopy.

Calculation of the hourly stomatal conductance of ozone (g_{sto})

The basis of the approach used for calculating phytotoxic ozone doses is the calculation of an instantaneous stomatal conductance g_{sto} in the given hour H, according to the equation

$$g_{sto} = g_{max} * [min(f_{phen}, f_{O3})] * f_{light} * max\{f_{min}, (f_{temp} * f_{VPD} * f_{SW})\} \quad \text{(A1.9)}$$

where g_{sto} is the actual stomatal conductance in [mmol O_3 m^{-2} PLA s^{-1}];
g_{max} is the species-specific maximum stomatal conductance in [mmol O_3 m^{-2} PLA s^{-1}]; see Table A1.2;
f_{phen} is the relative proportion function for the phenology for the different stage of growing;
f_{O3} is the relative proportion function for the influence of ozone on stomatal flux by promoting premature senescence;
f_{min} is the species-specific relative minimum stomatal conductance that occurs during daylight hours, see Table A1.2;
f_{temp}, f_{VPD}, f_{SW}, f_{light} are relative proportion functions for leaf stomata respond to temperature, air humidity, soil moisture and light.

Parameters f_{phen}, f_{O3}, f_{light}, f_{temp}, f_{VPD}, f_{SW} and f_{min} are expressed as relative proportion functions, taking values between 0 and 1 as a proportion of g_{max}. These functions allow taking into account irradiance (f_{light}), temperature (f_{temp}), water vapour deficit at leaves level (f_{vpd}), soil moisture (f_{sw}), phenology for the different stage of growing (f_{phen}) and the influence of ozone on stomatal flux by promoting premature senescence (f_{O3}). f_{min} is the minimum relative value of stomatal conductance during the daylight.

The parameter f_{phen} is calculated based on the accumulation of thermal time over the growing season of the crop being considered (Colette, 2018), according to CLRTAP (2017a). For wheat and potato, the accumulation period is defined for each year using the effective temperature sum (*ETS*) in ˚C for days in excess of 0 ˚C, while for tomato for days in excess of 10 ˚C.

For wheat, the total accumulation period during which wheat is sensitive to ozone exposure is 200 °C days and 300 °C days before mid-anthesis (mid-point in flowering) to 700 °C days to 550 °C days after mid-anthesis for Atlantic, Boreal and Continental regions and Mediterranean region, respectively. The timing of mid-anthesis is estimated by starting at the first date after 1 January (or just 1 January) when the temperature exceeds 0 °C. The mean daily temperature is then accumulated (temperature sum), and mid-anthesis is estimated to be a temperature sum of 1075 °C days for Atlantic, Boreal and Continental regions and 1250 °C days for Mediterranean region, which in general corresponds to bread wheat.

For potato, the accumulation period stands between 330 °C days before the tuber initiation date and 800 °C days after this date. The tuber initiation date is considered to be homogeneous throughout Europe. The reasons for its simplification are a) heterogeneous climatic conditions in the European countries naturally lead to different time of potato planting (Pedersen et al., 2005) followed by different time of the tuber initiation b) lack of detailed local data availability for modelling and mapping.

As discussed ([7]) with the French national Chamber of agriculture (APCA, http://chambres-agriculture.fr), the tuber initiation starts 15 days after the transplantation in the field, which occurs in May. Therefore, the fixed date for the tuber initiation was set to June 1st.

For tomato, the accumulation period is from 250 ˚C days to 1500 ˚C days after transplantation in the field over a base temperature of 10 °C. The timing of the transplantation is set on the date June 1st.

The parameter f_{phen} is calculated according to equation

in the case of wheat:

$$f_{phen} = 1 \quad \text{when} \quad (f_{phen\_2\_ETS} + f_{phen\_1\_ETS}) \leq ETS \leq (f_{phen\_2\_ETS} + f_{phen\_3\_ETS})$$

$$= 1 - \left(\frac{f_{phen\_a}}{f_{phen\_4\_ETS} - f_{phen\_3\_ETS}}\right) * (ETS - f_{phen\_3\_ETS})$$

$$\text{when} \quad (f_{phen\_2\_ETS} + f_{phen\_3\_ETS}) < ETS \leq (f_{phen\_2\_ETS} + f_{phen\_4\_ETS})$$

$$= f_{phen\_e} - \left(\frac{f_{phen\_e}}{f_{phen\_5\_ETS} - f_{phen\_4\_ETS}}\right) * (ETS - f_{phen\_4\_ETS})$$

$$\text{when} \quad (f_{phen\_2\_ETS} + f_{phen\_4\_ETS}) < ETS \leq f_{phen\_5\_ETS} \qquad \text{(A1.9a)}$$

in the case of potato (formulated based on CLRTAP, 2017b):

$$f_{phen} = 1 - \left(\frac{1 - f_{phen\_a}}{f_{phen\_1\_ETS}}\right) * ETS \quad \text{when} \quad f_{phen\_1\_ETS} \leq ETS < 0$$

$$= 1 - \left(\frac{1 - f_{phen\_e}}{f_{phen\_2\_ETS}}\right) * ETS \quad \text{when} \quad 0 < ETS \leq f_{phen\_2\_ETS} \qquad \text{(A1.9b)}$$

in the case of tomato (formulated based on CLRTAP, 2017b):

$$f_{phen} = \frac{ETS - f_{phen\_2\_ETS}}{A_{start\_ETS} - f_{phen\_2\_ETS}} \quad \text{when } A_{start\_ETS} \leq ETS < A_{end\_ETS} \qquad \text{(A1.9c)}$$

where *ETS* is the effective temperature sum in ˚C days using a base temperature of 0 ˚C for wheat and potato and a base temperature of 10 °C for tomato (see Table A1.2); for wheat, ETS is set to 0 °C days at mid-anthesis day. Then A_{start_ETS} will be at 200 ˚C days before mid-anthesis, and A_{end_ETS} will be at 700 ˚C days after mid-anthesis over a base temperature of 0 °C;
for potato, ETS is set to 0 °C days at tuber initiation day. Then A_{start_ETS} will be at 330 ˚C days before tuber initiation and A_{end_ETS} at 800 ˚C days after tuber initiation over a base temperature of 0 °C;
for tomato, ETS is set to 0 °C days at transplantation day in the field. Then A_{start_ETS} will be at 250 ˚C days after transplantation in the field and A_{end_ETS} at 1500 ˚C days after transplantation in the field over a base temperature of 10 °C,

([7]) There is a lack of information on a date of potato tuber initiation in Europe. It should ideally rely on existing models based on agricultural practices, local climatology, ground properties, and location. INERIS, while developing the POD script, relied on contents of discussions with the French National Chamber of Agriculture (personal consultation, Quentin Mathieu, APCA, March 2018; Deumier and Hannon, 2010). Based on the information given that the tuber initiation starts 15 days after the transplantation in the field, which occurs in May in France, it has chosen a fixed date of June 1st for France and for Europe. This date might be revised according to the availability of more accurate information on potato plantations in Europe.

f_{phen_a}, f_{phen_e} is the phenology function, which consists of terms describing rate changes of g_{max} expressed as fractions (see Table A1.2),

$f_{phen\_1\_ETS}$, $f_{phen\_2\_ETS}$, $f_{phen\_3\_ETS}$, $f_{phen\_4\_ETS}$, $f_{phen\_5\_ETS}$ are °C days (see Table A1.2; $f_{phen\_1\_ETS}$ and $f_{phen\_5\_ETS}$ define period crops to be sensitive to ozone exposure),

A_{start_ETS} and A_{end_ETS} are the effective temperature sums (counted from the day of the mid-anthesis for wheat, from the day of the tuber initiation for potato and from the day of the transplantation in the field for tomato) above a base temperature of 0 ˚C for wheat and potato and 10 ˚C for tomato at the start and end of the O_3 accumulation period respectively; see Table A1.2.

The parameter f_{O3} in the case of wheat is calculated according to equation

$$f_{O3} = ((1+(POD_0/14)^8)^{-1} \quad \text{(A1.9d)}$$

while $$POD_0 = \sum_{n=A_{start}}^{H-1} F_{sto}(n) \cdot \frac{3600}{10^6} \quad \text{(A1.9e)}$$

where POD_0 is the ozone flux already accumulated since the beginning of the vegetation period A_{start} up to the last hour H-1,

$F_{sto}(n)$ is the hourly ozone flux in the hour n, calculated in the previous steps based on Equation 2.4, while $F_{sto}(A_{start})$ is equal to 0.

The parameter (ozone function) f_{O3} in the case of potato is calculated according to equation

$$f_{O3} = ((1+(AOT0/40)^5)^{-1} \quad \text{(A1.9f)}$$

where *AOT0* is accumulated ozone concentration from the start of the vegetation period A_{start} up to the last hour H-1.

The parameter (ozone function) $\boldsymbol{f_{O3}}$ in the case of tomato is not determined.

The parameter f_{light} is calculated according to

$$f_{light} = 1 - EXP((-light\_a)*PPFD) \quad \text{(A1.9g)}$$

while $$PPFD = SSRD * 0.5 * 4.5 \quad \text{(A1.9h)}$$

where *PPFD* represents the photosynthetic photon flux density [μmol m^{-2} s^{-1}],
light_a is a light parameter (see Table A1.2),
SSRD represents the surface net solar radiation in [W.m^{-2}].

The parameter f_{temp} is calculated according to:

$$f_{temp} = \max\{f_{min}, [(T - T_{min}) / (T_{opt} - T_{min})] * [(T_{max} - T) / (T_{max} - T_{opt})]^{bt}\} \quad \text{when } T_{min} < T < T_{max}$$
$$= f_{min} \quad \text{when } T_{min} > T > T_{max} \quad \text{(A1.9i)}$$

while $$bt = (T_{max} - T_{opt}) / (T_{opt} - T_{min}) \quad \text{(A1.9j)}$$

where T_{min}, T_{max} and T_{opt} are minimum, maximum and optimum temperatures determining leaf stomata opening (see Table A1.2)

The parameter f_{VPD} is calculated according to:

$$f_{VPD} = \min\{1,\max\{f_{min}, ((1-f_{min})*(VPD_{min} - VPD) / (VPD_{min} - VPD_{max})) + f_{min}\}\} \quad \text{(A1.9k)}$$

while $$VPD = e_s(Ta) * (1-hr) \quad \text{(A1.9l)}$$

$$e_s(Ta) = a \exp(bT_a/(T_a+c)) \quad \text{(A1.9m)}$$

where VPD_{min} is the minimum vapour pressure deficit determining leaf stomata opening
VPD_{max} is the maximum vapour pressure deficit determining leaf stomata opening
T_a is the air temperature [°C]
h_r is the relative humidity [%]/100
$e_s(Ta)$ is the potential (saturation) water vapour pressure

a, *b*, *c* are the empirical constants (a = 0.611 kPa, b = 17.502, c = 240.97°C)

The ΣVPD (i.e., the function describing stomatal re-opening in the afternoon) is not taken into account.

Table A1.2: Parametrisation for POD_6SPEC for wheat flag leaves and the upper-canopy sunlit leaves of potato and tomato, for different biogeographical regions

Parameter	Units	(Bread) Wheat		Potato	Tomato
		Atlantic, Boreal, Continental *(Pannonia, Steppic)*	Mediterranean	Atlantic, Boreal, Continental *(Mediterranean Pannonia, Steppic)*	Mediterranean
g_{max}	mmol $O_3.m^{-2}$ PLA.s^{-1}	500	430	750	330
f_{min}	fraction	0.01	0.01	0.01	0.06
light_a	-	0.0105	0.0105	0.005	0.0125
T_{min}	°C	12	12	13	18
T_{opt}	°C	26	28	28	28
T_{max}	°C	40	39	39	37
VPD_{max}	kPa	1.2	3.2	2.1	1
VPD_{min}	kPa	3.2	4.6	3.5	4
f_{O3}	POD0 mmol $O_3.m^{-2}$.PLA s^{-1}	14	-	-	-
f_{O3}	AOT0, ppmh	-	-	40	-
f_{O3}	exponent	8	-	5	-
Astart_ETS	ºC day	-	-	-	250
Aend_ETS	ºC day	-	-	-	1500
Leaf dimension	cm	2	2	4	3
Canopy height	m	1	0.75	1	2
f_{phen_a}	fraction	0.3	0.5	0.4	1
f_{phen_b}	fraction	-	-	-	-
f_{phen_c}	fraction	-	-	-	-
f_{phen_d}	fraction	-	-	-	-
f_{phen_e}	fraction	0.7	0.5	0.2	0.0
$f_{phen\_1\_ETS}$	°C day	-200	-300	-330	0
$f_{phen\_2\_ETS}$	°C day	0	0	800	2770
$f_{phen\_3\_ETS}$	°C day	100	70	-	-
$f_{phen\_4\_ETS}$	°C day	525	312	-	-
$f_{phen\_5\_ETS}$	°C day	700	550	-	-
mid-anthesis	°C day	1075	1250	-	-

Source: CLRTAP, 2017a; González-Fernández et al., 2013; González-Fernández (personal communication, May 2021)

The parameter f_{SW} is replaced by f_{SMI} (where *SMI* represents Soil Moisture Index with maximum at field capacity), taking values between 0 and 1 as a proportion of g_{max} (with 0 for soil moisture at and below wilting point), following the parameterization given in Simpson et al. (2012), similar to the plant available water (*PAW*) parameterization f_{PAW} as defined for wheat in CLRTAP (2017a). The basic equation used for f_{SW} resp. f_{SMI} is:

$$f_{SMI} = 0 \quad \text{for SMI} \leq 0$$
$$= \frac{\text{SMI}}{\text{PAW}_t} \quad \text{for } 0 < \text{SMI} \leq PAW_t$$
$$= 1 \quad \text{for SMI} > PAW_t \qquad \text{(A1.9n)}$$

while $$\text{SMI} = \frac{\text{SWLL} - \text{PWP}}{\text{FC} - \text{PWP}} \qquad \text{(A1.9o)}$$

where PAW_t is the threshold amount of water in the soil available to the plants, above which stomatal conductance is at a maximum, set to 0.5

$SWLL$ is the soil moisture in [m^3 m^{-3}]

PWP is the permanent wilting point in [cm^3 cm^{-3}]

FC is the field capacity in [cm^3 cm^{-3}]

The Soil Moisture Index using the EMEP methodology as described in Simpson et al. (2012) and CLRTAP (2020) is used. It is computed using the soil moisture variable available from a meteorological model, which represents the water content in m^3 of water per m^3 of ground [m^3. m^{-3}] in a specific ground level, in dependence on the available dataset. For soil moisture, the ECWMF's ERA5-Land variable Volume of water in soil layer 3 (i.e. 28-100 cm) has been used, see Section 3.3. The level of soil layer was chosen based on recommendation of Haberle and Svoboda **(**2015**).** The soil moisture is quite a sensitive parameter in the calculation of the POD. Next to the soil moisture, the soil moisture index also takes into account the permanent wilting point and the field capacity; they are taken from JRC soil database (JRC, 2016), see Annex 2, Section A2.3.

No limitation of stomatal conductance due to soil moisture can be assumed for tomato, since it is an irrigated horticultural crop. Thus, f_{SMI} for this crop could be established to f_{SMI} = 1 over the whole range of SMI values to remove limitation due to soil moisture deficit.

Modelling the hourly stomatal flux of ozone (F_{sto})

Once the hourly stomatal conductance of ozone (g_{sto}) and all relevant variables are computed, the stomatal flux of ozone (F_{sto}) can be calculated, based on the assumption that the concentration of ozone at the top of the canopy represents a reasonable estimate of the concentration at the upper surface of the laminar layer for a sunlit upper canopy leaf. F_{sto} is calculated according to the CLRTAP (ICP Vegetation) methodology, thus the fraction of the ozone taken up by the stomata is given using a combination of the stomatal conductance, the external leaf, or cuticular, resistance and the leaf surface resistance. The hourly stomatal flux in the given hour H is calculated according to

$$F_{sto} = c(z_1) * g_{sto} * \frac{r_c}{r_b + r_c} \quad \text{(A1.10)}$$

where F_{sto} is the hourly stomatal flux of ozone in [nmol.m^{-2} PLA.s^{-1}]

$c(z_1)$ is the concentration of ozone at canopy top in [nmol.m^{-3}]

r_b is the quasi-laminar resistance in [s.m^{-1}]

r_c is the leaf surface resistance in [s.m^{-1}]

g_{sto} is the actual stomatal conductance in [m.s^{-1}],

while $r_c = 1/(g_{sto} + g_{ext})$ (A1.10a)

$$r_b = 1.3 * 150 * \sqrt{\frac{L}{u(z_1)}} \quad \text{(A1.10b)}$$

where g_{ext} is the external leaf, or cuticular, resistance in [m.s^{-1}], equal to 1/2500 m.s^{-1}

$u(z_1)$ is the wind speed at height z_1 (z_1 is the canopy top)

L is the cross-wind leaf dimension (2 cm, see Table A1.2)

while
$$u_{(z1)} = \frac{u*}{k} * ln\left(\frac{z_1 - d}{z_0}\right) \quad \text{(A1.10c)}$$

where k is the von Kármán constant (equal to 0.41)

d is the displacement height usually assumed as 2/3 of the canopy height,

z_1 is the top of the canopy

z_0 is the roughness length usually assumed as 1/10 of the canopy height

$u*$ is the friction velocity

Box A1.1 shows the conversion of stomatal conductance and ozone concentration to units demanded for POD_Y calculation.

Box A1.1: Conversion of stomatal conductance g_{sto} and ozone concentration to units demanded for POD_y calculation

Stomatal conductance g_{sto} has to be converted from units $mmol \cdot m^{-2} \cdot s^{-1}$ to units $m \cdot s^{-1}$ (since all the resistances are expressed in the unit of $s \cdot m^{-1}$). At standard temperature (20 °C) and air pressure (1.013 x 10^5 Pa), the conversion is made by dividing the conductance in $mmol \cdot m^{-2} \cdot s^{-1}$ by 41 000 to give conductance in $m \cdot s^{-1}$.

To convert the **ozone concentration (C)** at canopy height from $\mu g \cdot m^{-3}$ resp. ppb to nmol m^{-3}, the following equation should be used:

$$C\,[nmol \cdot m^{-3}] = C\,[ppb] * P/(R \cdot T) = C\,[\mu g \cdot m^{-3}] / 2 * P/(R \cdot T) \quad (A1.11)$$

where P is the atmospheric pressure in Pa,

R is the universal gas constant of 8.31447 J $mol^{-1} \cdot K^{-1}$

T is the air temperature in Kelvin.

At standard temperature (20 °C) and air pressure (1.013 x 10^5 Pa), the concentration in ppb should be multiplied by 41.56 to calculate the concentration in $nmol.m^{-3}$.

Source: CLRTAP, 2017a

In the routine used in this report (Section 2.3), an alternative conversion of the ozone concentrations from $\mu g \cdot m^{-3}$ resp. ppb to $nmol \cdot m^{-3}$ is done, using the air density instead of the atmospheric pressure, according to

$$C\,[nmol \cdot m^{-3}] = C\,[ppb] * \rho / N_a * 10^6 = C\,[\mu g \cdot m^{-3}] / 2 * \rho / N_a * 10^6 \quad (A1.12)$$

where ρ is the air density showing the number of the molecules in cm^{-3},
N_a is the Avogadro constant, which is equal to $6.022 \cdot 10^{23}$ mol^{-1}.

Calculation of POD_Y from F_{sto}

Hourly averaged stomatal ozone fluxes (F_{sto}) in excess of a Y threshold are accumulated over a species or vegetation-specific accumulation period using the following equation:

$$POD_Y = \sum_n (F_{sto}(n) - Y) \cdot \frac{3600}{10^6} \quad (A1.13)$$

while Y (for wheat, potato or tomato) = 6 nmol m^{-2} PLA s^{-1}

where POD_Y is the phytotoxic ozone dose related to the threshold Y, in [$mmol.m^{-2}$ PLA]
$F_{sto}(n)$ is the hourly ozone flux in the hour n of the accumulation period.

The value Y (in [nmol m^{-2} PLA s^{-1}]) is subtracted from each hourly averaged F_{sto} (in [nmol m^{-2} PLA s^{-1}]) value and the F_{sto} (after the subtracting of Y) is accumulated only when F_{sto}>Y, during daylight hours (when global radiation is more than 50 W m^{-2}). The value is then converted to hourly fluxes by multiplying by 3600 and to mmol by dividing by 10^6 to get the stomatal ozone flux in mmol m^{-2} PLA.

Calculation of exceedance of flux-based critical levels

If the calculated POD_Y value is larger than the flux-based Critical Level (CL) for O_3, then there is exceedance of the Critical Level ($CL_{exceedance}$). Exceedance of the Critical Level is calculated at follows:

$$CL_{exceedance} = POD_Y - CL \quad (A1.14)$$

A1.4 Methods for uncertainty analysis

The uncertainty estimation of the European map is based on leave-one-out cross-validation. This cross-validation method computes the quality of the spatial interpolation for each point of measurement (i.e., monitoring station) from all available information except from the point in question, i.e., it withholds one data point and then makes a prediction at the spatial location of that point. This procedure is repeated for all measurement points in the available set. The predicted and measurement values at these points are plotted in the form of a scatter plot. With help of statistical indicators, the quality of the predictions is demonstrated objectively. The advantage of the nature of this cross-validation technique is that it enables evaluation of the quality of the predicted values at locations without measurements, as long as they are within the area covered by the measurements.

In addition, a simple comparison is made between the point measurement data and the estimated values of the 1x1 km^2 grid cells (for PM and NO_2) or the 10x10 km^2 grid cells (for ozone) for the separate rural and urban maps and the 1x1 km^2 grid cells for the final combined maps, for the health-related indicators, resp. the 2x2 km^2 grid cells in the case of AOT40 and NO_x. Note that the grid cell value is the mean estimated value of this grid cell area. The estimated value within a grid cell will only approximate the predicted value(s) at the station(s) lying within that cell.

Another method to estimate uncertainties is based on geostatistical theory: together with the prediction, the prediction standard error is computed at all the grid cells, which represents in fact the interpolation uncertainty map (see Cressie, 1993 for a detailed discussion). Based on the concentration and the uncertainty map, the exceedance probability map is created.

Cross-validation

The results of cross-validation are described by the statistical indicators and scatter plots. The main indicator used is root mean squared error (RMSE) and the additional one is bias (mean prediction error, MPE):

$$RMSE = \sqrt{\frac{1}{N}\sum_{i=1}^{N}\left(\hat{Z}(s_i) - Z(s_i)\right)^2} \qquad \text{(A1.15)}$$

$$bias(MPE) = \frac{1}{N}\sum_{i=1}^{N}\left(\hat{Z}(s_i) - Z(s_i)\right) \qquad \text{(A1.16)}$$

where Z is the air quality indicator value derived from the measured concentration at the i^{th} point, i = 1, …, N,
is the air quality estimated indicator value at the i^{th} point using other information, without the indicator value derived from the measured concentration at the i^{th} point,
N is the number of the measuring points.

Next to the RMSE expressed in the absolute units, one could express this uncertainty in relative terms by relating the RMSE to the mean of the air pollution indicator value for all stations:

$$RRMSE = \frac{RMSE}{\bar{Z}}.100 \qquad \text{(A1.17)}$$

where *RRMSE* is the relative RMSE, expressed in percent,
$\bar{Z}$ is the arithmetic average of the indicator values $Z(s_1), \ldots, Z(s_N)$, as derived from measurement concentrations at the stations $i = 1, \ldots, N$.

Other indicators are R^2 and the regression equation (y = a.x + c) parameters slope (a) and intercept (c), following from the scatter plot between the predicted (using cross-validation) and the observed concentrations.

RMSE should be as small as possible, bias (MPE) should be as close to zero as possible, R^2 should be as close to 1 as possible, slope *a* should be as close to 1 as possible, and intercept *c* should be as close to zero as possible (in the regression equation $y = a.x + c$).

In the cross-validation of $PM_{2.5}$ and NO_x, only stations with $PM_{2.5}$, resp. NO_x, measurement data are used (not the pseudo $PM_{2.5}$, resp. NO_x, stations, see Annex 1 Section A1.1).

Comparison of the point measurement and interpolated grid values

The comparison of point measurement and predicted grid values is described by the linear regression equation and its parameters and statistical values. The comparison is executed separately for rural and urban background maps and for the final combined map. In the case of $PM_{2.5}$ and NO_x, only the stations with actual $PM_{2.5}$ resp. NO_x measurement data are used (not the pseudo $PM_{2.5}$ resp. NO_x stations).

The point observation – point cross-validation prediction analysis (Annex 3, sections "Uncertainty estimated by cross-validation") describes interpolation performance at point locations when there is no observation (as it follows the leave-one-out approach). In this case, the smoothing effect of the interpolation is most prevalent.

The point observation – grid prediction approach indicates performance of the value for the 10x10 km^2 (resp. 2x2 km^2 or 1x1 km^2) grid cell with respect to the observations that are located within that cell. As such, some variability is due to smoothing but it also includes smoothing due to spatial averaging into the 10x10 km^2 (2x2 km^2, 1x1 km^2) grid cells. As such, the point-grid validation approach tells us how well our interpolated and aggregated grid values approximate the measurements at the actual station (point) locations. Whereas the point-point approach tells us how well our interpolated values estimate the indicator at a point where there is no actual measurement at that location, under the constraint that the point lies within the area covered by measurements.

Annex 2
Input data

The types of input data in this paper are similar as in Horálek et al. (2021), supplemented with the NO_2 satellite data from Sentinel 5P (Veefkind et al., 2012). The air quality, modelling, satellite and meteorological data has been updated. For readability of this paper, the list of the input data is reproduced here. The key data is the air quality measurements at the monitoring stations extracted from the Air Quality e-Reporting database, including geographical coordinates (*latitude*, *longitude*). The supplementary data cover the whole mapping domain and are converted into the EEA reference projection ETRS89-LAEA5210 on a 1 x 1 km^2 grid resolution (for health-related indicators apart from ozone) resp. a 10x10 km^2 grid resolution (ozone). The data for the maps of vegetation related indicators (particularly AOT40) were converted – like in the previous reports (Horálek et al., 2021, and references cited therein) – into a 2 x 2 km^2 resolution to allow accurate land cover exposure estimates to be prepared for use in the Core Set Indicator 005 of the EEA (EEA, 2021b).

A2.1 Air quality monitoring data

Air quality station monitoring data for the relevant year as extracted from the official EEA Air Quality e-Reporting database, EEA (2021a) in March 2021 has been used. This data set is supplemented with several EMEP rural stations from the database EBAS (NILU, 2021) not reported to the Air Quality e-Reporting database. Specifically, 4 additional stations for PM_{10}, 3 for $PM_{2.5}$, 6 for NO_2 and 3 for NO_x from the EBAS database are added.

The following pollutants and aggregations are considered:

PM_{10} – annual average [$\mu g \cdot m^{-3}$], year 2019
– 90.4 percentile of the daily average values [$\mu g \cdot m^{-3}$], year 2019

$PM_{2.5}$ – annual average [$\mu g \cdot m^{-3}$], year 2019

Ozone – 93.2 percentile of the maximum daily 8-hour average values [$\mu g \cdot m^{-3}$], year 2019
– SOMO35 [$\mu g \cdot m^{-3} \cdot day$], year 2019
– SOMO10 [$\mu g \cdot m^{-3} \cdot day$], year 2019
– AOT40 for vegetation [$\mu g \cdot m^{-3} \cdot hour$], year 2019
– AOT40 for forests [$\mu g \cdot m^{-3} \cdot hour$], year 2019
– hourly values [$\mu g \cdot m^{-3}$], all hours of the year 2019 (for the purpose of POD_6 mapping)

NO_2 – annual average [$\mu g \cdot m^{-3}$], year 2019

NO_x – annual average [$\mu g \cdot m^{-3}$], year 2019

NO – annual average [$\mu g \cdot m^{-3}$], year 2019 (for the purposes of NO_x mapping only)

The exact values of percentiles are actually 90.41 in the case of PM_{10} daily means and 93.15 in the case of ozone maximum daily 8-hour means.

For a considerable number of stations NO_x is measured, but it is not reported as such but separately as NO and NO_2. For these stations reporting NO and NO_2 separately, the NO_x concentrations were derived according to the equation

$$NO_x = NO_x + \frac{46}{30} \cdot NO \qquad \text{(A2.1)}$$

In this equation, all components are expressed in $\mu g \cdot m^{-3}$, with a molecular mass for NO of 30 $g \cdot mol^{-1}$ and for NO_2 of 46 $g \cdot mol^{-1}$.

SOMO35 is the annual sum of the differences between maximum daily 8-hour concentrations above 70 $\mu g \cdot m^{-3}$ (i.e. 35 ppb) and 70 $\mu g \cdot m^{-3}$. SOMO10 is the annual sum of the differences between maximum daily 8-hour means above 20 µg·m^{-3} (i.e. 10 ppb) and 20 µg·m^{-3}. AOT40 is the sum of the differences between hourly concentrations greater than 80 µg·m^{-3} (i.e. 40 ppb) and 80 µg·m^{-3}, using only observations between 08:00 and 20:00 CET, calculated over the three months from May to July for AOT40 for vegetation and over the six months from April to September for AOT40 for forests.

Only the stations with annual data coverage of at least 75 percent are used. In the case of SOMO35, SOMO10 and AOT40 indicators, a correction for the missing data is applied according to the equation

$$I_{corr} = \mathrm{I} \cdot \frac{N_{max}}{N} \quad \text{(A2.2)}$$

where I_{corr} is the corrected indicator (SOMO35, SOMO10 or AOT40 for vegetation or for forests),
I is the value of the given indicator without any correction,
N is the number of the available daily resp. hourly data in a year for the given station,
N_{max} is the maximum possible number of the days or hours applicable for the indicator.

For the indicators relevant to human health (i.e. for all PM_{10} and $PM_{2.5}$ indicators, ozone indicators 93.2 percentile of maximum daily 8-hour means, SOMO35 and SOMO10, and NO_2 annual average), data from stations classified as *background* (for all the three types of area, *rural*, *urban* and *suburban*) are considered; for PM_{10} and $PM_{2.5}$ and NO_2, also *urban* and *suburban traffic* stations are considered. (Throughout the paper, the urban and suburban stations are handled together). *Industrial* stations are not considered, as they represent local concentration levels that cannot be easily generalized for the whole map. For the indicators relevant to vegetation damage (i.e., for ozone AOT40 and POD_6 parameters and NO_x annual average), only *rural background* stations are considered; the relevant maps are constructed (and applicable) for rural areas only. In case of existing data (with sufficient annual time coverage) from two or more different measurement devices in the same station location, the average of these data is used.

The stations from French overseas areas (departments), Svalbard, Azores, Madeira and Canary Islands were excluded. These areas outside the EEA map extent Map_2c (EEA, 2018) were excluded from the interpolation and mapping domain, as the interpolation should be performed across generally compact territory.

Table A2.1 shows the number of the measurement stations selected for the individual pollutants and their respective indicators.

Table A2.1: Number of stations selected for each pollutant indicator and area type, 2019

Station type	**PM_{10}**		**$PM_{2.5}$**	**Ozone**				**NO_2**	**NO_x**
	Ann. avg.	**90.4 perc. of d. m.**	**Ann. avg.**	**Health related**	**AOT40 for veg.**	**AOT40 for for.**	**POD_6**	**Ann. avg.**	**Ann. avg.**
Rural background	381	375	220	550	546	546	593	480	393
Urban/suburb. backgr.	1452	1441	768	1201	-	-	-	1381	-
Urban/suburban traffic	775	766	379	-	-	-	-	1060	-

Compared to 2018, the number of the rural background stations increased by about 5 % for $PM_{2.5}$, decreased by about 3 % for NO_2, while it remained almost the same for other pollutants. The number of the urban/suburban background stations increased by approximately 12 % for $PM_{2.5}$ and by about 2-3 % for PM_{10} and NO_2, while it remained almost the same for ozone. The number of the urban/suburban traffic stations increased by about 9 % for $PM_{2.5}$, 4 % for NO_2 and 2 % for PM_{10}.

For the $PM_{2.5}$ mapping, in addition to the $PM_{2.5}$ stations, 184 rural background, 722 urban/suburban background and 412 urban/suburban traffic PM_{10} stations (at locations without $PM_{2.5}$ measurement) have been also used for the purpose of calculating the pseudo $PM_{2.5}$ station data.

In the case of NO_x, 340 stations with NO_x reported data have been used, while for 53 stations NO_x values are calculated from reported NO_2 and NO data using Eq. A2.1. Next to this, for the NO_x

mapping 75 additional rural background NO_2 stations (at locations without NO_x measurement) were also used for the purpose of calculating the pseudo NO_x station data.

A2.2 EMEP MSC-W model output

The chemical dispersion model used in this paper is the EMEP MSC-W (formerly called Unified EMEP) model (version rv4.35), which is an Eulerian model. Simpson et al. (2012) and https://wiki.met.no/emep/page1/emepmscw_opensource (web site of Norwegian Meteorological Institute) describe the model in more detail. Emissions for the previous year 2018 (Mareckova et al., 2020) are used and the model is driven by ECMWF meteorology for the relevant year 2019. EMEP (2020) provides details on the EMEP modelling for 2019 using 2018 emission. The resolution of the model is 0.1°x0.1°, i.e. circa 10x10 km^2. For the third time, the model output based on the emission for the previous (not actual) year has been used, in agreement with conclusion of Horálek et al. (2016b), in order to enable the map creation a half year earlier than using the model results based on the actual emission.

The EMEP data were downloaded from NMI (2021) in the form of annual means, daily means and hourly means. Where relevant, these primary have been aggregated data to the same set of parameters as for the air quality observations:

PM_{10} – annual average [$\mu g \cdot m^{-3}$], year 2019
– 90.4 percentile of the daily means [$\mu g \cdot m^{-3}$], year 2019 (aggregated from daily means)

$PM_{2.5}$ – annual average [$\mu g \cdot m^{-3}$], year 2019

Ozone – 93.2 percentile of the highest maximum daily 8-hour average value [$\mu g \cdot m^{-3}$], year 2019 (aggregated from hourly means)
– SOMO35 [$\mu g \cdot m^{-3} \cdot day$], year 2019 (aggregated from hourly means)
– SOMO10 [$\mu g \cdot m^{-3} \cdot day$], year 2019 (aggregated from hourly means)
– AOT40 for vegetation [$\mu g \cdot m^{-3} \cdot hour$], year 2019 (aggregated from hourly means)
– AOT40 for forests [$\mu g \cdot m^{-3} \cdot hour$], year 2019 (aggregated from hourly means)

NO_2 – annual average [$\mu g \cdot m^{-3}$], year 2019

NO_x – annual average [$\mu g \cdot m^{-3}$], year 2019

Due to the complete temporal data coverage available at the modelled data, the PM_{10} indicator 90.4 percentile of daily means is identical with the 36th highest daily mean and the ozone indicator 93.2 percentile of maximum daily 8-hour means is identical with the 26th highest maximum daily 8-hour mean.

The data were re-gridded into the reference EEA 10x10 km^2 grid (for ozone health related indicators), 1x1 km^2 grid (for PM and NO_2) and 2x2 km^2 grid (for vegetation related indicators).

A2.3 Other supplementary data

Meteorological parameters

The meteorological data used are the ECWMF data extracted from the CDS (Climate Data Store, https://cds.climate.copernicus.eu/cdsapp#!/home). Hourly data for 2019 are used. Most of the data come from the reanalysed data set ERA5-Land in 0.1°x0.1° resolution (of CDS), namely the indicators:

Surface solar radiation [$MWs.m^{-2}$] – variable "Surface solar radiation downwards"
Temperature [K] – variable "2m temperature"
Wind speed [$m.s^{-1}$] – calculated based on variables "10m u-component of wind" and "10m v-component of wind"
Relative humidity [%] – calculated based on variables "2m temperature" and "2m dewpoint temperature"

Soil water – variable "Volumetric soil water layer 3", i.e. layer of 28-100 cm (used for POD only)

Wind speed (WV) is derived from the "10m u-component of wind" (10U) and "10m v-component of wind" (10V) according to relation

$$WV = \sqrt{(10U)^2 + (10V)^2} \quad \text{(A2.3)}$$

Relative humidity (RH) is derived by means of the saturated water vapour pressure (e_t) as a function of "2m temperature" (2T) and "2m dew point temperature" (2D) according to relation

$$RH = \frac{e_{2D}}{e_{2T}} \cdot 100\text{, with} = e_t = 6.1365^{\frac{17.502 \cdot t}{24097 + t}} \quad \text{(A2.4)}$$

where t is 2T and 2D, respectively.

In the coastal areas (where the data from ERA5-Land are not available), the same parameters from the reanalysed data set ERA5 in 0.25°x0.25° resolution are applied. Next to this, the following data (not available in the ERA5-Land data set) from the ERA5 data set is also used:

Friction velocity [$m.s^{-1}$] – variable "Friction velocity". The friction velocity (also known as the shear-stress velocity) has the dimensions of velocity.

Next to the meteorological data of ERA5-Land and ERA5, the following indicators based on the meteorological ECWMF's IFS (Integrated Forecasting System) data and coming from the CHIMERE pre-processing are used, being the hourly data for 2019 in 0.1°x0.1° resolution:

Obukhov length [m] – the stability of the atmospheric surface layer expressed in terms of the Obukhov length L (1/L = 0 if the atmosphere is neutral, 1/L < 0 if the atmosphere is unstable, 1/L > 0 if the atmosphere is stable).
Air density [$molec.cm^{-3}$] – expressed the number of the molecules in cm^{-3}.

Most of the meteorological parameters are used for POD_6 maps only. For other maps than POD_6, annual aggregations based on hourly data are used, namely for the parameters:

Wind speed	– annual average [$m \cdot s^{-1}$], year 2019
Relative humidity	– annual average [%], year 2019
Surface solar radiation	– annual average of daily sum [$MWs.m^{-2}$], year 2019

All meteorological data were re-gridded and converted into the reference EEA 1x1 km^2 grid, 10x10 km^2 grid and 2x2 km^2 grid, in the ETRS89-LAEA5210 projection.

Altitude

The altitude data field (in meters) of Global Multi-resolution Terrain Elevation Data 2010 (GMTED2010) is used, with an original grid resolution of 15x15 arcseconds (some 463x463 m at 60N). Source: U.S. Geological Survey Earth Resources Observation and Science, see Danielson et al. (2011). The field is converted into the ETRS 1989 LAEA projection. (The resolution after projection was in 449.2x449.2 m). In the following step, the raster dataset was resampled to 100x100 m^2 resolution and shifted it to the extent of EEA reference grid. As a final step, the dataset was spatially aggregated into 1x1 km^2, 2x2 km^2 and 10x10 km^2 resolutions.

Population density and population totals

Population density (in $inhbs.km^{-2}$, census 2011) is based on Geostat 2011 grid dataset, Eurostat (2014). The dataset is in 1x1 km^2 resolution, in the EEA reference grid.

For regions not included in the Geostat 2011, alternative sources were used. Primarily, JRC (Joint Research Centre) population data in resolution 100x100 m^2 were used (JRC, 2009). The JRC 100x100 m^2 population density data is spatially aggregated into the reference 1x1 km^2 EEA grid. For regions that are neither included in the Geostat 2011 nor in the JRC database, population density data from ORNL LandScan Global Population Datase, https://landscan.ornl.gov/ was used. This dataset in 30x30 arcsec resolution; based on the annual mid-year national population estimates for 2008 (from the Geographic Studies Branch, US Bureau of Census, http://www.census.gov) was earlier re-projected and converted from its original WGS1984 30x30 arcsecs grids into EEA's reference projection ETRS89-LAEA5210 at 1x1 km^2 resolution by the EEA (EEA, 2010).

The areas lacking Geostat 2011 data, and supplemented with JRC or ORNL data were: Gibraltar (JRC); Faroe Islands, British crown dependencies (Jersey, Guernsey and Man) and northern Cyprus (ORNL). As such, the Geostat 2011 1x1 km^2 data and these supplements cover the entire mapping area.

To verify the consistency of merging Geostat 2011 with JRC and ORNL data, the Geostat 2011 data were compared to the JRC supplemented with ORNL data on the basis of the national population totals of the individual countries. Additionally, the national population totals for the Geostat 2011 gridded data were verified with the Eurostat national population data for 2019 (Eurostat, 2021). Figure A2.1 presents both comparisons. From these verifications, one can conclude a high correlation of the national population totals of each data source. Slight underestimation of the supplemented JRC and ORNL data in comparison with the Geostat 2011 data can be seen, which is caused by the fact that the Geostat 2011 data is more up-to-date than both the JRC and the ORNL data source. Geostat 2011 and Eurostat 2019 data correlate even better and leads to a similar conclusion. Based on this, in the further calculations on national population totals the actual Eurostat data for 2019 (Eurostat, 2021) were used, as described further.

Figure A2.1: Correlation of national population totals for JRC supplemented with ORNL (left) and Eurostat 2019 (right) with Geostat 2011

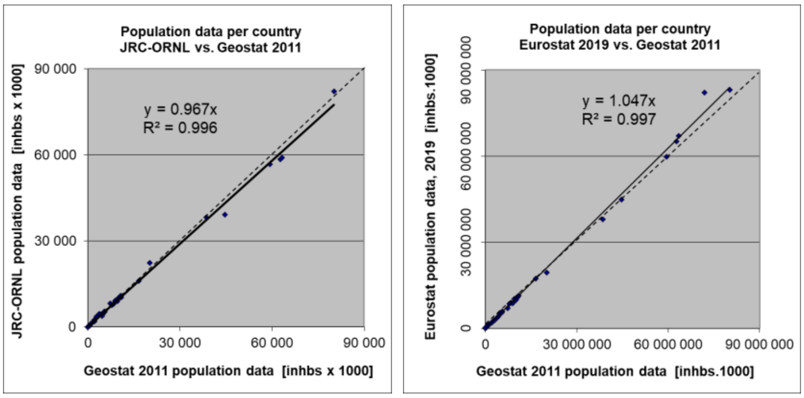

Population density data can be used to classify the spatial distribution of each type of area (rural, urban or mixed population density) in Europe. This information is used to select and weight the air quality values, grid cell by grid cell and merge them into a final combined map (Annex 1). Furthermore, It is used to estimate population health exposure and exceedance numbers per country, EU-28 and for the total mapping area, including involved uncertainties. These activities take place on the 1x1 km^2 resolution grid in accordance with the recommendations of Horálek et al. (2010). The supplemented Geostat data (as described above) are used in all the calculations.

National population totals presented in the exposure tables of this paper are based on Eurostat national population data for 2019 (Eurostat, 2021). For France, Portugal and Spain, the population totals of areas outside the mapping area (i.e. French oversea departments Azores, Madeira and Canarias) are subtracted. For Faroe Islands and Crown dependencies not included in the Eurostat database, the population totals are based on UN (2020). For Cyprus, population of the northern part of Cyprus (based on http://www.devplan.org) is added to the population total based on Eurostat.

Land cover

CORINE Land Cover 2018 (CLC2018) – grid 100 x 100 m^2, Version 2020_20 is used (EU, 2020). For Andorra that is missing is this database, World Land Cover at 30m resolution from MDAUS BaseVue 2013 (MDA, 2015) resampled to 100m resolution is used. For areas that are neither included in the

CLC2018 nor in the World Land Cover database (i.e., Jan Mayen and some border areas), ESA Climate Change Initiative Global Land Cover for 2018 (ESA, 2019) is used, resampled to 100m resolution.

In agreement with Horálek et al. (2017b), the 44 CLC classes have been re-grouped into the 8 more general classes. In this paper four of these general classes are used, see Table A2.2.

Table A2.1: General land cover classes, based on CLC2018 classes, used in mapping

Label	General class description	CLC classes grid codes	CLC classes codes	CLC classes description
HDR	High density residential areas	1	111	Continuous urban fabric
LDR	Low density residential areas	2	112	Discontinuous urban fabric
AGR	Agricultural areas	12 - 22	211 - 244	Agricultural areas
NAT	Natural areas	23 - 34	311 - 335	Forest and semi natural areas

Two aggregations are used, i.e., into 1x1 km^2 grid and into the circle with radius of 5 km. For each general CLC class, the high land use resolution is spatially aggregated into the 1x1 km^2 EEA standard grid resolution. The aggregated grid square value represents for each general class the total area of this class as percentage of the total 1x1 km^2 square area. For details, see Horálek et al. (2017b).

Road type vector data

GRIP (Meijer et al., 2018) vector road type data base provided by the Netherlands Environmental Assessment Agency (PBL) is used. The road types are distributed into 5 classes, from highways to local roads and streets. In agreement with Horálek et al. (2017b), road classes No. 1 “Highways”, No. 2 “Primary roads” and No. 3 “Secondary roads” are used.

Percentage of the area influenced by traffic is represented by buffers around the roads: for the individual classes 1-3 and for classes 1-3 together, at all 1x1 km^2 grid cells; a buffer of 75 metres distance at each side from each road vector is taken for the roads of classes 1 and 2, while a buffer of 50 metres is taken for the roads of class 3. For details, see Horálek et al. (2017b).

Satellite data

The annual average NO_2 dataset was constructed based on data from the TROPOspheric Monitoring Instrument (TROPOMI) onboard of the Sentinel-5 Precursor satellite (Veefkind et al., 2012). All available swath-based Level-2 data with an irregular pixel geometry was acquired for the year 2019. Until August 2019, the spatial resolution was approximately 7 km by 3.5 km at nadir; after August 2019 this was reduced to 5.5 km by 3.5 km. The product used is the S5P_OFFL_L2__NO2 product (van Geffen et al., 2020; Van Geffen et al., 2019) and it provides the tropospheric vertical column density of NO_2, i.e. a vertically integrated value over the entire troposphere. All overpasses for a specific day were then mosaicked using HARP (https://stcorp.github.io/harp/doc/html/index.html) and retrievals with a quality assurance values greater than 0.75 (indicating high quality and cloud-free conditions) were gridded to a regular projected grid for all area with a 1x1 km^2 spatial resolution in a ETRS89 / ETRS-LAEA (EPSG 3035) projection. The daily gridded files were subsequently averaged to an annual mean. I.e., the parameter used is

NO_2 – annual average tropospheric vertical column density (VCD) [number of NO_2 molecules per cm^2 of earth surface], year 2019 (aggregated from cloud-free high-quality daily data).

Soil hydraulic properties data

JRC data called "Maps of indicators of soil hydraulic properties for Europe" in 1x1 km^2 resolution are used for POD_6 calculations, JRC (2016). Namely the following indicators are used:

Wilting Point – water content at wilting point [$cm^3 \cdot cm^{-3}$]
Field Capacity – water content at field capacity [$cm^3 \cdot cm^{-3}$]

Annex 3
Technical details and mapping uncertainties

This annex contains technical details on the linear regression models and the residual kriging, including the performance. Furthermore, uncertainty estimates for the maps of the indicators are given.

A3.1 PM_{10}

Technical details on the mapping and uncertainty estimates for both PM_{10} indicators maps annual average (Map 2.1) and 90.4 percentile of daily means (Map 2.2) are presented in this section.

Technical details on the mapping

Table A3.1 presents the estimated parameters of the linear regression models (c, a_1, a_2, …) and of the residual kriging (nugget, sill, range) and includes the statistical indicators of both the regression and the kriging, for both PM_{10} indicators. The linear regression and ordinary kriging of its residuals are applied on the logarithmically transformed data of both measurement and modelled PM_{10} values. In Table A3.1 the standard error and variogram parameters (nugget, sill and range) refer to these transformed data, whereas RMSE and bias refer to the interpolation after a back-transformation.

Since 2017 maps, an updated methodology as developed and tested under Horálek et al. (2019) has been used, i.e., including land cover among the supplementary data and using the traffic urban map layer.

The adjusted R^2 and standard error are indicators for the fit of the regression relationship, where the adjusted R^2 should be as close to 1 as possible and the standard error should be as small as possible. The adjusted R^2 for the rural areas was 0.64 at the annual average and 0.58 at the P90.4; for the urban background areas 0.35 at the annual average and 0.31 at the P90.4; for the urban traffic areas 0.43 at the annual average and 0.33 at the P90.4.

Table A3.1: Parameters and statistics of linear regression model and ordinary kriging of PM_{10} indicators annual average and 90.4 percentile of daily means for 2019 in rural, urban background and urban traffic areas for the final combined map

		Annual average			90.4 percentile of daily means		
		Rural areas	Urb. b. ar.	Urb. tr. ar.	Rur. ar.	Urb. b. ar.	Urb. tr. ar.
Linear regresion model (LRM, Eq. A1.3)	c (constant)	1.31	1.14	1.62	1.73	1.40	2.29
	a1 (log. EMEP model)	0.652	0.721	0.56	0.568	0.673	0.46
	a2 (altitude GMTED)	-0.00029			-0.00023		
	a3 (wind speed)	-0.037			-0.041		-0.054
	a4 (relative humidity)						
	a5 (land cover NAT)	-0.001			-0.002		
	Adjusted R^2	**0.64**	**0.35**	**0.43**	**0.58**	**0.31**	**0.33**
	Stand. Error [μg.m^{-3}]	**0.24**	**0.31**	**0.25**	**0.24**	**0.33**	**0.27**
Ordinary kriging (OK) of LRM residuals	nugget	0.021	0.013	0.013	0.023	0.018	0.017
	sill	0.049	0.068	0.042	0.051	0.083	0.050
	range [km]	1000	640	330	1000	640	330
LRM + OK of its residuals	**RMSE [μg.m^{-3}]**	**3.0**	**6.5**	**4.3**	**6.0**	**12.5**	**8.0**
	Relative RMSE [%]	**20.0**	**28.7**	**19.3**	**22.9**	**31.6**	**20.6**
	Bias (MPE) [μg.m^{-3}]	**0.0**	**-0.1**	**-0.1**	**0.0**	**-0.3**	**-0.1**

RMSE (the smaller the better) and bias (the closer to zero the better), highlighted by orange, are the cross-validation indicators, showing the quality of the resulting map. The bias indicates to what extent the predictions are under- or overestimated on average. Further in this section, more detailed uncertainty analysis is presented.

Uncertainty estimated by cross-validation

Using RMSE as the most common indicator, the absolute mean uncertainty of the final combined map at areas 'in between' the station measurements (i.e., at locations without measurements, as long as they are within the area covered by the measurements) can be expressed in $\mu g \cdot m^{-3}$. Table A3.1 shows that the absolute mean uncertainty of the final combined map of PM_{10} annual average and 90.4 percentile of daily means expressed by RMSE is 3 0 $\mu g \cdot m^{-3}$ and 6.0 $\mu g \cdot m^{-3}$ for the rural areas, 6.5 $\mu g \cdot m^{-3}$ and 12.5 $\mu g \cdot m^{-3}$ for the urban background areas, and 4.3 $\mu g \cdot m^{-3}$ and 8.0 $\mu g \cdot m^{-3}$ for the urban traffic areas, respectively. Alternatively, one can express this uncertainty in relative terms by relating the absolute RMSE uncertainty to the mean air pollution indicator value for all stations. This relative mean uncertainty (Relative RMSE) of the final combined map of PM_{10} annual average and 90.4 percentile of daily means is 20.0 % and 22.9 % for rural areas, 28.7 % and 31.6 % for urban background areas, and 19.3 % and 20.6 % for urban traffic areas, respectively. These quite high numbers in urban background areas compared to previous years up to 2015 are caused by inclusion of Turkey since 2016 mapping. For the mapping results without Turkey, the relative mean uncertainty is 17.6 % and 19.7 % for rural areas, 19.8 % and 20.8 % for urban background areas and 17.5 % and 18.8 % for urban traffic areas, respectively. Nevertheless, the relative uncertainty values including Turkey fulfil the data quality objectives for models as set in Annex I of the Air Quality Directive (EC, 2008).

Figure A3.1 shows the cross-validation scatter plots, obtained according to Annex 1, Section A1.4 for rural, urban background and urban traffic areas, for both PM_{10} indicators. The R^2 indicates that the variability is attributable to the interpolation for about 74 % and 68 % at the rural areas, for about 65 % and 62 % at the urban background areas, and for about 54 % and 75 % at the urban traffic areas, for the PM_{10} indicators annual average and the 90.4 percentile of daily means, respectively.

Figure A3.1: Correlation between cross-validated predicted (y-axis) and measurement values for PM_{10} indicators annual average (top) and 90.4 percentile of daily means (bottom) for 2019 for rural (left), urban background (middle) and urban traffic (right) areas

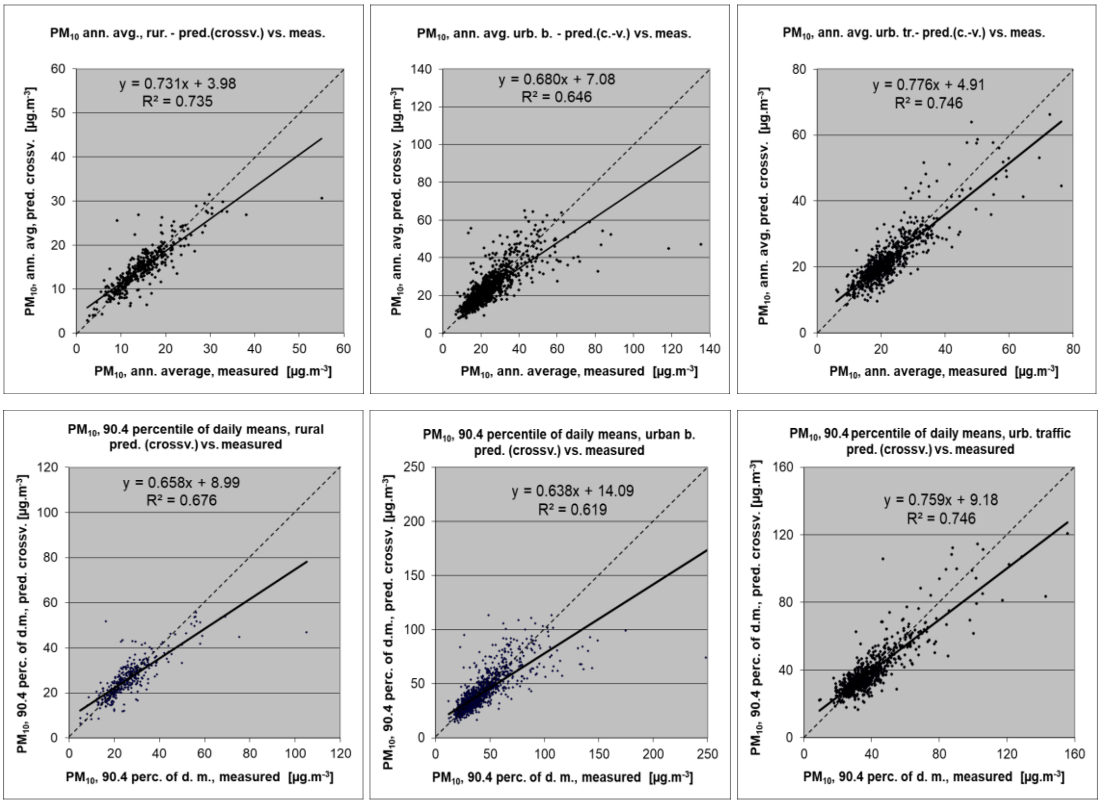

The trend line in the scatter-plots deviates at the lowest values somewhat above, and at higher values below the symmetry axis, indicating that the interpolation methods tend to underestimate the high concentrations and overestimate the low concentrations. For example, in rural areas for annual average an observed value of 30 μg·m^{-3} is estimated in the interpolations to be about 26 μg·m^{-3}, about 14 % lower. This underestimation at high values is common to all spatial interpolation methods. It could be reduced by either using a higher number of stations with an improved spatial distribution, or by introducing an improved regression that uses either other supplementary data or more advanced chemical transport model (resp. model in finer resolution).

Comparison of point measurement values with the predicted grid value

In addition to the above point observation – point prediction cross-validation, a simple comparison has been made between the point observation values and interpolated prediction values spatially averaged at grid cells. This point observation – grid averaged prediction comparison indicates to what extent the predicted value of a grid cell represents the corresponding measurement values at stations located in that cell. The comparison has been made primarily for the separate rural, urban background and urban traffic map layers at 1x1 km^2 resolution. (One can directly relate this comparison result to the cross-validation results of Figure A3.1). Apart from this, the comparison has been done also for the final combined maps at the same 1x1 km^2 resolution. Figure A3.2 shows the scatterplots for these comparisons, for PM_{10} annual average only as an illustration. The results of the point observation – point prediction cross-validation of Figure A3.1 and those of the point observation – grid averaged prediction validation for separate rural, urban background and urban traffic map layers, and for the final combined maps are summarised in Table A3.2 for both PM_{10} indicators.

Figure A3.2: Correlation between predicted grid values from rural (upper left), urban background (upper middle) and urban traffic (upper right) map layer and final combined map (all bottom) (y-axis) versus measurements from rural (left), urban/suburban background (middle) and urban/suburban traffic stations (right) (x-axis) for PM_{10} annual average 2019

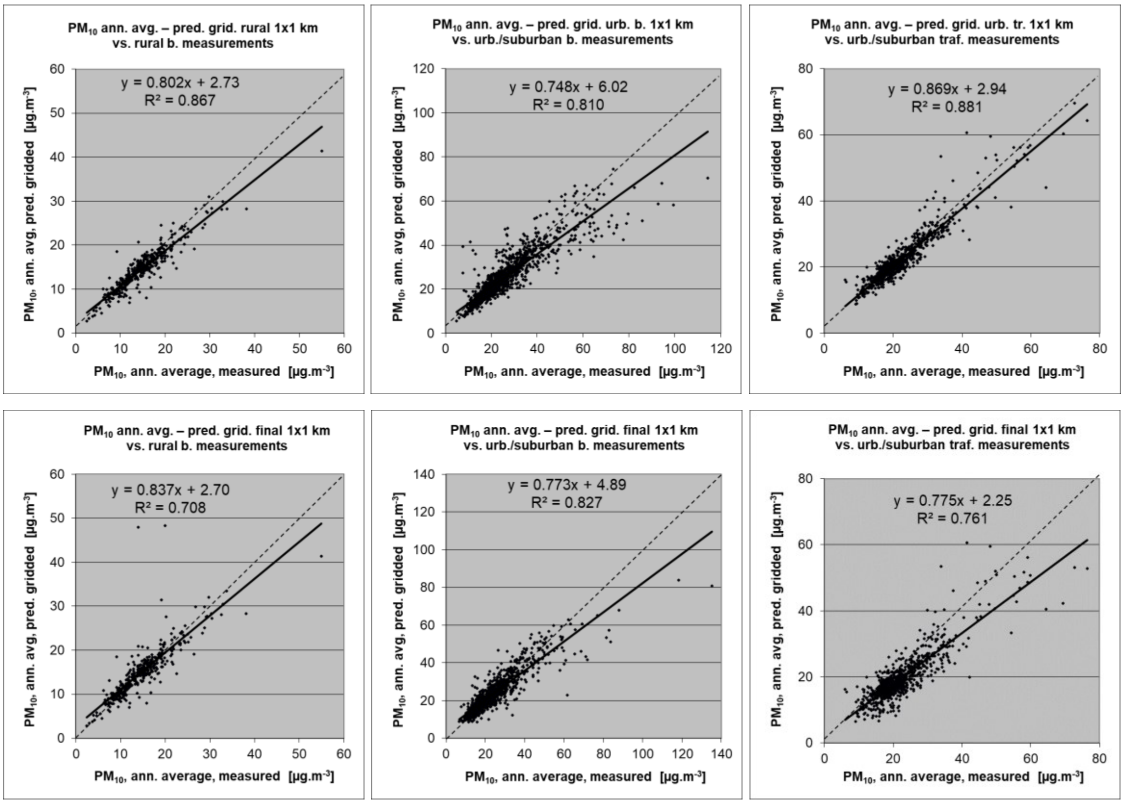

Table A3.2: Statistical indicators from the scatter plots for the predicted grid values from separate (rural, urban background or urban traffic) map layers and final combined map versus the measurement point values for rural (upper left), urban background (upper right) and urban traffic (bottom left) stations for PM_{10} indicators annual average (top) and 90.4 percentile of daily means (bottom) for 2019

PM_{10}	rural backgr. stations				urban/suburban backgr. stations			
	RMSE	bias	R^2	lin. r. equation	RMSE	bias	R^2	lin r. equation
Annual average								
cross-val. prediction, separate (r or ub) map layer	3.0	0.0	0.735	y = 0.731x + 3.98	6.5	-0.1	0.646	y = 0.680x + 7.08
grid prediction, 1x1 km² separ. (r or ub) map layer	2.1	-0.2	0.867	y = 0.802x + 2.73	4.2	-0.2	0.810	y = 0.748x + 6.02
grid prediction, 1x1 km² final combined map	3.2	0.3	0.708	y = 0.837x + 2.70	4.6	-0.2	0.827	y = 0.773x + 4.89
90.4 percentile of daily means								
cross-val. prediction, separate (r or ub) map layer	6.0	0.0	0.676	y = 0.658x + 8.99	12.5	-0.3	0.619	y = 0.638x + 14.09
grid prediction, 1x1 km² separ. (r or ub) map layer	4.4	-0.4	0.843	y = 0.738x + 6.49	8.5	-0.4	0.836	y = 0.745x + 9.67
grid prediction, 1x1 km² final combined map	5.8	0.4	0.708	y = 0.774x + 6.37	9.1	-0.6	0.806	y = 0.731x + 10.06

PM_{10}	urban/suburban traffic stations			
	RMSE	bias	R^2	lin. r. equation
Annual average				
cross-valid. prediction, urban traffic map layer	4.3	-0.1	0.746	y = 0.776 + 4.91
grid prediction, 1x1km² urban traffic map layer	2.9	0.0	0.881	y = 0.869x + 2.94
grid prediction, 1x1 km² final combined map	5.0	-2.8	0.761	y = 0.775x + 2.25
90.4 percentile of daily means				
cross-valid. prediction, urban traffic map layer	8.0	-0.1	0.746	y = 0.759x + 9.18
grid prediction, 1x1km² urban traffic map layer	17.9	16.3	0.888	y = 0.857x + 5.55
grid prediction, 1x1 km² final combined map	13.8	11.6	0.742	y = 0.736x + 5.49

By comparing the scatterplots and the statistical indicators for the separate rural, urban background and urban traffic map layers with the final combined map, one can evaluate the level of representation of the rural, urban background and urban traffic areas in the final combined map. Both the rural and the urban air quality are fairly well represented in the 1x1 km² final combined map, while the traffic air quality is underestimated in this spatial resolution. One can conclude that the final combined map in 1x1 km² resolution is representative for rural and urban background areas, but not for urban traffic areas.

The Table A3.2 shows a better relation (i.e., lower RMSE, higher R^2, smaller intercept and slope closer to 1) between station measurements and the interpolated values of the corresponding grid cells at either rural, urban background or urban traffic areas than it does at the point cross-validation predictions. That is because the simple comparison between point measurements and the gridded interpolated values shows the uncertainty at the actual station locations (points), while the point cross-validation prediction simulates the behaviour of the interpolation at point positions assuming no actual measurement would exist at that point. The uncertainty at measurement locations is introduced partly by the smoothing effect of the interpolation and partly by the spatial averaging of the values in the 1x1 km² grid cells. The level of the smoothing effect leading to underestimation at areas with high values is there smaller than in situations where no measurement is represented in such areas. For example, in rural areas the predicted interpolation gridded annual average value in the separate rural map will be about 27 $\mu g \cdot m^{-3}$ at the corresponding station with the measurement value of 30 $\mu g \cdot m^{-3}$. This means an underestimation of about 11 %. It is a slightly less than the prediction underestimation of 14 % at the same point location, when leaving out this one actual measurement point and the interpolation is done without this station (see the previous subsection).

A3.2 $PM_{2.5}$

Technical details and uncertainty estimates for Map 3.1 with the $PM_{2.5}$ annual average are presented in this section.

Technical details on the mapping

Like for PM_{10}, an updated methodology as developed and tested under Horálek et al. (2019) has been used, i.e., including the land cover among supplementary data and using the traffic urban map layer.

Table A3.3 presents the regression coefficients determined for pseudo $PM_{2.5}$ stations data estimation, based on the 864 rural and urban/suburban background and 349 urban/suburban traffic stations that have both $PM_{2.5}$ and PM_{10} measurements available (see Section 2.1.1).

Table A3.3: Parameters and statistics of linear regression model for generating pseudo $PM_{2.5}$ annual average data for 2019 in rural and urban background (left) and urban traffic (right) areas

		Rural and urban background areas	Urban traffic areas
Linear regresion model (LRM, Eq. A1.1)	c (constant)	28.4	42.3
	b (PM_{10} measurement data)	0.649	0.471
	a1 (surface solar radiation)	-1.021	-1.103
	a2 (latitude)	-0.334	-0.544
	a3 (longitude)	0.079	0.064
	Adjusted R^2	**0.83**	**0.72**
	Standard Error [μg.m^{-3}]	**2.0**	**2.3**

Table A3.4 presents the estimated parameters of the linear regression models (c, a_1, a_2,…) and of the residual kriging (nugget, sill, range) and includes the statistical indicators of both the regression and the kriging of its residuals. The same supplementary data as in Horálek et al. (2019) has been used, apart from the land cover, which was found not significant. Like in the case of PM_{10}, the linear regression is applied on the logarithmically transformed data of both measurement and modelled $PM_{2.5}$ values. Thus, the standard error and variogram parameters refer to these transformed data, whereas RMSE and bias refer to the interpolation after the back-transformation.

Table A3.4: Parameters and statistics of linear regression model and ordinary kriging of $PM_{2.5}$ annual average 2019 in rural, urban background and urban traffic areas for final combined map

$PM_{2.5}$		**Annual average**		
		Rural areas	**Urban b. areas**	**Urban tr.. areas**
Linear regresion model (LRM, Eq. A1.3)	c (constant)	0.78	1.00	1.01
	a1 (log. EMEP model)	0.792	0.66	0.653
	a2 (altitude GMTED)	-0.00044		
	a3 (wind speed)	-0.043		
	a4 (land cover NAT1)	*non signif.*		
	Adjusted R^2	**0.68**	**0.38**	**0.59**
	Standard Error [μg.m^{-3}]	**0.28**	**0.29**	**0.23**
Ordinary kriging (OK) of LRM residuals	nugget	0.045	0.015	0.011
	sill	0.066	0.063	0.046
	range [km]	1000	410	160
LRM + OK of its residuals	**RMSE [μg.m^{-3}]**	**2.0**	**2.7**	**3.1**
	Relative RMSE [%]	**20.5**	**20.5**	**26.0**
	Bias (MPE) [μg.m^{-3}]	**0.0**	**0.1**	**-0.1**

The adjusted R^2 and standard error are indicators for the quality of the fit of the regression relation. The adjusted R^2 is 0.68 for the rural areas, 0.38 for urban background areas and 0.59 for urban traffic areas. Quite weaker regression relation in the urban background areas causes a higher impact of the interpolation part of the interpolation-regression-merging mapping methodology in these areas.

RMSE and bias – highlighted in orange – are the cross-validation indicators, showing the quality of the resulting map; the bias indicates to what extent the predictions are under- or overestimated on average. Only stations with $PM_{2.5}$ measurement data are used for calculating the RMSE and the bias (i.e., the pseudo $PM_{2.5}$ stations are not used). These statistical indicators are calculated excluding the pseudo stations because they are estimated values only, not actual measurement values. According to Denby et al (2011b), the pseudo $PM_{2.5}$ data does not satisfy the quality objectives for fixed monitoring alone. The pseudo stations are used as they improve the mapping estimate, whereas the actual measurements can be used for evaluating the quality of the map. For the future, it will be considered to quit the application of the $PM_{2.5}$ pseudo stations as the current number of the actual $PM_{2.5}$ measurement stations has increased over time such that the use of pseudo $PM_{2.5}$ stations may not contribute enough any longer to improve the mapping estimates.

Due to the lack of rural stations in Turkey for $PM_{2.5}$, no proper interpolation results could be presented for this country in a rural map, so the estimated $PM_{2.5}$ values for Turkey are not presented in the final map. Thus, the stations located in Turkey have not been used in the uncertainty estimates (although used in the mapping process), as they lie outside the mapping area.

Uncertainty estimated by cross-validation

Table A3.4 shows that the absolute mean uncertainty of the final combined map of $PM_{2.5}$ annual average expressed as RMSE is 2.0 $\mu g{\cdot}m^{-3}$ for the rural areas and 2.7 $\mu g{\cdot}m^{-3}$ for the urban background areas and 3.1 $\mu g{\cdot}m^{-3}$ for the urban traffic areas. On the other hand, the relative mean uncertainty (Relative RMSE) of the final combined map of $PM_{2.5}$ annual average is 20.5 % for both rural and urban background areas and 26.0 % for urban traffic areas. These relative uncertainty values fulfil the data quality objectives for models as set in Annex I of the Air Quality Directive (EC, 2008).

Figure A3.3 shows the cross-validation scatter plots, obtained according to Section A1.3, for different area types. The R^2 indicates that about 81 % of the variability is attributable to the interpolation for the rural areas, 75 % for the urban background areas and 73 % for the urban traffic areas.

Figure A3.3: Correlation between cross-validated predicted and measurement values for $PM_{2.5}$ annual average 2019 for rural (left), urban background (middle) and urban traffic (right) areas

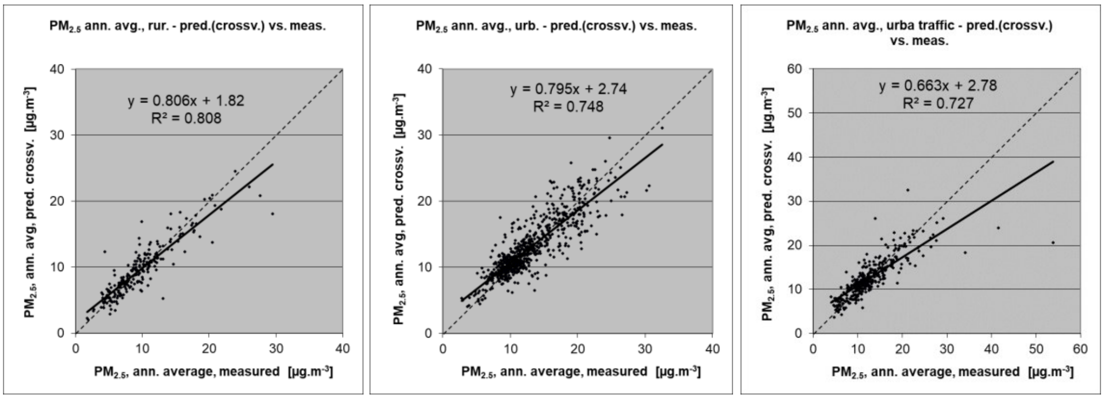

The scatter plots indicate that in areas with high concentrations the interpolation methods tend to underestimate the levels. For example, in rural areas an observed value of 25 $\mu g{\cdot}m^{-3}$ is estimated in the interpolations to be about 22 $\mu g{\cdot}m^{-3}$, which is an underestimated prediction of about 12 %. This underestimation at high values is an inherent feature of all spatial interpolations. It could be reduced by either using a higher number of the stations at improved spatial distribution, or by introducing a closer regression that uses either other supplementary data or more improved CTM output.

Comparison of point measurement values with the predicted grid value

Like for PM_{10}, a simple comparison has been made between the point observation values and interpolated prediction values spatially averaged in grid cells, in addition to the cross-validation.

The comparison has been made primarily for the separate rural, urban background and urban traffic map layers at 1x1 km^2 resolution. Next to this, the comparison has been done also for the final combined maps at the same 1x1 km^2 resolution. Figure A3.4 shows the scatterplots for these comparisons.

The results of the point observation – point prediction cross-validation of Figure A3.3 and those of the point observation – grid averaged prediction validation of Figure A3.4 for separate map layers and for the final combined map are summarised in Table A3.5.

Figure A3.4: Correlation between predicted grid values from rural (upper left), urban background (upper middle) and urban traffic (upper right) map layer and final combined map (all bottom) (y-axis) versus measurements from rural (left), urban/suburban background (middle) and urban/suburban traffic stations (right) (x-axis) for $PM_{2.5}$ annual average 2019

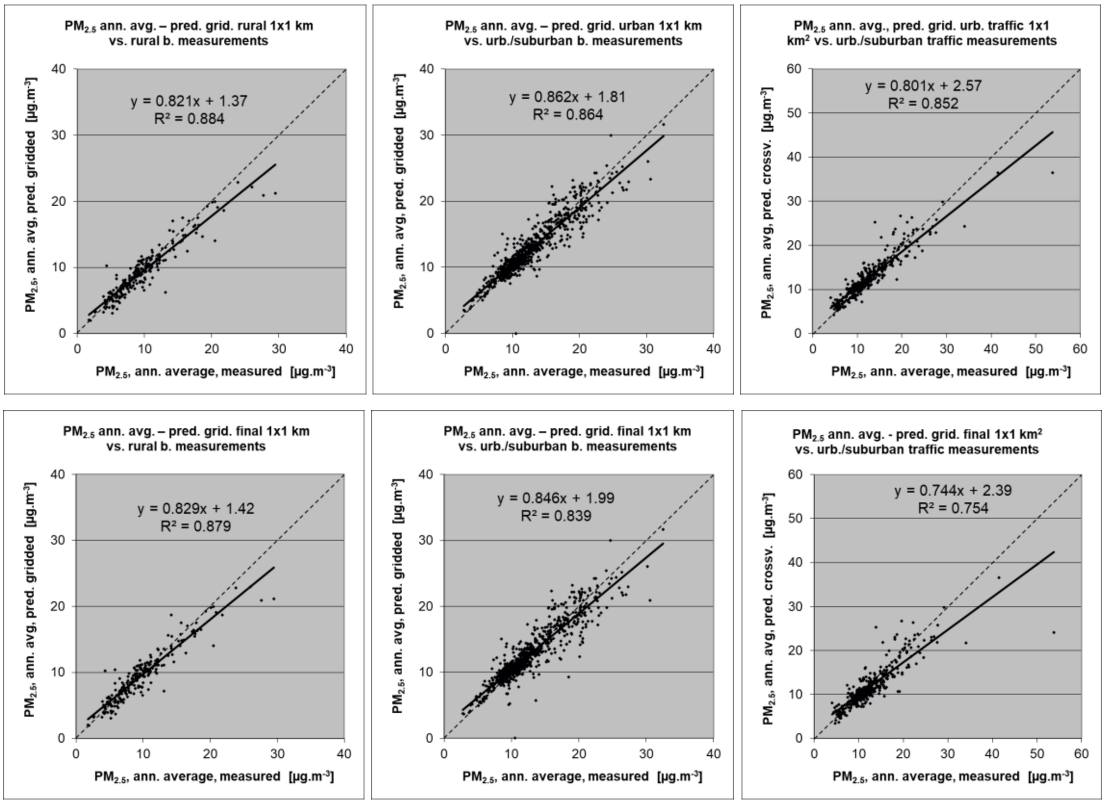

By comparing the scatterplots and the statistical indicators for separate rural, urban background and urban traffic map layers with the final combined maps, one can evaluate the level of representation of the rural, urban background and urban traffic areas in the final combined map. Similar results as for PM_{10} can be observed: the final combined map in 1x1 km^2 resolution is fairly well representative for rural and urban background areas, but not for urban traffic areas.

Like in the case of PM_{10}, Table A3.5 shows a better correlated relation with the station measurements (i.e., lower RMSE, higher R^2, smaller intercept and slope closer to 1) for the simply interpolated gridded values than for the point cross-validation predictions, at rural, urban background and urban traffic map areas. That is because the simple comparison shows the uncertainty at the actual station locations, while the cross-validation prediction simulates the behaviour of the interpolation (within the area covered by measurements) at point positions assuming no actual measurements would exist at these points.

The uncertainty at measurement locations is introduced partly by the smoothing effect of the interpolation and partly by the spatial averaging of the values in the 1x1 km^2 grid cells. For example, in urban background areas the predicted interpolation gridded value in the final map will be about 28 µg·m^{-3} at the corresponding station with the measurement value of 30 µg·m^{-3} (calculated based on the linear regression equation), which coincides with an underestimation of about 8 %.

Table A3.5: Statistical indicators from the scatter plots for the predicted grid values from separate (rural, urban background or urban traffic) map layers and final combined map versus the measurement point values for rural (upper left), urban background (upper right) and urban traffic (bottom left) stations for $PM_{2.5}$ annual average 2019

$PM_{2.5}$	rural backgr. stations				urban/suburban backgr. stations			
	RMSE	bias	R^2	lin. r. equation	RMSE	bias	R^2	lin. r. equation
cross-val. prediction, separate (r or ub) map layer	1.8	0.0	0.808	y = 0.806x + 1.82	2.3	0.1	0.748	y = 0.795x + 2.74
grid prediction, 1x1 km^2 separ. (r or ub) map layer	1.5	-0.3	0.884	y = 0.821x + 1.37	1.7	0.0	0.864	y = 0.862x + 1.81
grid prediction, 1x1 km^2 final merged map	1.5	-0.2	0.879	y = 0.829x + 1.42	1.9	0.0	0.839	y = 0.846x + 1.99

$PM_{2.5}$	urban/suburban traffic stations			
	RMSE	bias	R^2	lin. r. equation
cross-val. prediction, urban traffic map layer	2.3	0.0	0.727	y = 0.663x + 2.78
grid prediction, 1x1 km^2 urban traffic map layer	1.6	0.1	0.852	y = 0.801x + 2.57
grid prediction, 1x1 km^2 final merged map	2.1	-0.8	0.754	y = 0.744x + 2.39

A3.3 Ozone

In this section, the technical details and the uncertainty estimates are presented for the maps of ozone health-related indicators 93.2 percentile of maximum daily 8-hour means, SOMO35 and SOMO10 (Maps 4.1-4.3), as well as for the maps of ozone vegetation-related indicators AOT40 for vegetation and AOT40 for forests (Maps 4.4 and 4.5). Next to this, the details of POD_6 maps are presented.

Technical details on the mapping

Table A3.6 presents the estimated parameters of the linear regression models and of the residual kriging, including the statistical indicators of both the regression and the kriging.

The adjusted R^2 and standard error show the quality of the fit of the regression relation. For the rural areas, all indicators show the value of the adjusted R^2 between 0.48 and 0.60. For the urban areas, the adjusted R^2 is 0.44 for 93.2 percentile of daily 8-hour maximums, 0.29 for SOMO35 and 0.22 for SOMO10. For the vegetation-related indicators the urban maps are not constructed. RMSE and bias – highlighted by orange – are the cross-validation indicators, showing the quality of the resulting map.

Table A3.6: Parameters and statistics of linear regression model and ordinary kriging for ozone indicators 93.2 percentile of maximum daily 8-hourly means, SOMO35 and SOMO10 in rural and urban areas for the final combined map and for O_3 indicators AOT40 for vegetation and for forests in rural areas for 2019

		93.2 perc. of dmax 8h		SOMO35		SOMO10		AOT40v	AOT40f
		Rur. areas	Urb. ar.	Rur. ar.	Urb.ar.	Rur. ar.	Urb.ar.	Rur. ar.	Rur. ar.
Linear regresion model (LRM, Eq. A1.3)	c (constant)	-3.3	9.9	-430	428	4027	5654	-2428	-1649
	a1 (EMEP model)	1.10	0.98	0.72	0.62	0.63	0.48	0.89	0.66
	a2 (altitude GMTED)	0.0022		0.86		1.80		2.17	4.76
	a3 (wind speed)		-1.30		*n.sign.*		*n. sign.*		
	a4 (s. solar radiation)	*n.sign.*	*n.sign.*	152.3	84.3	250.2	260.7	519.8	910.4
	Adjusted R^2	**0.51**	**0.44**	**0.51**	**0.29**	**0.48**	**0.22**	**0.60**	**0.52**
	Stand. Err. [µg.m^{-3}.x]*	**9.0**	**11.6**	**1784**	**1901**	**2606**	**3194**	**5886**	**10024**
Ord. krig. (OK) of LRM	nugget	22	54	1.7E+06	1.6E+06	3.8E+06	3.0E+06	1.8E+07	4.2E+07
	sill	65	81	2.6E+06	2.4E+06	5.6E+06	5.7E+06	3.9E+07	7.3E+07
	range [km]	230	140	170	300	140	530	180	860
LRM + OK of its residuals	**RMSE [µg.m^{-3}.x]***	**8.3**	**10.1**	**1777**	**1569**	**2585**	**2616**	**5507**	**9609**
	Relative RMSE [%]	**7.1**	**8.9**	**29.6**	**32.1**	**11.7**	**13.4**	**32.1**	**32.6**
	Bias (MPE) [µg.m^{-3}.x]*	**0.0**	**0.0**	**0**	**-7**	**-19**	**-16**	**-11**	**-41**

* Units: 93.2 percentile of daily 8-h maximums: [µg·m^{-3}], SOMO35 and SOMO10: [µg·m^{-3}·d], AOT40v and AOT40f: [µg·m^{-3}·h].

Uncertainty estimated by cross-validation

The basic uncertainty analysis is provided by cross-validation. Table A3.6 shows both absolute and relative mean uncertainty, expressed by RMSE and Relative RMSE. The relative mean uncertainty of the 2019 ozone map is at the 93.2 percentile of daily 8-h maximums about 8 % for rural areas and 10 % for urban areas, around 30-32 % for SOMO35, around 12-13 % for SOMO10 and around 32-33 % at AOT40 indicators. The small levels of the relative uncertainty for the 93.2 percentile of maximum daily 8-h means and SOMO10 are highly influenced by the low ratio between the relevant standard error and mean calculated based on all annual station concentration data: for these two indicators the ratio is at the level of about 0.11- 0.19, while for SOMO35 and for both AOT40 indicators it is at the level of about 0.42-0.54.

Figure A3.5 shows the cross-validation scatter plots for both the rural and urban areas of the 2019 map for the health-related ozone indicators.

Figure A3.5: Correlation between cross-validated predicted (y-axis) and measurement values for ozone indicators 93.2 percentile of max. daily 8-hourly means (top), SOMO35 (middle) and SOMO10 (bottom) for 2019 for rural (left) and urban (right) areas

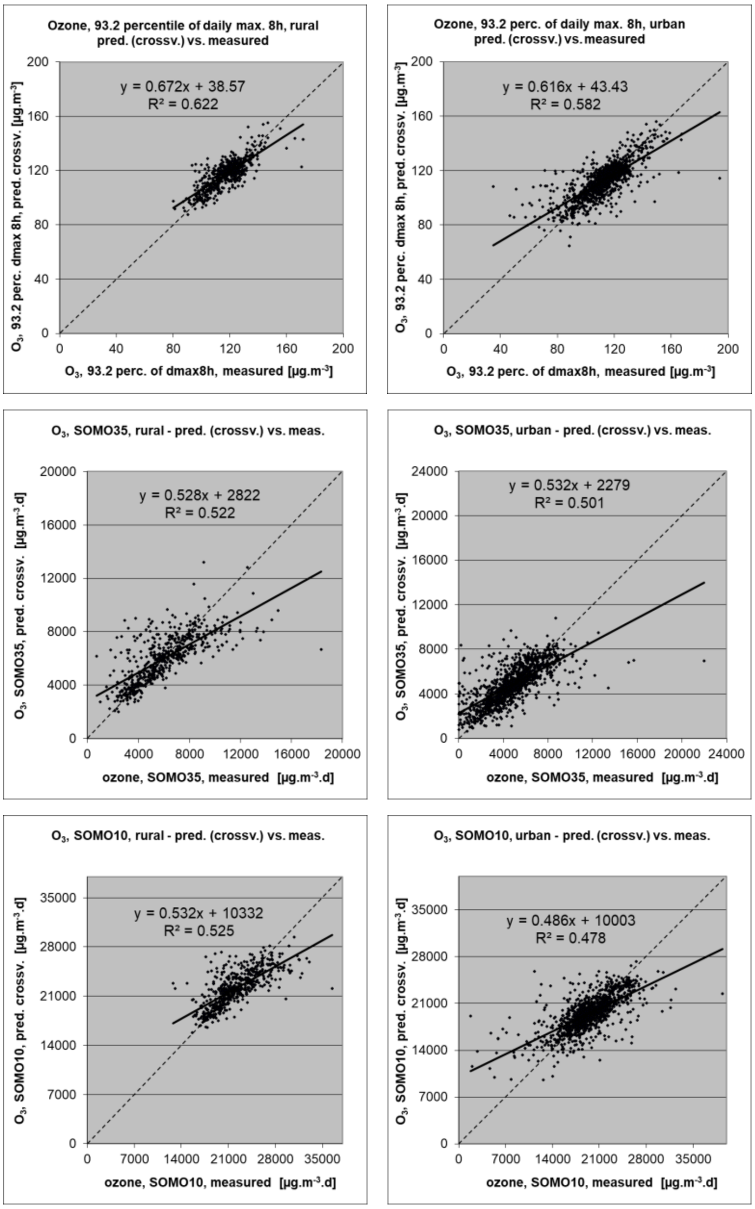

The R^2, an indicator for the interpolation correlation with the observations, shows that for the health related ozone indicators, about 52-62 % is attributable to the interpolation in the rural areas, while in the urban areas it is about 48-58 %.

The scatter plots indicate that the higher values are underestimated and the lower values somewhat overestimated by the interpolation method; a typical smoothing effect inherent to the interpolation method with the linear regression and its residuals kriging. For example, in the case of the 93.2 percentile of daily 8-h maximums, in urban areas (Figure A.3.5, upper right panel) an observed value of 160 µg·m^{-3} is estimated in the interpolation as 142 µg·m^{-3}, which is 11 % lower. Or, in the case of SOMO35, in rural areas (Figure A3.5, middle left panel) an observed value of 9 000 µg·m^{-3}·d is estimated in the interpolation as about 7 600 µg·m^{-3}·d, which is 16 % lower.

Figure A3.6 shows the cross-validation scatter plots of the AOT40 for both vegetation and forests. R^2 indicates that about 65 % of the variability is attributable to the interpolation in the case of AOT40 for vegetation, while for AOT40 for forests it is about 56 %.

The cross-validation scatter plots show again that in areas with higher accumulated ozone concentrations the interpolation methods tend to deliver underestimated predicted values. For example, in agricultural areas (Figure A3.6, left panel) an observed value of 30 000 µg·m^{-3}·h is estimated in the interpolation as about 25 700 µg·m^{-3}·h, i.e., an underestimation of about 14 %. In addition, an overestimation at the lower end of predicted values occurred. One could reduce this under- and overestimation by extending the number of measurement stations and by optimising the spatial distribution of those stations, specifically in areas with elevated values over years.

Figure A3.6: Correlation between cross-validated predicted (y-axis) and measurement values for ozone indicators AOT40 for vegetation (left) and AOT40 for forests (right) for 2019 for rural areas

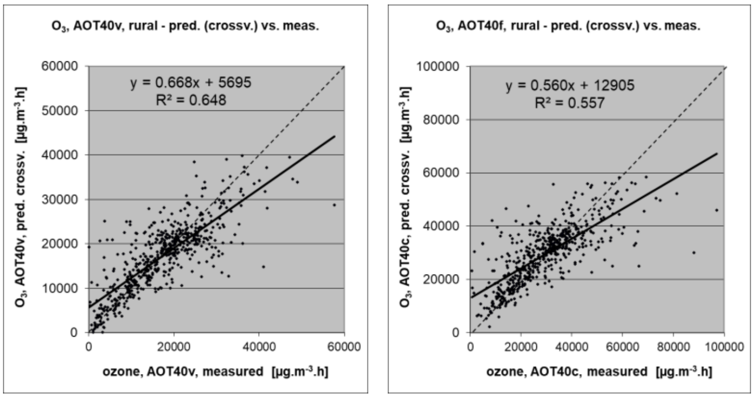

Comparison of point measurement values with the predicted grid value

In addition to the above point observation – point prediction cross-validation, a simple comparison has been made between the point observation values and interpolated predicted grid values.

For health related indicators, the comparison has been made primarily for the separate rural and separate urban background maps at 10x10 km^2 resolution. (One can directly relate this comparison result to the cross-validation of the previous section.) Next to this, the comparison has been done also for the final combined maps at 1x1 km^2 resolution.

Figure A3.7 shows the scatterplots for these comparisons, for ozone indicator 93.2 percentile of maximum daily 8-hour means only, as an illustration.

The results of the point observation – point prediction cross-validation of Figure A3.5 and those of the point observation – grid averaged prediction validation for the separate rural and the separate urban background map, and for the final combined maps are summarised in Table A3.7. By comparing the scatterplots and the statistical indicators for the separate rural and separate urban background map with the final combined maps, one can evaluate the level of representation of the rural resp. urban background areas in the final combined maps. Both the rural and the urban air quality are fairly well represented in the 1x1 km² final combined map.

Figure A3.7: Correlation between predicted grid values from rural 10x10 km² (upper left), urban 10x10 km² (bottom left) and final combined 1x1 km² (both right) map (y-axis) versus measurements from rural (top), resp. urban/suburban (bottom) background stations (x-axis) for ozone indicator 93.2 percentile of daily max. 8-hourly means for 2019

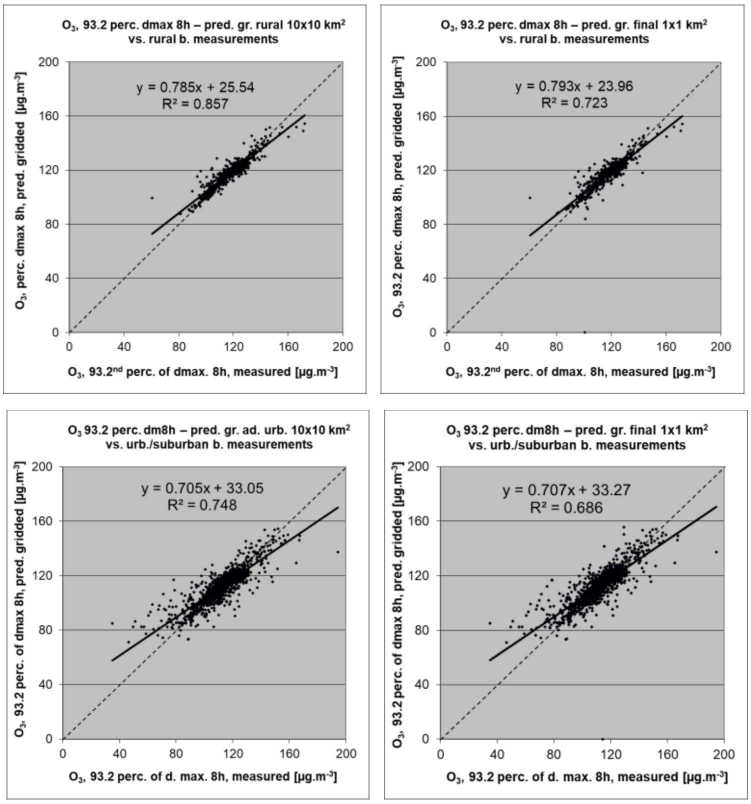

Table A3.7: Statistical indicators from the scatter plots for the predicted point values based on cross-validation and the predicted grid values from separate (rural resp. urban) 10x10 km² and final combined 1x1 km² map versus the measurement point values for rural (left) and urban (right) background stations for ozone indicators 93.2 percentile of daily max 8h means (top), SOMO35 (middle) and SOMO10 (bottom) for 2019

Ozone	rural backgr. stations				urban/suburban backgr. stations			
	RMSE	Bias	R^2	lin. r. equation	RMSE	Bias	R^2	lin r. equation
93.2 percentile of daily max. 8-hour means								
cross-val. prediction, separate (r or ub) map layer	8.3	0.0	0.622	y = 0.672x + 38.57	10.1	0.0	0.582	y = 0.616x + 43.43
grid prediction, 10x10 km² separate (r or ub) map l.	6.9	0.1	0.857	y = 0.785x + 25.54	7.8	-0.3	0.748	y = 0.705x + 33.05
grid prediction, 1x1 km² final merged map	5.4	-0.2	0.723	y = 0.793x + 23.96	8.1	0.2	0.686	y = 0.707x + 33.27
SOMO35								
cross-val. prediction, separate (r or ub) map layer	1777	0	0.522	y = 0.528x + 2822	1569	-7	0.501	y = 0.532x + 2279
grid prediction, 10x10 km² separate (r or ub) map l.	1324	20	0.747	y = 0.652x + 2114	1357	-4	0.628	y = 0.590x + 1979
grid prediction, 1x1 km² final merged map	1323	-108	0.741	y = 0.653x + 1976	1395	79	0.606	y = 0.607x + 1998
SOMO10								
cross-val. prediction, separate (r or ub) map layer	2585	-19	0.525	y = 0.532x + 10332	2616	-16	0.478	y = 0.486x + 10003
grid prediction, 10x10 km² separate (r or ub) map l.	2087	-27	0.748	y = 0.634x + 8086	2168	-28	0.650	y = 0.575x + 8260
grid prediction, 1x1 km² final merged map	1959	-289	0.721	y = 0.656x + 7307	2234	180	0.623	y = 0.592x + 8138

The uncertainty of the rural and urban background maps at measurement locations is caused partly by the smoothing effect of interpolation and partly by the spatial averaging of the values in the 10x10 km^2 grid cells. The level of smoothing, which leads to underestimation in areas with high values, is weaker in areas where measurements exist than in areas where a measurement point is not available. For example, in the case of the SOMO35, in rural areas an observed value of 9 000 $\mu g \cdot m^{-3} \cdot d$ is estimated in the interpolation as about 8 000 $\mu g \cdot m^{-3} \cdot d$, which is about 11 % lower. It is less than the cross-validation underestimation of 16 % at the same point location, when leaving out this one actual measurement point and the interpolation without this station is done (see the previous subsection).

Table A3.8 presents the results of the point observation – point prediction cross-validation of Figure A3.6 and those of the point-grid validation for the rural map, for vegetation related indicators AOT40 for vegetation and AOT40 for forests. Again, one can see for both indicators a better correlation between the station measurements and the averaged interpolated predicted values of the corresponding grid cells, than at the point cross-validation predictions, of Figure A3.6.

Table A3.8: Statistical indicators from the scatter plots for predicted point values based on cross-validation and predicted grid values from rural 2x2 km^2 map versus measurement point values for rural background stations for ozone indicators AOT40 for vegetation (top) and forests (bottom) for 2019

Ozone	rural backgr. stations			
	RMSE	bias	R^2	linear regression equation
AOT40 for vegetation				
cross-valid. prediction, rural map	5507	-11	0.648	y = 0.668x + 5695
grid prediction, 2x2 km^2 rural map	3706	-8	0.845	y = 0.781x + 3762
AOT40 for forests				
cross-valid. prediction, rural map	9609	-41	0.557	y = 0.560x + 12905
grid prediction, 2x2 km^2 rural map	6114	-14	0.835	y = 0.727x + 8036

Details of POD_6 maps

POD_6 maps have been calculated using the ozone based on the hourly ozone rural maps, hourly meteorological data and soil hydraulic properties data, according to the methodology described in Annex 1, Section A1.3.

The hourly ozone maps needed for POD_6 calculation have been calculated at the 2x2 km^2 resolution, based on rural background measurements. The maps for each hour of the year 2019 have been constructed using the same methodology as for the annual maps, i.e., the multiple linear regression followed by the kriging of its residuals (see Annex 1, Section A1.1) based on the measurement data, EMEP model output, altitude and the surface solar radiation. Table A3.9 presents the summary results of the RMSE, RRMSE and bias for the whole year, based on the annual average and percentiles of these three statistics. For bias, annual sum is also shown in addition.

Table A3.9: Annual statistics average, 2nd percentile, 25th percentile, 50th percentile (median), 75th percentile, 98th percentile and sum (where relevant) for average ozone concentration, number of stations considered, and cross-validation parameters RMSE, RRMSE and Bias of hourly ozone maps, 1.1.2019-31.12.2019. Units: $\mu g \cdot m^{-3}$ apart from N and RRMSE.

	Rural background areas						
	avg	p2	p25	p50	p75	p98	Sum
N	501	468	485	492	529	549	
avg	63.6	36.9	49.2	60.0	76.1	106.7	
RMSE	**16.2**	10.1	13.3	**15.6**	18.5	25.9	
RRMSE	**27.9%**	11.7%	18.4%	**27.6%**	35.8%	49.6%	
Bias	**-0.05**	-0.64	-0.21	**-0.05**	0.09	0.58	**-467**

Figure A3.8 and A3.9 presents the averages of the cross-validation indicators Bias and RMSE in the individual hours of the year 2019.

Figure A3.8: Cross-validation statistical indicator Bias of hourly ozone maps, average at rural background stations, 1.1.2019-31.12.2019

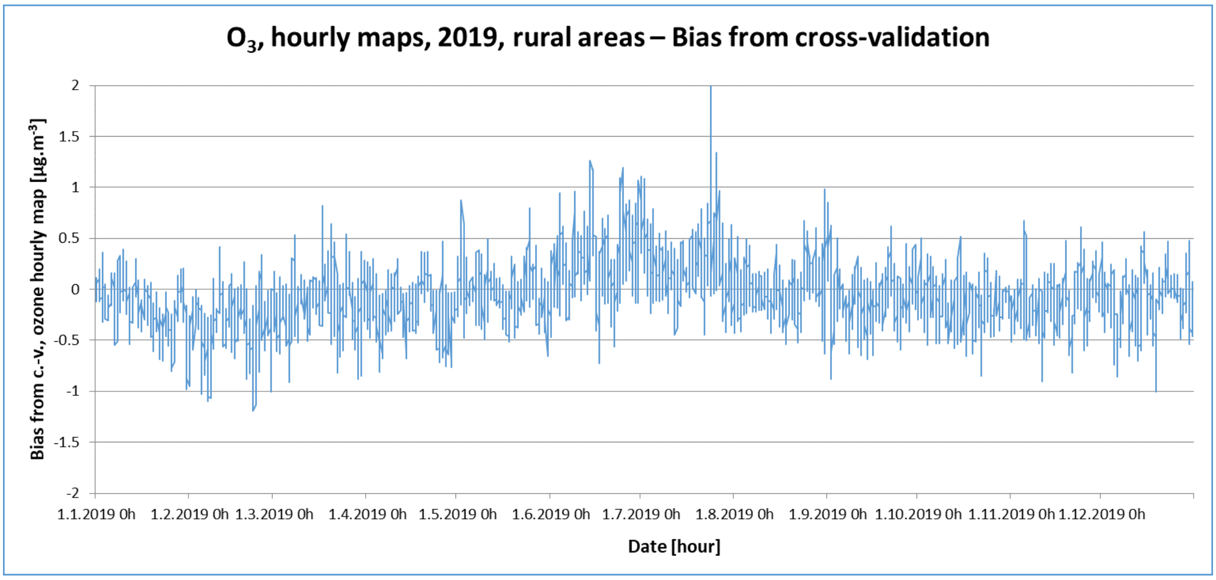

Figure A3.9: Cross-validation statistical indictor RMSE of hourly ozone maps, average at rural background stations, 1.1.2019-31.12.2019

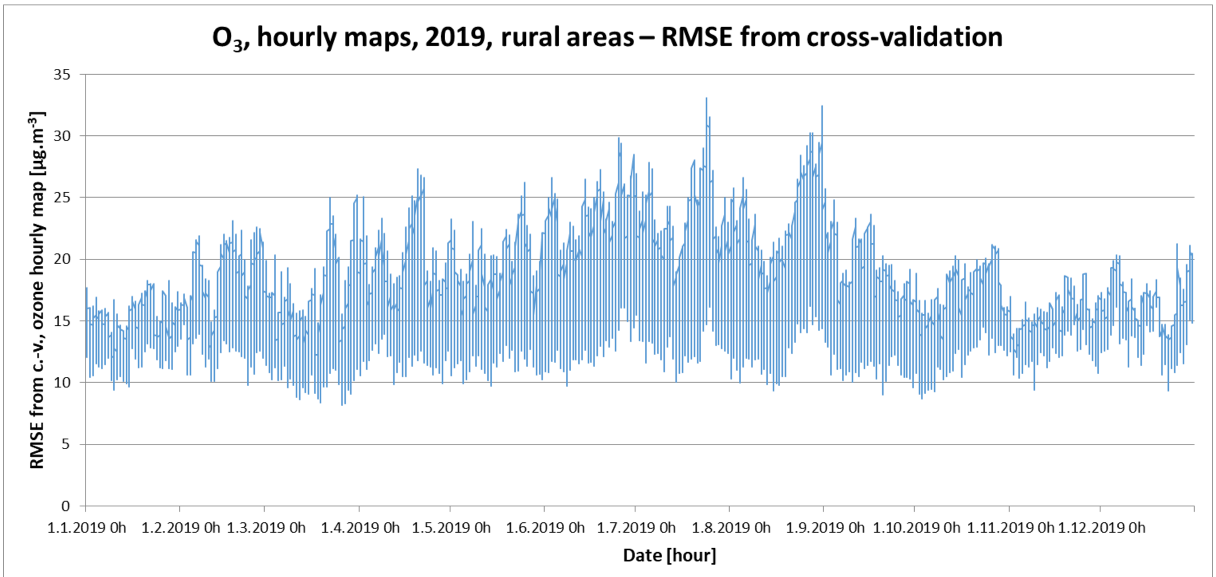

In the POD_6 calculations, the module to estimate phytotoxic ozone doses from a given atmospheric ozone exposure developed by INERIS has been used.

During the POD_6 maps calculation, different biogeographical regions were considered. Plant stomatal functioning varies per plant species and can vary by biogeographical region, reflecting different adaptations of plants to climate and soil water in these regions. Parametrization for POD_6 (i.e., for wheat, potato and tomato) is currently available for all different biogeographic regions of Europe apart from Alpine region, i.e., for Atlantic, Boreal, Continental, Pannonian, Steppic, and Mediterranean regions (CLRTAP, 2017a). In the case of wheat, the parametrization is the same for most of these regions (namely Atlantic, Boreal, Continental, Pannonian, and Steppic), while for Mediterranean regions is different. Thus, these areas are calculated separately. For Alpine region, the parametrisation of the Continental and several other regions are used. For potato and tomato, only one parametrisation exists – in the case of potato, the parametrisation is set for all regions apart from the Alpine one, while for tomato for the Mediterranean region only (see Table 1.2). In the calculations, the existing parametrisation has been applied for the entire mapping area.

The values calculated in 0.1° x 0.1° resolution were converted into the standard ETRS89-LAEA5210 projection and transferred into the EEA 2x2 km^2 grid.

A3.4 NO_2 and NO_x

In this section, the technical details and the uncertainty estimates for the maps of NO_2 annual average and NO_x annual average, for Maps 5.1 and 5.2, are presented.

Technical details on the mapping

In agreement with Horálek et al. (2007) and Annex 1, the NO_x measurements are supplemented by the so-called pseudo NO_x stations. The pseudo NO_x data are calculated based on the NO_2 data, using quadratic regression Eq. A1.2. The regression coefficients were estimated based on the rural background stations with both NO_x and NO_2 measurements (see Section 2.1.1). The number of such stations is 391. The estimated coefficients of Eq. A1.2 are: a = 0.0348, b = 0.802, c = 1.39. Adjusted R^2 is 0.95, the standard error is 1.8 µg·m^{-3}.

Table A3.10 presents the estimated parameters of the linear regression models and of the residual kriging and includes the statistical indicators of both the regression and the kriging.

Table A3.10: Parameters and statistics of linear regression model and ordinary kriging of NO_2 annual average for 2019 in rural, urban background and urban traffic areas for the final combined map (left) and NO_x annual average for 2019 in rural areas (right)

		NO_2 Annual average			NO_x Annual average
		Rural areas	Urb. b. areas	Urb. tr. areas	Rural areas
Linear regresion model (LRM, Eq. A1.3)	c (constant)	4.7	15.8	22.63	4.8
	a1 (EMEP model)	0.405	*non signif.*	*non signif.*	1.042
	a2 (altitude)	-0.0066		*non signif.*	-0.0051
	a3 (altitude_5km_radius)	0.0063		*non signif.*	
	a4 (wind speed)	-0.82	-2.05	-1.56	-1.97
	a5 (solar radiation)				0.47
	a6 (satellite TROPOMI)	1.79	2.24	2.29	
	a7 (population*1000)	0.00098	0.00024		
	a8 (NAT_1km)		-0.0501		
	a9 (AGR_1km)		-0.0356		
	a10 (TRAF_1km)		0.0865		
	a11 (LDR_5km_radius)	*non signif.*	*non signif.*	0.1243	
	a12 (HDR_5km_radius)		0.1394	0.2517	
	a13 (NAT_5km_radius)	-0.0334			
	Adjusted R^2	**0.80**	**0.50**	**0.36**	**0.61**
	Standard Error [µg.m^{-3}]	**2.3**	**5.8**	**8.8**	**5.2**
Ordinary kriging (OK) of LRM residuals	nugget	1	13	36	3
	sill	5	21	60	24
	range [km]	16	56	58	28
LRM + OK of its residuals	**RMSE [µg.m^{-3}]**	**2.3**	**5.0**	**7.6**	**4.9**
	Relative RMSE [%]	**30.7**	**26.8**	**24.2**	**47.7**
	Bias (MPE) [µg.m^{-3}]	**0.0**	**1.0**	**0.0**	**0.1**

In agreement with the analysis on both 2018 and 2019 data, the Sentinel-5P TROPOMI satellite data have been used as a supplementary parameter instead of the previously used OMNO2 satellite data.

Only stations with actual measurement data of the relevant pollutant (i.e., not the pseudo stations) are used for calculating the cross-validation parameters RMSE and bias.

Uncertainty estimated by cross-validation

Table A3.10 shows both absolute and relative mean uncertainty, expressed by RMSE and Relative RMSE. The absolute mean uncertainty of the final combined map of NO_2 annual average expressed as RMSE is 2.3 µg·m^{-3} for the rural areas, 5.0 µg·m^{-3} for the urban background areas and 7.6 µg·m^{-3} for the urban traffic areas. For the NO_x rural map it is 4.9 µg·m^{-3}.

The relative mean uncertainty of the NO_2 annual average map is 31 % for rural, 27 % for urban background areas and 24 % for the urban traffic areas. The NO_x annual average rural map has a relative mean uncertainty of 48 %.

Figure A3.10 shows the point observation – point prediction cross-validation scatter plots for NO_2 annual average. The R^2 indicates that about 80 % of the variability is attributable to the interpolation for the rural areas, while for the urban background areas it is 63 % and for the urban traffic 52 %.

Figure A3.10: Correlation between cross-validated predicted and measurement values for NO_2 annual average 2019 for rural (left), urban background (middle) and urban traffic (right) areas

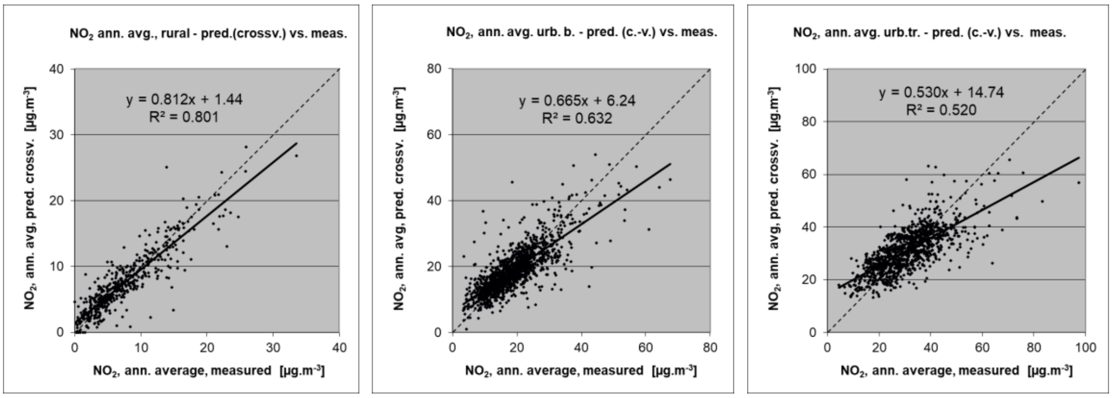

Like in the case of other pollutants, the cross-validation scatter plots show the underestimation of predictions at high concentrations at locations with no measurements. For example, in urban background areas an observed value of 40 µg·m^{-3} is estimated in the interpolations to be about 33 µg·m^{-3}, which is an underestimated prediction of about 18 %.

Figure A3.11 shows the cross-validation scatter plot for NO_x annual average rural map. The R^2 indicates that about 62 % of the variability is attributable to the interpolation.

Figure A3.11: Correlation between cross-validated predicted and measurement values for NO_x annual average 2019 for rural areas

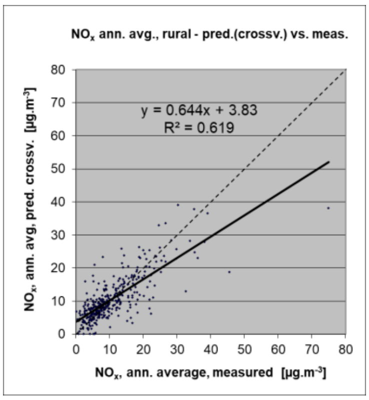

Comparison of point measurement values with the predicted grid value

Next to the above presented cross-validation, a simple comparison was made between the point observation values and interpolated predicted 1x1 km^2 resp. 2x2 km^2 grid values.

For NO_2 annual average, the comparison has been made primarily for the separate rural, separate urban background and separate urban traffic map layers at 1x1 km^2 resolution. Besides, the comparison has been done also for the final combined map. Table A3.11 presents the results of this comparison, together with the results of cross-validation prediction of Figure A3.10. One can conclude that the final combined map in 1x1 km^2 resolution is representative for rural and urban background areas, but not for urban traffic areas.

Table A3.11: Statistical indicators from the scatter plots for the predicted grid values from separate (rural, urban background or urban traffic) map layers and final combined map versus the measurement point values for rural (upper left), urban background (upper right) and urban traffic (bottom left) stations for NO_2 annual average 2019

NO_2	rural backgr. stations				urban/suburban backgr. stations			
	RMSE	Bias	R^2	lin. r. equation	RMSE	Bias	R^2	lin r. equation
cross-val. prediction, separate (r or ub) map layer	2.3	0.0	0.801	y = 0.812x + 1.44	5.0	0.1	0.632	y = 0.665x + 6.24
grid prediction, 1x1 km^2 separate (r or ub) map layer	1.2	-0.3	0.954	y = 0.911x + 0.39	3.6	0.1	0.811	y = 0.768x + 4.44
grid prediction, 1x1 km^2 final merged map	2.0	0.2	0.866	y = 0.973x + 0.45	4.0	0.6	0.762	y = 0.796x + 4.38

NO_2	urban/suburban traffic stations			
	RMSE	Bias	R^2	lin. r. equation
cross-valid. prediction, urban traffic map layer	7.6	0.0	0.520	y = 0.530x + 14.74
grid prediction, 1x1 km^2 urban traffic map layer	5.3	0.0	0.776	y = 0.675x + 10.20
grid prediction, 1x1 km^2 final merged map	12.5	-9.6	0.481	y = 0.457x + 7.41

Table A3.12 presents the cross-validation results of Figure A3.11 and those of the point observation – grid averaged prediction validation for the rural map of NO_x annual average.

Table A3.12: Statistical indicators from the scatter plots for predicted point values based on cross-validation and predicted grid values from rural 2x2 km^2 map versus measurement point values for rural background stations for NO_x annual average 2019

NO_x	rural background stations			
	RMSE	Bias	R^2	linear regression equation
cross-valid. prediction, rural map	4.9	0.1	0.619	y = 0.644x + 3.83
grid prediction, 2x2 km^2 rural map	0.8	0.0	0.992	y = 0.948x + 0.56

Annex 4
Concentration change in 2019 in comparison to the five-year mean 2014-2018

In this annex, air concentration changes in 2019 in comparison to the five-year mean 2014-2018 are presented, both for the mapped concentrations and for the population-weighted and vegetation-weighted concentrations. In all cases, the maps for 2014-2018 presented in Horálek et al. (2017, 2018, 2019, 2020, and 2021) have been used. In the case of PM_{10} and $PM_{2.5}$, the maps constructed using the updated methodology have been used since 2015 maps, while for 2014 the maps constructed the olde methodology has been used.

A4.1 PM_{10}

Concentration maps

Map A4.1 presents the difference between 2019 and five-year mean 2014-2018 for annual average and the 90.4 percentile of daily means for PM_{10}. Orange to red areas show an increase of PM_{10} concentration in 2019, while blue areas show a decrease.

Map A4.1: Difference concentrations between 2019 and five-year mean 2014-2018 for PM_{10} indicators annual average (left) and 90.4 percentile (right)

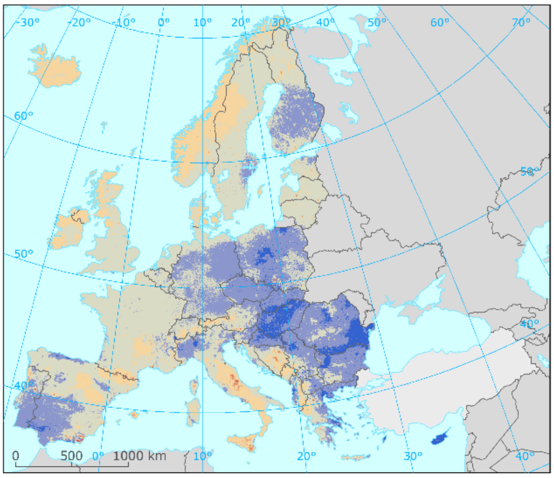

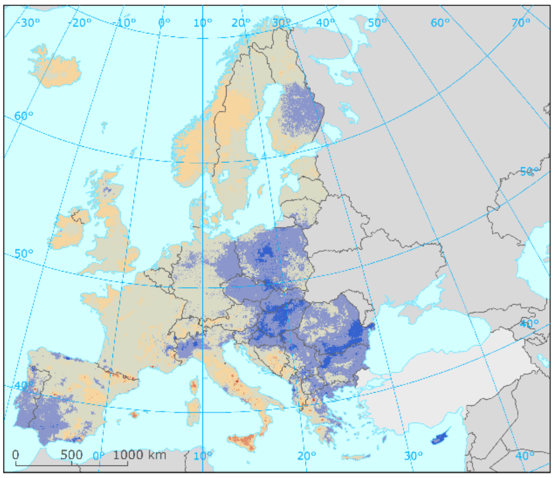

Particulate Matter (PM_{10}), Annual Average
Difference between 2019 and Five-year Mean 2014-2018
Difference: 2019 - avg(2014-2018)
Combined Rural and Urban (incl. Traffic) Map, Resolution 1x1 km²

- ≤ - 5 μg.m⁻³
- - 5 – - 2 μg.m⁻³
- - 2 – 0 μg.m⁻³
- 0 – 2 μg.m⁻³
- 2 – 5 μg.m⁻³
- > 5 μg.m⁻³
- no available data
- unmapped countries

Particulate Matter (PM_{10}), 90.4 Percentile of Daily Means
Difference between 2019 and Five-year Mean 2014-2018
Difference: 2019 - avg(2014-2018)
Combined Rural and Urban (incl. Traffic) Map, Resolution 1x1 km²

- ≤ - 10 μg.m⁻³
- - 10 – - 4 μg.m⁻³
- - 4 – 0 μg.m⁻³
- 0 – 4 μg.m⁻³
- 4 – 10 μg.m⁻³
- > 10 μg.m⁻³
- no available data
- unmapped countries

At the annual average PM_{10} difference map the highest increases are observed in south and south-eastern Europe (central and southern Italy, Bosnia and Herzegovina, Montenegro, parts of Albania, Greece and Spain), in western and central Europe (parts of Ireland, the United Kingdom, France, Austria and Switzerland) and in northern Europe (most of Iceland and Norway and part of Sweden). Nevertheless, the observed increase in annual average PM_{10} concentrations has been up to 5 $\mu g \cdot m^{-3}$ in most of these areas. Increase higher than 5 $\mu g \cdot m^{-3}$ has occurred only locally. Contrary to that, decreases occur in parts of Portugal, Spain, Italy (the Po Valley), Finland, Germany, Poland, Czechia, Slovakia, Hungary and in parts of most of the countries in the south-eastern Europe (mainly in Bulgaria, Serbia and Romania) and in Cyprus. At the 90.4 percentile of daily means for PM_{10} the highest increases and decreases are seen in similar parts of Europe.

Be it noted that besides the actual changes in the concentrations, the variability of the linear regression model and variogram parameters, changes in the measurement network and changes in the dispersion model may cause minor differences in the concentration levels estimated.

Population exposure

Table A4.1 shows the difference of the population-weighted concentrations between 2019 and five-year mean 2014-2018 for PM_{10} annual average and the 90.4 percentile of daily PM_{10} means, for individual countries, EU-28 and for the total mapping area (without Turkey).

In 2019, the overall average population-weighted annual mean PM_{10} concentration for the total mapping area was 18.7 $\mu g \cdot m^{-3}$, i.e., its value decreased by about 2.2 $\mu g \cdot m^{-3}$ compared to the previous five-year mean. The steepest decreases per country were detected in North Macedonia (more than 10 $\mu g.m^{-3}$), the highest (but less than 1 $\mu g.m^{-3}$) increases were estimated in Andorra.

In the case of the 90.4 percentile of daily means, the overall average population-weighted concentration for 2019 is estimated at 32.8 $\mu g \cdot m^{-3}$, which is of about 3.8 $\mu g \cdot m^{-3}$ less than five-year mean. The steepest decreases were estimated in North Macedonia (28 $\mu g \cdot m^{-3}$), while the highest increases in Andorra (less than 3 $\mu g.m^{-3}$).

Table A4.1: Population-weighted concentration in 2019 and five-year mean 2014-2018 and its difference between 2019 and five-year mean for PM_{10} indicators annual average (left) and 90.4 percentile of daily means (right)

Country	ISO	Population-weighted concentration [$\mu g \cdot m^{-3}$]						Country	ISO	Population-weighted concentration [$\mu g \cdot m^{-3}$]					
		Annual average			90.4 percentile of daily means					Annual average			90.4 percentile of daily means		
		2019	5-year mean	Diff.	2019	5-year mean	Diff.			2019	5-year mean	Diff.	2019	5-year mean	Diff.
Albania	AL	27.2	31.6	**-4.4**	50.4	58.5	**-8.0**	Luxembourg	LU	14.9	17.3	**-2.4**	26.3	28.8	**-2.4**
Andorra	AD	23.1	22.3	**0.8**	44.1	41.5	**2.6**	Malta	MT	27.9	28.3	**-0.4**	42.2	42.9	**-0.7**
Austria	AT	16.1	18.0	**-1.9**	28.3	32.1	**-3.8**	Monaco	MC	22.2	22.0	**0.2**	34.3	34.3	**-0.1**
Belgium	BE	18.5	20.1	**-1.6**	33.1	34.6	**-1.5**	Montenegro	ME	24.7	26.9	**-2.2**	50.2	53.1	**-2.9**
Bosnia & Herzegovina	BA	29.8	29.3	**0.5**	59.6	60.6	**-1.0**	Netherlands	NL	18.1	19.0	**-0.9**	30.4	31.5	**-1.0**
Bulgaria	BG	27.2	33.5	**-6.3**	46.8	62.3	**-15.5**	North Macedonia	MK	31.3	42.2	**-11.0**	60.1	88.1	**-28.0**
Croatia	HR	21.1	24.3	**-3.2**	39.8	47.2	**-7.4**	Norway	NO	10.0	11.1	**-1.1**	19.1	20.0	**-0.9**
Cyprus	CY	26.3	34.6	**-8.3**	42.6	52.4	**-9.8**	Poland	PL	25.1	29.6	**-4.5**	45.0	54.5	**-9.5**
Czechia	CZ	19.3	23.7	**-4.5**	34.4	43.2	**-8.8**	Portugal (excl. Az., Mad.)	PT	17.3	18.3	**-1.0**	28.3	31.2	**-2.9**
Denmark (incl. Faroes)	DK	16.2	16.6	**-0.4**	28.0	28.5	**-0.5**	Romania	RO	22.2	25.5	**-3.3**	38.2	43.7	**-5.4**
Estonia	EE	11.1	12.4	**-1.3**	20.4	21.8	**-1.5**	San Marino	SM	21.9	21.9	**0.0**	38.9	39.6	**-0.7**
Finland	FI	9.2	10.0	**-0.8**	17.2	17.9	**-0.8**	Serbia (incl. Kosovo*)	RS	29.3	34.8	**-5.5**	55.9	67.8	**-11.9**
France (metropolitan)	FR	16.1	17.3	**-1.2**	27.8	29.0	**-1.2**	Slovakia	SK	20.5	25.5	**-5.0**	37.5	46.6	**-9.1**
Germany	DE	15.3	17.8	**-2.5**	26.9	30.3	**-3.5**	Slovenia	SI	18.8	22.2	**-3.4**	33.6	41.1	**-7.6**
Greece	GR	25.3	30.7	**-5.3**	41.3	52.0	**-10.7**	Spain (excl. Canarias)	ES	19.3	20.7	**-1.4**	30.9	33.9	**-3.0**
Hungary	HU	21.9	26.1	**-4.3**	38.6	47.2	**-8.6**	Sweden	SE	10.9	12.3	**-1.4**	20.8	21.8	**-0.9**
Iceland	IS	8.9	10.7	**-1.8**	17.9	18.3	**-0.4**	Switzerland	CH	13.2	15.8	**-2.6**	24.5	27.7	**-3.1**
Ireland	IE	12.4	12.3	**0.0**	22.1	21.8	**0.4**	United Kingdom (& Cr. d.)	UK	15.0	15.5	**-0.5**	26.5	26.5	**0.0**
Italy	IT	23.3	25.2	**-1.9**	40.9	44.4	**-3.5**	**Total without Turkey**		**18.7**	**20.9**	**-2.2**	**32.8**	**36.6**	**-3.8**
Latvia	LV	17.6	17.7	**-0.1**	30.2	31.1	**-0.9**	**EU-28**		**18.5**	**20.7**	**-2.1**	**32.2**	**35.8**	**-3.6**
Liechtenstein	LI	12.0	13.9	**-1.9**	21.9	25.5	**-3.6**	Kosovo*	KS	27.7	37.1	**-9.5**	56.5	76.3	**-19.8**
Lithuania	LT	19.4	19.2	**0.2**	32.9	34.3	**-1.4**	Serbia (excl. Kosovo*)	RS-	29.7	34.3	**-4.5**	55.8	65.8	**-10.0**

(*) under the UN Security Council Resolution 1244/99.

Notes: 5-year mean, i.e., five-year mean 2014-2018. Diff., i.e., difference concentrations between 2019 and five-year mean 2014-2018.

A4.2 $PM_{2.5}$

Concentration maps

Map A4.2 presents the difference between 2019 and five-year mean 2014-2018 for annual average $PM_{2.5}$.

The increases up to 1.5 µg·m^{-3} are seen parts of Ireland, the United Kingdom, Spain, France, Italy and Portugal. The higher increases are observed in the areas around the cities in south and south-eastern Europe and in the Krakow – Katowice (PL) – Ostrava (CZ) industrial region. The highest decreases are estimated in the Po Valley in northern Italy, most of Slovakia and parts of Czechia, Poland, Hungary, Romania and Croatia.

Map A4.2: Difference $PM_{2.5}$ annual average concentrations between 2019 and five-year average 2014-2018

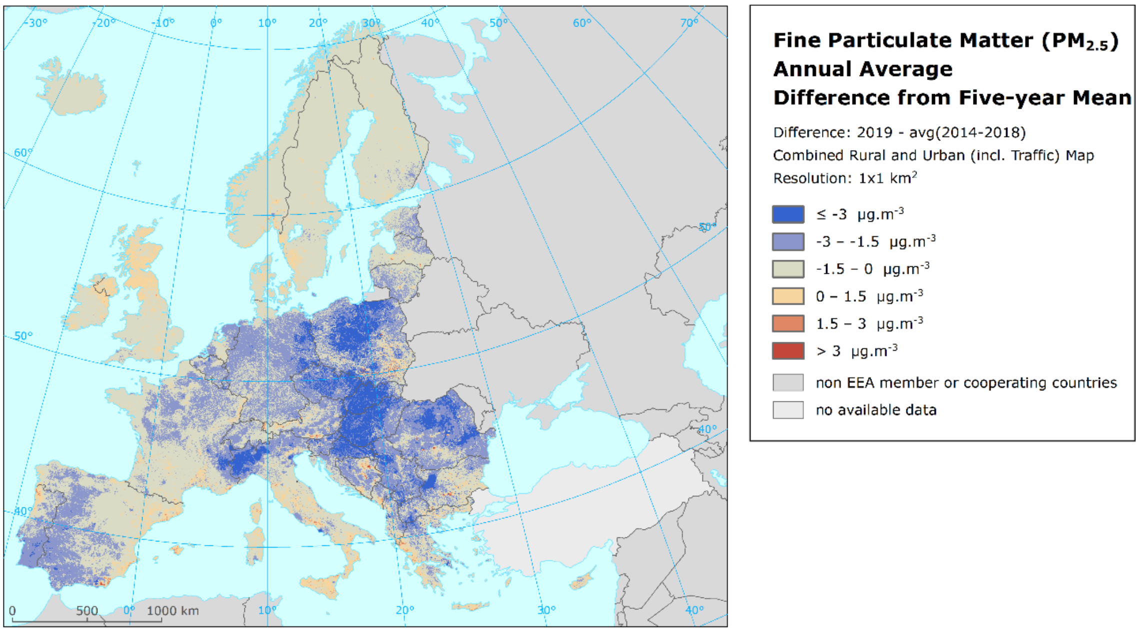

Population exposure

Table A4.2 presents the difference of the population-weighted concentrations between 2019 and five-year mean 2014-2018 for $PM_{2.5}$ annual average, for individual countries and for Europe as a whole (without Turkey, which is not mapped for this pollutant).

In 2019, the average overall population-weighted concentration is estimated at 11.8 µg·m^{-3}, which means a decrease of 2.1 µg·m^{-3} compared to five-year mean. The decrease in concentrations in 2019 compared to five-year mean has been observed in all countries. The change of concentrations is from -0.3 µg.m^{-3} in Ireland to the steepest decreases in North Macedonia (more than -11 µg·m^{-3}).

Table A4.2: Population-weighted concentration in 2019 and five-year mean 2014-2018 and its difference between 2019 and five-year mean for $PM_{2.5}$ annual average

Country	ISO	Population-weighted concentration [μg·m⁻³] Annual average			Country	ISO	Population-weighted concentration [μg·m⁻³] Annual average		
		2019	5-year mean	Diff.			2019	5-year mean	Diff.
Albania	AL	17.5	21.1	**-3.6**	Luxembourg	LU	8.1	11.1	**-3.0**
Andorra	AD	10.8	11.1	**-0.3**	Malta	MT	12.2	12.1	**0.1**
Austria	AT	11.3	12.8	**-1.5**	Monaco	MC	12.9	13.4	**-0.5**
Belgium	BE	11.0	12.9	**-1.9**	Montenegro	ME	18.4	18.8	**-0.4**
Bosnia & Herzegovina	BA	21.6	22.0	**-0.5**	Netherlands	NL	10.7	12.2	**-1.5**
Bulgaria	BG	18.0	23.0	**-5.0**	North Macedonia	MK	20.6	32.0	**-11.4**
Croatia	HR	14.6	17.6	**-3.0**	Norway	NO	5.4	6.1	**-0.7**
Cyprus	CY	14.7	16.0	**-1.3**	Poland	PL	17.6	21.7	**-4.1**
Czechia	CZ	13.8	17.6	**-3.7**	Portugal (excl. Az., Mad.)	PT	8.3	9.1	**-0.8**
Denmark (incl. Faroes)	DK	9.4	9.9	**-0.6**	Romania	RO	15.1	17.6	**-2.5**
Estonia	EE	5.5	6.8	**-1.3**	San Marino	SM	13.0	14.2	**-1.2**
Finland	FI	5.0	5.7	**-0.7**	Serbia (incl. Kosovo*)	RS	20.6	25.4	**-4.8**
France (metropolitan)	FR	9.5	11.1	**-1.6**	Slovakia	SK	14.5	18.6	**-4.1**
Germany	DE	10.1	12.4	**-2.3**	Slovenia	SI	13.1	16.1	**-3.0**
Greece	GR	15.7	21.0	**-5.3**	Spain (excl. Canarias)	ES	10.2	11.4	**-1.2**
Hungary	HU	14.5	18.3	**-3.9**	Sweden	SE	5.4	6.1	**-0.7**
Iceland	IS	3.9	5.5	**-1.5**	Switzerland	CH	8.7	10.7	**-2.0**
Ireland	IE	7.7	7.3	**0.3**	United Kingdom (& Cr. dep.)	UK	9.7	10.0	**-0.3**
Italy	IT	14.5	16.7	**-2.2**	**Total without Turkey**		**11.8**	**11.8**	**13.9**
Latvia	LV	10.1	11.7	**-1.5**	**EU-28**		**11.7**	**11.7**	**13.6**
Liechtenstein	LI	8.1	9.7	**-1.6**	Kosovo*	KS	20.1	27.8	**-7.7**
Lithuania	LT	12.1	12.6	**-0.6**	Serbia (excl. Kosovo*)	RS-	20.8	24.9	**-4.1**

(*) under the UN Security Council Resolution 1244/99.

Notes: 5-year mean, i.e., five-year mean 2014-2018. Diff., i.e., difference concentrations between 2019 and five-year mean 2014-2018.

A4.3 Ozone

Concentration maps

In Map 4.3, the difference concentrations between 2019 and five-year average 2014-2018 for both the health related ozone indicators (i.e., for 93.2 percentile of maximum daily 8-hour means and SOMO35) and the vegetation related ozone indicators (i.e., for AOT40 for vegetation and AOT40 for forests) are presented. In all the maps, orange and red areas show an increase of ozone concentrations, while blue areas show a decrease.

In general, increases are shown for the two health related indicators. The highest increases for 93.2 percentile of maximum daily 8-hour means have been observed in northern Europe, in large areas in Ireland, the United Kingdom, France and Germany and in smaller areas in south and south-eastern Europe. Contrary to that, one can see a decline in several coastal parts in southern and south-eastern Europe, in larger areas of Romania and Hungary and on the borders of Czechia, Poland and Slovakia. The difference pattern for SOMO35 is quite similar to that of the percentile indicator.

In the case of both AOT40 indicators, the state is very similar to the health-related indicators, apart from some areas of the west Balkan and most of the Mediterranean coast, where decreases are found.

Map A4.3: Difference concentrations between 2019 and five-year average 2014-2018 for ozone indicators 93.2 percentile of daily 8-hour maximums (top left), SOMO35 (top right), AOT40 for vegetation (bottom left) and AOT40 for forests (bottom right)

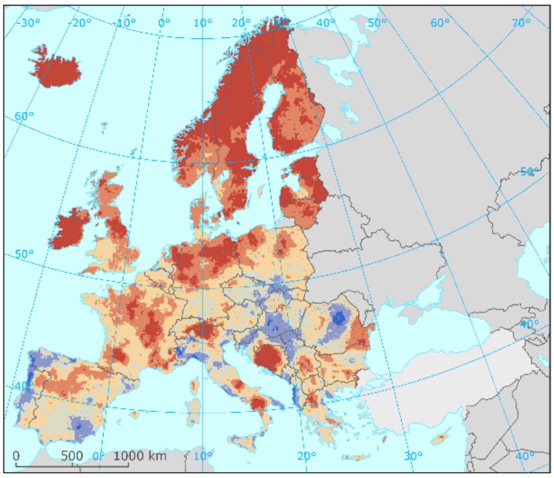

Ozone, 93.2 Percentile of Maximum daily 8-hour Means
Difference between 2019 and Five-year Mean 2014-2018

Difference: 2019 - avg(2014-2018)
Combined Rural and Urban Background Map, Resolution 1x1 km²

- ≤ - 10 µg.m⁻³
- - 10 – - 4 µg.m⁻³
- - 4 – 0 µg.m⁻³
- 0 – 4 µg.m⁻³
- 4 – 10 µg.m⁻³
- > 10 µg.m⁻³
- no available data
- unmapped countries

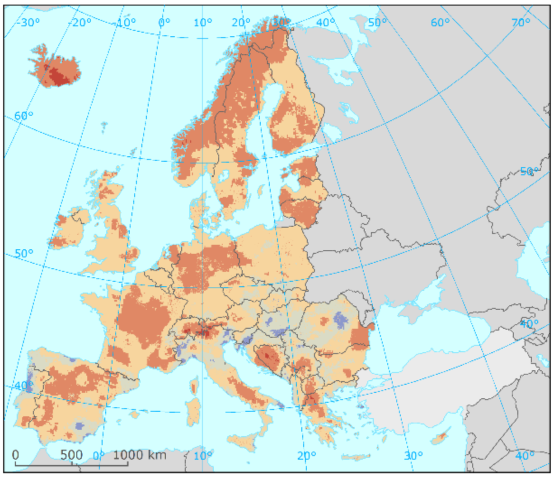

Ozone, SOMO35
Difference between 2019 and Five-year Mean 2014-2018

Difference: 2019 - avg(2014-2018)
Combined Rural and Urban Background Map, Resolution 1x1 km²

- ≤ - 2000 µg.m⁻³.d
- - 2000 – - 800 µg.m⁻³.d
- - 800 – 0 µg.m⁻³.d
- 0 – 800 µg.m⁻³.d
- 800 – 2000 µg.m⁻³.d
- > 2000 µg.m⁻³.d
- no available data
- unmapped countries

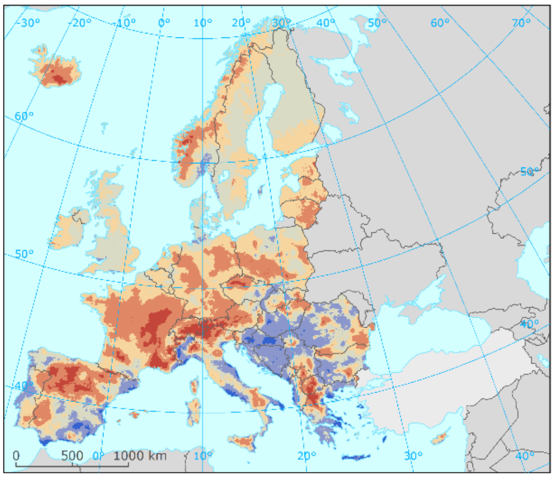

Ozone, AOT40 for Vegetation
Difference between 2019 and Five-year Mean 2014-2018

Difference: 2019 - avg(2014-2018)
Rural Map, Resolution 2x2 km²

- ≤ - 6000 µg.m⁻³.h
- - 6000 – - 2000 µg.m⁻³.h
- - 2000 – 0 µg.m⁻³.h
- 0 – 2000 µg.m⁻³.h
- 2000 – 6000 µg.m⁻³.h
- > 6000 µg.m⁻³.h
- no available data
- unmapped countries

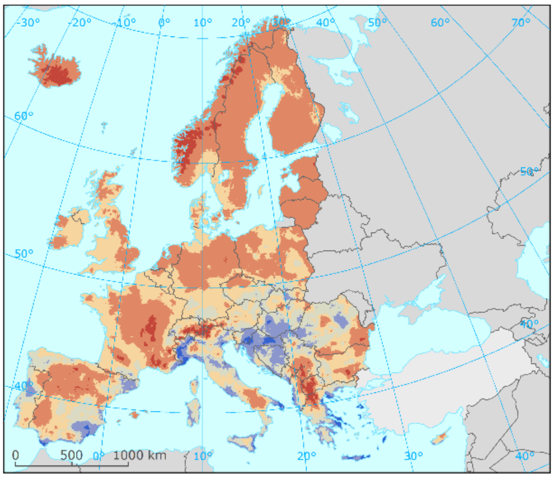

Ozone, AOT40 for Forests
Difference between 2019 and Five-year Mean 2014-2018

Difference: 2019 - avg(2014-2018)
Rural Map, Resolution 2x2 km²

- ≤ - 10000 µg.m⁻³.h
- - 10000 – - 4000 µg.m⁻³.h
- - 4000 – 0 µg.m⁻³.h
- 0 – 4000 µg.m⁻³.h
- 4000 – 10000 µg.m⁻³.h
- > 10000 µg.m⁻³.h
- no available data
- unmapped countries

Population exposure

Table A4.3 provides the difference of the population-weighted concentrations between 2019 and five-year mean 2014-2018 for ozone health related indicators 93.2 percentile of 8-houry daily maximums and SOMO35, for individual countries, for EU-28 and for the total mapping area (without Turkey). Additionally, the difference of the population-weighted concentrations between 2019 and 2018 is presented for SOMO10, for which the five-year time series is not available.

Table A4.3: Population-weighted concentration in 2019 and five-year mean 2014-2018 and its difference between 2019 and five-year mean for ozone indicators 93.2 percentile of 8-h daily maximums (left) and SOMO35 (middle) and population-weighted concentration in 2018 and 2019 and its difference between 2019 and 2018 for ozone indicator SOMO10 (right)

Country	ISO	Population-weighted concentration								
		93.2 perc. of 8-h d. max [μg·m^{-3}]			SOMO35 [μg·m^{-3}·d]			SOMO10 [μg·m^{-3}·d]		
		2019	5-year mean	Diff.	2019	5-year mean	Diff.	2019	2018	Diff.
Albania	AL	109.2	113.1	**-3.9**	5 727	5 913	**-186**	21 910	20 980	**930**
Andorra	AD	116.5	112.9	**3.6**	7 536	5 788	**1 748**	22 728	20 618	**2 111**
Austria	AT	119.9	119.3	**0.6**	5 802	5 431	**370**	20 707	21 481	**-774**
Belgium	BE	107.7	106.0	**1.7**	3 336	2 829	**508**	17 237	17 689	**-452**
Bosnia & Herzegovina	BA	123.5	111.8	**11.6**	7 062	5 300	**1 763**	22 745	19 449	**3 296**
Bulgaria	BG	99.2	100.5	**-1.3**	3 515	3 550	**-35**	17 138	17 679	**-541**
Croatia	HR	116.0	115.7	**0.3**	6 191	5 838	**352**	21 625	21 002	**623**
Cyprus	CY	113.5	106.4	**7.1**	5 653	6 060	**-407**	21 304	20 042	**1 262**
Czechia	CZ	118.1	118.6	**-0.5**	5 400	4 997	**404**	20 475	22 084	**-1 609**
Denmark (incl. Faroe Islands)	DK	103.3	95.5	**7.8**	3 477	2 536	**941**	18 918	19 523	**-605**
Estonia	EE	100.7	91.5	**9.2**	2 739	1 994	**745**	17 594	17 625	**-31**
Finland	FI	97.5	88.4	**9.1**	2 297	1 597	**699**	16 872	17 276	**-404**
France (metropolitan)	FR	112.8	108.8	**4.0**	4 791	4 107	**685**	20 273	20 509	**-236**
Germany	DE	118.5	113.7	**4.8**	4 612	3 962	**649**	18 720	19 874	**-1 154**
Greece	GR	113.2	112.8	**0.4**	7 094	6 344	**750**	22 955	21 685	**1 270**
Hungary	HU	108.3	112.8	**-4.5**	4 473	4 806	**-333**	18 649	20 124	**-1 475**
Iceland	IS	92.8	77.3	**15.5**	1 662	751	**911**	16 807	16 593	**214**
Ireland	IE	90.2	76.3	**13.9**	2 125	1 404	**720**	17 436	17 966	**-530**
Italy	IT	123.6	124.1	**-0.5**	6 659	6 476	**183**	21 625	20 793	**832**
Latvia	LV	98.8	95.1	**3.7**	2 552	2 367	**185**	16 339	17 310	**-971**
Liechtenstein	LI	122.9	122.2	**0.8**	5 719	5 439	**280**	20 049	21 454	**-1 405**
Lithuania	LT	105.2	96.5	**8.7**	3 222	2 446	**776**	17 584	17 694	**-110**
Luxembourg	LU	111.3	108.7	**2.6**	3 808	3 230	**578**	18 126	19 011	**-885**
Malta	MT	106.0	107.3	**-1.4**	5 872	6 079	**-206**	23 683	23 185	**497**
Monaco	MC	121.0	121.2	**-0.2**	6 930	7 644	**-715**	23 101	23 313	**-212**
Montenegro	ME	112.3	111.4	**1.0**	6 017	5 698	**318**	21 930	20 646	**1 284**
Netherlands	NL	106.5	102.2	**4.2**	3 331	2 650	**681**	17 232	17 331	**-99**
North Macedonia	MK	103.7	103.3	**0.4**	4 038	4 325	**-287**	18 335	17 214	**1 120**
Norway	NO	98.6	89.1	**9.5**	2 709	1 991	**719**	17 338	18 569	**-1 230**
Poland	PL	112.6	110.7	**1.9**	4 390	3 972	**418**	18 784	19 612	**-829**
Portugal (excl. Azores, Madeira)	PT	96.5	105.0	**-8.5**	3 332	4 034	**-702**	18 010	20 823	**-2 813**
Romania	RO	97.5	93.6	**3.9**	3 222	2 969	**253**	16 828	17 557	**-729**
San Marino	SM	119.0	123.6	**-4.5**	5 956	6 537	**-580**	21 020	21 121	**-100**
Serbia (incl. Kosovo*)	RS	104.9	102.4	**2.5**	4 143	3 994	**150**	17 627	16 999	**628**
Slovakia	SK	110.9	114.3	**-3.4**	4 778	5 004	**-226**	19 636	20 940	**-1 304**
Slovenia	SI	116.1	119.4	**-3.3**	5 758	6 054	**-296**	20 963	21 481	**-518**
Spain (excl. Canarias)	ES	111.6	112.0	**-0.5**	5 816	5 582	**235**	21 951	21 732	**219**
Sweden	SE	103.0	93.2	**9.7**	3 148	2 265	**883**	18 368	18 940	**-573**
Switzerland	CH	123.2	122.5	**0.7**	5 847	5 586	**262**	20 521	21 770	**-1 249**
United Kingdom (& Crown dep.)	UK	89.9	86.7	**3.1**	1 892	1 465	**427**	15 662	16 089	**-427**
Total without Turkey		**109.9**	**107.5**	**2.4**	**4 478**	**4 057**	**421**	**19 147**	**19 519**	**-372**
EU-28		**109.9**	**107.5**	**2.4**	**4 454**	**4 032**	**421**	**19 127**	**19 539**	**-412**
Kosovo*	KS	104.9	102.8	**2.2**	4 378	4 581	**-203**	18 702	17 687	**1 015**
Serbia (excl. Kosovo*)	RS-	104.9	102.3	**2.6**	4 086	3 850	**236**	17 364	16 831	**533**

(*) under the UN Security Council Resolution 1244/99.

Notes: 5-year mean, i.e., five-year mean 2014-2018. Diff., i.e., difference concentrations between 2019 and five-year mean 2014-2018 for 93.2 percentile of 8-h daily maximums and SOMO35; difference concentrations between 2019 and 2018 for SOMO10.

In 2019 the overall population-weighted concentration for ozone indicator 93.2 percentile of maximum daily 8-hour means was about 109.9 μg·m^{-3}, i.e., of about 2.5 μg·m^{-3} higher than five-year mean concentration. The highest increases are found in countries of northern Europe (maximum of

15.5 µg·m^{-3} in Iceland, then in Ireland, Sweden and Norway) and in Bosnia and Herzegovina, the highest decreases are shown in countries of southern and central Europe (maximum of 8.5 µg·m^{-3} in Portugal, then in Hungary, Albania, Slovakia).

In the case of SOMO35, the average overall population-weighted concentration for 2019 is estimated at about 4 478 µg·m^{-3}·d, which is of about 421 µg·m^{-3}·d higher than five-year mean SOMO35 value. The highest increases are found in Bosnia and Herzegovina (1 763 µg·m^{-3}) and Andorra and in countries of northern Europe (Denmark, Iceland, Sweden), the steepest decreases are found in Monaco and Portugal (more than 700 µg·m^{-3}).

Vegetation exposure

Table A4.4 provides the difference of the agricultural-weighted concentrations for AOT40 for vegetation and the forest-weighted concentrations for AOT40 for forests between 2019 and five-year mean of AOT40.

Table A4.4: Agricultural weighted (left) and forest-weighted (right) concentration in 2019 and five-year mean 2014-2018 and its difference between 2019 and five-year mean for ozone indicators AOT40 for vegetation (left) and AOT40 for forests (right)

Country	ISO	Agriculture-weighted concentration AOT40 for vegetation [µg·m^{-3}·h]			Forest-weighted concentration AOT40 for forests [µg·m^{-3}·h]		
		2019	5-year mean	Differ.	2019	5-year mean	Differ.
Albania	AL	18 774	21 392	**-2 618**	42 927	40 930	**1 997**
Andorra	AD	20 912	19 488	**1 424**	34 385	34 012	**373**
Austria	AT	11 589	11 211	**378**	21 931	19 701	**2 230**
Belgium	BE	12 216	16 306	**-4 090**	26 768	31 179	**-4 412**
Bosnia & Herzegovina	BA	11 897	12 116	**-219**	30 832	29 504	**1 327**
Bulgaria	BG	13 282	17 711	**-4 428**	26 114	32 909	**-6 795**
Croatia	HR	21 921	21 911	**11**	44 369	44 825	**-456**
Cyprus	CY	19 380	18 141	**1 239**	33 242	32 345	**897**
Czechia	CZ	5 931	6 816	**-885**	14 564	11 328	**3 236**
Denmark (incl. Faroe Islands)	DK	4 773	3 436	**1 337**	12 953	6 421	**6 532**
Estonia	EE	3 162	2 940	**221**	9 167	4 495	**4 672**
Finland	FI	14 222	11 354	**2 868**	28 949	25 032	**3 917**
France (metropolitan)	FR	15 709	14 167	**1 542**	30 180	26 473	**3 706**
Germany	DE	20 493	22 969	**-2 476**	41 861	43 121	**-1 260**
Greece	GR	14 505	15 777	**-1 272**	27 964	30 665	**-2 702**
Hungary	HU	946	620	**326**	7 805	1 531	**6 273**
Iceland	IS	2 431	2 222	**209**	7 534	3 996	**3 538**
Ireland	IE	23 990	24 711	**-722**	41 710	43 244	**-1 534**
Italy	IT	5 680	4 147	**1 533**	14 162	7 795	**6 366**
Latvia	LV	24 253	18 943	**5 310**	38 591	35 834	**2 757**
Liechtenstein	LI	7 202	5 453	**1 750**	17 618	10 636	**6 982**
Lithuania	LT	14 338	13 883	**455**	23 793	21 787	**2 006**
Luxembourg	LU	18 774	21 392	**-2 618**	42 927	40 930	**1 997**
Malta	MT	21 420	24 546	**-3 126**	42 655	46 997	**-4 343**
Monaco	MC	0	13 970	**-13 970**	31 606	34 435	**-2 829**
Montenegro	ME	16 557	18 516	**-1 959**	36 934	36 110	**824**
Netherlands	NL	9 828	8 632	**1 197**	19 025	13 983	**5 042**
North Macedonia	MK	21 866	19 106	**2 760**	46 398	39 870	**6 529**
Norway	NO	2 872	3 451	**-579**	12 494	6 608	**5 886**
Poland	PL	13 242	12 168	**1 074**	25 901	22 069	**3 832**
Portugal (excl. Azores, Madeira)	PT	10 919	10 541	**378**	20 008	21 539	**-1 531**
Romania	RO	9 394	9 775	**-381**	20 239	21 723	**-1 484**
San Marino	SM	19 720	25 334	**-5 614**	35 994	40 886	**-4 892**
Serbia (incl. Kosovo*)	RS	14 445	15 555	**-1 110**	34 236	31 508	**2 727**
Slovakia	SK	15 630	15 572	**59**	28 223	28 573	**-350**
Slovenia	SI	17 836	20 415	**-2 579**	31 664	36 202	**-4 537**
Spain (excl. Canarias)	ES	18 956	18 194	**762**	31 203	29 796	**1 408**
Sweden	SE	5 212	5 349	**-137**	11 808	6 760	**5 047**
Switzerland	CH	22 888	19 470	**3 418**	37 919	34 721	**3 198**
United Kingdom (& Crown dep.)	UK	3 642	4 184	**-542**	8 582	5 364	**3 218**
Total without Turkey		**13 735**	**13 131**	**604**	**22 343**	**19 655**	**2 688**
EU-28		**13 721**	**13 033**	**688**	**22 331**	**19 773**	**2 558**
Kosovo*	KS	19 574	16 927	**2 647**	42 600	34 828	**7 772**
Serbia (excl. Kosovo*)	RS-	13 943	15 414	**-1 471**	32 660	30 879	**1 781**

(*) under the UN Security Council Resolution 1244/99.

Notes: 5-year mean, i.e., five-year mean 2014-2018. Differ., i.e., difference concentrations between 2019 and five-year mean 2014-2018.

In 2019, the agricultural-weighted concentration of vegetation-related AOT40 shows an increase of ca. 604 $\mu g \cdot m^{-3} \cdot h$ compared to five-year mean; the forest-weighted concentration of forest-related AOT40 shows an increase of about 2 688 $\mu g \cdot m^{-3} \cdot h$ compared to five-year mean. The highest increases of vegetation-related AOT40 are seen in Liechtenstein and Switzerland, while the steepest decreases in Croatia and Bosnia and Herzegovina. The highest increases of forest-related AOT40 are seen in Kosovo, Lithuania and Estonia, while the steepest decreases in Croatia and Slovenia.

A4.4 NO_2 and NO_x

Concentration maps

Map A4.4 presents the difference concentrations between 2019 and five-year average 2014-2018 for NO_2 and NO_x annual averages. Orange and red areas show an increase of concentration in 2019, while blue areas show a decrease.

For NO_2, the decreases are shown in some parts of Italy, Spain and France and countries in central Europe. The highest increases are seen in northern Europe, Ireland, the United Kingdom and parts of south and south-eastern Europe.

In the case of NO_x, notable decreases are seen in north-eastern Spain, western and northern France, northern Italy, Serbia, North Macedonia and Finland. The highest increases can be seen in coastal parts of Ireland, Cyprus, Bulgaria and Greece. In this context, note the lack of stations in the south-east Balkan.

Map A4.4: Difference concentrations between 2019 and five year average 2014-2018 for NO_2 annual average (left) and NOx annual average (right)

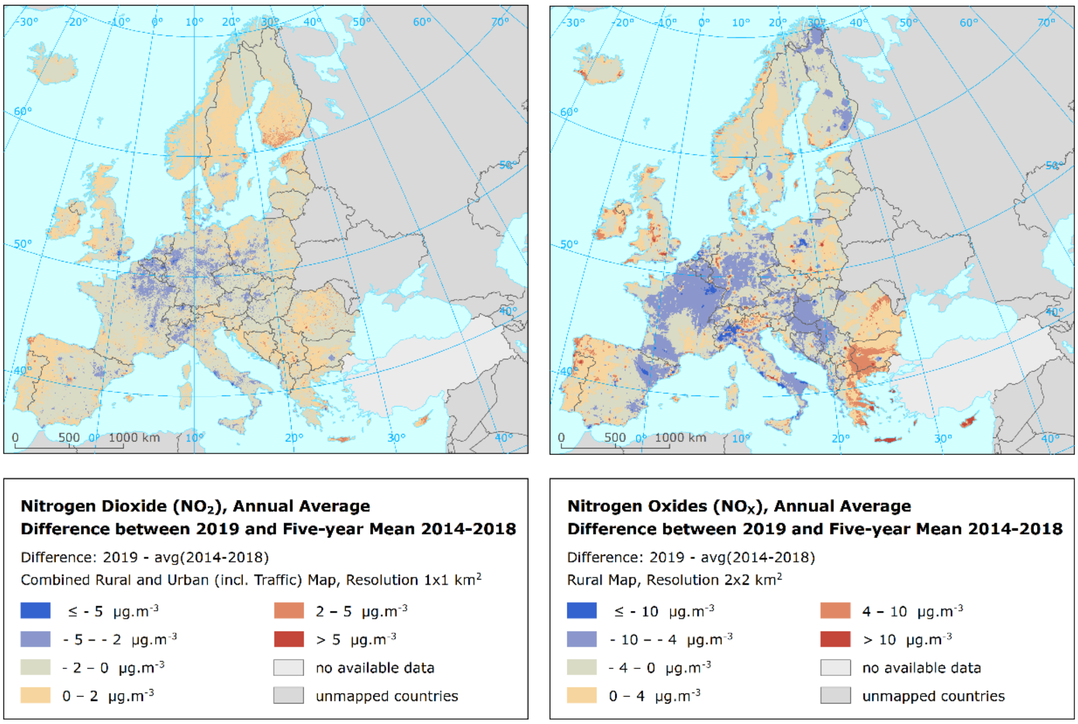

Population exposure

Table A4.5 provides the difference between 2019 annual average and five-year mean 2014-2018 for NO_2. In 2019 the overall population-weighted concentration for NO_2 annual average was 16.8 μg·m^{-3}, i.e., 1.6 μg·m^{-3} lower than for five-year mean. The steepest decreases (ca. 3 μg.m^{-3}) are shown in Malta, Switzerland and Belgium, while the highest increases (above 2 μg.m^{-3}) in Kosovo and Cyprus.

Table A4.5: Population-weighted concentration in 2019 and five-year mean 2014-2018 and its difference between 2019 and five-year mean for NO_2 annual average

Country	ISO	Population-weighted concentration [μg·m^{-3}] Annual average			Country	ISO	Population-weighted concentration [μg·m^{-3}] Annual average		
		2019	**5-year mean**	**Diff.**			**2019**	**5-year mean**	**Diff.**
Albania	AL	15.2	15.6	**-0.4**	Luxembourg	LU	18.4	20.0	**-1.6**
Andorra	AD	20.0	18.5	**1.6**	Malta	MT	11.5	14.8	**-3.3**
Austria	AT	16.4	18.9	**-2.5**	Monaco	MC	23.9	26.5	**-2.6**
Belgium	BE	18.5	21.2	**-2.6**	Montenegro	ME	14.9	14.2	**0.8**
Bosnia & Herzegovina	BA	14.3	14.8	**-0.5**	Netherlands	NL	19.1	20.7	**-1.6**
Bulgaria	BG	18.6	17.9	**0.7**	North Macedonia	MK	18.0	18.0	**0.0**
Croatia	HR	14.2	15.5	**-1.3**	Norway	NO	9.6	11.5	**-1.9**
Cyprus	CY	20.9	18.8	**2.1**	Poland	PL	14.2	15.3	**-1.1**
Czechia	CZ	14.2	15.8	**-1.6**	Portugal (excl. Az., Mad.)	PT	14.9	15.3	**-0.4**
Denmark (incl. Faroes)	DK	9.0	10.1	**-1.1**	Romania	RO	19.5	17.4	**2.0**
Estonia	EE	7.5	7.7	**-0.2**	San Marino	SM	15.8	15.2	**0.6**
Finland	FI	8.2	8.3	**-0.1**	Serbia (incl. Kosovo*)	RS	17.9	18.3	**-0.4**
France (metropolitan)	FR	15.2	17.1	**-2.0**	Slovakia	SK	13.5	15.0	**-1.5**
Germany	DE	17.5	19.8	**-2.3**	Slovenia	SI	14.3	15.6	**-1.3**
Greece	GR	19.0	19.4	**-0.5**	Spain (excl. Canarias)	ES	18.6	20.4	**-1.9**
Hungary	HU	16.6	17.3	**-0.7**	Sweden	SE	8.0	9.6	**-1.6**
Iceland	IS	11.0	10.7	**0.3**	Switzerland	CH	16.7	19.7	**-3.0**
Ireland	IE	10.5	9.0	**1.5**	United Kingdom (& Cr. dep.)	UK	18.7	20.5	**-1.8**
Italy	IT	20.0	22.3	**-2.4**	**Total without Turkey**		**16.8**	**18.4**	**-1.6**
Latvia	LV	10.4	11.9	**-1.5**	**EU-28**		**16.9**	**18.5**	**-1.6**
Liechtenstein	LI	16.5	18.3	**-1.8**	Kosovo*	KS	17.5	15.3	**2.2**
Lithuania	LT	11.0	11.9	**-0.9**	Serbia (excl. Kosovo*)	RS-	18.0	19.1	**-1.1**

(*) under the UN Security Council Resolution 1244/99.

Notes: 5-year mean, i.e., five-year mean 2014-2018. Diff., i.e., difference concentrations between 2019 and five-year mean 2014-2018.

Annex 5
Concentration maps including stations

Throughout the report, the concentration maps presented do not include the concentration values measured at the stations. The reason is to better visualise the health related indicators with their distinct concentration levels at the more fragmented and smaller urban areas.

As presented in Annex 3, the kriging interpolation methodology somewhat smooths the concentration field. Therefore, it is valuable to present in this Annex 5 the indicator maps including the concentration values resulting from the measurement data at the stations. These points provide important additional visual information on the smoothing effect caused by the interpolation. For instance, maps A5.1 and A5.2 present PM_{10} indicators annual average and 90.4 percentile of daily means and include the stations points used in the interpolation. They correspond to Maps 2.1 and 2.2 of the main report, which do not have stations. Table A5.1 provides an overview on the maps of the main report and the corresponding maps including stations point values as presented in this annex.

Both the rural and the urban/suburban background stations and also urban/ traffic stations for PM and NO_2 are included in the maps of the health related indicators, while the rural stations only are shown in the maps of vegetation related indicators. For $PM_{2.5}$ and NO_x, only the stations with relevant measured data (i.e., not the pseudo stations) are presented.

Table A5.1: Overview of maps presented in this Annex 5 and their relation with the maps presented in the main report

Air pollutant	Indicator	Map including stations	Map without stations
PM_{10}	Annual average	A5.1	2.1
	90.4 percentile of daily means	A5.2	2.2
$PM_{2.5}$	Annual average	A5.3	3.1
Ozone	93.2 percentile of maximum daily 8-hour means	A5.4	4.1
	SOMO35	A5.5	4.2
	SOMO10	A5.6	4.3
	AOT40 for vegetation ([a])	A5.7	4.4
	AOT40 for forests ([a])	A5.8	4.5
NO_2	Annual average	A5.9	5.1
NO_x	Annual average ([a])	A5.10	5.2

([a]) Rural map, applicable for rural areas only.

Map A5.1: Concentration map of PM_{10} annual average including station measurement values, 2019

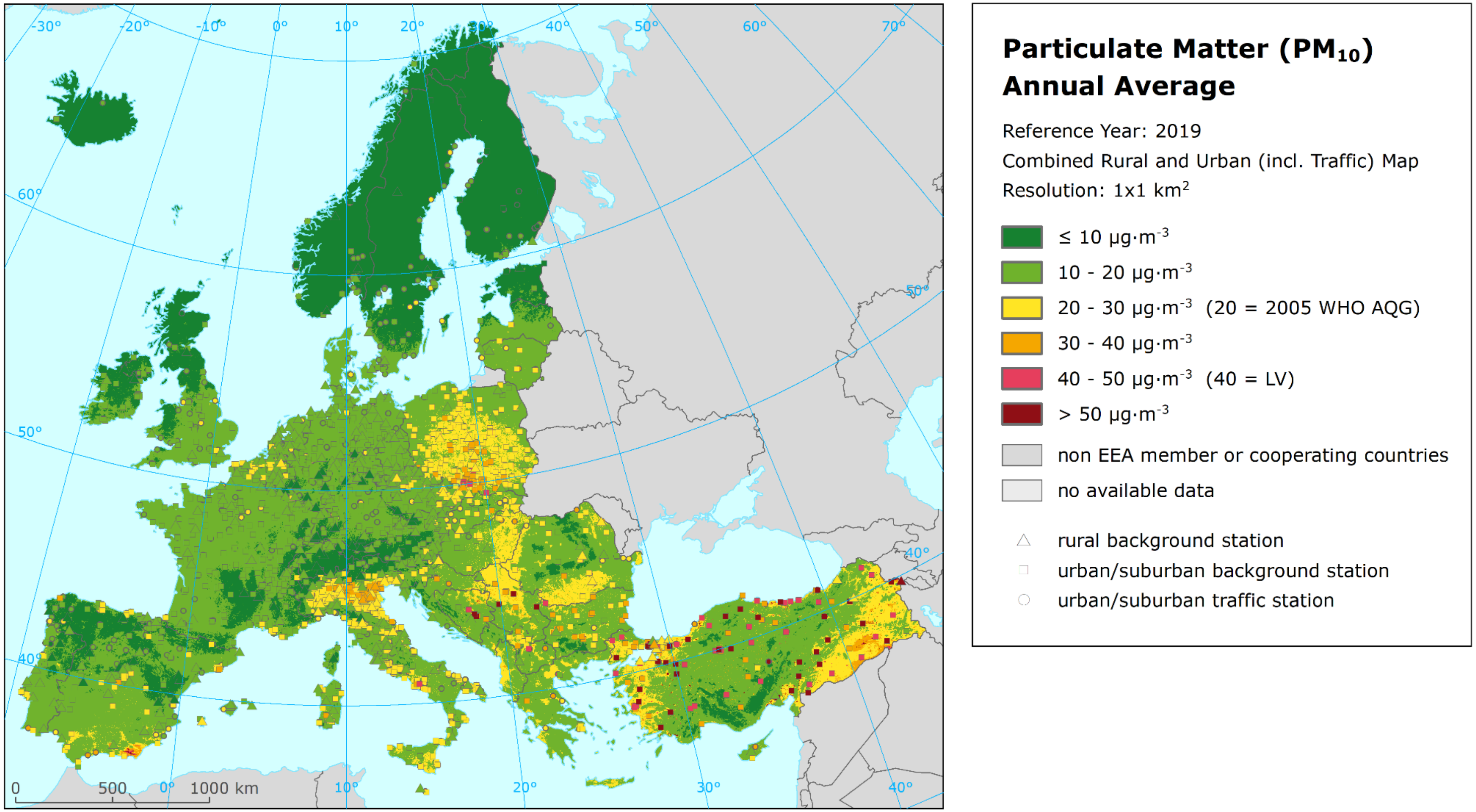

Map A5.2: Concentration map of PM_{10} indicator 90.4 percentile of daily means including station measurement values, 2019

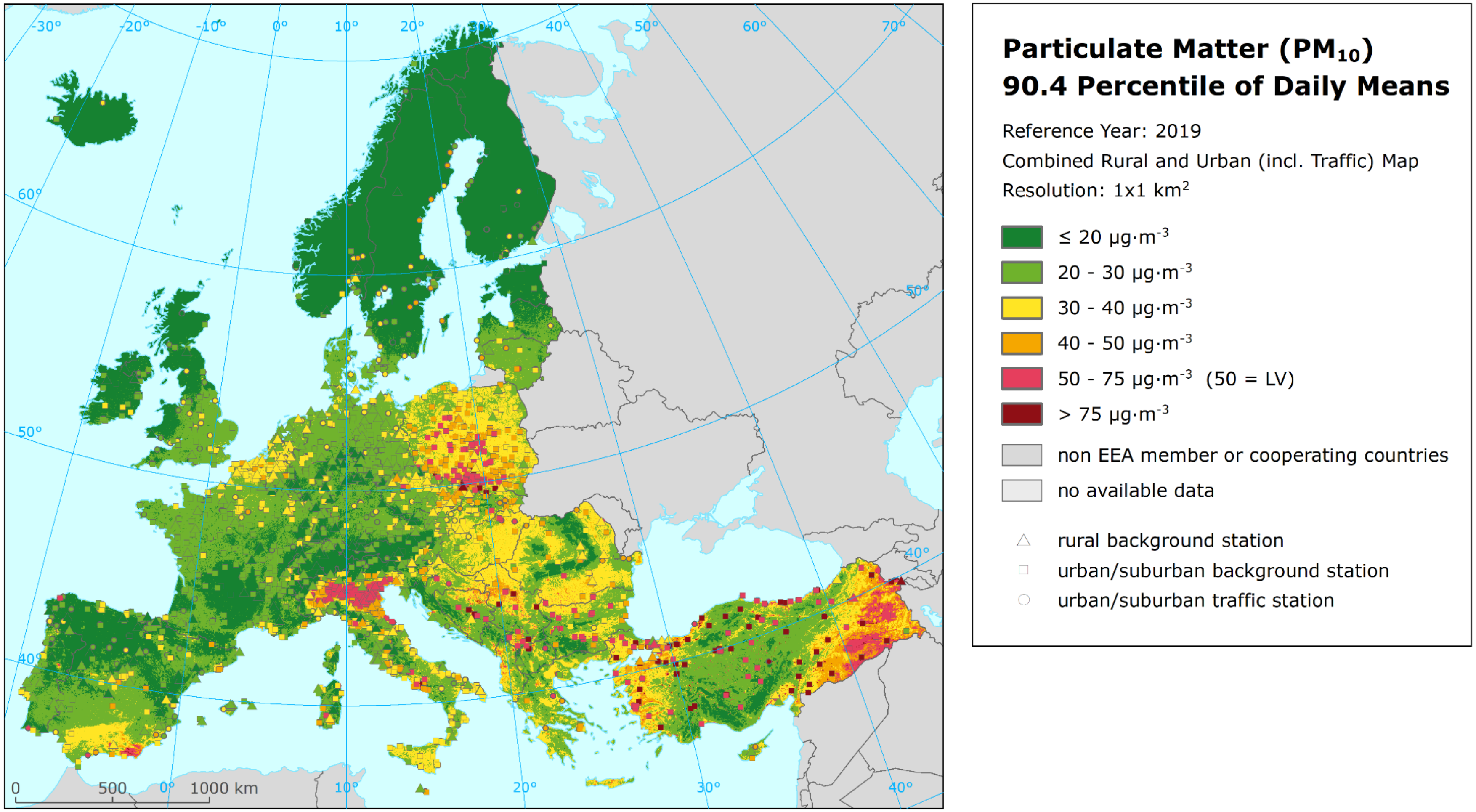

Map A5.3: Concentration map of $PM_{2.5}$ annual average including station measurement values, 2019

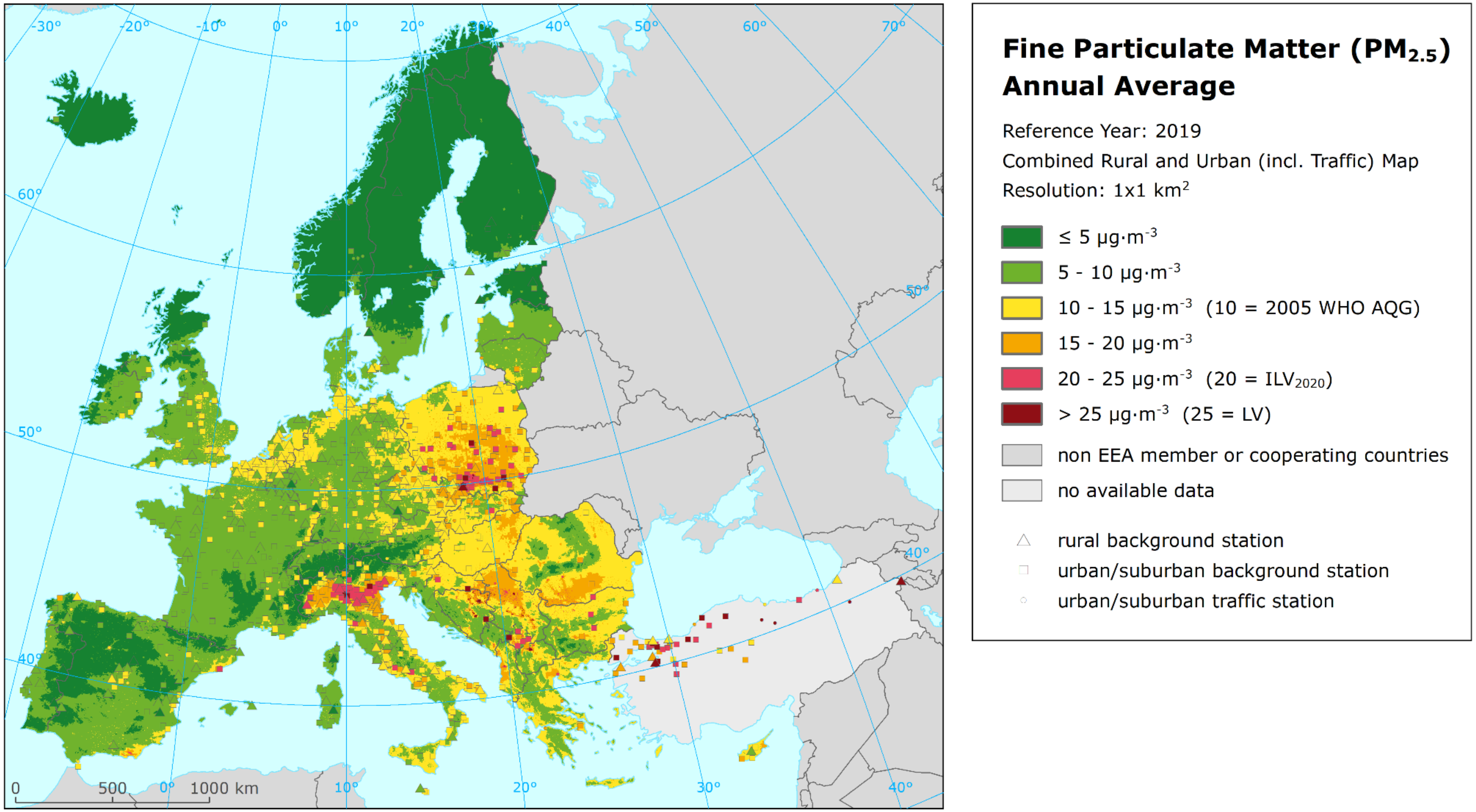

Map A5.4: Concentration map of ozone indicator 93.2 percentile of maximum daily 8-hour means including station measurement values, 2019

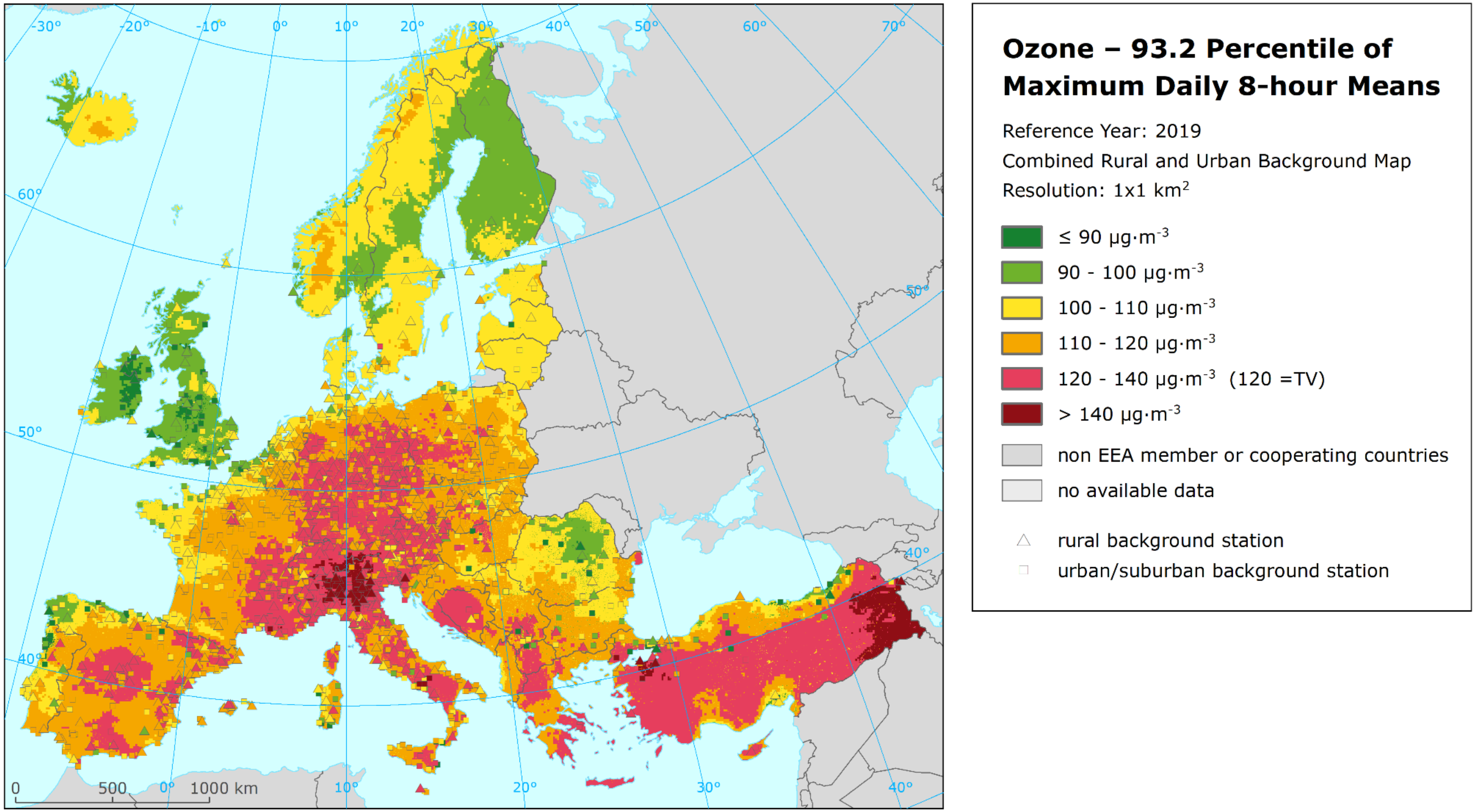

Map A5.5: Concentration map of ozone indicator SOMO35 including station measurement values, 2019

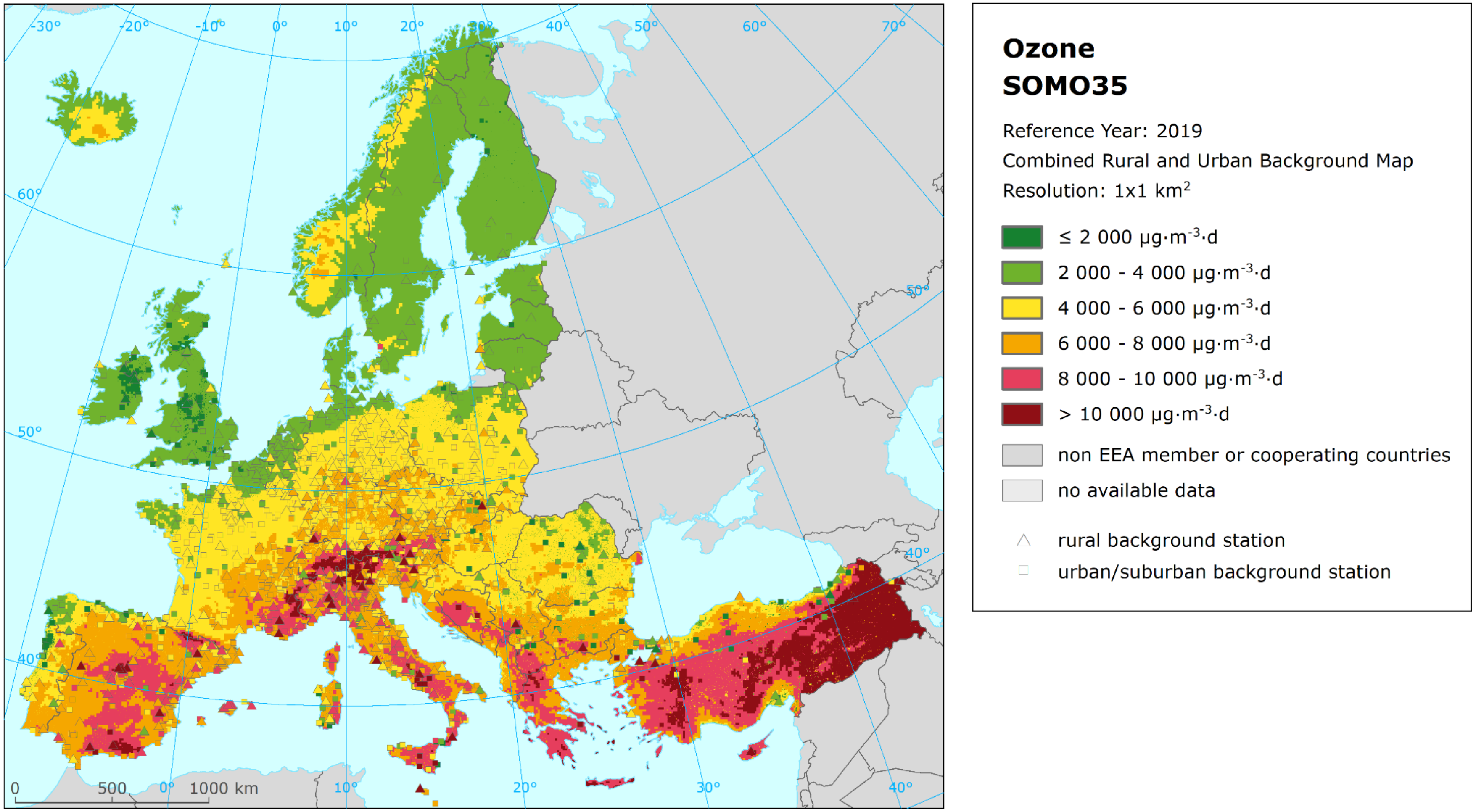

Map A5.6: Concentration map of ozone indicator SOMO10 including station measurement values, 2019

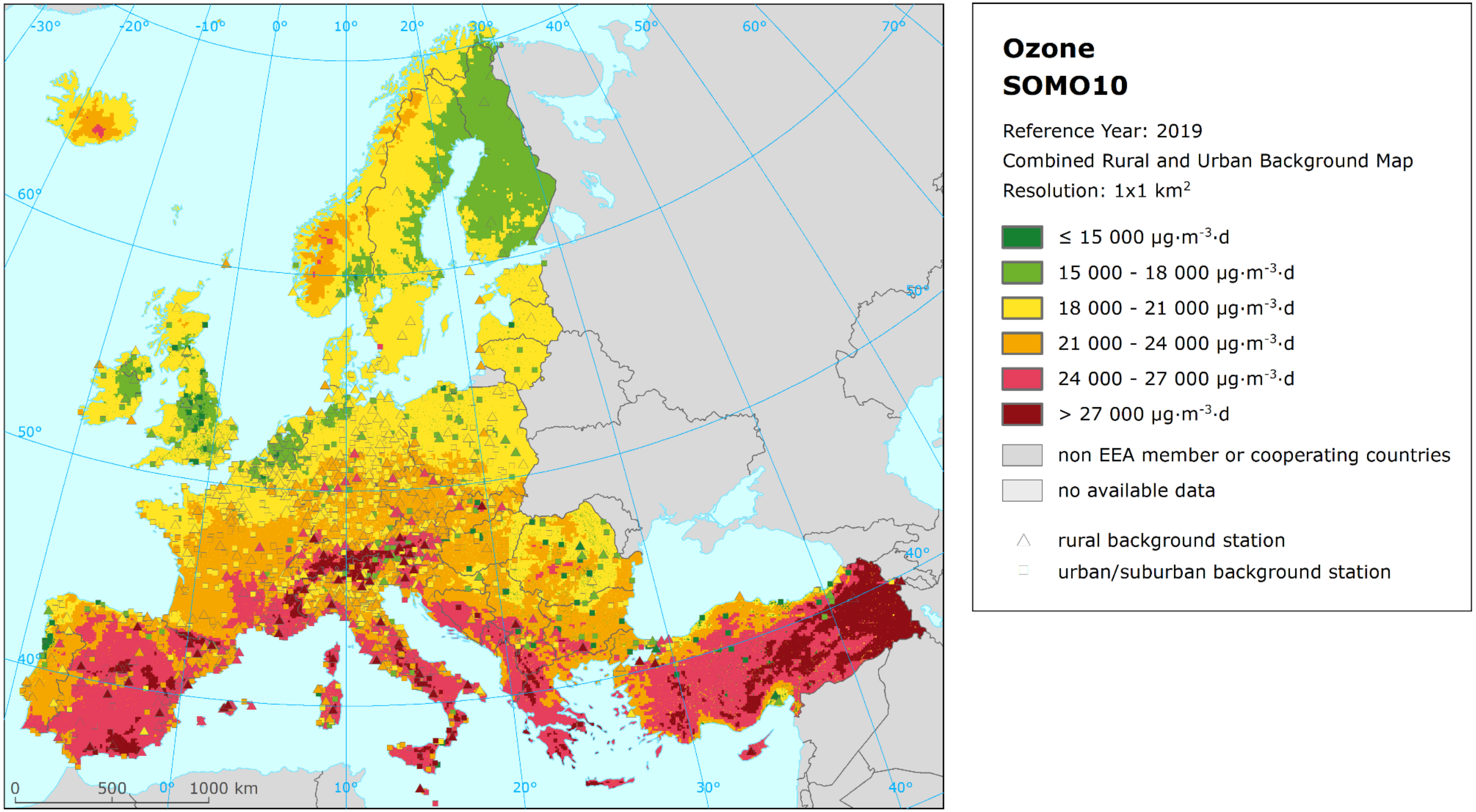

Map A5.7: Concentration map of ozone indicator AOT40 for vegetation including station measurement values, rural air quality, 2019

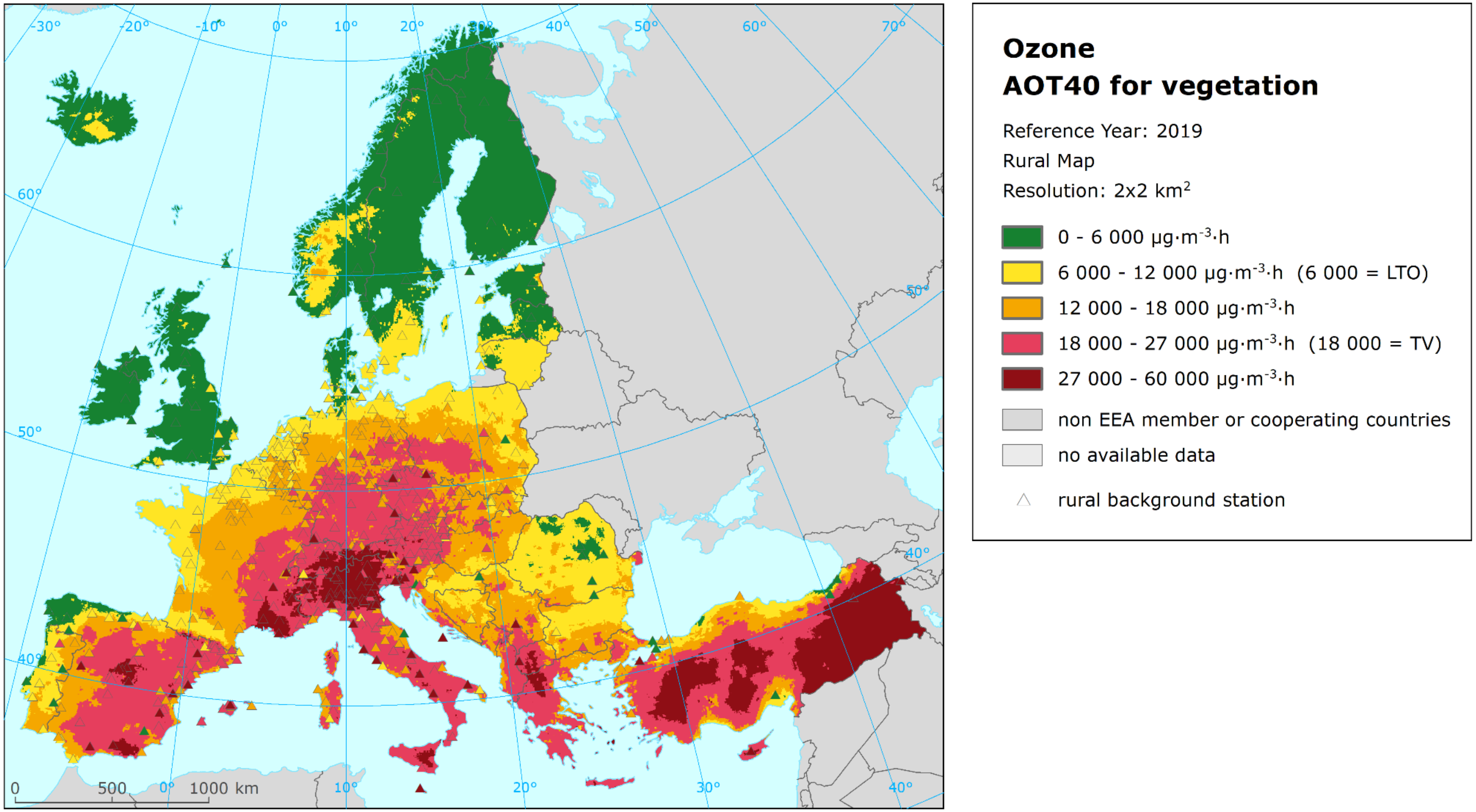

Map A5.8: Concentration map of ozone indicator AOT40 for forests including station measurement values, rural air quality, 2019

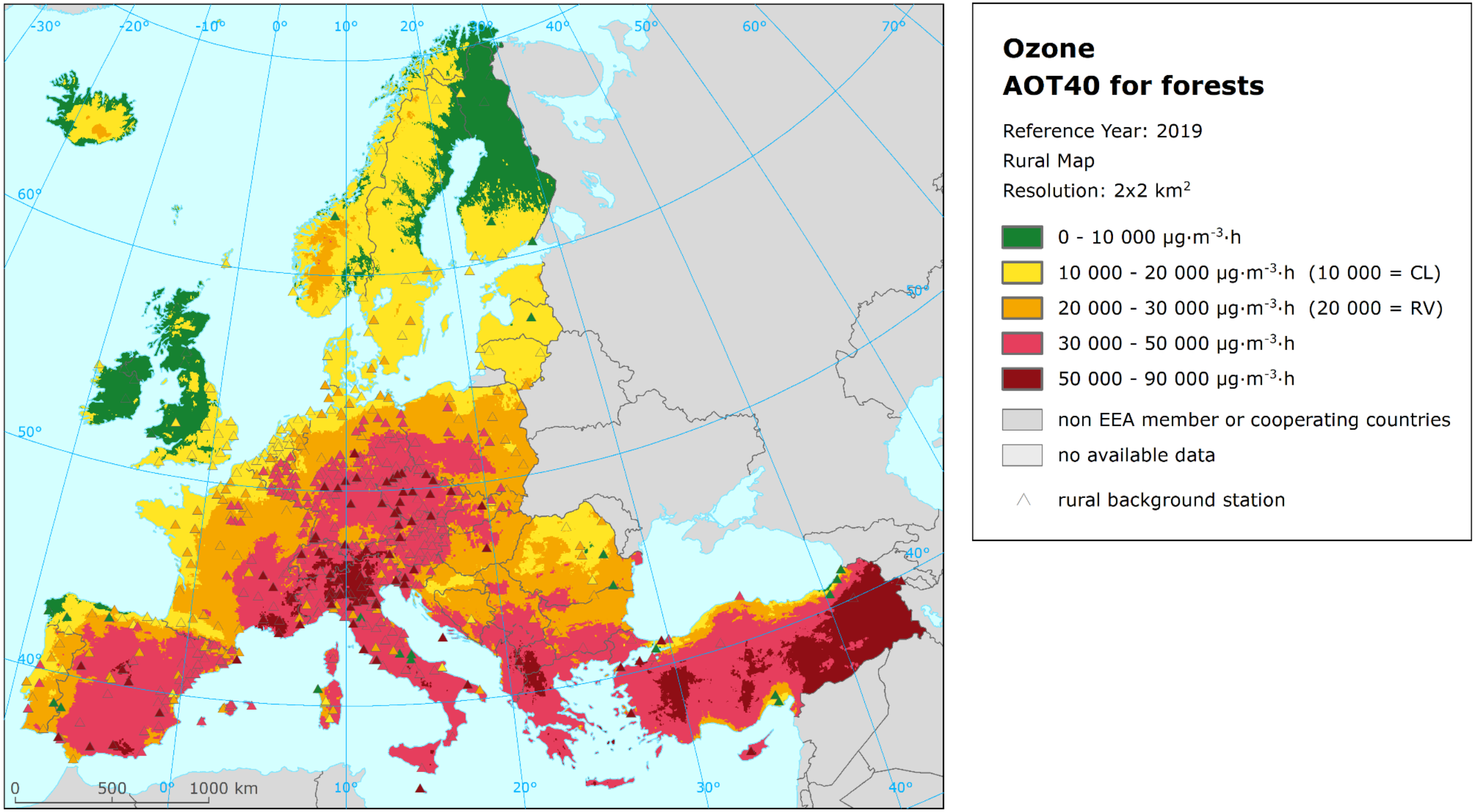

Map A5.9: Concentration map of NO_2 annual average including station measurement values, 2019

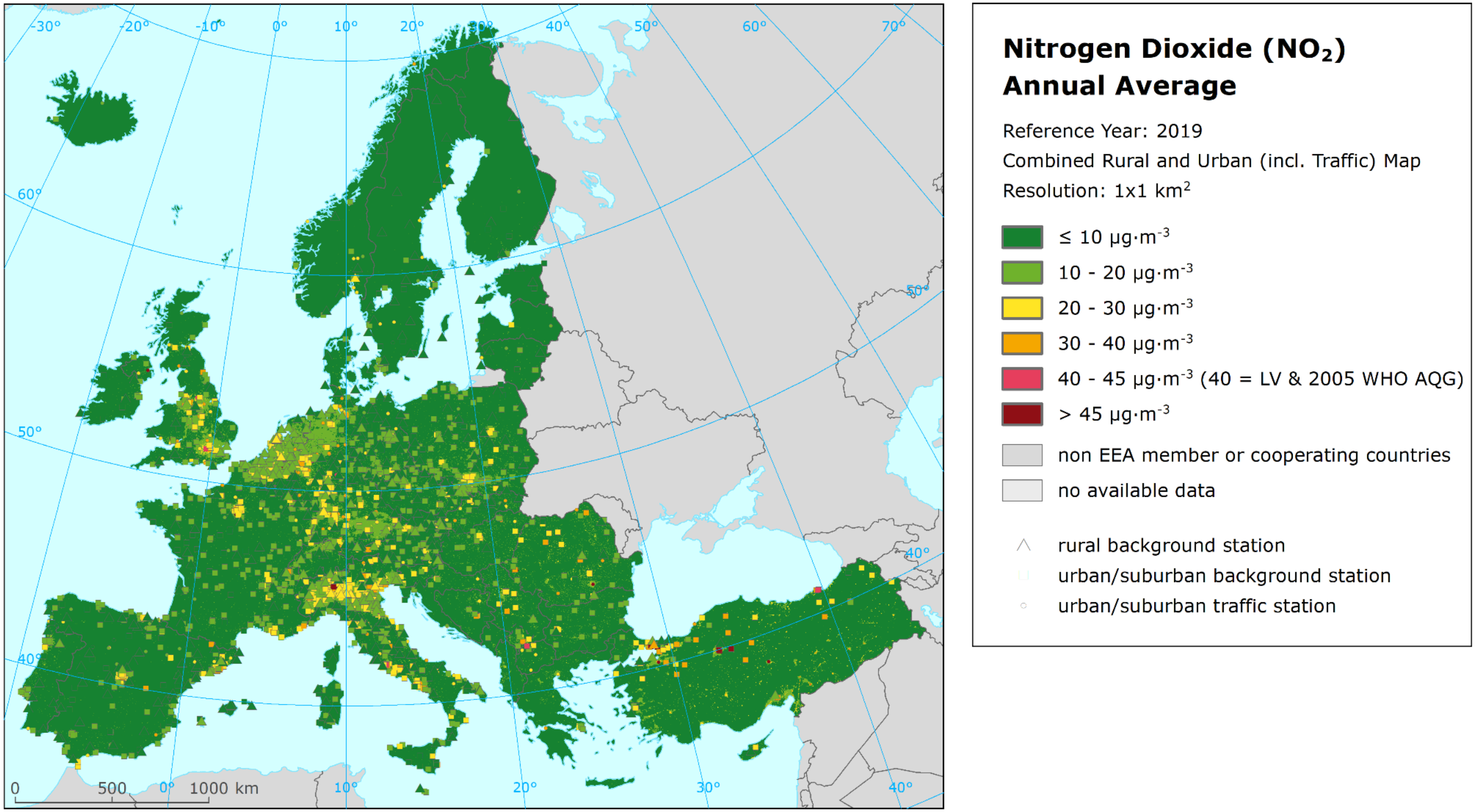

Map A5.10: Concentration map of NO_x annual average including station measurement values, rural air quality, 2019

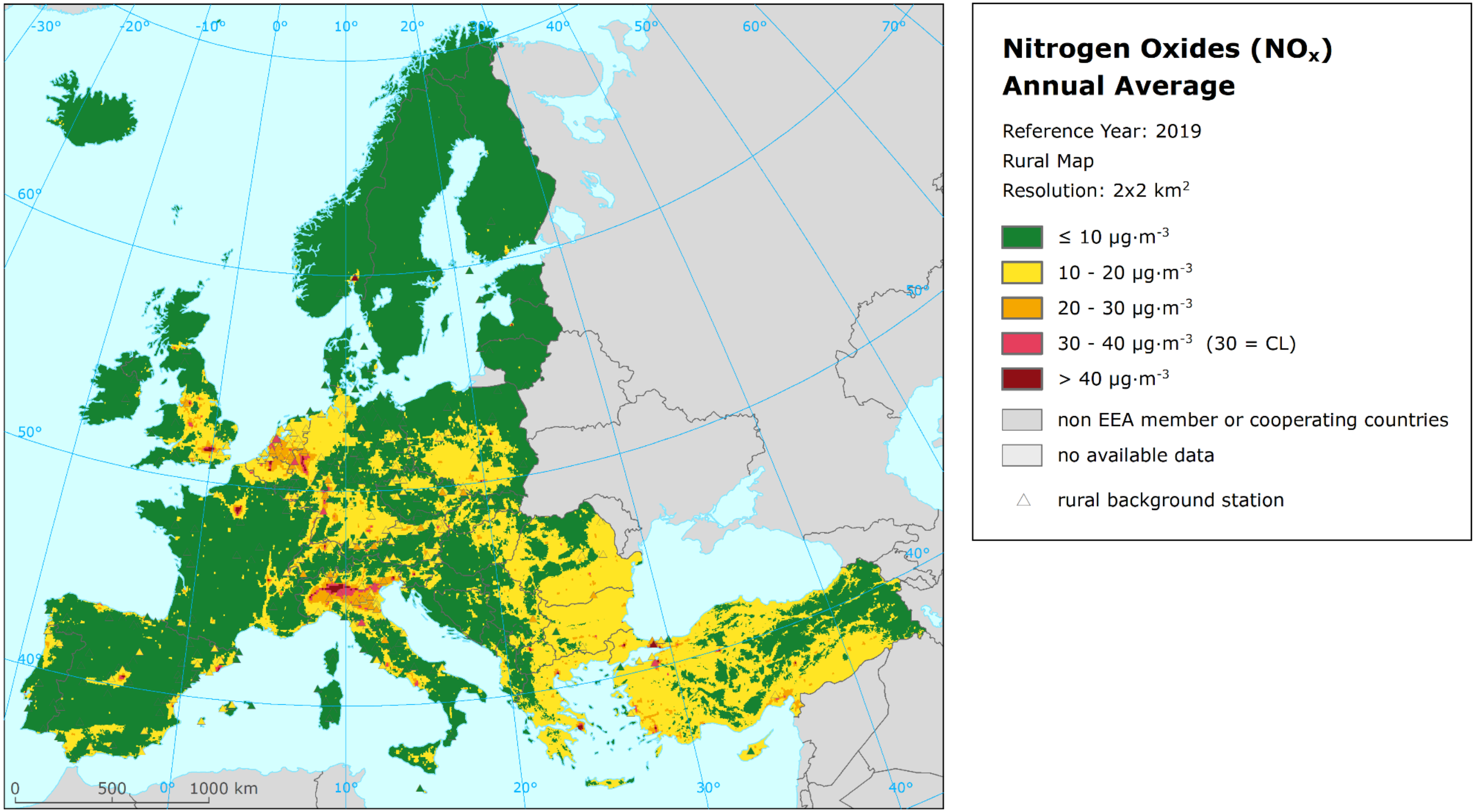

European Topic Centre on Air pollution,
transport, noise and industrial pollution
c/o NILU – Norwegian Institute for Air Research
P.O. Box 100, NO-2027 Kjeller, Norway
Tel.: +47 63 89 80 00
Email: etc.atni@nilu.no
Web : https://www.eionet.europa.eu/etcs/etc-atni

The European Topic Centre on Air pollution, transport, noise and industrial pollution (ETC/ATNI) is a consortium of European institutes under a framework partnership contract to the European Environment Agency.

European Environment Agency
European Topic Centre on Air pollution,
transport, noise and industrial pollution